1-1-2013

Experimental Investigation of Steady Flows at a Breached Levee

Cyrus K. Riahi-Nezhad
University of South Carolina

Experimental Investigation Of Steady Flows At A Breached Levee

By

Cyrus Khezr Riahi-Nezhad

Bachelor of Science
Tennessee Technological University, 1990

Master of Science
University of Tennessee, 2002

Master of Science
University of Tennessee, 2004

Submitted in Partial Fulfillment of the Requirements

For the Degree of Doctor of Philosophy in

Civil Engineering

College of Engineering and Computing

University of South Carolina

2013

Accepted by:

M. Hanif Chaudhry, Major Professor and Advisor

Jasim Imran, Co-Advisor

Jamil Khan, Committee Member

Jonathan L. Goodall, Committee Member

Lacy Ford, Vice Provost and Dean of Graduate Studies

DEDICATION

First and last, great thanks are due to "**ALLAH**", the only true God for the whole universe, without his will nothing can be achieved. This work is dedicated to HIM.

I wish to express my gratitude to my mom Fatemeh Karami and my dad Gholam-Ali for their love, support, encouragement and showing permanent interest in my work, as well as to my brothers and sister as follows:

Nabiollah (Businessman), his wife Noora (Teacher) and his two children Ida (M.Sc. Architectural Engr.) and Ali-Reza (Civil Engr. Student);

Habibollah (Businessman), his wife Behnoosh (Teacher) and his two children Pedram (M.Sc. Architectural Engr.) and Pegah (Law School);

Masoud (Orthopedist) and Hossein (Economist);

Masoumeh (Teacher), her husband Jalil alias Amir (Businessman) and her daughter Shaghayegh (M.D.) and Shahrbanoo (Teacher) and her husband Mahmood (Businessman).

ACKNOWLEDGMENTS

The author wishes to thank National Science Foundation (NSF) for providing the financial support which made this work possible. Several people contributed in significant measure to this program. The author's deepest appreciation and thanks go to the following people:

Dr. M. Hanif Chaudhry, Major Professor (Mr. and Mrs. Irwin B. Kahn Professor, Winner of Hunter Rouse Hydraulic Engineering Award, Associate Dean for International Programs and Continuing Education), for his invaluable guidance, technical advice and friendship.

Dr. Jasim Imran, Co-Advisor, Distinguished Professor, for his comments, encouragement, contributions, kindness, and suggestions;

Dr. Jamil Khan (Chairman, Mechanical Engineering), committee member, for his kindness, understanding and suggestions;

Dr. Jonathan L. Goodall, committee member, for his kindness, technical advice and suggestions;

Dr. Pranab Mohapatra (Research Associate Professor), for his invaluable support and suggestions for the Generalized Model and Analytical Model.

My heartfelt thanks to the following colleagues for their friendship, partnership, suggestions, encouragement and providing me the required data for my research and publications:

Mohamed El-Kholy (post-doc), Prashanth H. Reddy (post-doc), Ali Asghari Tabrizi (PhD candidate) and Jose A. Feliciano (M.Sc.).

In addition, Drs. Robert L. Mullen (Chairman, Civil and Environmental Engineering), Anthony S. McAnally, Michael Meadows and Enrica Viparelli, for their kindness, encouragement, friendship and understanding.

Special thanks are to Mrs. Karen Ammarel and Ms. Rebecca Rinehart, for their secretarial services, kindness and organizing the date for my dissertation defense and the technical staff(s) for constructing the experimental set-up.

The author also wishes to thank the following colleagues at Oak Ridge National Laboratory for their kindness, invaluable guidance, encouragement and friendship for the past 15 years:

Drs. Leonard E. McNeese (Ex. Director, Chemical Technology Division, ORNL) and his wife Barbara J. Redmon, Ali Kashani (Distinguished Staff Scientist at Atlas Scientific-NASA), Walter F. Silva-Araya (Professor and Director of the Research and Development Center at University of Puerto Rico, Mayaguez, Associate Director of Puerto Rico Water Resources) Costas Tsouris (Distinguished Staff Scientist), Abdolreza Zaltash, Moonis R. Ally (Distinguished Staff Scientist), Jack S. Watson (Ex. Editor, Journal of Separation Science and Technology, ex. Senior Scientist at ORNL and professor at UT-Knoxville), Steven H. Overbury (Distinguished Research Staff and Group Leader, Heterogeneous Catalysis), Sheng Dai (Distinguished Staff Scientist and Group Leader).

Sincere thanks to all of my colleagues at College of Engineering and Computing as well as to the authors and coauthors of the scientific publications presented within this dissertation.

VITA

Cyrus Khezr Riahi-Nezhad was born in suburb of the city of Noor (Vanoosh) near the coast of Caspian Sea located in Mazandaran province in the North of Iran (Persia). He has attended Reza Pahlavi and Shareef High School in city of Chalus, Mazandaran and obtained his high-school diploma with honors in 1973. After finishing his tour of duty (Army) in fall of 1976, he came to U.S.A. to pursue his undergraduate and graduate studies in Chemical Engineering. In 1990, he has earned his B.S. in Chemical Engineering from Tennessee Technological University at Cookeville, TN. In December 2001, he has obtained his first Master of Science in Chemical Engineering with thesis entitled "*The effect of electric field on moving aqueous aerosol suspended in a dynamic fluid chamber*" from University of Tennessee at Knoxville, TN. In August 2004, he has obtained his second Master of Science in Environmental Engineering from University of Tennessee at Knoxville, TN. The thesis was entitled "*The synthesis and characterization of mesoporous uranium oxide catalyst for oxidative destruction of volatile organic compounds and clean air protection*". He is currently a U.S. Citizen and after working for eight years for U.S. Department of Energy at Oak Ridge National Laboratory at Oak Ridge, TN, he has been admitted to the graduate studies in Civil and Environmental Engineering at University of South Carolina, Columbia, SC under Dr. M. Hanif Chaudhry (Mr. and Mrs. Irwin B. Kahn Professor, Winner of Hunter Rouse Hydraulic

Engineering Award, Associate Dean for International Programs and Continuing Education) in the area of Hydraulics and Fluid Mechanics. He has obtained his Ph. D. in May 2013. The title of dissertation is "*Experimental investigation of steady flows at a breached levee*". During his graduate studies at University of South Carolina, he has several presentations at the following cities / countries: San Juan / Puerto Rico; Cairo / Egypt; Louvain-La-Neuve / Belgium; Auckland / New Zealand. He has a number of research publications in journals and conferences. He is a member of American Institute of Chemical Engineering (AIChE) and American Society of Civil Engineering (ASCE).

ABSTRACT

Steady flow at a breached levee is studied in this dissertation through a generalized model and a case study. The generalized experimental set-up consists of a main channel with an opening in its side wall and an adjustable sluice gate at its downstream end. Water surface elevation and the three-dimensional velocity field are measured by a point gauge and an Acoustic Doppler Velocimeter (ADV), respectively. Time-averaged measured values of velocity field and free surface elevation are presented. In addition, Froude Number, turbulent kinetic energy (TKE) and bed shear stress are computed from the measured results. Results show that the flow is one-dimensional near the inlet and outlet of the main channel. However, it is three-dimensional near the breach. There is a zone of depression having dimensions less than the breach length near the breach in the surface profile. The Froude Number indicates the flow is critical near the breach. The bed shear stress shows that the breach area is prone to erosion. A generalized analytical model is developed to predict the approximate flow depth and velocity at the breach by knowing the flow depths at inlet and outlet, discharge at inlet, channel widths and breach length. The 17th Street Canal breach is employed as a case study. Detailed measurements of the flow field are performed in a 1:50 scale hydraulic model. On the model, the actual topography of the channel bed and the area beside the breach are reproduced. The flow in the channel is one-dimensional near the inlet, it becomes two-dimensional as it approaches the breach and finally it becomes three-dimensional at the breach. A

recirculating zone in the channel downstream of the breach exists due to no flow at the downstream boundary. Depth-averaged velocities, turbulent kinetic energy and bed shear stress are determined from the measured velocities. In addition, results for water surface profile and the effect of nearby structures on the flow field are presented. Trends for the Froude Number, TKE and bed shear stress are similar to those observed in the generalized experimental model. In addition, the generalized analytical model is used to predict the approximate flow depth and velocity at the 17th Street Canal Breach. Comparison of results obtained from the detailed measurements and from the analytical model suggests that the flow depth is over-predicted by the analytical model.

TABLE OF CONTENTS

LIST OF TABLES

LIST OF FIGURES

LIST OF SYMBOLS

$a = \frac{B_1}{y_1}$	Ratio of channel width over flow depth at the inlet
B_1, B_2, B_3	Width of channel at inlet, breach and outlet (m)
C_d	Coefficient of discharge through sluice gate
C*	Non-dimensional roughness coefficient
F_1	Inlet Froude Number
g	Acceleration of gravity, 9.81 m/s^2
go	Opening of the sluice gate (m)
h	Height of water behind sluice gate (m)
K	Correction factor for streamline curvature at breach
K_E	Turbulent Kinetic Energy (cm^2/s^2)
L_1, L_2	Length of control volumes 1 and 2, respectively
Q_1, Q_2, Q_3	the discharge at inlet, breach and outlet (m^3/s)
Q_g	Discharge through sluice gate (m^3/s)
$\overline{u'^2}$, $\overline{v'^2}$, $\overline{w'^2}$	Variance of fluctuation x, y and z-component
V_x, V_y, V_z	Velocities in x, y and z- direction (cm/s)
V_1, V_2, V_3	Velocities at inlet, breach and outlet (m/s)
y_1, y_2, y_3	Flow depth at inlet, breach and outlet (m)

$\xi = \frac{Q_2}{Q_1}$	Breach discharge ratio
η_2, η_3	Depth ratio at breach and outlet, respectively
ω_2, ω_3	Width ratios at breach and outlet, respectively
τ	Bed shear stress N/m^2

Chapter 1

INTRODUCTION

1.1 Levee breach flow

Breaching of levees in a river or in a canal is the most common cause of flooding. The breach may be natural or artificial. The breaching of levees begins with the partial failure of the levee followed by enlargement of the opening and the formation of scour holes resulting in complete breakage of the embankment (Fujita et al. 1987). Sometimes, breaching of a levee is purposefully engineered to manage a flood (Jaffe and Sanders, 2001). A depression known as a kolk lake may be formed behind the breach, due to high intensity of flow through the breach associated with scour of bed. A levee breach causes mega flood leading to enormous losses to lives and properties. Some examples of levee breaches in the recent past are (place, country, month, year): Thatta, Pakistan, August 2010; Bihar, India, August 2008; Louisiana, USA, August 2005. A list of historic events of levee breach is presented in Appendix-1. Understanding the levee breach flow helps in many engineering applications such as, (i) estimation of the flood inundation area/flood plain zoning; (ii) efficient way of closing the breach; (iii) design of the embankment; and (iv) assessment of impact of flood wave on the structures in the vicinity. The research reported in this dissertation is for understanding the hydraulics of steady flow at a breached levee.

The characteristics of divided, open-channel flow due to a levee breach are complicated. The occurrence of a levee breach triggers the propagation of flood wave in a region external to the main channel. It also affects the flow field in the main channel. It is important to estimate the outgoing discharge through the breached levee and the water surface profiles in the main channel and in the flooding zone outside the breaches. The velocity field near the breach is highly complicated and is associated with high degree of turbulence, energy loss and three-dimensional flow field. Flow separation and trans-critical flow may be present. The changed water flow features also influence the sediment transport in the whole system. A definition sketch for divided flow in an open channel due to a levee breach is presented in Fig. 1.1.

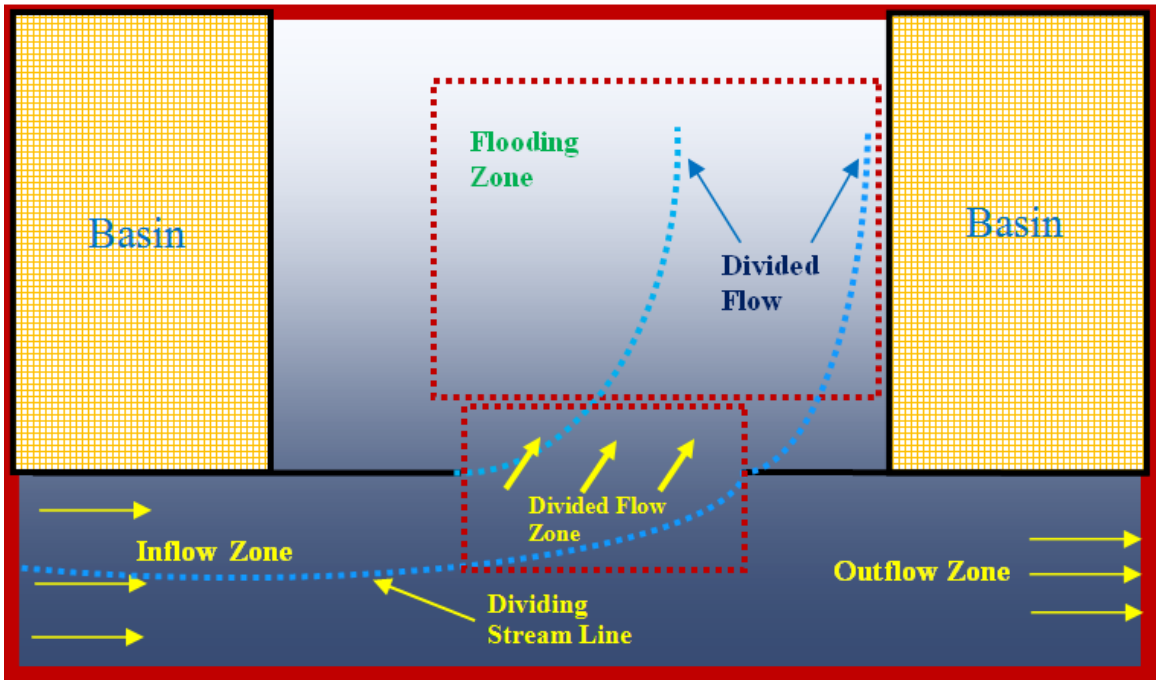

Figure 1.1: Definition sketch of divided flow due to a levee breach

Divided open channel flow due to levee breach is studied in the present work and the 17th street canal breach is used as a case study. A brief description of the event is presented in the following paragraphs.

1.2 17th Street Canal Breach

The City of New Orleans is surrounded by an intricate network of floodwalls and dikes built to protect the city from flooding from the Mississippi River and Lake Pontchartrain. On August 29, 2005, Hurricane Katrina, a category 4 hurricane, led to over 20 levee breaches in the City of New Orleans within 24 hours of the passage of the storm and 80 percent of the city was submerged by the flooding, with some parts under 15 feet of water (Wikipedia 2012). The worst of these breaches occurred on the 17th Street Canal, with an overall length of 465 feet. About 100,000 citizens were trapped in the city without power, food, and drinking water. This failure has been cited as an 'engineering failure' (Walsh 2006). There were approximately 2000 deaths and total properties damages of cost $500 billion (Robert et al. 2008).

The US Army Corps of Engineers started the closure of the 17th Street breach by placing 3000 lb sandbags by helicopters. Later the size of the sandbags was increased to 6000 and 7000 lbs because the lighter bags were washed away by the flow through the breach. Plans in the field for breach closure were changed a couple of times because of the absence of standard procedures. The measured maximum breach discharge was 31,699 cfs as compared to about 29,000 cfs as calculated in the (USACE 2007). The measured flooding depths in the vicinity of the breach ranged from 4 ft to 6 ft and then decreased to an average value of 2.2 ft at about 400 ft from the breach, which are very close to high water marks of elevations 2.3 ft to 2.8 ft collected at 400 ft from the breach and the scaled video recording of 4-5 ft near the breach (UACE 2007).

1.3 Objectives

The main purpose of the present study is to understand the hydraulic behavior of steady flow past a breached levee. Specific objectives of this dissertation are (i) to measure the detailed flow field in a generalized model set-up; (ii) to develop an analytical model to predict the approximate flow conditions at the breach; (iii) to measure the detailed flow field for a real-life case of levee breach flow; and, (iv) to verify the performance of the analytical model to predict the real-life case using the hydraulic model study of the 17th Street Canal breach.

1.4 Organization

The dissertation is divided into six chapters. Importance and characteristics of levee breach flow are presented in the present chapter. In addition, the objectives are identified. Literature relevant to the present study is reviewed in the next chapter. The third chapter presents the experimental setup and procedure. Results of the generalized model are presented in chapter four and results for the 17th Street Canal breach are reported in chapter five. Important conclusions from the present research and scope of future work are outlined in the last chapter. Experimental results are included in Appendix…

Chapter 2

REVIEW OF LITERATURE

Importance of divided flow in an open channel due to a levee breach is discussed in the previous chapter and the objectives of the present study are presented. Literature relevant to the divided open channel flow (DOCF) in general and flow due to levee breach in particular is reviewed in this chapter. The presentation is divided into three parts: (i) divided flow in open channels; (ii) flow due to levee breach; and (iii) 17th Street canal breach.

2.1 Divided flow in open channels

Considering the methodology to study divided flows in open channels, analytical, numerical and experimental approaches have been reported in the literature. Shabayek et al. (1999) presented an analytical model for subcritical dividing flows in open channel junctions. Separate control volumes for the main channel flow and for the lateral channel flow were considered. The momentum principle was applied in the stream-wise direction together with mass conservation. Given the discharge ratio and the upstream Froude number, the proposed model was used to solve for the downstream flow depths for the main and the lateral channel.

Ramamurthy et al. (1990) presented a model for dividing flow at right-angle junctions of rectangular open channels and obtained an estimate of the discharge ratio as a function of the Froude number in the main channel upstream and downstream of the junction. The proposed model was verified by experimental data. Various aspects of divided open channel flows have been reported in the literature. Yue et al. (2005) presented coherent structures in open-channel flows over a fixed dune. Turbulent open-channel flow over a two-dimensional laboratory-scale dune was studied using large eddy simulation. Level set method was used for surface tracking. The numerical simulations for mean flow field and turbulence statistics were in good agreement with the experimental data. Ramamurthy et al. (2007) also presented a three-dimensional turbulence model to investigate the dividing open-channel flow. The simulated flow characteristics were validated using experimental data. Data related to secondary flows provided information vital to bank stability. Pirzadeh and Shamloo (2008) presented numerical investigation of velocity field in dividing open-channel flow by applying FLUENT for lateral intake flow and compared the numerical results and measured experimental velocities. Kesserwani and Vazquez (2010) presented a mathematical model for predicting the division of unsteady flow at a right-angle open-channel junction. They assumed a side weir with zero crest height at the junction to take into account the divided flow. An upwind, implicit numerical solver is employed to compute the governing equations. In all the tests, lateral-to-upstream discharge ratios are successfully reproduced by the present technique with a maximum error of less than nine percent. All the works cited above are numerical. However, many experimental works are also reported in the literature and some relevant works are discussed in the following paragraphs.

Lakshmana et al. (1970) presented flow characteristics such as surface profiles, dividing streamlines at the bed and on the surface, and return flow in the branch channel. The division of flow was correlated with Froude numbers in the main and branch channels. Neary and Odgaard (1993) showed that the flow at an open channel diversion is three-dimensional, exhibiting similar characteristics to river bend flows. They advocated that the sediment transport behavior at diversions required the understanding of three-dimensional flow structure. Hsu et al. (2002) found that the contraction coefficient at the maximum width-contracted section in the recirculation region was almost inversely related to the main channel upstream-to-downstream discharge ratio. The energy heads upstream and downstream of the division in the main channel were found to be almost equal. The energy-loss coefficient of the division was expressed in terms of discharge ratio, upstream Froude number and depth ratio. An expression to determine the maximum possible branch-channel discharge at a given upstream discharge with a prescribed downstream Froude number was presented. El Kadi et al. (2011) presented characteristics of dividing critical flows with various inflow discharges and downstream boundary conditions. Four main flow patterns were identified considering the location and length of the developed hydraulic jumps. A relationship between the discharge division ratio and the tail water Froude number was established. Ramamurthy et al. (2007) used point gauge and laser Doppler anemometer to measure flow depth and velocities, respectively and data were used to develop a numerical model.

Barkdoll et al. (1998) compared experimental results for velocity and water-surface elevation between open-channel free surface and duct symmetry plane. The differences in

velocity were attributed to secondary currents in open-channel flow. They also found that centrifugal forces caused up to 2.1 percent super elevation of the water surface in the junction. Ye et al. (1995) used LDA to measure and study the dividing flows in channels. The flow patterns, distribution of velocities and pressure, and the allotment of flow volumes were obtained in detail. The results showed that the dividing flow was very complicated. The dimensions of the breach, shape and backpressure in the downstream channel affect the flow patterns of the dividing flow. Agelinchaab and Tachie (2008) used particle image velocimeter (PIV) to study the mean and turbulent fields of separated and redeveloping flow over blocks of different shapes fixed to the bed.

In view of the literature review presented in the above paragraphs, it may be remarked that divided open channel flows have been studied primarily by employing branched channels. However, some studies for flow past levee breach available in the literature are presented in the following section.

2.2 Flow due to levee breach

Han et al. (1998) presented flood inundation analysis resulting from a levee-break, by using one- and two-dimensional numerical models. Zhang and Yu (2001) presented numerical simulation of bed deformation in dike burst. Sarma and Das (2003) presented analytical solution of a flood wave resulting from dike failure. Faeh (2007) presented a numerical model taking into account the breach erosion of the river. The sensitivity of the discharge through the breach related to different processes and material parameters was compared with the experimental and field data. Yu et al. (2009) presented two-

dimensional numerical simulations of the levee breach flows under complex boundary conditions. Vorogushyn et al. (2010) proposed an Inundation Hazard Assessment Model (IHAM) comprising of three models that are coupled dynamically: (1) one-dimensional unsteady hydrodynamic model for river channel and floodplain between dikes; (2) probabilistic dike breach model which determines possible dike breach locations, breach widths and breach outflow discharges; and (3) two-dimensional raster-based inundation model for the dike-protected floodplain areas. Savant et al. (2011) presented an efficient implicit, finite-element method for the dam and levee breach by using the concept of a pseudo-transient continuation (PTC) flow model.

Only few experimental studies simulating flow past a breached levee are reported in the literature. Fujita et al. (1987) presented the process of enlargement of breaches in flood levees on alluvial plains. The hydraulic characteristics and the mechanisms for the enlargement of a breach were discussed and methods for the prevention or mitigation of breach enlargement were considered. Different aspects of side weir flow have been studied in details. Some recent studies have been reported by Emiroglu (2011), Prastowo et al. (2009), Kotowski and Wojtowicz (2007), Zhicheng et al. (2007), and Onen (2007). However, these studies were with a finite weir height.

2.3 17th Street Canal Breach

Different aspects of the 17th Street Canal breach have been reported: Hou et al. 2006 described the pathogen indicator microbes and heavy metals in lake Pontchartrain following Hurricane Katrina. Rogers et al. (2008) and Dunbar et al. (2008) studied the

geologic conditions underlying the 2005 17th Street Canal levee failure. Sasanakul et al. (2008), Seed et al. (2008) and Steedman et al. (2011) analyzed different geotechnical aspects of the levee failure at the 17th street canal breach. Duncan et al. (2008) presented the stability of I-walls in New Orleans during Hurricane Katrina.

Seaberg (2010) utilized a 1:50 scale physical model to simulate the wave and water velocity conditions in the 17th Street Canal during the time period leading up to the breaching of the floodwall. This physical model study indicated wave-attenuating processes occurring as waves approached the location of the breach. Wave heights near the lakeside of the bridge were 0.3 to 0.9 m in height, reduced from 1.8 to 2.7 m wave heights in the open lake. Waves on the south side of the bridge, near the breach, were further reduced to heights below 0.3 m. These results supported the conclusion that the waves were not a significant factor for the 17th Street Canal floodwall failure. Other IPET investigations determined that the floodwall failure was of a geotechnical nature due to the high surge water level. The effects of debris on the flow and waves after the breach were also investigated.

Sattar et al. (2008) used a 1:50 scale physical model of the 17th Street Canal breach to study the closure procedures. It is assumed in the model that the bed is fixed and the levee below the flood wall remains intact during breach closure. Because of the many uncertainties in the values of various variables, a range of conditions were tested on the model in an attempt to bracket the results for the flooding depths and the initial failed attempts to close the breach. Then, various possible methods for breach closure were

investigated utilizing the procedures developed for cofferdam closure for river diversion, e.g., toe dumping, transverse dumping, single- and multi-barrier embankments, etc.

Emlen et al. (2012) presented a two-dimensional depth-averaged finite-volume numerical model and found that the transient part of the flood is quite short in comparison with the long flood in the city under steady-state conditions. Comparison between the simulated results and experimental measurements for steady-state flow was satisfactory. The depth-average model could predict the average velocity values satisfactorily, even at the breach location.

2.4 Summary

Based on the review of literature presented in the previous sections, following remarks may be made:

1. A generalized approach for the hydraulics of steady flow in a breached levee is not available.
2. The characteristics of sediment transport including the aggradation and degradation of bed due to a levee breach has not been studied.
3. Detailed measurements in the flow field in a levee breach environment are unavailable.
4. The development of a numerical model to assess the wall stresses for bed scour and/or enlargement of the breach will be very useful.
5. The hydraulics of the steady flow past a breached levee have been studied experimentally by using the 17th Street Canal breach as a case study.

Chapter 3

EXPERIMENTAL INVESTIGATIONS

The experimental study for this dissertation is performed in the Hydraulics Laboratory of the University of South Carolina. The experimental set-up, instrumentation used and procedure followed to study the generalized model and the hydraulic model of the 17th Street Canal Breach are described in this chapter.

3.1 The generalized model

The experimental set-up for A generalized model was built by using marine plywood as shown in Fig. 3.1. The main channel is 12.90 m long, 0.61 m wide and 0.3 m high. The flooded area is 6.1 m long and 2.96 m wide and it is separated by the left bank of the main channel. The model was built on a raised platform to allow the outflow from the flooded zone and to prevent backing up of the water into the model. Two axial pumps supplied the flow to the channel inlet. The discharges were measured by an electromagnetic flow meter in the pump delivery line. A number of valves were used to control the inlet discharge. A honey comb was used at the canal entrance followed by a flow straightner to reduce the turbulence. A wave suppressor was installed before the model inlet to reduce the waves and fluctuations on the water surface. The sluice gate at the downstream end of the channel controls the outlet discharge. A 16 MHz 3-

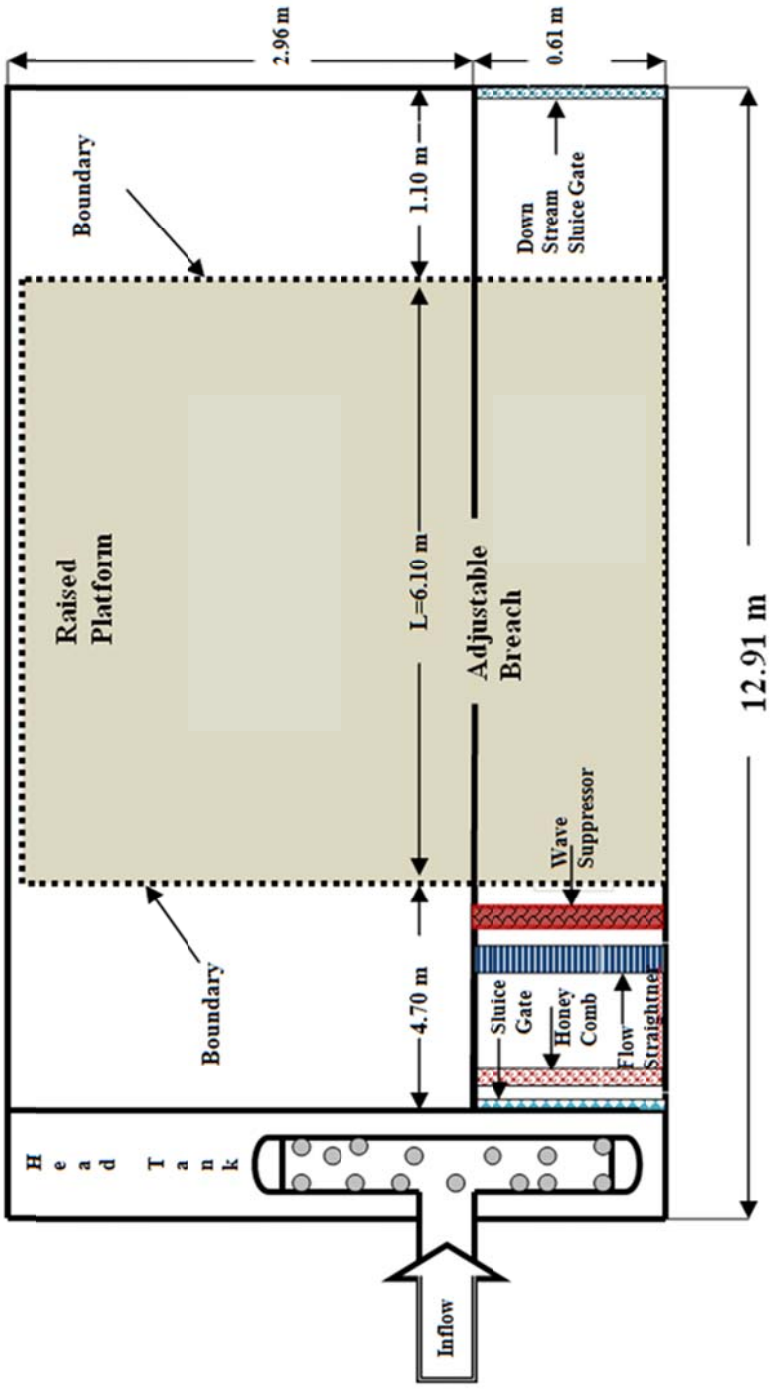

Figure 3.1. Schematic of the generalized model set-up

component Sontek micro ADV was used to measure the vertical distribution of the velocity components at selected locations on a measuring grid. Three-dimensional velocitiy profiles were measured at each selected locations from ~ 0.5 cm above the bed to about 1 cm below the water surface. Water surface elevation at the grid points were measured by a point gauge. The grids are 0.15 m x 0.15 m. Fig. 3.2 shows an aerial view of the model.

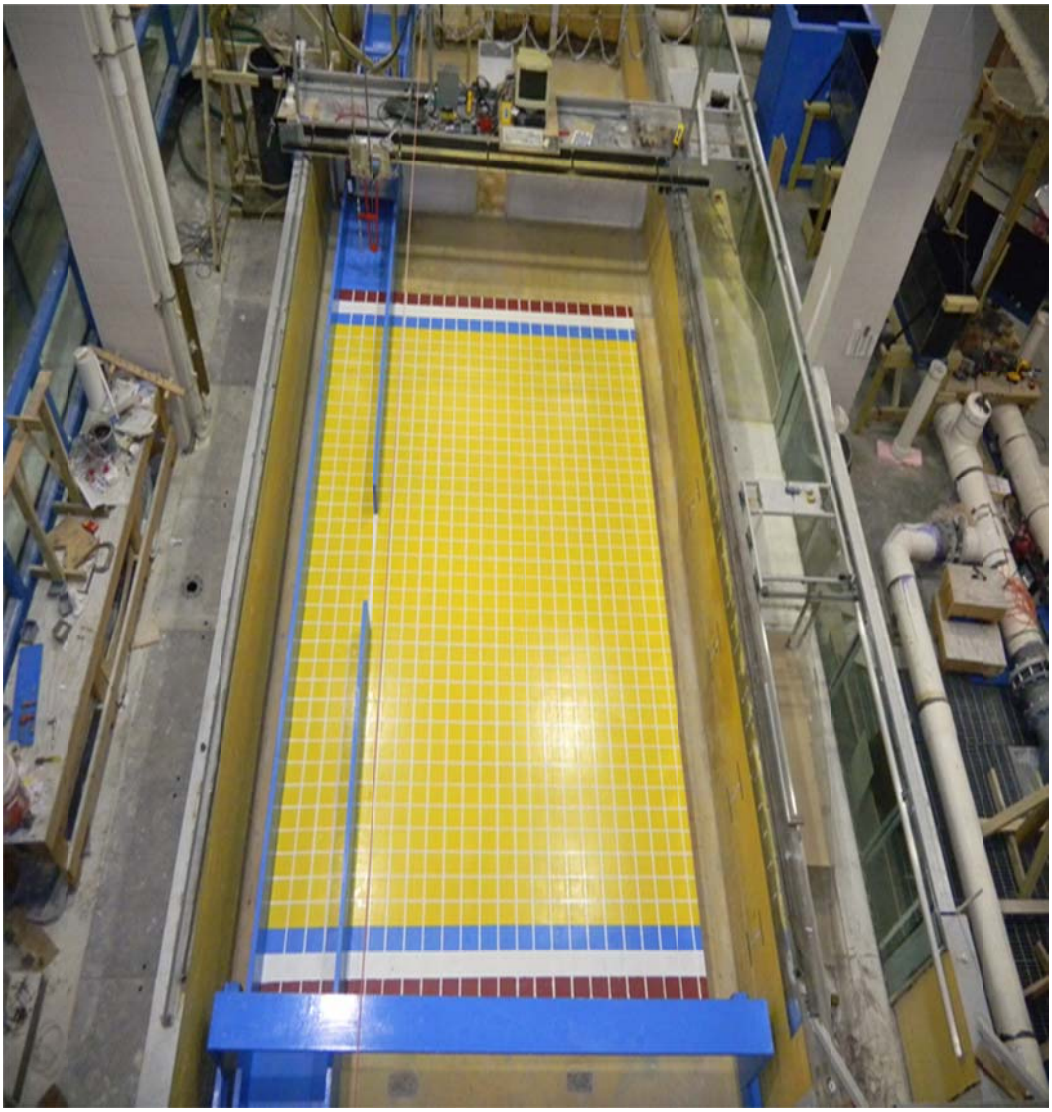

Figure 3.2. Aerial view of the generalized model set-up

3.2 Hydraulic model of the 17th Street Canal breach

The hydraulic model study of the 17th Street Canal breach was conducted on 1:50 scale model. This model scale is selected to minimize the effects of viscosity and surface tension in the hydraulic model (Chanson 1999; Chaudhry et al. 2010). The flows in the model are studied by Froude Number similitude. All dimensions in this chapter refer to the laboratory model and the scales of Table 3.1 may be used to convert the model parameters to corresponding field values. The hydraulic model consists of the main channel that is 12.91 m long and 1.22 m wide, and the flooded urban area which is separated by the breached levee (Fig. 3.3). The topographic data used to build the model was adopted from the final report, IPET of USACE (2007). The flooded neighborhood and the building blocks were reproduced using the rectangle wooden blocks; the flooded area was built on a raised platform to allow outflow in all three direction to avoid backing up of the water level into the model.

Table 3.1: Scales used in the hydraulic model

Parameter	Scale = model/prototype	Remarks
Length/Width/Depth	1:50	Undistorted Model
Discharge	1:17677.67	Froude Similarity
Velocity	$1:\sqrt{50}$	
Time	$1:\sqrt{50}$	

Figure 3.3: Aerial view of the 17th Street Channel breach model

A field survey (USACE 2007) showed that the crest of the levee on the canal side remained in place after the breach. Therefore, the levee and the bed section at the breach location on the physical model were non-erodible. Two axial pumps were used to supply the water into canal entrance and the flow discharges were measured by an electromagnetic flow meter in the pump delivery system. A honey-comb was used at the canal entrance, followed by a flow straightener to reduce the turbulences. A wave suppressor was installed downstream the model entrance to reduce the water surface fluctuations and downstream end of the canal was closed by a sluice gate to force the

entire flow to exit through the breach. This is to simulate the dead end condition in the real canal (USACE 2007).

An aerial view and schematic of the physical model are presented in Figs. 3.3 and 3.4. The bathymetry and topography of the breach area are accurately reproduced in the model (Fig. 3.5). In particular, the significant erosion in the breached section and immediately downstream are incorporated in the model. According to the survey sections (USACE 2007; Sattar et al., 2008), the crest elevation of the breach had an average value of zero meters (0 ft). The floodwalls had an average elevation of 3.65 m (12 ft) throughout the modeled canal section. Digital photographs (USACE 2007) were used to determine the exact location and dimensions of the houses in the vicinity of the breach. The hydraulic model included a 570 m (1, 870 ft) section of the 17th Street Canal South of the Old Hammond Highway Bridge where the breach occurred and a small part of the neighborhood, 3.172 hectares (7.84 acres) in the vicinity of the breach where major flooding occurred. The model was constructed of sealed plywood. The plywood sheets in the channel and in the neighborhood were covered with two layers of thick plastic (3 mm) to ensure waterproofing followed by one layer of metal wire mesh for strong bonding of the mixture used to construct the topography of the model. The non-erodible topography of the canal, breach, and the flooded area were reproduced using a mixture of cement sand, and zonolite. Irregular topography of the breach and the area in its vicinity were reproduced using plywood frames cut to the exact dimensions of the sections and moved over the specified section in the wet mixtures.

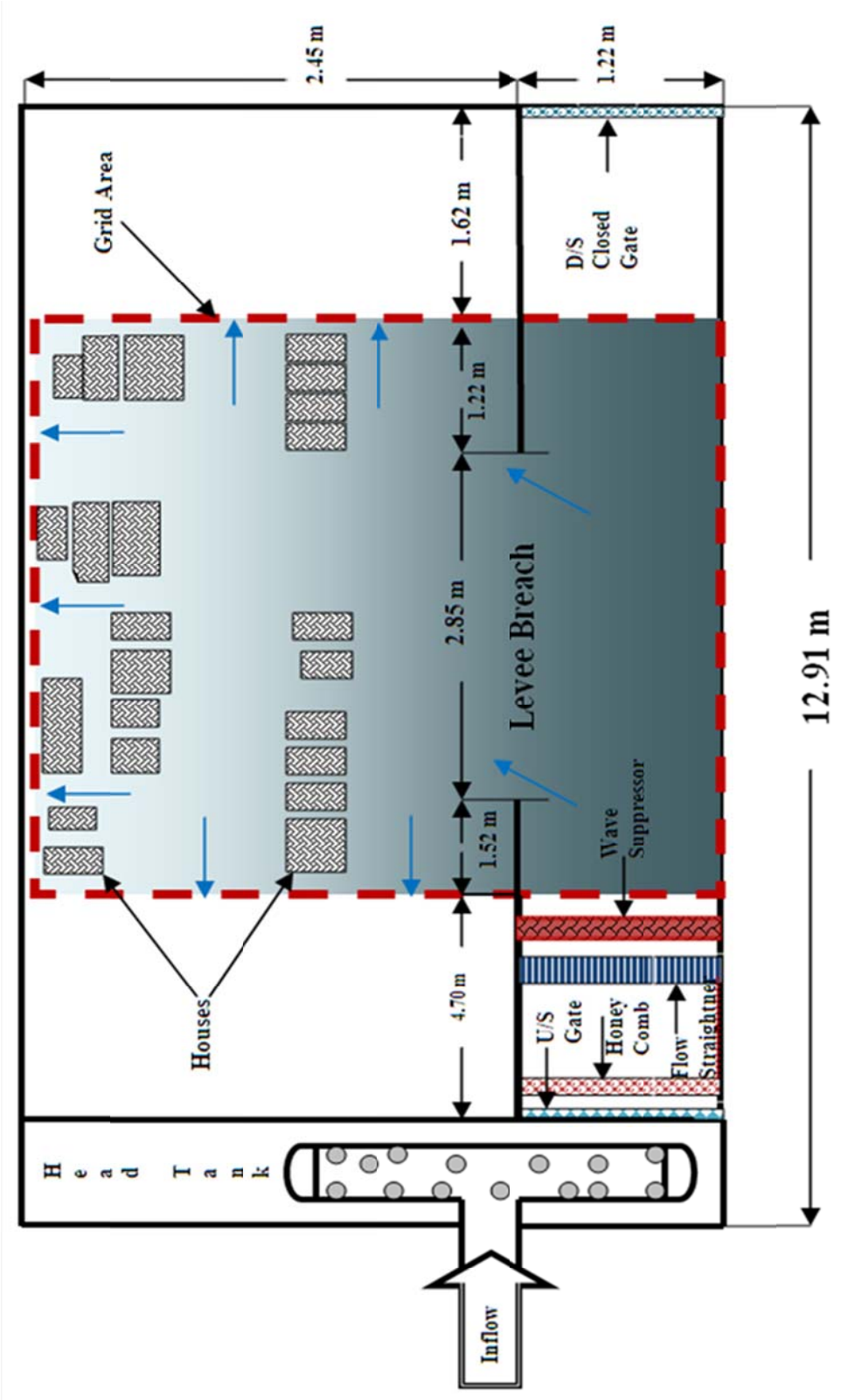

Figure 3.4: Physical model set-up

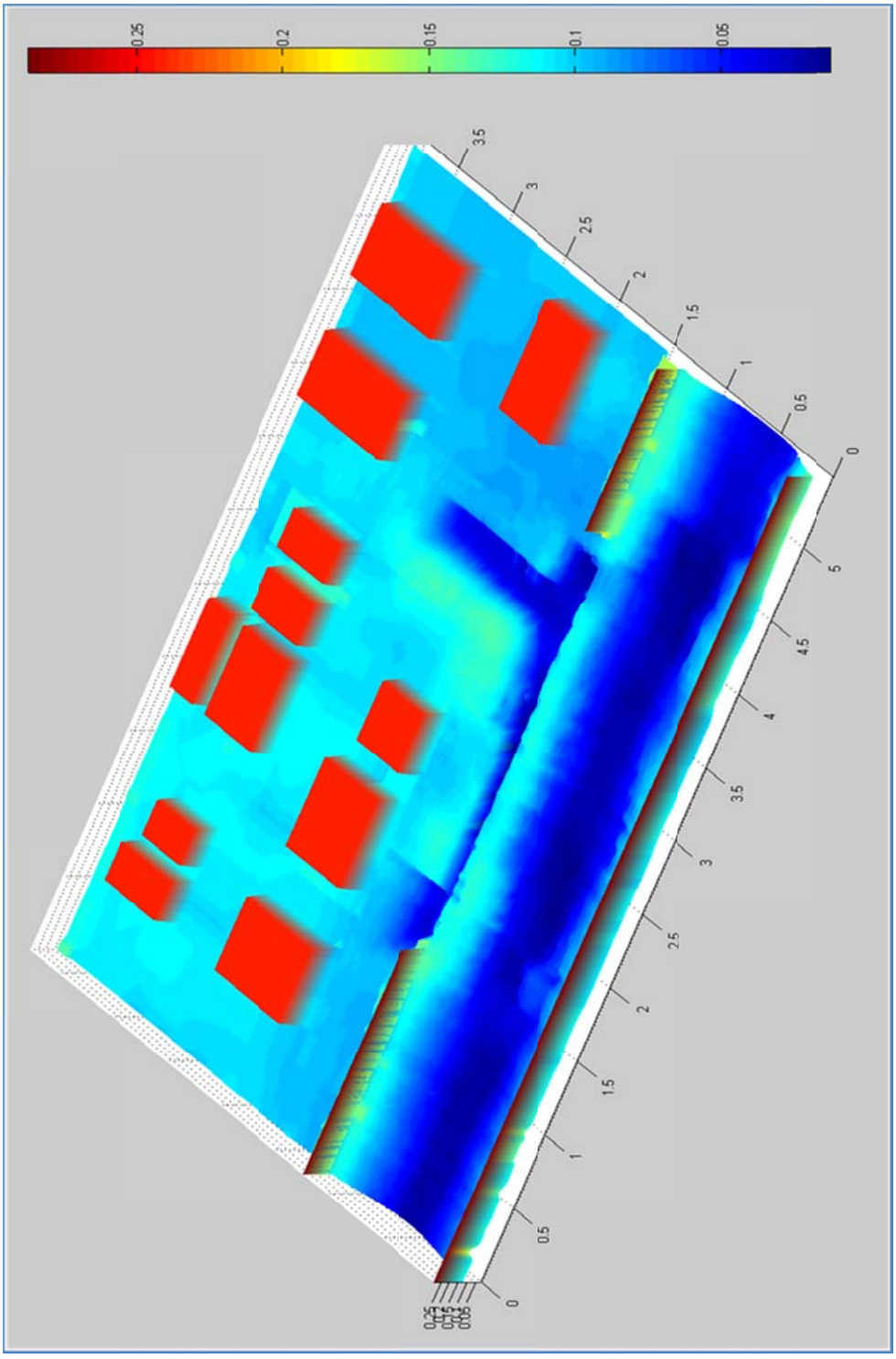

Figure 3.5: A 3-D elevation map of the model

3.3 Equipment

The following equipment are used in the present experimental study.

1. Accuostic Doppler Velocimeter for velocity;
2. A high speed digital camera for the free surface velocity;
3. Point gauge for the bed and water surface elevation; and ;
4. Baumer for topography of dry-bed.

A brief description of the equipments are presented below.

3.3.1 Acoustic Doppler Velocimeter (ADV)

The instantaneous velocity components are measured by using a 16-MHZ Sontek micro ADV (Sontek, 2001). The instrument is highly advanced as compared to other velocity measurement devices, i.e propeller or mechanical gauge, electromagnetic current meter, hot films anemometer, Pitot tube and Hydrogen Bubble technique. An ADV is useful for many different applications in hydraulics, coastal engineering and oceanography. The commonly used velocity measurement tools, such as mechanical or electromagnetic current meters measure only the 2-D velocity data, cause disturbance in the flow due to their relatively large size, and are not appropriate for capturing the fine turbulence scales due to their slow response (Sontek San Diego, 2001).

ADV consists of a central circular transmitter surrounded by three equally spaced receivers (Fig. 3.6a). The sampling volume is located at the intersection of the transmitted and received beams, 5 cm from the probe. Therefore, the presence of probe does not distort the velocity measurement. Velocity can be measured in any water containing

acoustic scatters, or scattering particles such as walnut shell powder (Kraus et al. 1994; Voulgaris et al. 1998; Chanson 2008). For each sample, it records nine values: three velocity values (one for each component), three signal strength values (one for each receiver) and three correlation values (one for each receiver). Figure 3-6b shows the 16-MHz cable ADV used in the present study.

A windows interface, Horizon ADV was used to collect and save the raw data. Post processing software, WinADV was utilized to analyze the raw data (Wahl 2000). WinADV provides routines for processing an entire ADV file or portions of ADV files defined by sampling windows to obtain average velocities, turbulence parameters, and aggregated measures of data quality. A single or collections of ADV file may be viewed and processed. Signal strength is accessed as signal-to-noise ratio (SNR), in dB. SNR is derived from signal amplitude by subtracting the ambient noise level and converting to units of dB. The main function of the signal strength data is to verify that there is sufficient particulate matter in the water. If the water is too clear, the return signal may not be stronger than the ambient electronics noise level. As SNR decreases, the noise in ADV velocity measurements increases. For high-resolution measurements (e.g. sampling at 25 Hz), it is recommended to maintain SNR of at least 15 dB. The ADV correlation coefficient is a data quality parameter that is a direct output of Doppler velocity calculations. Correlation is expressed as a percentage. Perfect correlation of 100 percent indicates reliable, low-noise velocity measurements; 0 percent correlation indicates the output velocity is dominated by noise (i.e., no coherent signal).

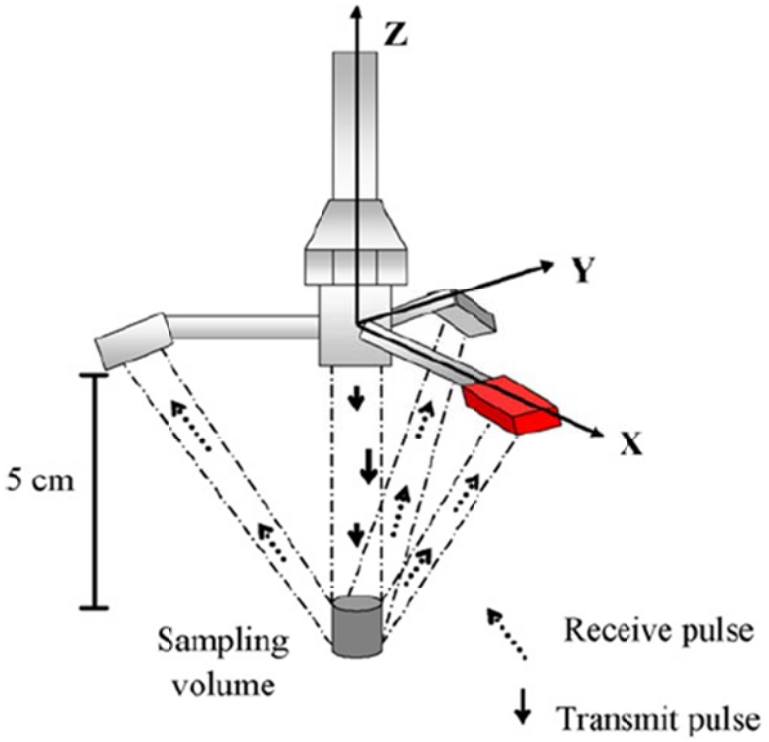

(a) Main component (sensor), (Sontek 2001)

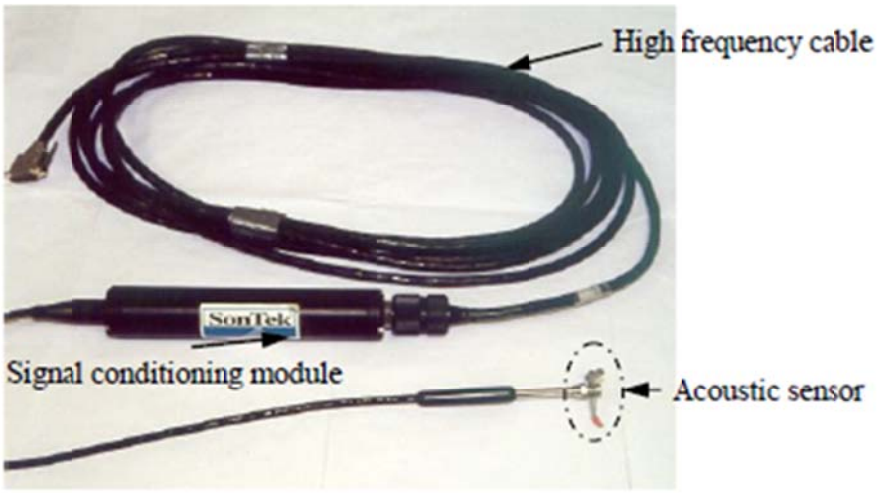

(b) 16-MHZ Cable

Fig. 3.6: Acoustic Doppler Velocimeter

Correlation can be used to monitor data quality during collection and to edit data in post processing. Ideally, correlation values should be between 70 percent and 100 percent (Sontek San Diego, 2001).

3.3.2 Digital Video Camera Recorder (DCR-SR47)

Water surface velocity is measured by using Digital Particle Tracking Velocimetry (DPTV) technique (Elkholy 2009). A video camera Sony-SR47 (60x optical / 2000x digital zoom) is used to measure the surface velocities (Fig. 3.7). A plastic ball (ID=1cm) is tracked by the video camera. The entire hydraulic model is painted in white and the balls are painted in black to easily identify and track. The balls are dropped at the entrance of the main channel and are collected by a mesh at the exit of the model. The camera is placed above the model at different locations to be able to track the motion of the balls in the entire model. Software based on DPTV technique is developed to track the motion of balls.

3.3.3 Baumer UNAM30/130 Series

Ultrasonic sensor baumer UNAM 30/130 (Fig. 3.8) is used for precise topography of dry-bed. Ultrasonic distance measuring sensor provides high-precision information on an absolute position of a target or moving object. The repeated accuracy is < 0.5 mm. (Wolfautomation, 2010).

Fig. 3.7: Sony-SR47 with 60x optical / 2000x digital zoom (Sony 2011)

Fig. 3.8: Baumer UNAM30

3.3.4 Point Gauge

A point gauge is used to measure bed and water surface elevations. The moving rod is divided vertically, is anchored in the canal, provides a needle point, so that the magnitude of the rise and fall of the water level can be observed directly and is minimized the meniscus error. It is graduated in millimeters, and vernier reads to one tenth of a millimeter (Fig. 3.9).

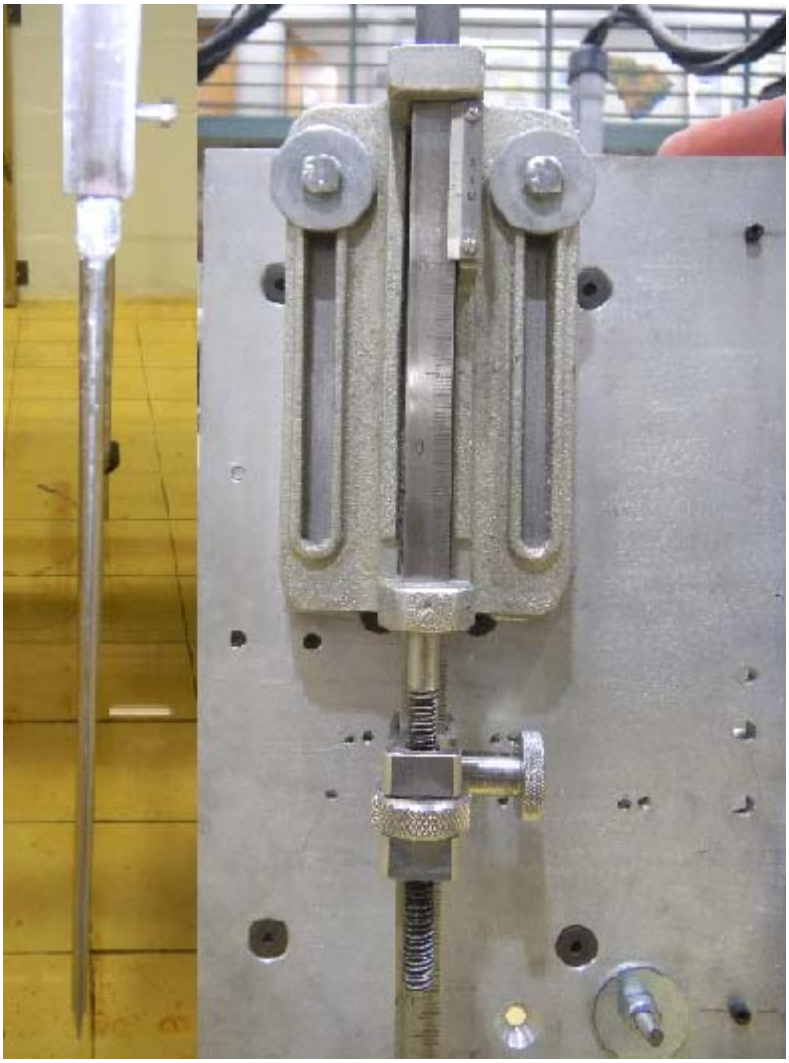

Fig. 3.9: Point Gauge

3.4 Experimental Procedure

A measurement grid was set up over a 5.59 m x 3.67 m of the model using nylon strings. The grid covered part of the canal, the breach where the dimension was 0.15 m x 2.85 m and the entire urban flooded area. The datum was set on top of the floodwall at grid node (x_0, y_0) which is the origin of the grid. Bed elevation was measured at each grid node using the Baumer. The flows of 0.056, 0.075 and 0.094 m^3/s were established using two axial flow pumps. The measurements were taken after circulating the flow through the model for a period of one hour, corresponding to the steady flow passing through the breach during the long period of flooding. The flow was strongly influenced by the topography showing large variation of the depth within the model. The measurements include water level and velocity profiles. The water surface elevation was measured for each flow at the grid crossings by using a point gauge. The distances between the neighboring measurement points are 0.15 m in the inner zone and 0.07 m near the boundary, respectively (Fig. 3.7).

Vertical velocity profiles in the three Cartesian directions are measured with a 16-MHz 3-Component Sontek micro ADV (Sontek 2001) at a limited number of grid points as shown in Fig. 3.10. Accurate velocity measurements using ADV require a minimum water depth of 6 cm, which occurs only in the canal and in some locations of the urban area for the given flow rates. Therefore, most of the available velocity profiles are in the main canal and in the eroded part of the flooded area near the breach. Furthermore, the measurement point is at least 0.5 cm above the bed, because the ADV probe uses a sampling volume located at a distance of 5 cm from the tip. The probe was moved

upward and was positioned at an interval of 0.5 cm. At each z (vertical) position, data were collected for 1 minute at a frequency of 50 Hz before moving the probe to the next vertical position. Note that the velocity data could not be collected in top 6 cm of the water depth. As a result, the number of data points was at limited locations with shallow water depth. Therefore, complementary velocity measurements have been taken at the water surface, using the particle tracking velocimetry (PTV) technique (Elkholy, 2009). These surface velocity measurements are added to the recorded velocity profiles by ADV.

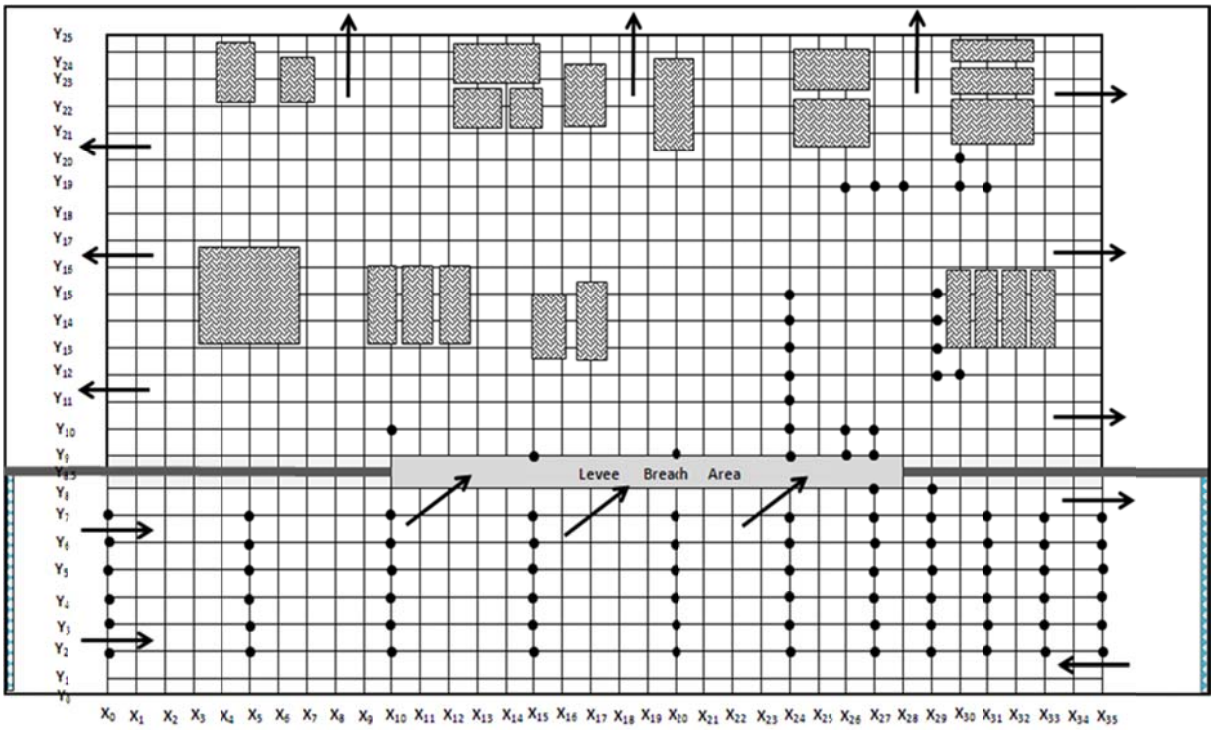

Fig. 3.10: Level measurement (grid crossing) and velocity measurement (dots)

The results of the present study are discussed in the next chapter.

Chapter 4

STEADY FLOWS IN A LEVEE BREACH IN GENERALIZED MODEL[1]

A generalized model describing the flow field due to steady flow in a breached levee is presented in this chapter. A generalized experimental set-up and an analytical model are used for the purpose. Dimensional analysis, results from the generalized breach experiments and results from the analytical model are presented in the following paragraphs.

4.1 Dimensional analysis

A dimensional analysis showing important parameters governing the flow in a breached levee is presented in this section. The flow is assumed to be steady. The flow in the main channel is divided due to the breach. The flow in the main channel from the inlet is divided and outflows at the outlet of the channel as well as through the breached levee. The flow field at the breach depends on the inflow conditions, outflow conditions and breach length. Thus, the following function may be written to represent the dependency of flow condition at the breach.

$$f_1(y_B, Q_B, B_B, B, Q_i, Q_o, y_i, y_o, C, g, S_o, \rho, \mu) = 0 \quad (4.1)$$

[1] This chapter is based on the following collaborative research:
Mohapatra, P. K., Riahi-Nezhad, C. K., Chaudhry, M. H., and Imran, J. (2013). "Steady flow at a breached levee", submitted to J. of Hydraulic Engineering, ASCE.

In Eq. 4.1, y_B and Q_B are the flow depth and the discharge at breach; Q_i and Q_o are the discharges at the channel inlet and outlet; y_i and y_o are the flow depths at channel inlet and outlet; B, S_0 and C are channel bed width, slope and roughness; B_B is breach length; g is acceleration due togravity; and ρ and μ are density and viscosity of the fluid in the channel. For steady flow at the breached levee, continuity equation is satisfied, $Q_i = Q_B + Q_o$. Thus, one out of the three discharges may be omitted in Eq. 4.1. Considering water as the fluid in the channel, density, ρ, may be assumed to be constant. The case being an open channel flow, the effect of viscosity may be assumed to be negligible. The experiments in the present study are performed on a horizontal bed, therefore, S_o may also be neglected. Thus, Eq. 4.1 is simplified to

$$f_2(y_B, Q_B, B_B, B, Q_i, y_i, y_o, C, g) = 0 \tag{4.2}$$

Equation 4.2 is written in non-dimensional form by applying the Buckingham Pi theorem (White 2008).

$$f_3(\pi_1, \pi_2, \pi_3, \pi_4, \pi_5, \pi_6, \pi_7) = 0 \tag{4.3}$$

Different πs in Eq. 4.2 are given below:

$$\pi_1 = \frac{y_B}{y_i};\ \pi_2 = \frac{Q_B}{Q_i};\ \pi_3 = \frac{B_B}{B};\ \pi_4 = \frac{Q_i^2}{gB^2y_i^3};\ \pi_5 = \frac{y_o}{y_i};\ \pi_6 = C^*;\ \pi_7 = \frac{B}{y_i} \tag{4.4}$$

Note that, π_4 is the inflow Froude Number and π_6 is the non-dimensional bed roughness.

4.2 Generalized experimental model

Flow in a breached levee is studied experimentally by using the generalized model set-up described in Chapter 3 (see 3.1). Cases studied, calibration of flow through the downstream sluice gate and results are presented in the following sub-sections.

4.2.1 Cases studied

Eleven cases are studied for different flow conditions in the breach flow by varying the inlet discharge, outlet discharge and breach lengths (Table 4.1). The inlet discharge is varied between 0.044 to 0.066 m^3/s. The outlet discharge is controlled by the sluice gate opening at the downstream end. Three different breach lengths are tested.

Table 4.1: Experimental runs in generalized model study

Run	Inlet discharge (m^3/s)	Gate opening at outlet (m)	Inlet flow depth	Outlet flow depth (m)	Breach length (m)	Remarks
G1	0.057	0.020	0.137	0.142	0.61	Flow depth
G2	0.057	0.025	0.135	0.138	0.61	Flow depth
G3	0.057	0.030	0.133	0.135	0.61	Flow depth
G4	0.06	0.020	0.146	0.148	0.61	Detailed
G5	0.066	0.030	0.145	0.147	0.61	Detailed
G6	0.044	0.020	0.142	0.144	0.35	Detailed
G7	0.051	0.020	0.158	0.159	0.35	Flow depth
G8	0.057	0.020	0.174	0.175	0.35	Detailed
G9	0.044	0.030	0.138	0.137	0.20	Detailed
G10	0.051	0.030	0.161	0.161	0.20	Flow depth
G11	0.057	0.030	0.184	0.185	0.20	Detailed

4.2.2 Calibration of the downstream sluice gate

The discharge through the downstream sluice gate is calibrated with no breach in the main channel. The discharge in the channel is known by the supply of flow from the pipe. The known discharge is correlated with the flow depth upstream of the gate and the gate opening. The effective head is calculated by subtracting half of the gate opening from the

flow depth upstream of the sluice gate. The following equation is used to determine the coefficient of discharge.

$$Q = C_d(go)B\sqrt{2gh} \quad (4.5)$$

Fifteen different runs are used to determine the C_d values which is correlated to the ratio of gate opening and flow depth upstream of gate, *go/h*. Calibration of C_d is shown in Table 4.2 and the variation of C_d with *go/h* is presented in Fig. 4.1. The fitted curve in Fig. 4.1 is

$$C_d = 0.7393+1.3042(go/h)-4.4801(go/h)^2+4.357(go/h)^3 \quad (4.6)$$

Equation 4.6 is with R^2=0.9899. Performance of Eq. 4.6 is shown in the last column of Table 4.2 and in Fig. 4.2. The computed discharges match well with the measured discharges for the flow under the sluice gate. Equations 4.5 and 4.6 are used in the generalized model set-up to estimate the outlet discharge in the main channel.

Table 4.2: Calibration of C_d for downstream sluice gate

Runs	Gate opening, go (m)	Flow depth at gate, h (m)	Measured discharge, Q_M (m^3/s)	go/h	C_d (from Eq. 4.5)
SG 1	0.015	0.160	0.012	0.094	0.862
SG 2	0.020	0.168	0.017	0.119	0.850
SG 3	0.035	0.098	0.024	0.357	0.835
SG 4	0.020	0.258	0.024	0.077	0.834
SG 5	0.035	0.139	0.028	0.251	0.833
SG 6	0.035	0.195	0.034	0.179	0.919
SG 7	0.050	0.110	0.034	0.454	0.910
SG 8	0.050	0.145	0.041	0.344	0.904
SG 9	0.035	0.240	0.041	0.145	0.890
SG 10	0.050	0.180	0.047	0.277	0.881
SG 11	0.040	0.115	0.031	0.347	0.916
SG 12	0.040	0.120	0.032	0.333	0.915
SG 13	0.035	0.165	0.034	0.212	0.914
SG 14	0.030	0.240	0.035	0.125	0.913
SG 15	0.035	0.190	0.037	0.184	0.910

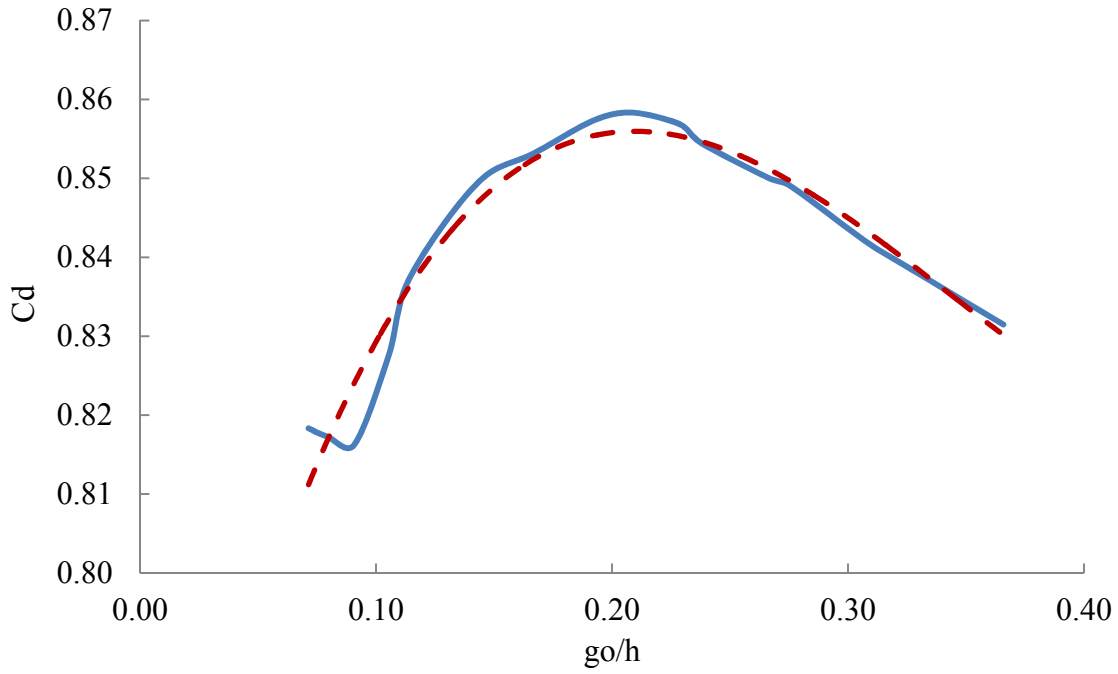

Fig. 4.1 Variation of C_d with *go/h*

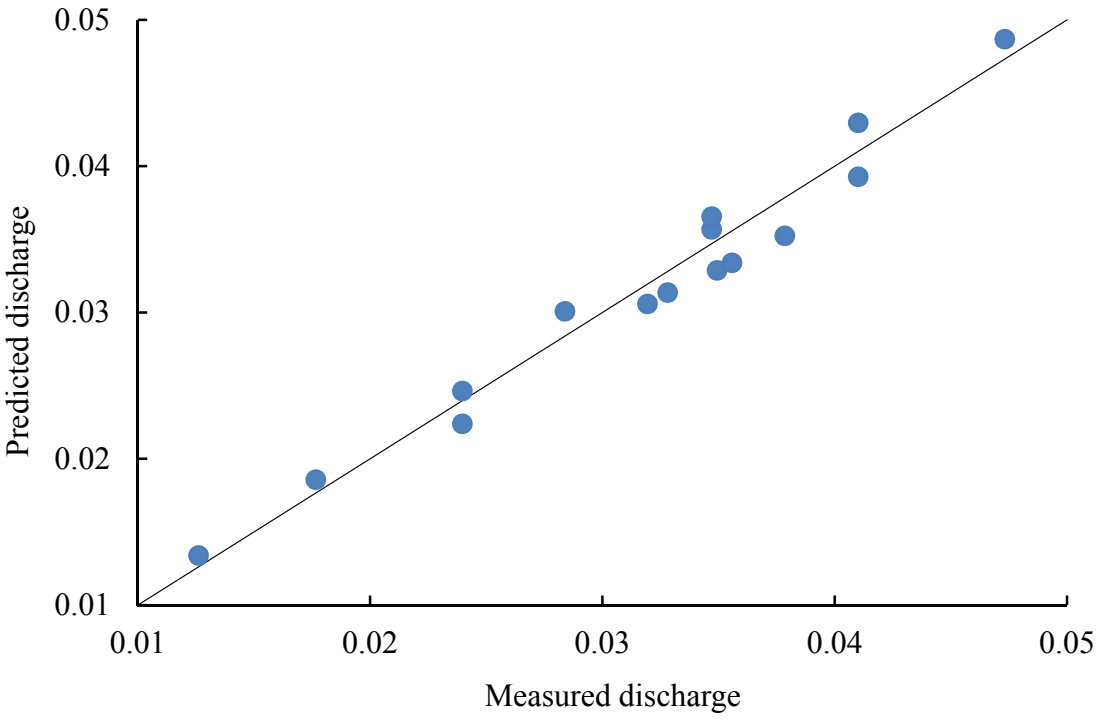

Fig. 4.2 Validation of C_d for the downstream sluice gate

Table 4.3: Validation of C_d for downstream sluice gate

Runs	Gate opening, go (m)	Flow depth at gate, h (m)	Measured discharge, Q_M (m^3/s)	go/h	C_d (from Eq. 4.6)	Computed discharge, Q_C (m^3/s)
SG16	0.015	0.160	0.012	0.093	0.825	0.013
SG17	0.020	0.168	0.017	0.119	0.838	0.018
SG18	0.035	0.098	0.023	0.357	0.832	0.024
SG19	0.020	0.258	0.023	0.077	0.815	0.022
SG20	0.035	0.139	0.028	0.251	0.853	0.030
SG21	0.035	0.195	0.034	0.179	0.854	0.035
SG22	0.050	0.110	0.034	0.454	0.815	0.036
SG23	0.050	0.145	0.041	0.344	0.834	0.042
SG24	0.035	0.240	0.041	0.145	0.847	0.039
SG25	0.050	0.180	0.047	0.277	0.849	0.048
SG26	0.040	0.115	0.031	0.347	0.834	0.030
SG27	0.040	0.120	0.032	0.333	0.837	0.031
SG28	0.035	0.165	0.034	0.212	0.855	0.032
SG29	0.030	0.240	0.035	0.125	0.840	0.033
SG30	0.035	0.190	0.037	0.184	0.854	0.035

4.2.3 Flow field

Results for the velocity field, water surface profile, turbulent kinetic energy and bed shear stress from the generalized experimental model (Case G4) are presented in this section. Results for other cases are presented in Appendix – 2.

The velocity field as measured in Case G4 are presented in Fig. 4.3. The indicated surface velocities are measured by a camera, all other velocities are measured by ADV. Velocity distribution along grid line Y1 indicates that the longitudinal velocity (Vx) is prominent and the lateral velocity (Vy) is almost negligible (Fig. 4.3 a). Thus, the velocity is one-dimensional. velocity is primarily one dimensional and the maximum velocity of 0.81 m/s is observed at 2.74 m from the inlet. Velocity distribution along Y2 also indicates the same trend (Fig. 4.3 b), the maximum velocity being marginally higher (0.89 m/s). The lateral velocity is marginally higher near the breach. Velocity distribution along Y3 indicates strong lateral velocity near the breach. The maximum lateral velocity is 0.75 m/s and it occurs on the breach. The flow becomes one-dimensional downstream of the breach. The flow is three-dimensional near the breach. Vertical velocity at two locations on the breach is shown in Figs. 4.3 (d) and 4.3 (e). The velocity vectors (for averaged velocities) are indicated in Fig. 4.4. As expected, the flow is divided into two parts: one part exits through the breach and the other part through the outlet in the main channel. In addition, a small localized recirculation zone is observed near the right bank downstream of the breach. Thus, the entire set-up has three different flow zones: (a) One-dimensional flow near the inlet and outlet of the main channel; (b) Three-dimensional turbulent flow near breach having strong lateral velocities; and (c) Flow in the flooded zone outside the

main channel. The present study is limited to the first two flow zones. Froude number is computed using the depth averaged velocities and the flow depth at grid points. Mapping of the Froude Number in the main channel shows that the flow is subcritical in the channel. However, there is an increase in the Froude Number as the flow approaches the breach. Critical flow condition exists in a small location at the breach before the flow is exposed to the vast area of the flooded zone (Fig. 4.5).

Contours of the water flow depths are presented in Fig. 4.6. The water surface slope along the longitudinal direction is mild. However, the water surface has steep slope near the breach, both in the longitudinal and lateral directions, due to the presence of a depression in the bottom. Variation of the flow depth along the left bank shows a dip (approximately 6 cm) in the water surface near the breach (Fig. 4.7). Note that the breach is from 2.89 m to 3.50 m (distance from inlet). This region (point of lowest flow depth) is also with the critical flow condition. This depression zone is also indicated in the photograph for the water surface near the breach (Fig. 4.8).

Variations of the turbulent kinetic energy and the bed shear stress are presented in Figs. 4.9 and 4.10, respectively. Procedures to compute turbulent kinetic energy and bed shear stress from the measured velocities are described elsewhere in this dissertation (see Sections 5.7 and 5.8). Variation of TKE along Y1, Y2 and Y3 are presented separately. Higher values of TKE near the breach indicate there is high degree of turbulence in the flow near the breach. As the flow passes through the breach, there are fluctuations in the velocity and water surface. This may be treated as an indicator for the impact the breach

flow may have on the nearby structures. In addition, TKE may be used to select proper breach closure procedures. Note that the breached levee has to be closed in order to make the flow limited to the main channel.

The bed shear stress attained in the channel is small. However, it attains a very high value (approximately 7 N/m2) near the breach. This is also an indication that this region is prone to scour. A regular phenomenon in the real-life levee breach flows is the formation of a lake just outside the breach. This may be attributed to the high value of bed shear stress.

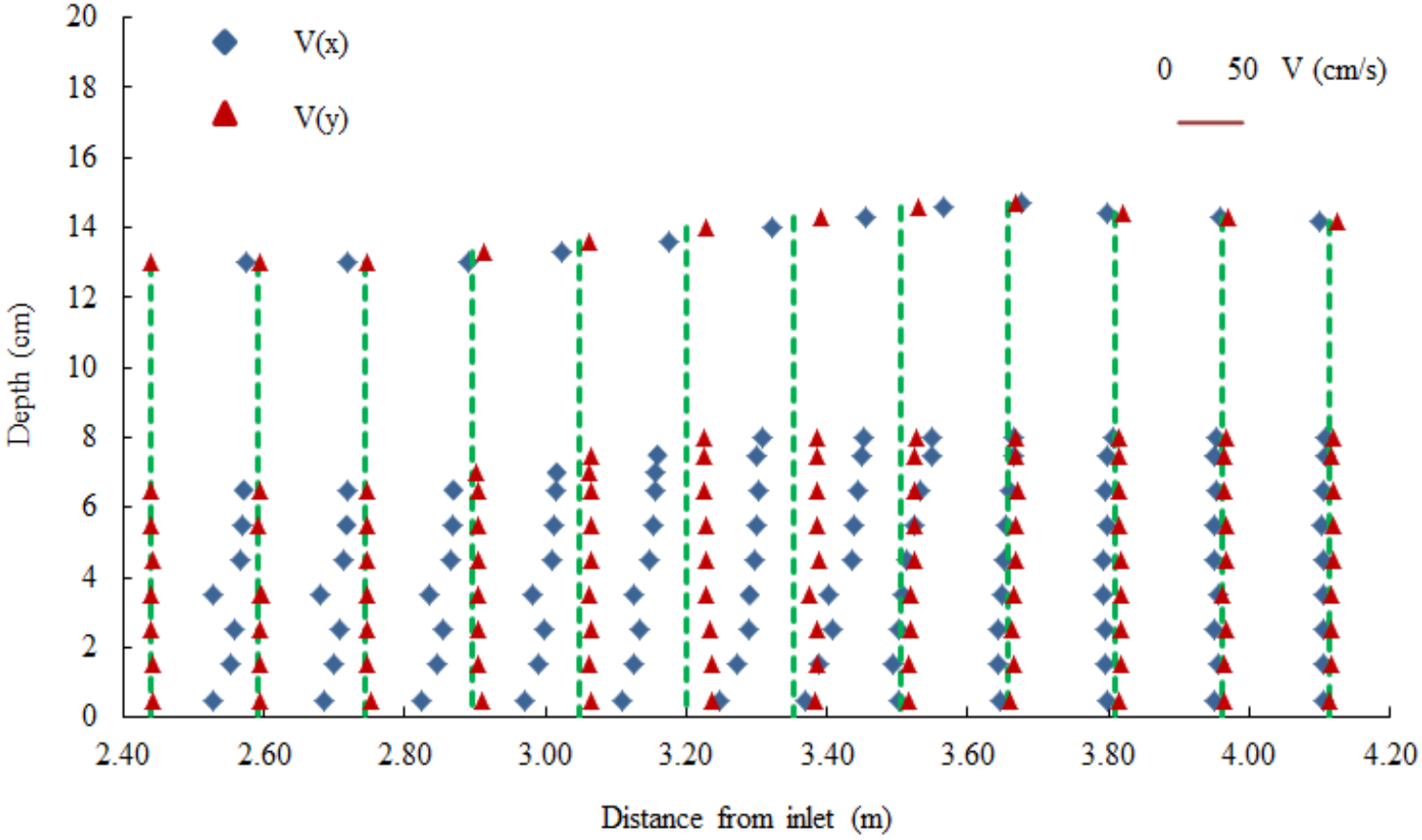

(a) Along Y1

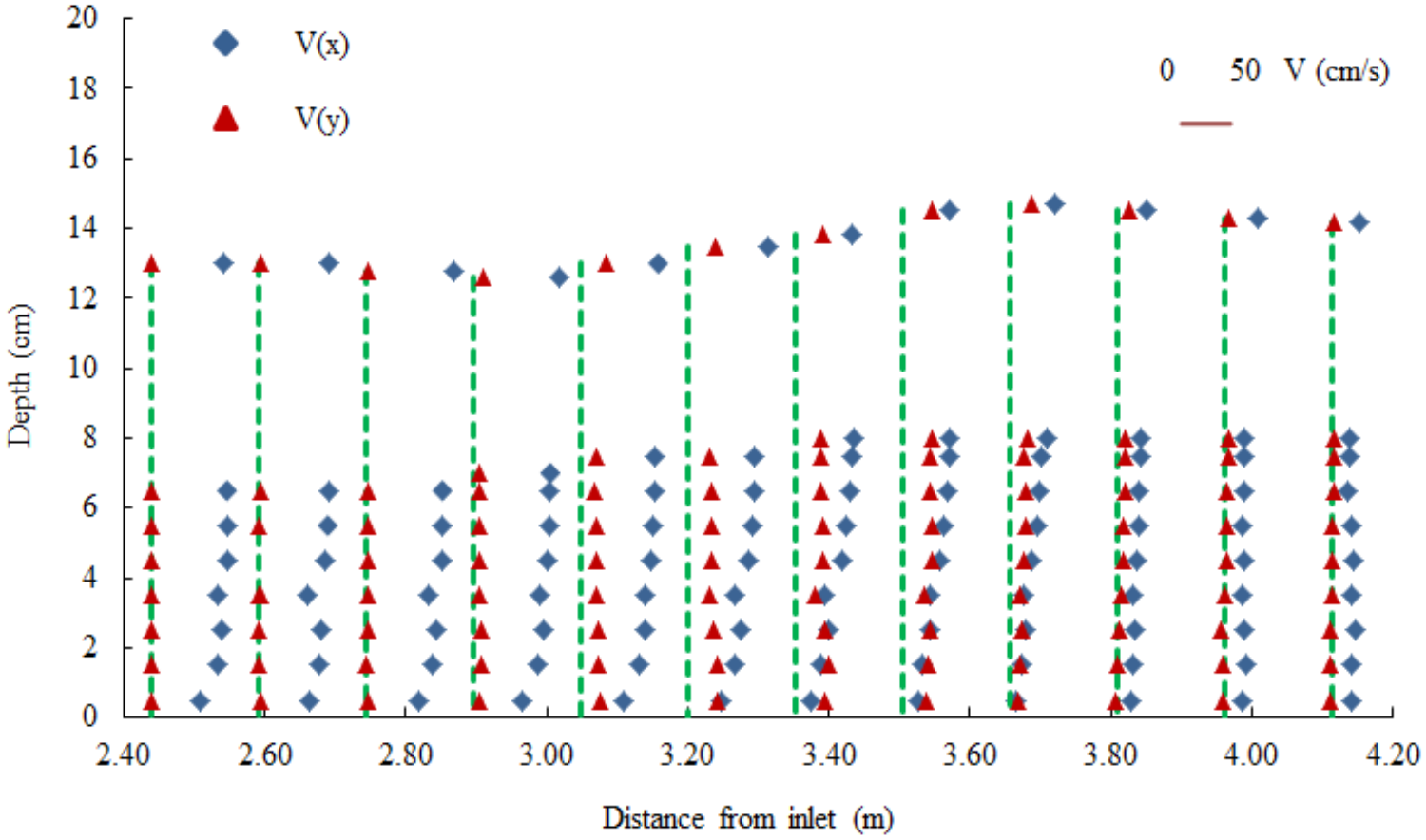

(b) Along Y2

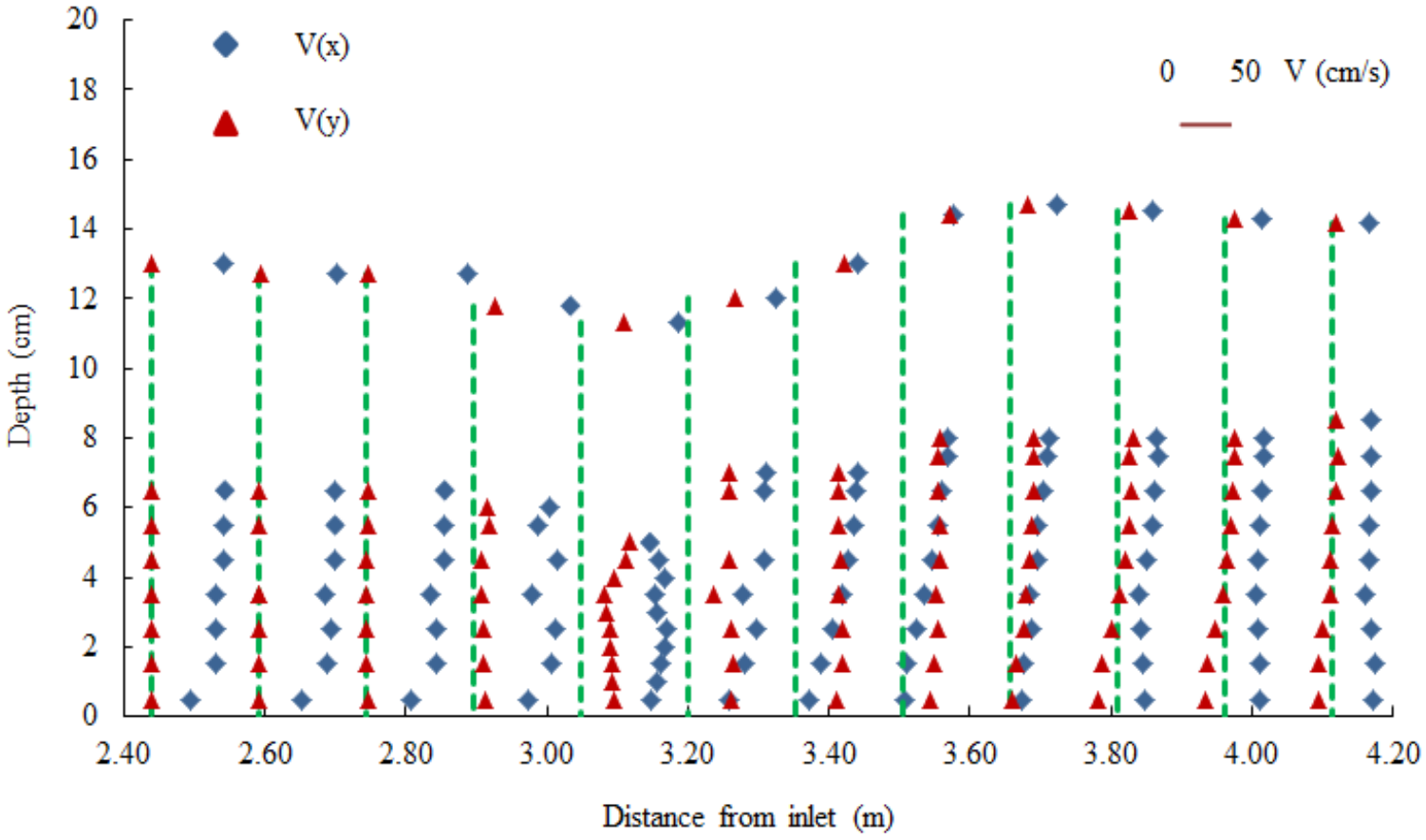

(c) Along Y3

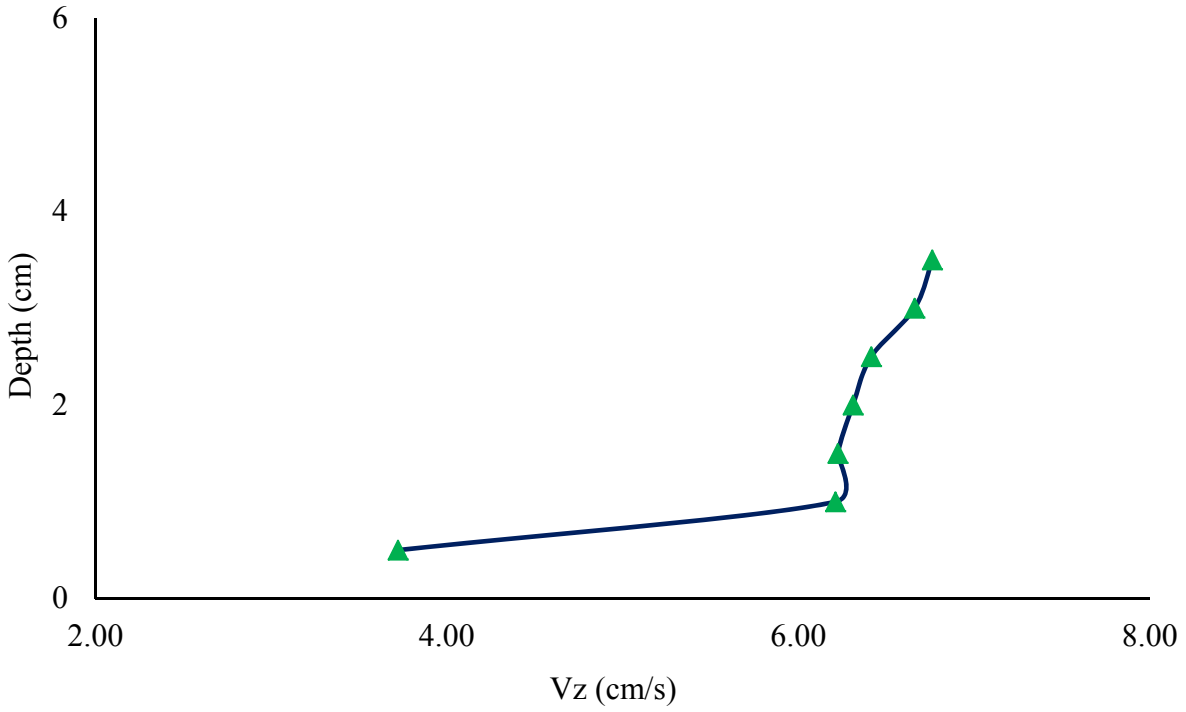

(d) Vertical velocity (Vz) at X21-Y4

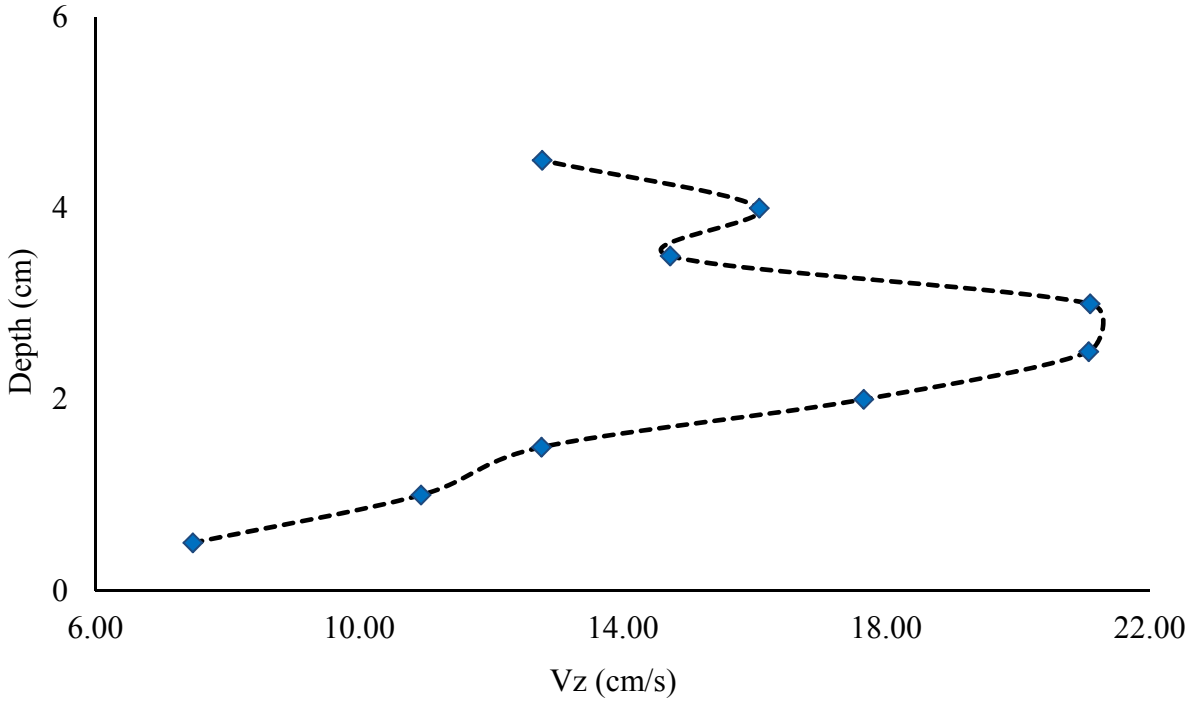

(e) Vertical velocity (Vz) at X23-Y4

Fig. 4.3 Measured results for velocity distribution (Case G4)

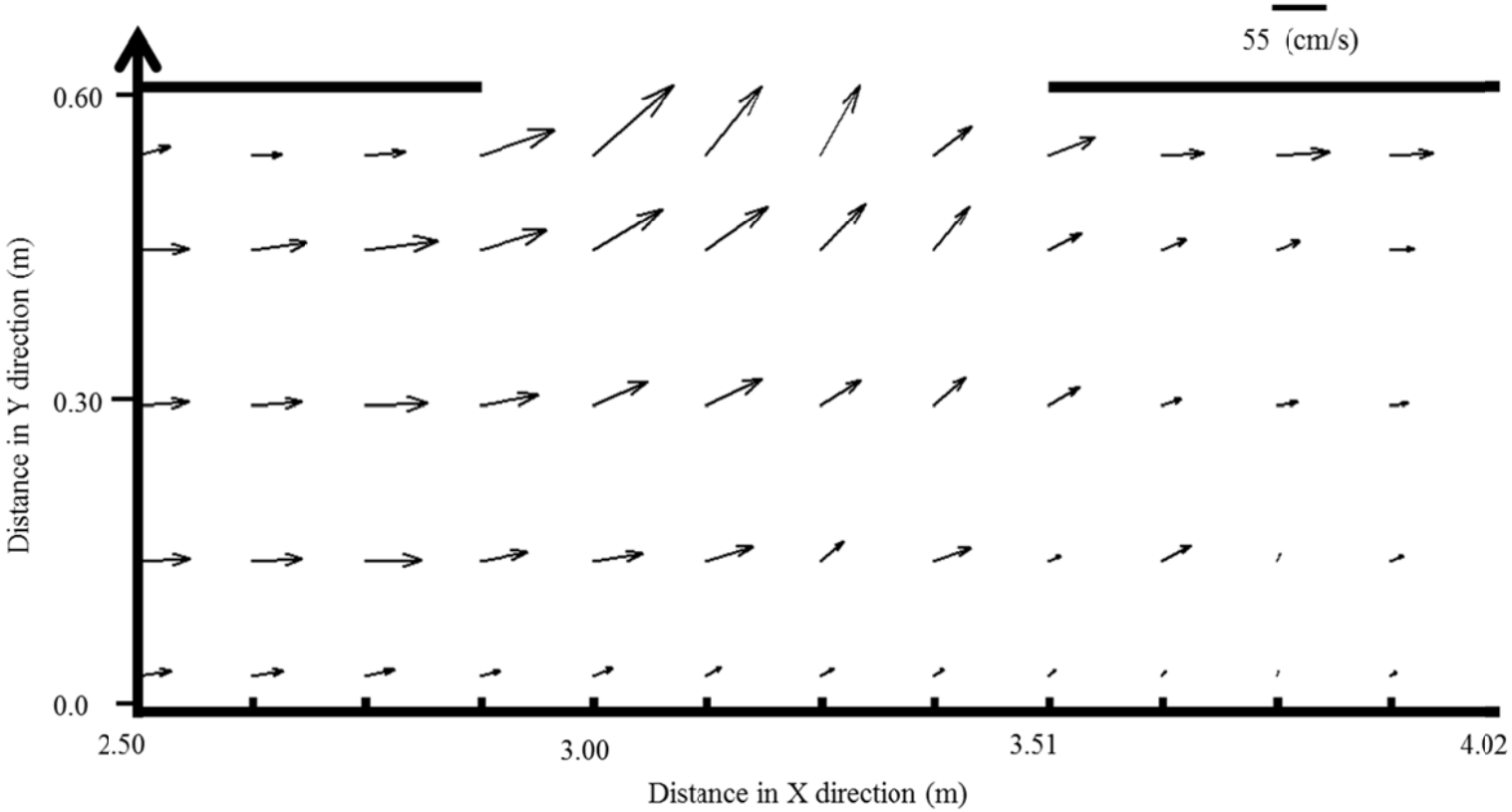

Fig. 4.4 Average velocities (Case G4)

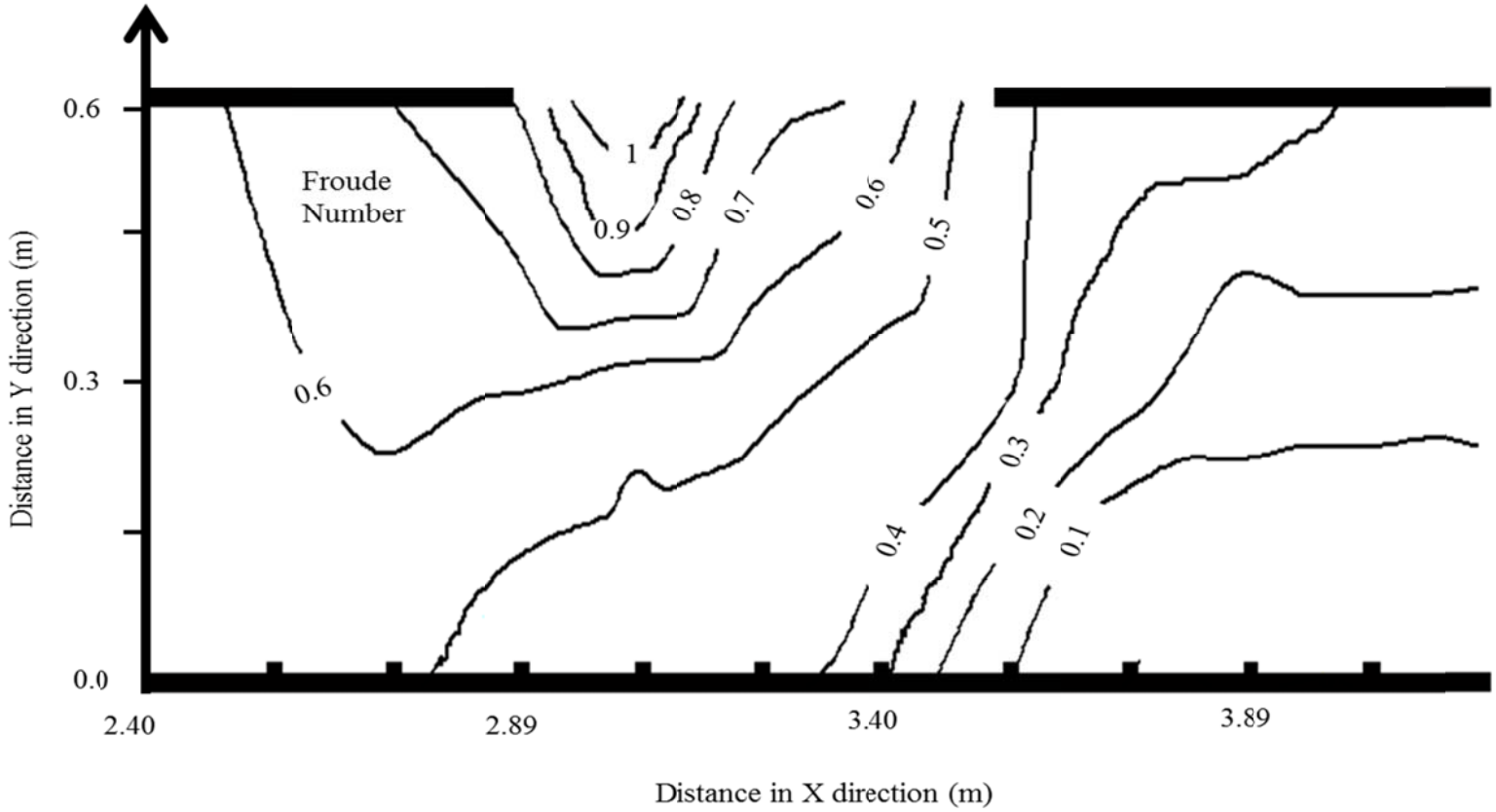

Fig. 4.5 Distribution of Froude Number

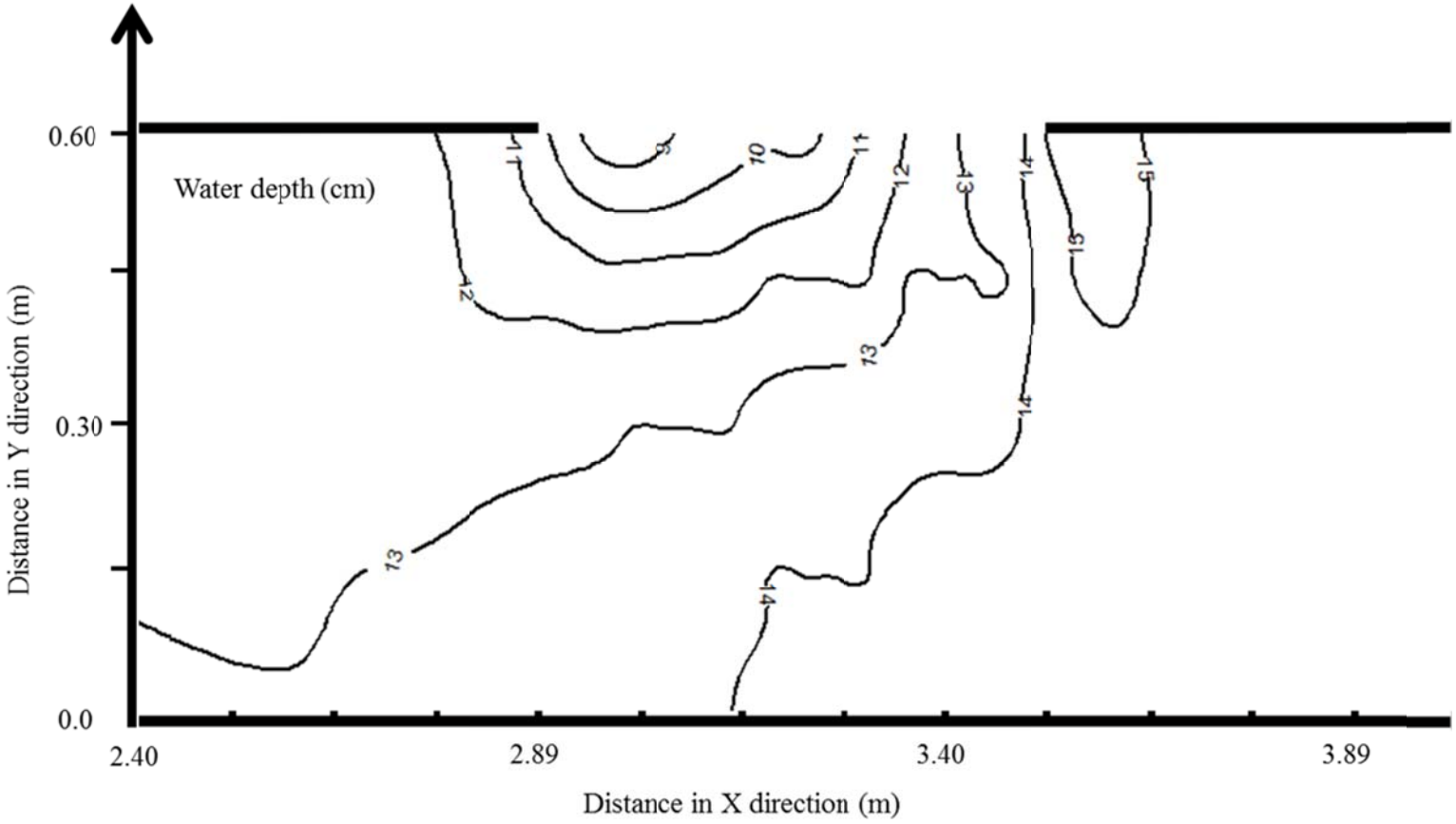

Fig. 4.6 Contours of flow depth (Case G4)

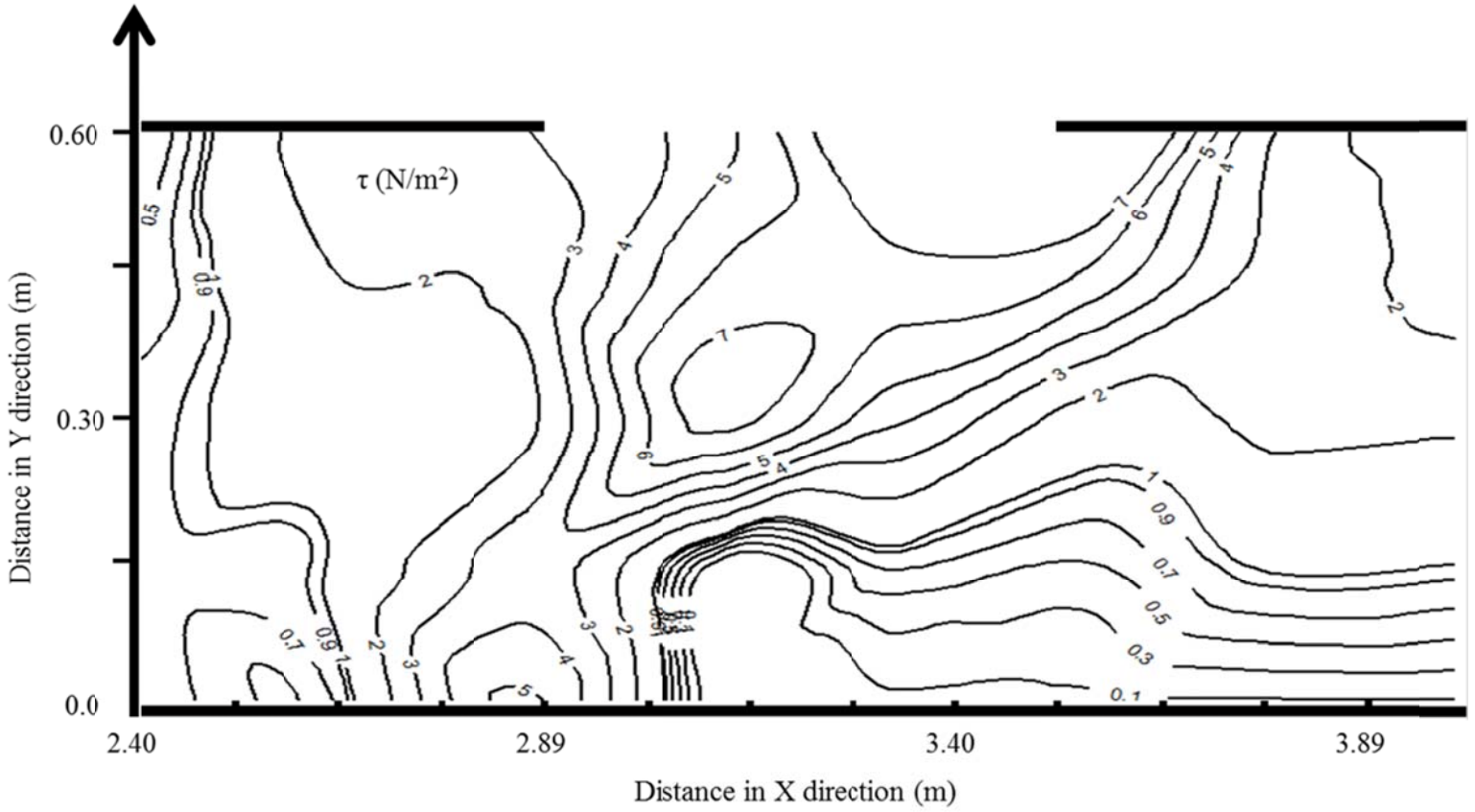

Fig. 4.7 Contours of bed shear stress (Case G4)

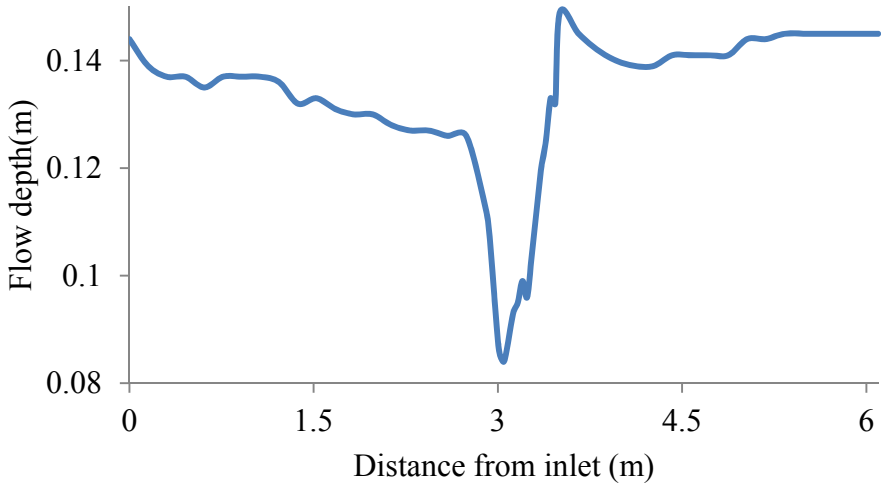

Fig. 4.8 Variation of flow depth along breach (Case G4)

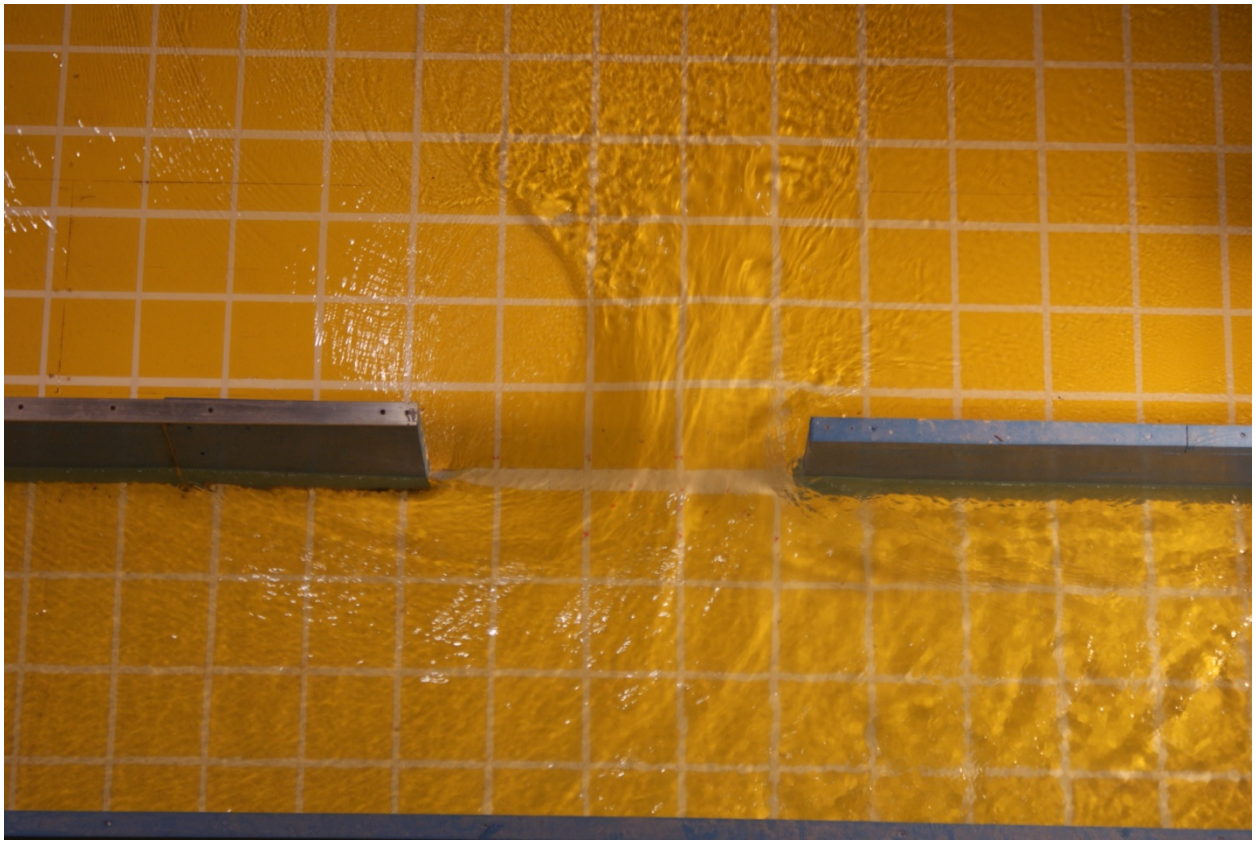

Fig. 4.9 Photograph of water surface profile near breach (Case G4)

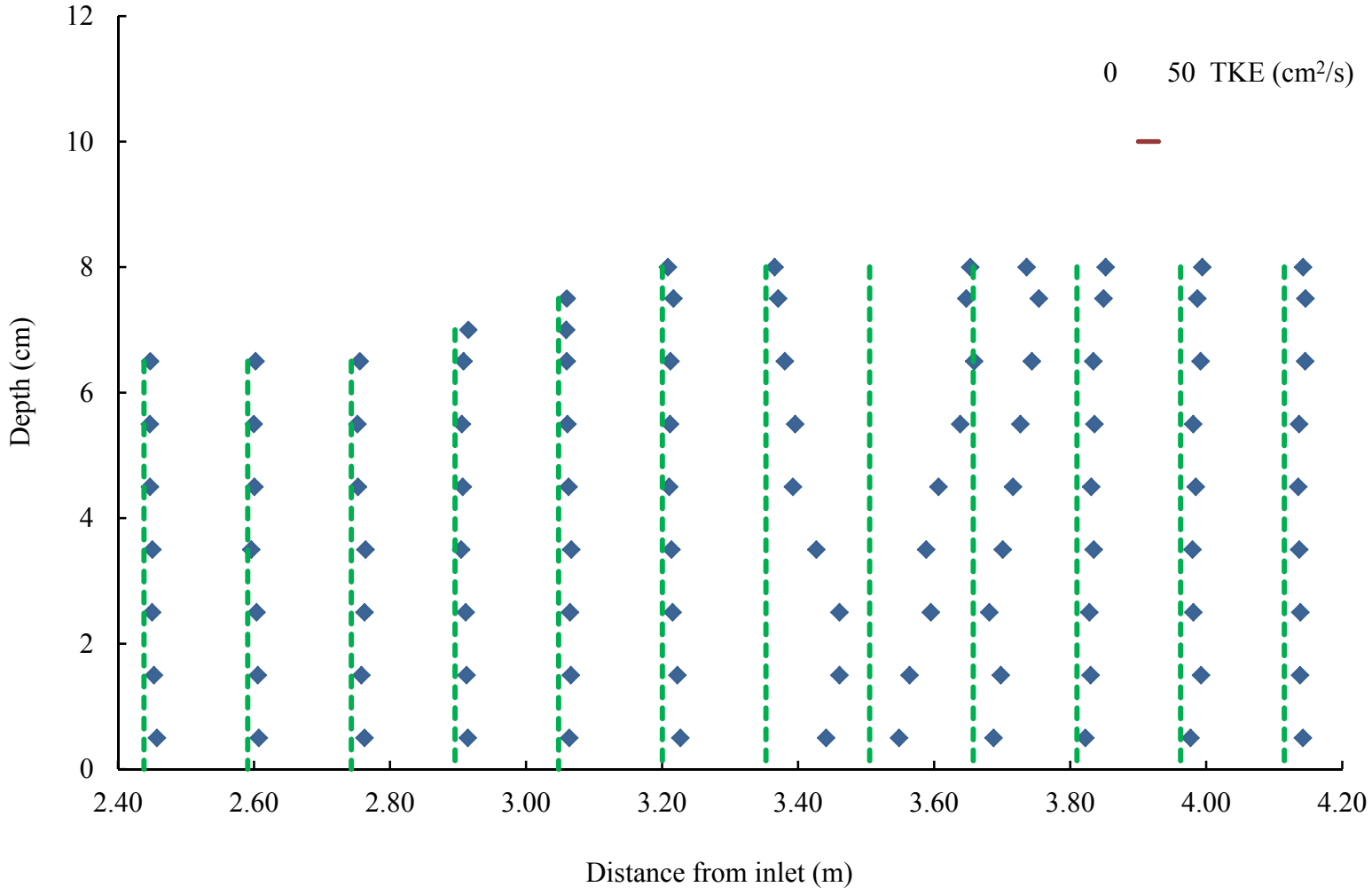

Fig. 4.10 (a) Distribution of TKE Along Y1 (Case G4)

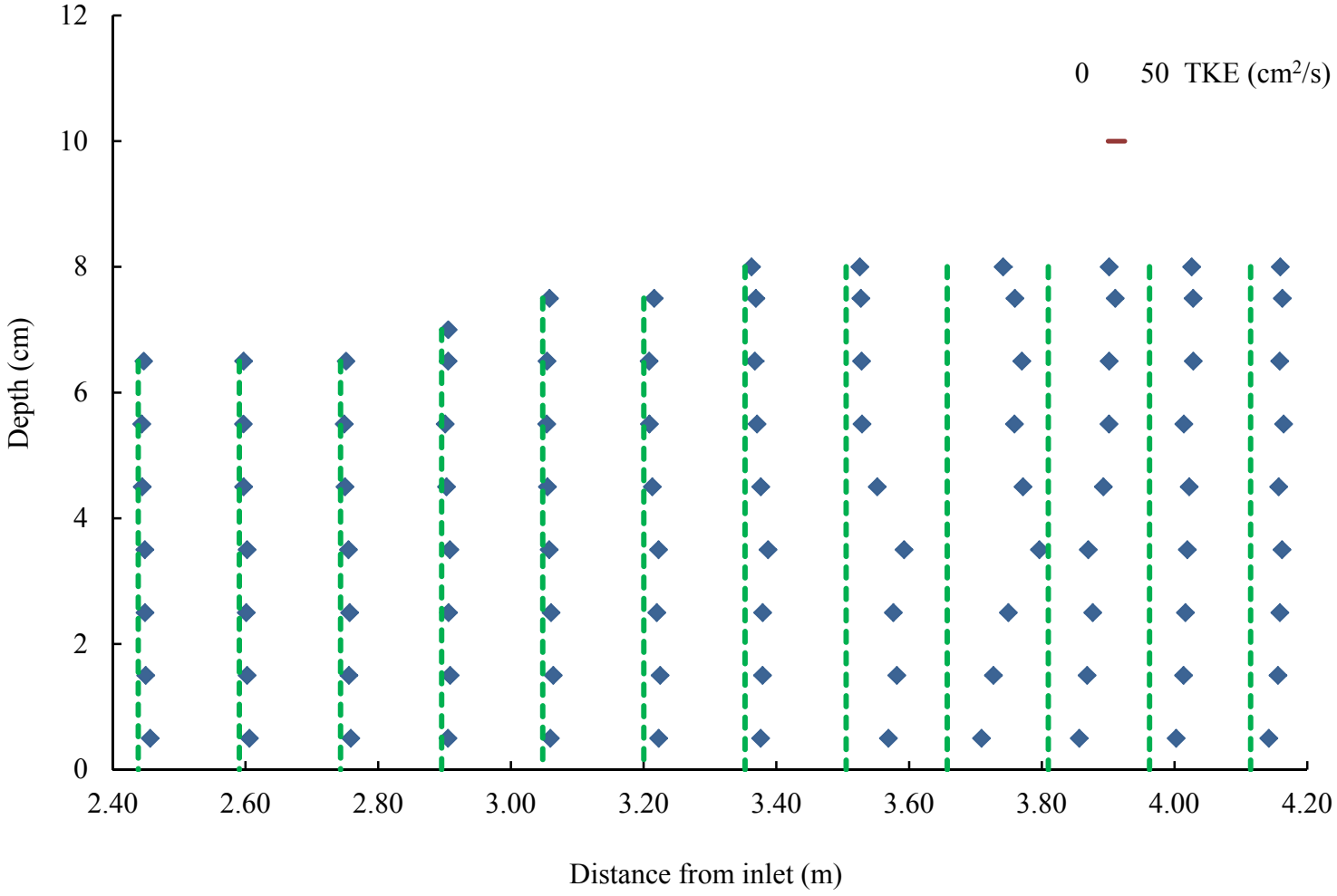

Fig. 4.10 (b) Distribution of TKE Along Y2 (Case G4)

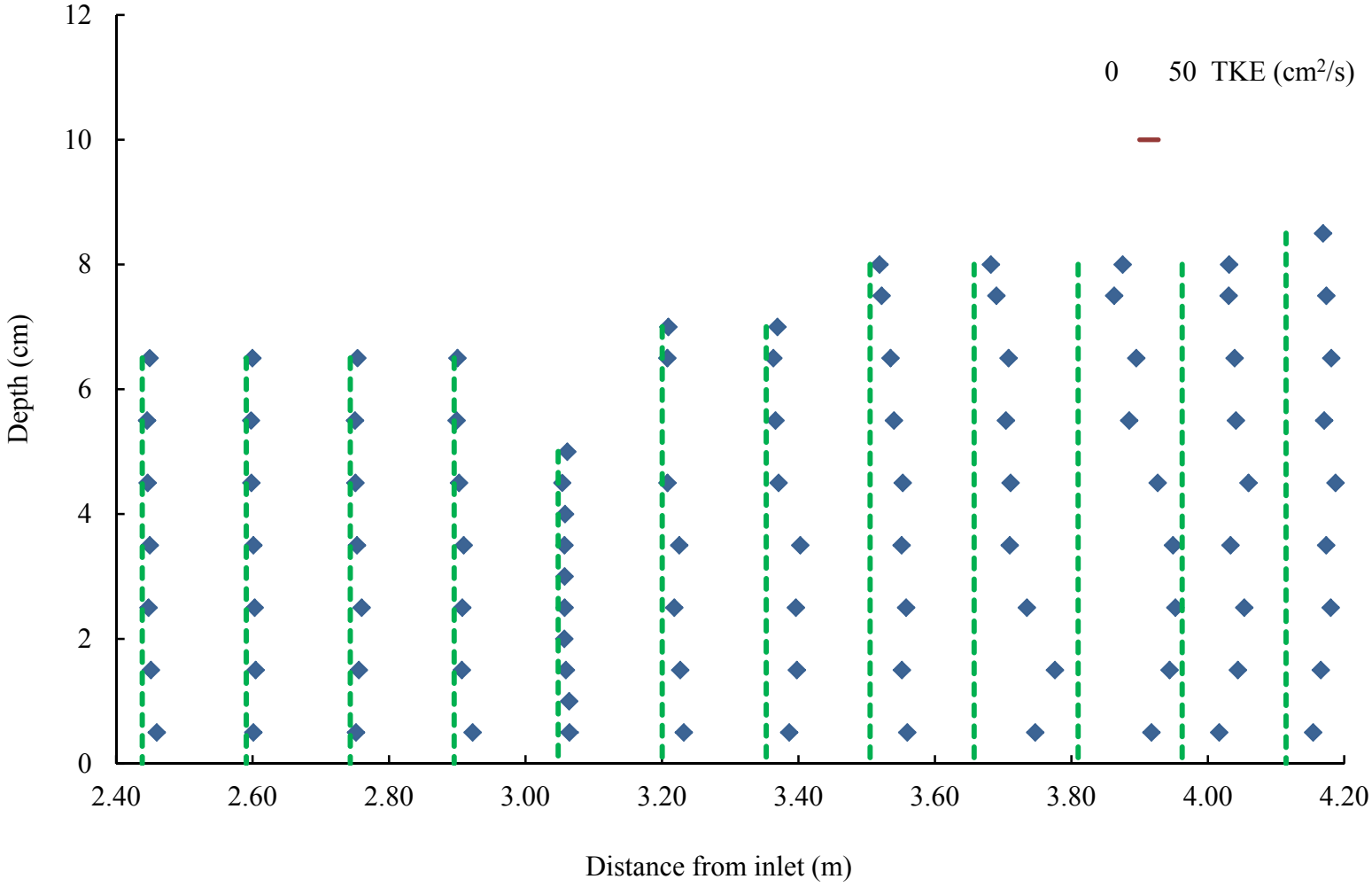

Fig. 4.10 (c) Distribution of TKE Along Y3 (Case G4)

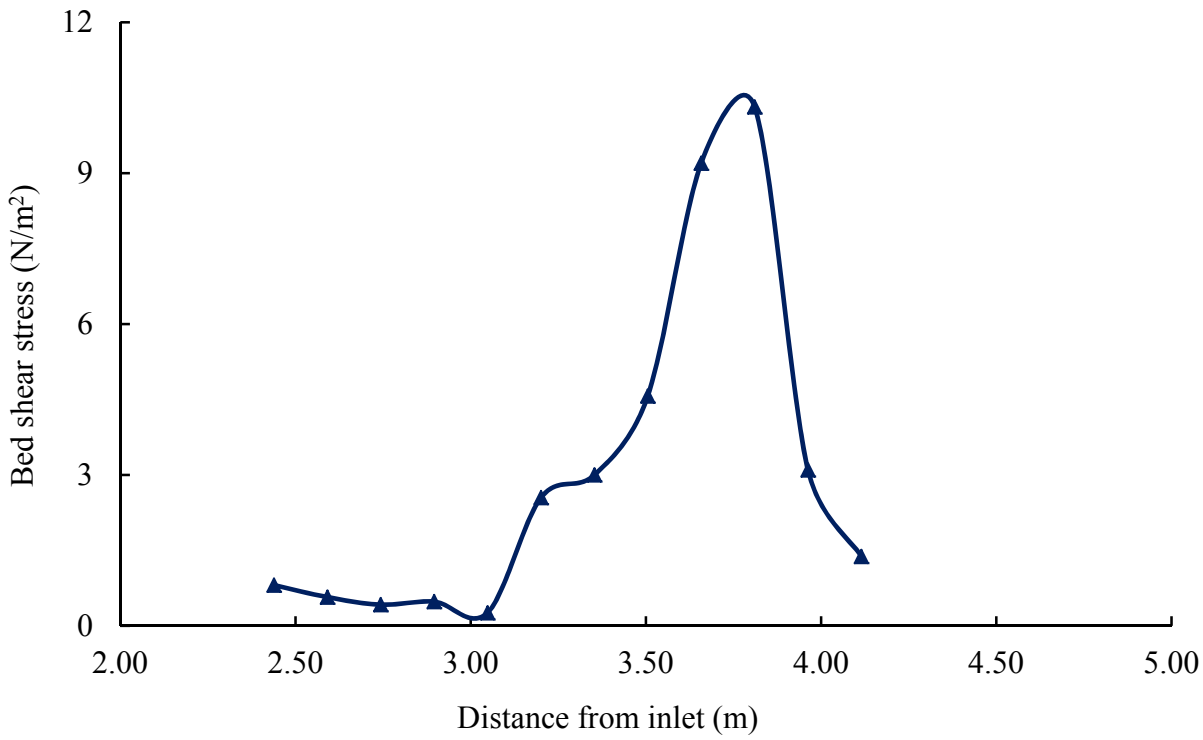

Fig. 4.11 Variation of bed shear stress along the breach

As observed in the several experiments for the generalized breach flow, the flow field near the breach is influenced by the inflow and outflow in the main channel and the breach length. The breach flow conditions may be used for engineering applications, such as identifying the flood inundation area and closure of the breach.

An analytical model is presented in the following section, to understand the general characteristics of breach flow.

4.3 Generalized analytical model

The flow field near the breach in steady flow past a breached levee is complicated. The definition sketch for steady flow at a breached levee is presented in Fig. 4.3. The analytical procedure adopted here is similar to that presented by Shabayek et al. (1999) for dividing flows in open channel junctions.

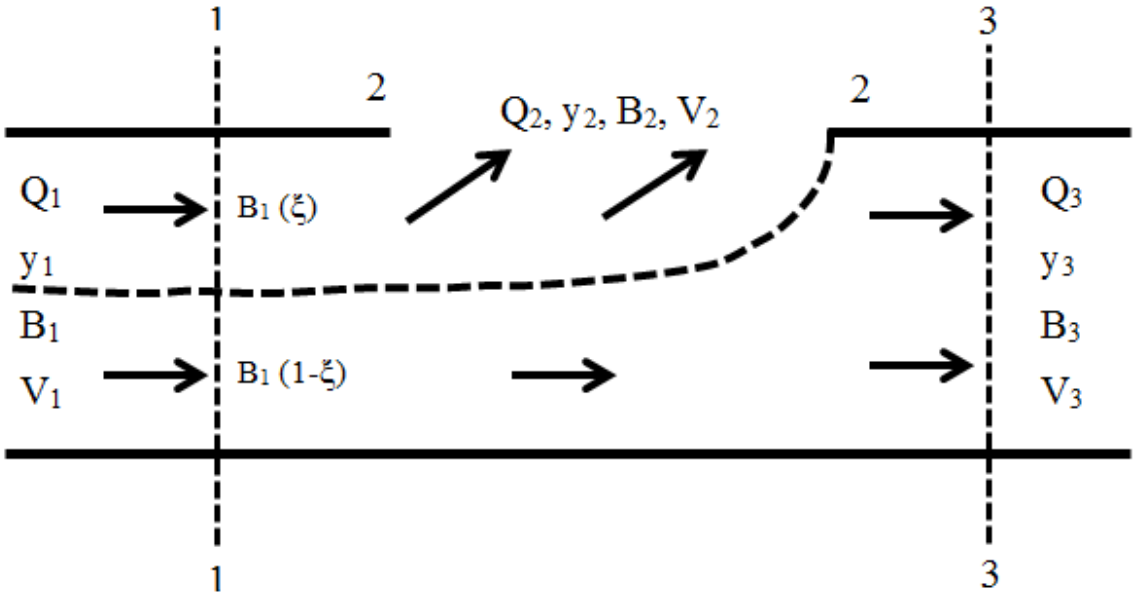

Fig. 4.12 Steady flow at a breached levee

The flow regime is divided into two parts: i.e., one part going through the channel outlet and the other through the breach. The flow width at section 1-1 is divided proportional to the discharge ratios. Thus, width B_1 is divided in to $\xi.B_1$ and $(1-\xi).B_1$ where, ξ is the discharge ratio (Q_2/Q_1). Two control volumes, one between sections 1 and 2 and the other between sections 1 and 3 are used to analyze the flow.

Continuity equation

$$Q_1 = Q_2 + Q_3 \tag{4.7}$$

Applying Reynolds Transport Theorem between sections 1 and 3, the momentum equation is written as

$$\rho Q_3 V_3 - \rho Q_3 V_1 = \frac{1}{2}\rho g y_1^2 B_1 (1-\xi) - \frac{1}{2}\rho g y_3^2 B_3 + \rho g \left(\frac{y_1 + y_3}{2}\right)^2 [B_3 - B_1(1-\xi)] - \frac{\rho V_1^2}{C^{*2}}[B_1(1-\xi) + y_1]L_1 \quad (4.8)$$

Similarly, the momentum equation for the control volume between sections 1 and 2 is

$$K\rho Q_2 V_2 - \rho Q_2 V_1 = \frac{1}{2}\rho g y_1^2 B_1 \xi - \frac{1}{2}\rho g y_2^2 B_2 + \frac{1}{2}\rho g y_1^2 (B_2 - B_1\xi) - \frac{\rho V_1^2}{C^{*2}}(B_1\xi + y_1)L_2 \quad (4.9)$$

Note that L_1 and L_2 are the lengths of the control volumes of part 1 and 2, respectively, C* is the non-dimensional bed roughness coefficient and K is a correction factor due to streamline curvature at section 2-2. Note that C* and K are the model parameters and have to be calibrated.

Eqs. 4.8 and 4.9 may be written in non-dimensional form by using the terms defined in Eq. 4.10 and Eq. 4.7,

$$\xi = \frac{Q_2}{Q_1}; \eta_2 = \frac{y_2}{y_1}; \eta_3 = \frac{y_3}{y_1}; \omega_2 = \frac{B_2}{B_1}; \omega_3 = \frac{B_3}{B_1}; a = \frac{B_1}{y_1}; F_1 = \frac{Q_1}{\sqrt{g B_1^2 y_1^3}} \quad (4.10)$$

$$\frac{(1-\xi)^2}{\eta_3\omega_3} - (1-\xi) = \frac{1}{8F_1^2}\left[(1-\xi)(3 - 2\eta_3 - \eta_3^2) + \omega_3(1 + 2\eta_3 - 3\eta_3^2)\right] - \frac{2\omega_3}{C^{*2}}[a(1-\xi)+1] \quad (4.11)$$

$$\frac{K\xi^2}{\eta_2\omega_2} - \xi = \frac{\omega_2}{2F_1^2}(1-\eta_2^2) - \frac{2\omega_2}{C^{*2}}(a\xi + 1) \quad (4.12)$$

Considering all the non-dimensional terms, ξ and η_2 are unknowns. Eqs. 4.11 and 4.12 are solved for ξ and η_2 for the known values of the other non-dimensional parameters. However, the model parameters, C^* and K are to be calibrated.

In the present study, the generalized experimental set-up is used for 11 different runs to estimate C* and K. This is presented in subsection 4.3.2.

4.3.1 Special cases

The channel width of the main channel is constant in the present experimental set-up. Thus, Eq. 4.11 may be further simplified by using $\omega_3 = 1$.

$$\frac{(1-\xi)^2}{\eta_3} - (1-\xi) = \frac{1}{8F_1^2}\left[(1-\xi)\left(3-2\eta_3-\eta_3^2\right)+\left(1+2\eta_3-3\eta_3^2\right)\right] - \frac{2}{C^{*2}}\left[a(1-\xi)+1\right] \tag{4.13}$$

Similarly, when the outlet discharge is zero, the condition $\xi = 1$ leads to

$$\frac{1}{8F_1^2}\left[\left(1+2\eta_3-3\eta_3^2\right)\right] - \frac{2}{C^{*2}} = 0 \tag{4.14}$$

$$\frac{K}{\eta_2\omega_2} - 1 = \frac{\omega_2}{2F_1^2}\left(1-\eta_2^2\right) - \frac{2\omega_2}{C^{*2}}(a+1) \tag{4.15}$$

Eq. 4.15 may further be simplified by assuming the breach length equal to the channel width.

$$\frac{K}{\eta_2} - 1 = \frac{1-\eta_2^2}{2F_1^2} - \frac{2}{C^{*2}}(a+1) \tag{4.16}$$

The downstream gate may be controlled such that $y_3 = y_1$, i.e., $\eta_3 = 1$. Thus, Eq. 4.13 becomes

$$(1-\xi)\left(\frac{2a}{C^{*2}}-\xi-\frac{1}{8F_1^2}\right)+\frac{2}{C^{*2}}=0 \qquad (4.17)$$

4.3.2 Model parameters

K and C* are the model parameters used in Eqs. 4.11 and 4.12. K is the correction factor for streamline curvature at section 2 and C* is a measure of the bed roughness. These parameters are estimated by utilizing the measurements of several experiments.

Consider Eqs. 4.11 and 4.12. C* can be computed knowing all other parameters in Eq. 4.11. Eq. 4.12 can be used to solve for K by using the known parameters including C*. The 11 cases used to estimate C* and K are presented in Table 4.3. Note that all other entries (except the entries in last two columns) are based on the experimental observations.

The channel bed roughness is assumed to be constant as the flow conditions are almost similar. Thus, an average value of C*=5.12 is obtained for the present study. However, K may be different as the streamline curvatures are different for different flow conditions. In this study, it is assumed that K is dependent on the breach length and the breach discharge. Thus, a regression analysis is used to correlate K with ω_2 and ξ. Based on the present set of observations, the following empirical relations are obtained.

$$K = \alpha\xi^{\beta} \qquad (4.18)$$

$$\alpha = -2.0273 * \omega_2^2 + 4.2102\omega_2 - 1.0477 \qquad (4.19)$$

$$\beta = -6.7525\omega_2^2 + 11.037\omega_2 - 5.385 \quad (4.20)$$

Based on the calibrated values of C* (= 5.12) and K (Eqs. 4.18 – 4.20), Eqs. 4.11 and 4.12 are used to predict the flow condition at the breach (ξ and η_2). The predicted and the measured values are compared in Figs. 4.10 and 4.11. Prediction of the flow depth (maximum error is approximately 12 %) is better as compared to that for discharge (maximum error is approximately 28 %). The discharge is over-predicted for the discharge ratios higher than 0.75.

Table 4.4 Calibration of C* and K ($\xi < 1.0$)

Case	Q_1 (m^3/s)	Q_2 (m^3/s)	Q_3 (m^3/s)	F_1	ξ	η_2	η_3	ω_2	a	C*	K
G1	0.057	0.040	0.017	0.588	0.698	0.667	1.036	1.000	4.453	5.710	1.710
G2	0.057	0.036	0.021	0.601	0.623	0.653	1.026	1.000	4.519	5.357	1.934
G3	0.057	0.032	0.025	0.615	0.553	0.638	1.015	1.000	4.586	5.253	2.255
G4	0.06	0.043	0.017	0.563	0.709	0.705	1.014	1.000	4.178	4.970	1.657
G5	0.066	0.039	0.027	0.626	0.597	0.710	1.014	1.000	4.207	4.975	1.887
G6	0.044	0.027	0.017	0.430	0.606	0.758	1.014	0.574	4.296	5.360	1.331
G7	0.0505	0.032	0.018	0.421	0.641	0.766	1.009	0.574	3.861	4.950	1.229
G8	0.057	0.038	0.019	0.409	0.668	0.772	1.006	0.574	3.506	4.658	1.175
G9	0.044	0.018	0.026	0.449	0.416	0.742	0.992	0.328	4.417	5.135	0.999
G10	0.0505	0.023	0.028	0.409	0.449	0.862	1.000	0.328	3.788	4.980	0.882
G11	0.057	0.027	0.030	0.378	0.475	0.951	1.005	0.328	3.315	4.971	0.714

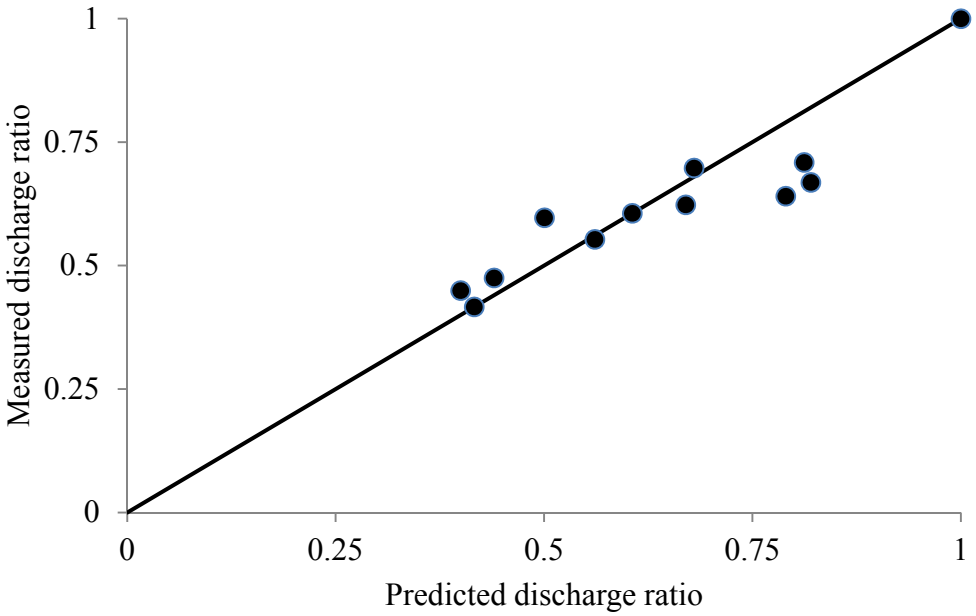

Fig. 4.13 Discharge ratio at the breach

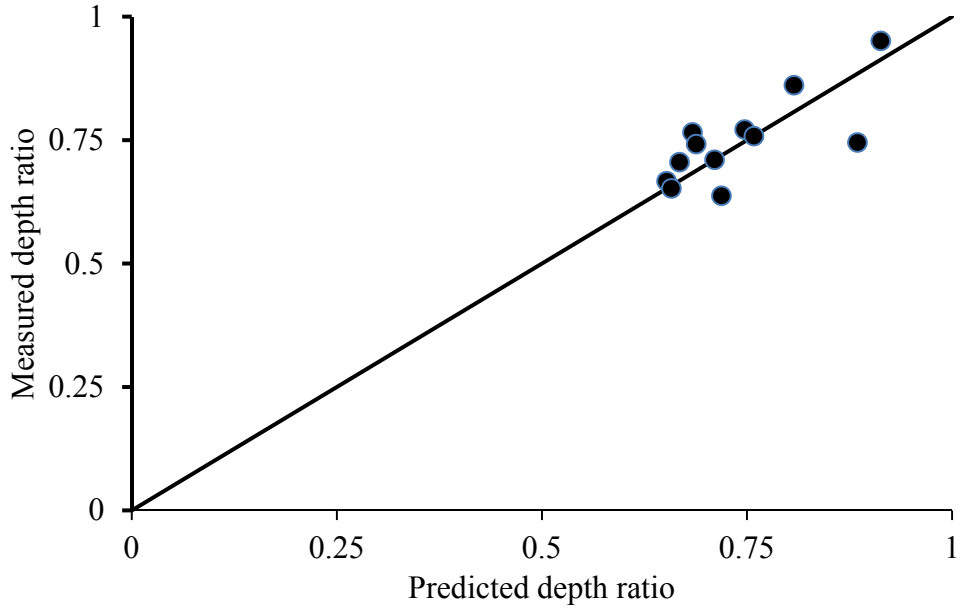

Fig. 4.14 Depth ratio at breach

Calibration of K for ξ = 1

All cases considered above are with ξ < 1. However, ξ = 1, if there is no discharge at the downstream end of the channel. Thus, K for this case depends on the breach length only. Average values of K for each breach size are obtained from 6 different experiments with ξ = 1 (Table 4.4) and the following equation is established by fitting a curve by least square error method.

$$K = -0.1065 + 2.1097\ \omega_2 - 0.5131\ \omega_2^2 \qquad (4.21)$$

Table 4.5 Calibration of K (ξ = 1.0)

Case	Q_1 (m^3/s)	F_1	η_2	η_3	ω_2	a	K
G12	0.063	0.439	0.798	0.983	1.0000	3.427	1.44
G13	0.057	0.429	0.745	0.988	1.0000	3.609	1.54
G14	0.050	0.291	0.868	1.024	0.5738	3.019	0.88
G15	0.044	0.280	0.822	1.010	0.5738	3.227	0.99
G16	0.031	0.175	0.887	1.000	0.3279	2.946	0.61
G17	0.037	0.185	0.950	1.008	0.3279	2.711	0.45

4.3.3 Computation to estimate breach flow

The breach flow may be estimated as follows:

1. Measure the channel width, flow depth and discharge at a section upstream of the breach, the channel width and flow depth at a section downstream of breach and the breach length.

2. Calculate all non-dimensional parameters excluding ξ and η_2 as defined in Eq. 4.10.

3. Solve Eq. 4.11 for ξ. and C* = 5.12.

4. From Eqs. 1.18 through 4.20, obtain K.

5. Solve Eq. 4.12 for η_2.

4.3.4 Remarks

The generalized model (Eqs. 4.11 and 4.12) may be used to predict the flow conditions at the breach. However, the assumption that the flow is divided into two parts in the breach region is a simplified one. As observed in the experiments, there is a lot of turbulence in his zone. In addition, the interface between these two zones of flows is not stable even though the flow is steady. The generalized model predicts a single value of flow depth at the breach. However, experiments show that the flow depth has undulations along the breach. First, it decreases till it attains a minimum value and then it increases. Similarly, the velocity along the breach varies. However, the predictions by using Eqs. 4.11 and 4.12 may be used in real life applications. For example, the predicted velocity at a breach may be used with a factor of safety to determine the maximum velocity at the breach, which may be utilized to develop procedures for closure. Similarly, the predicted breach discharge may be used to estimate the inundation area due to a breach. C* and K values

may be calibrated if past events of breach flow are available. In the absence of any data, C* may be estimated based on the channel bed material. K may be estimated by using Eqs. 4.18 – 4.20.

A generalized analytical model has been presented in this chapter. The model parameters are estimated by using the experimental results. A case study for the levee breach flow is presented in the next chapter.

Chapter 5

17th STREET CANAL BREACH – A CASE STUDY

The 17th Street Canal Breach is used as a case study to understand the performance of the generalized model for the steady flow at a breached levee presented in the previous chapter. The experimental set-up for the case study is presented in chapter 3.

The cases considered for the hydraulic model study of the 17th Street Canal Breach are listed first. The details of the measured velocity field and water surface profile are then discussed. In addition, results showing the effect of inflow and nearby structures on the flow field are included. Turbulent characteristics of the flow are presented through the turbulent kinetic energy (TKE) and bed shear stress. Results from the detailed experiments are compared against results obtained from the generalized model developed in chapter 4.

5.1 Cases considered

Six sets of experiments are conducted in the present study. Three different inflow discharges (0.057 m^3/s, 0.075 m^3/s and 0.095 m^3/s) are considered. The study also takes into account the effect of the structures in the flood plain on the flow field. Note that the breach size, bed topography and the downstream condition (zero flow) are as per the field

values and are kept constant in all the runs. Steady flow condition on rigid bed is maintained in the present study.

Table 5.1 Cases considered in the 17th Street Canal Breach

Case No.	Inflow (m^3/s)	Flood-plain condition
1	0.057	Structures
2	0.057	No structures
3	0.075	Structures
4	0.075	No structures
5	0.095	Structures
6	0.095	No structures

5.2 Uncertainty

The velocity and the water depth measurements are verified for uncertainty. The velocities measured by two different instruments (UVP and ADV) indicates matching each other. However, all velocity measurements in the present work are performed by using the ADV. Repeatability of the x- and y-components of the measured velocities at three grid points (X10-Y5; X24-Y5; and X24-Y12) for case 1 is presented in Fig. 5.1. Measurements from two different runs indicate that the maximum differences in the velocities along x- and y-directions are approximately six percent and two percent, respectively. Repeatability of measured flow depth for case 1 indicates the maximum difference between the measured values is less than 0.1 percent (Fig. 5.2). Thus, the repeatability for the present set of measurements is considered acceptable. The measured velocities and flow depths are used for further analysis.

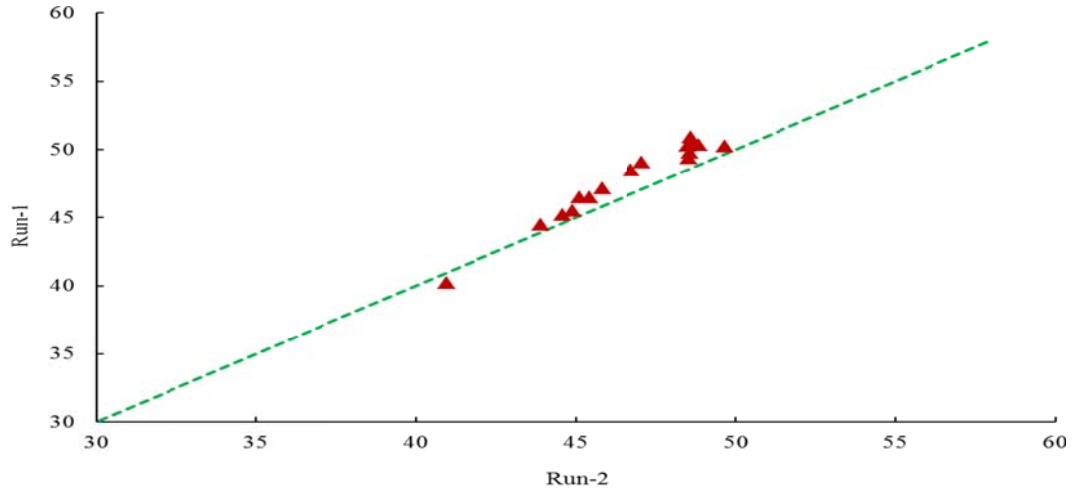

(a) X10-Y5

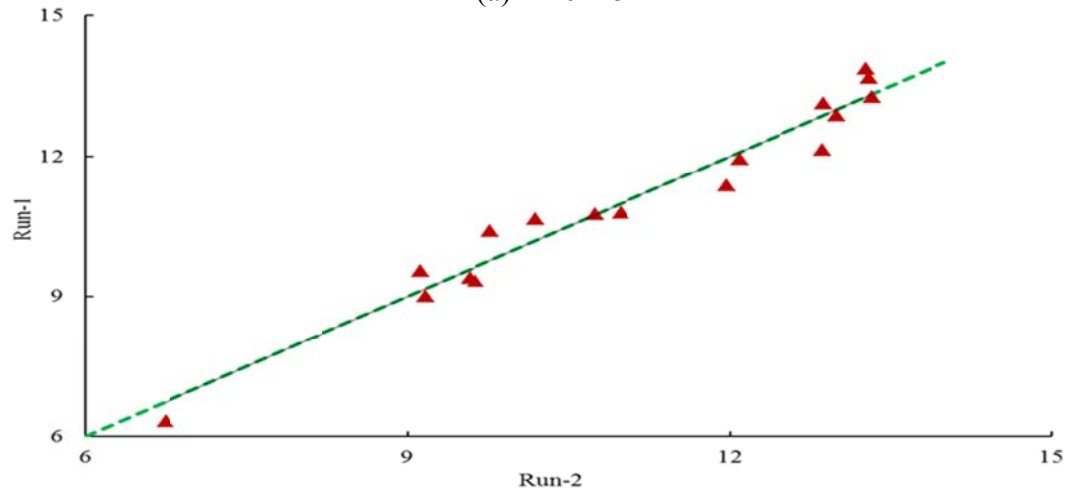

(b) X24-Y5

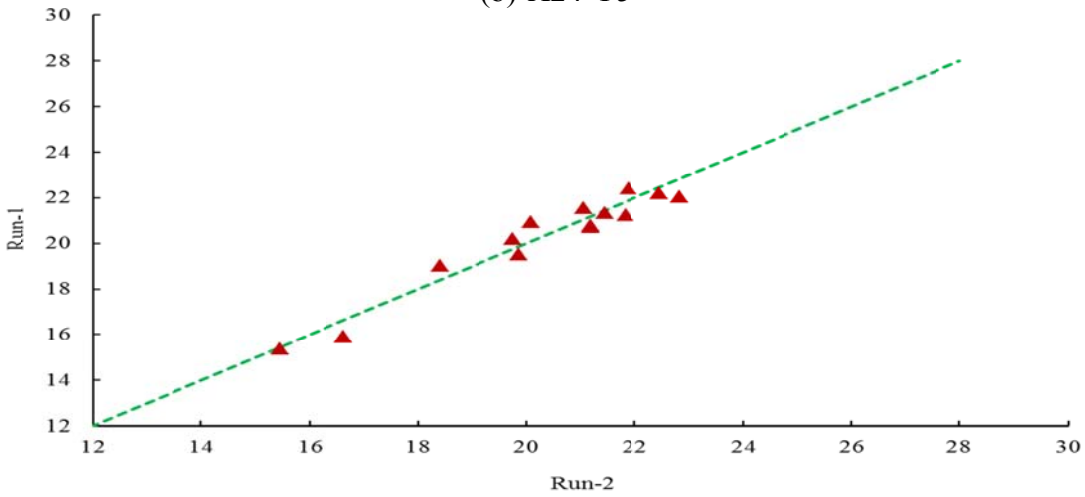

(c) X24-Y12

Figure 5.1 Repeatability of longitudinal velocities (cm/s) for case 1

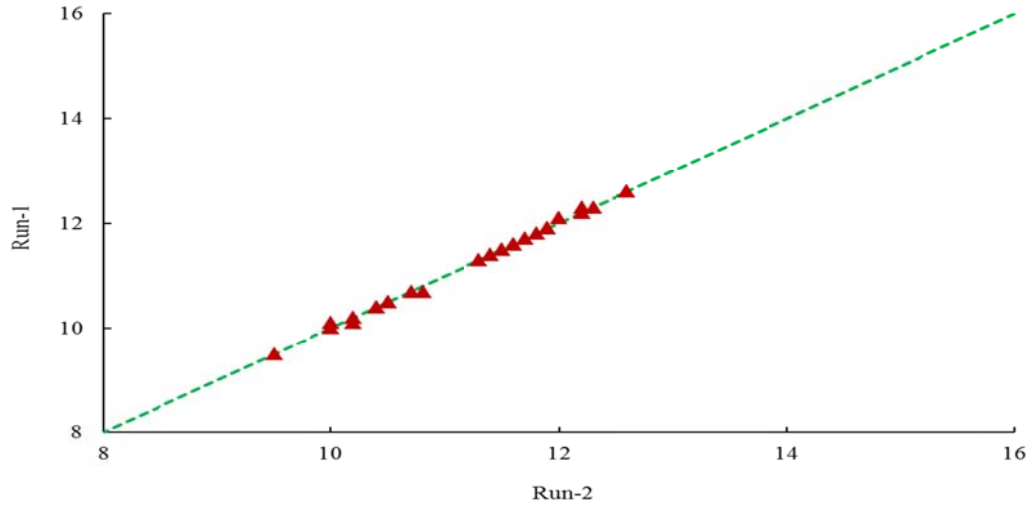

(a) Y3

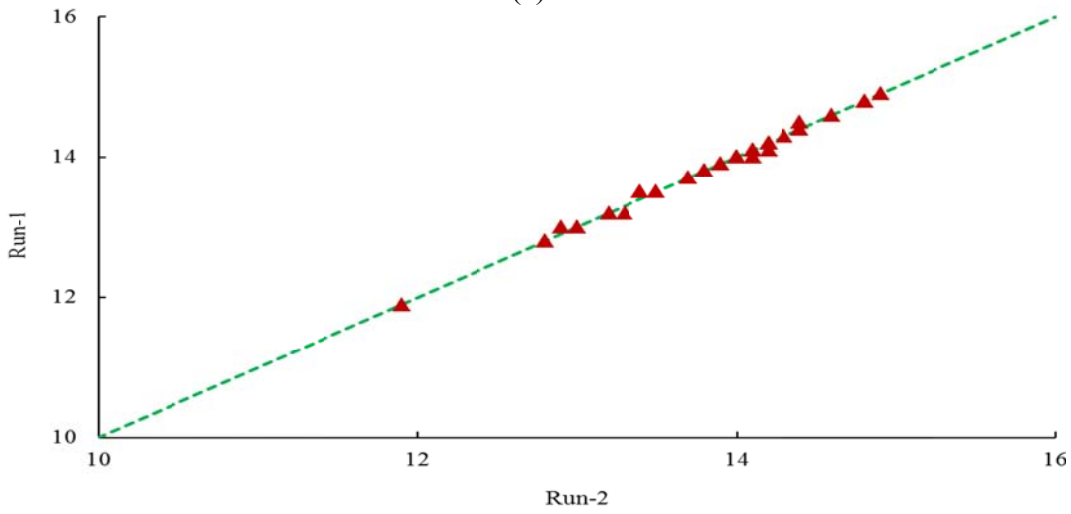

(b) Y5

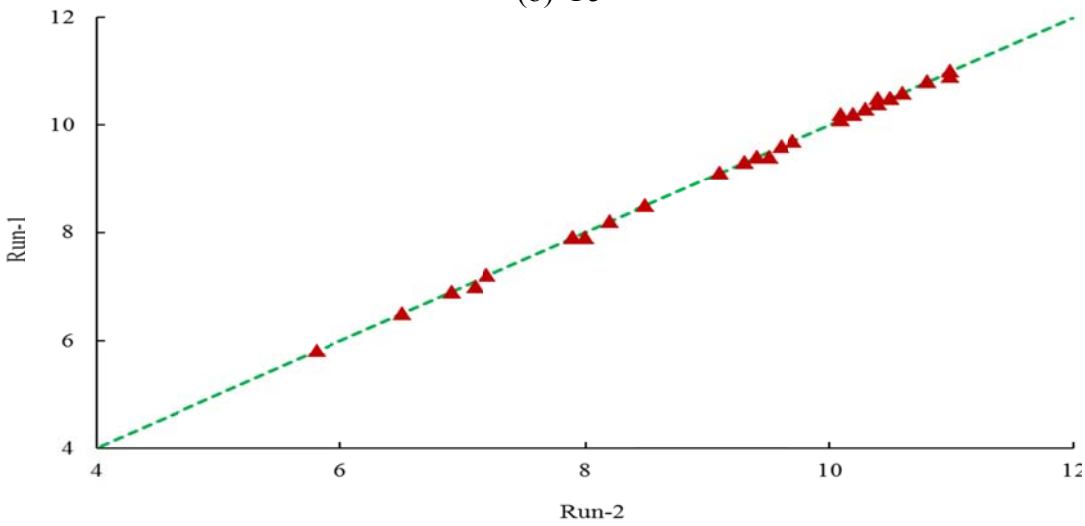

(c) Y7

Figure 5.2 Repeatability of flow depth (cm) for case 1

5.3 General description of flow

The topography and the geometry of the reproduced model flow area may be divided into following four zones: the upstream and downstream flow zones of the main canal, the breach zone and the urban flooded area zone, as shown in Fig. 5.3. The water depth in the upstream part of the channel does not vary and it is characterized by smooth subcritical flow.

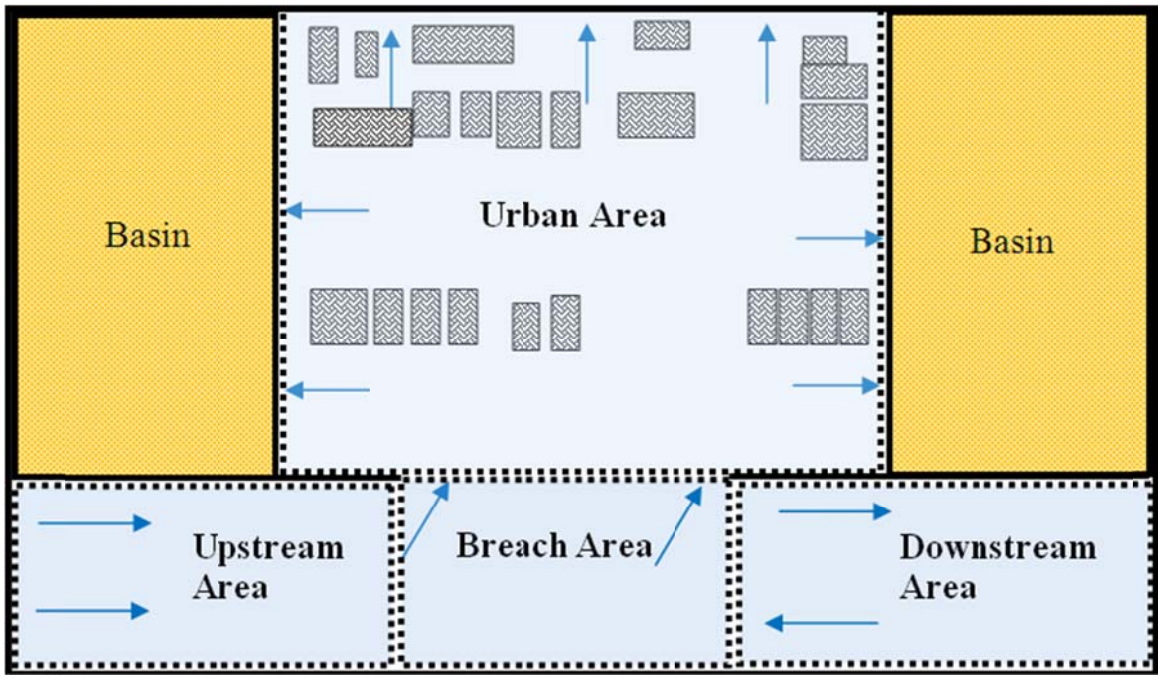

Figure 5.3 Different flow zones in the model

The flow is mostly one-dimensional (only in the *x*-direction) in the upstream zone, while it becomes two-dimensional as the flow approaches the breach. The downstream part of the channel is almost stationary flow, with near-constant water level and very low velocities as compared to the upstream. The closed gate at the downstream end of the channel prevents the flow from being significant in this area and the visual observation and velocity measurements confirm the recirculation of the flow in this area. The breach

zone is described as 3-D turbulent flow with the presence of standing waves and fluctuations. Prominent vertical-component of the velocity and significant turbulent kinetic energy are discussed elsewhere. The velocity measurements in this zone are less precise than elsewhere due to turbidity and fluctuations. The flow in the flooded urban area is characterized by shallow water depth. The presence of houses obstructs the flow and causes significant variations in the flow direction. The flow is considered as 2-D flow in this region. Velocity measurements are taken at limited locations in this zone due to the shallow water depths.

Results for the velocity field, water surface profile , turbulent kinetic energy and bed shear stress for Case 1 are presented in the following sections. Results for other cases are presented in Appendix 3.

5.4 Velocity field

The velocity field for Case 1 is presented in Figs. 5.4 through 5.7. The variation of X- and Y- components of velocities along the main channel as a function of depth is presented in Figs. 5.4 through 5.6. The velocity distribution at the inlet indicates that the X-component of the velocity is prominent and thus, the flow is one-dimensional. The maximum velocity in this zone is 52.2 cm/s and it occurs at grid point X5-Y4. The positive X-velocity along Y7 (Fig. 5.6) and the negative X-velocity along Y3 (Fig. 5.4) show that the recirculating flow zone on the downstream side is clockwise. This is due to the closed gate at the downstream end of the channel. Considering the velocity field along Y3, the X-velocity decreases and Y-velocity increases as the flow progresses

towards the breach (Fig. 5.4). The same trend is also observed along Y5 and Y7 (Figs. 5.5-5.6). However, the Y-velocities are higher in Y7 as this is close to the breach. Considering the breach zone in the main channel, the maximum X-velocity of 47.90 cm/s is measured at grid point X15-Y5.

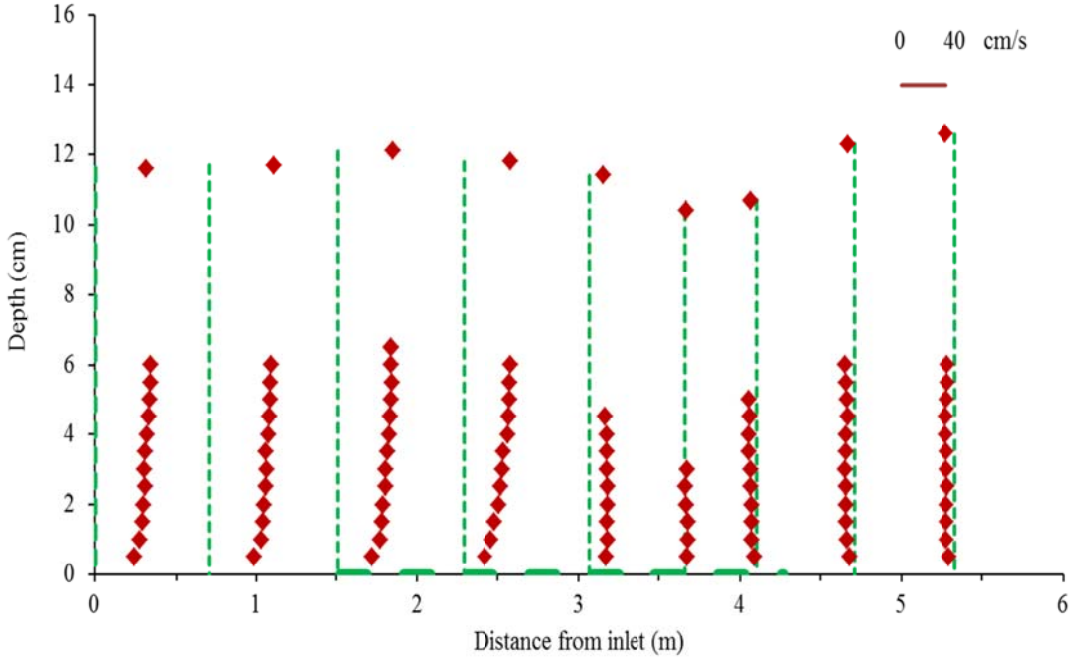

(a) X-velocity

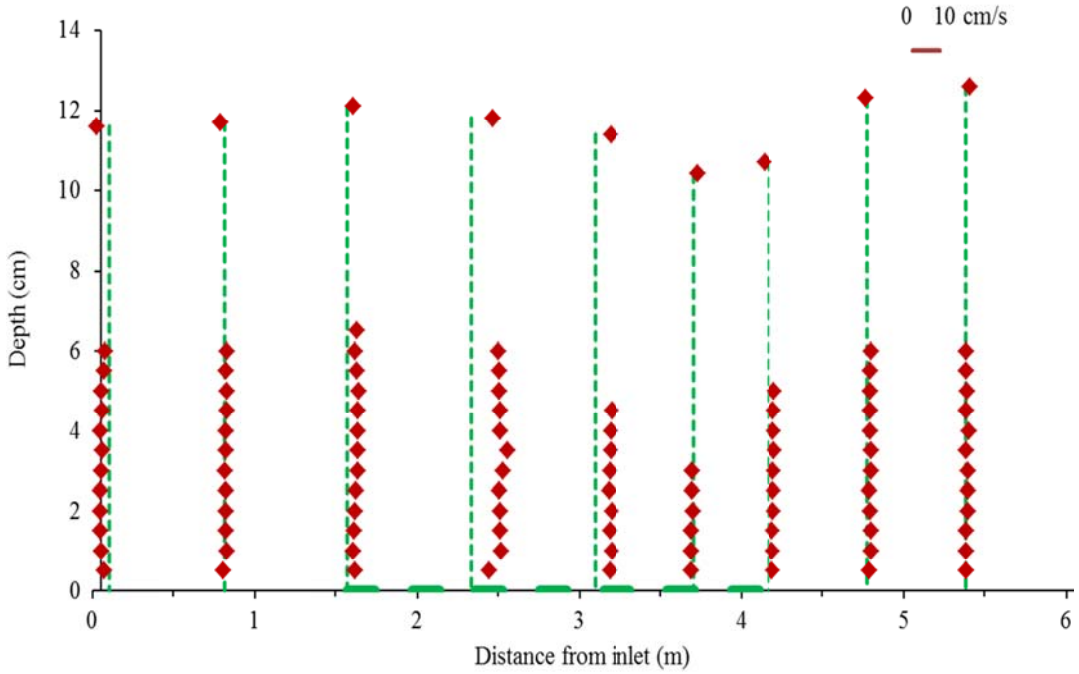

(b) Y-velocity

Fig. 5.4 Measured velocities along Y3 (case 1)

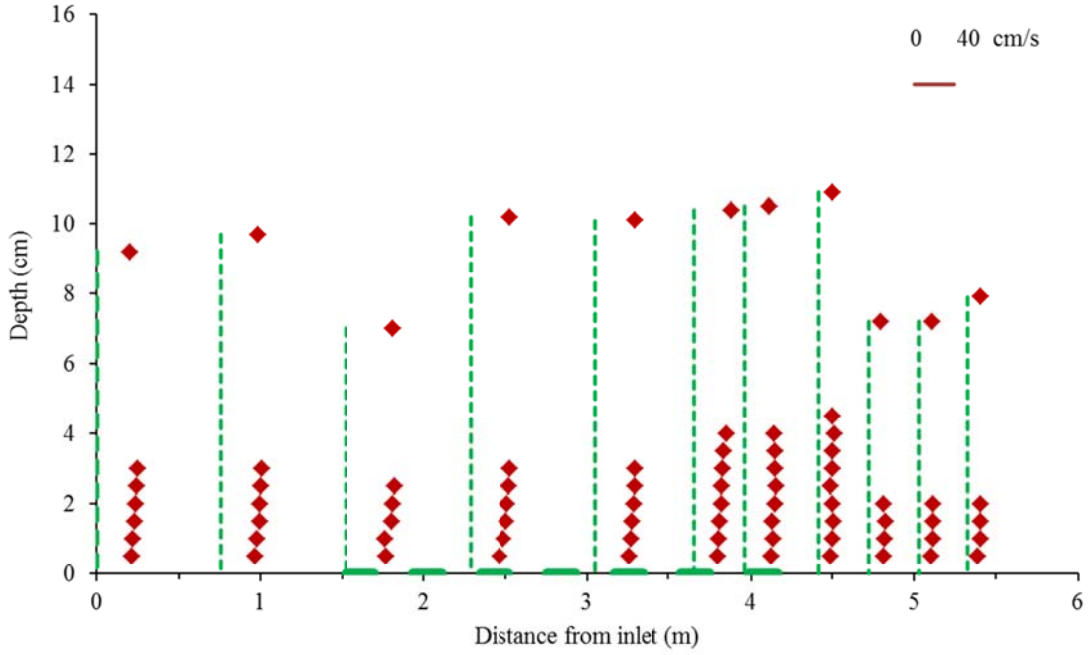

(a)

(a) X-velocity

(a)

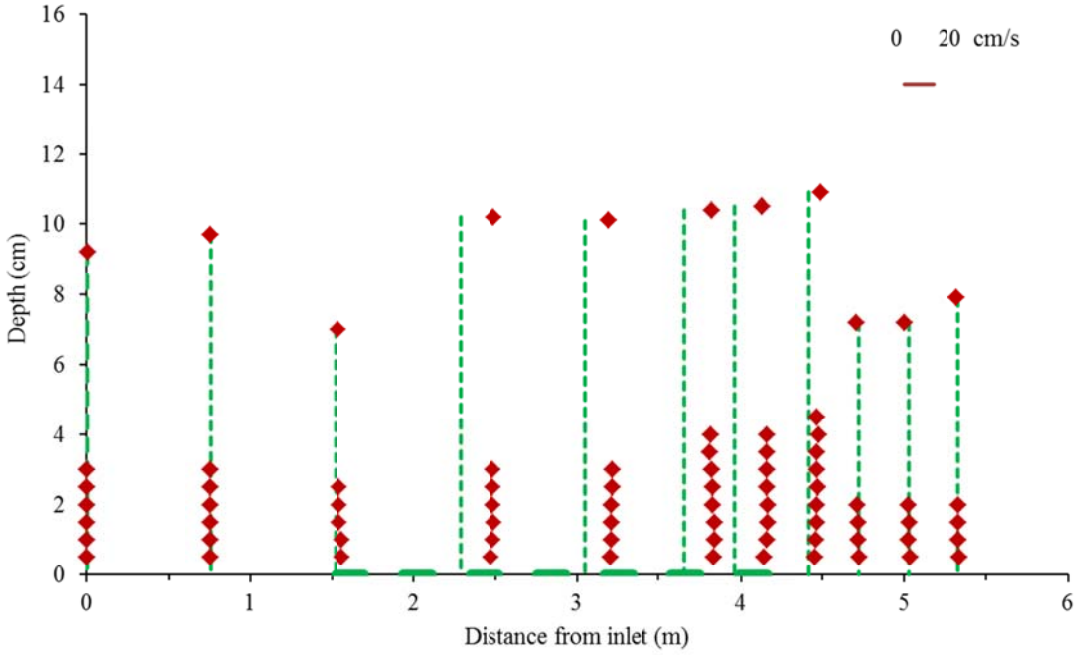

(b) Y-velocity

Fig. 5.5 Measured velocities along Y5 (case 1)

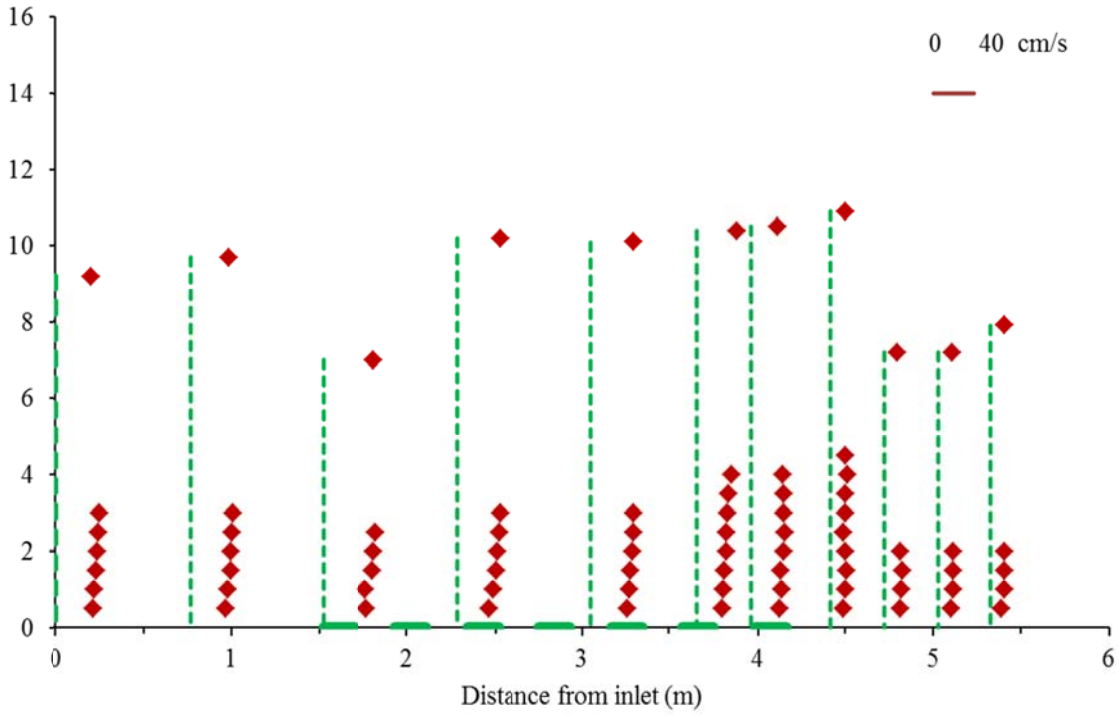

(a) X-velocity

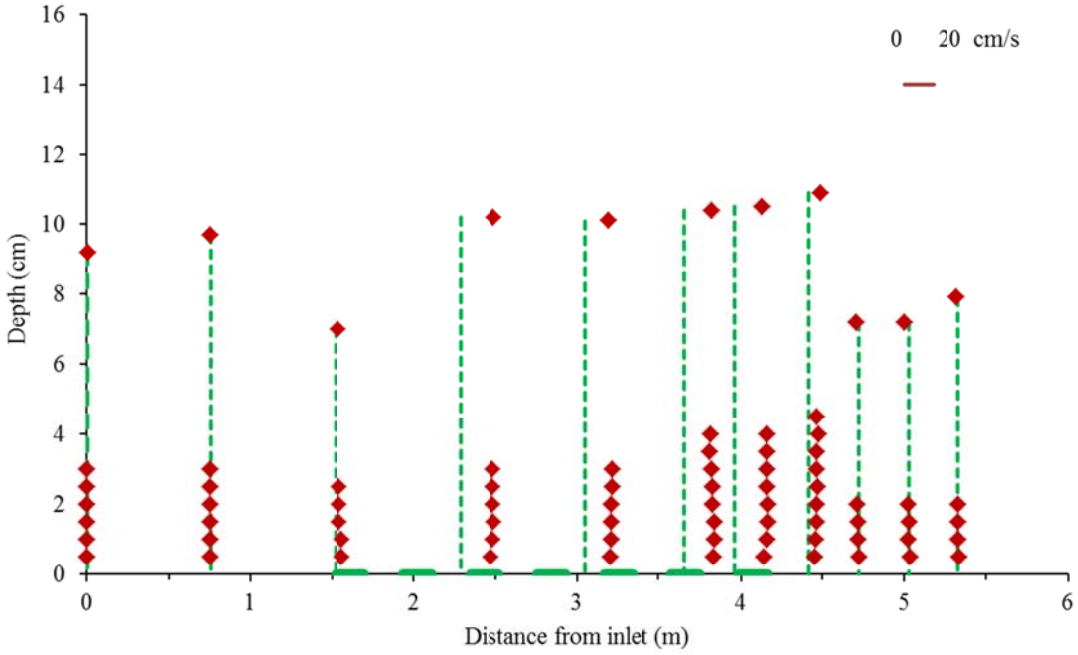

(b)Y-velocity

Fig. 5.6 Measured velocities along Y7 (case 1)

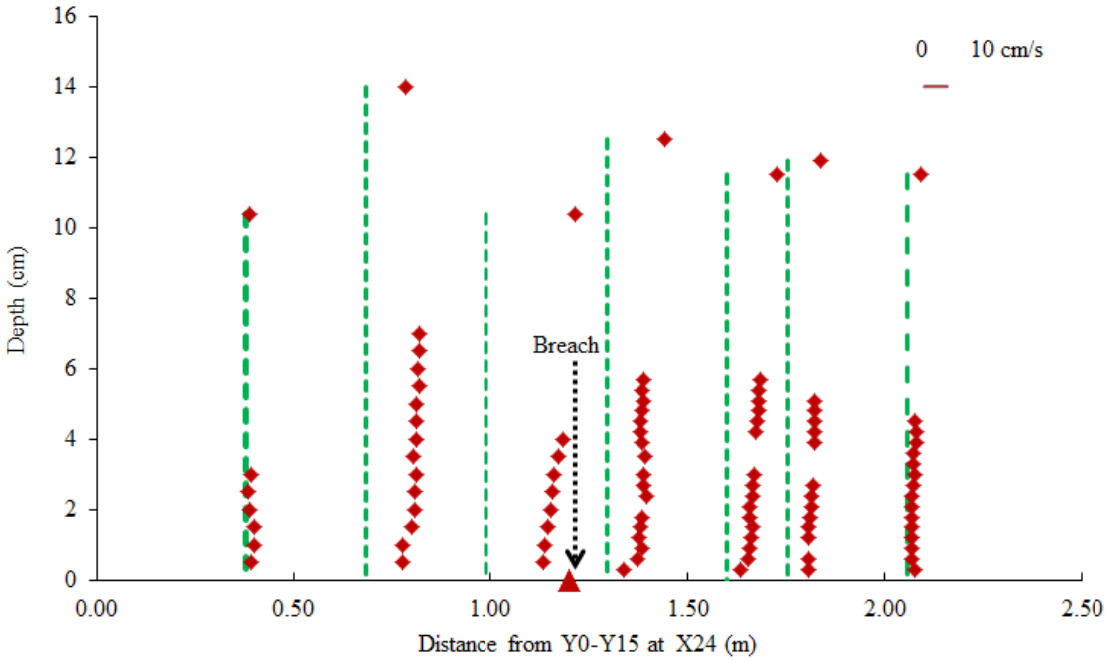

(a) X-velocity

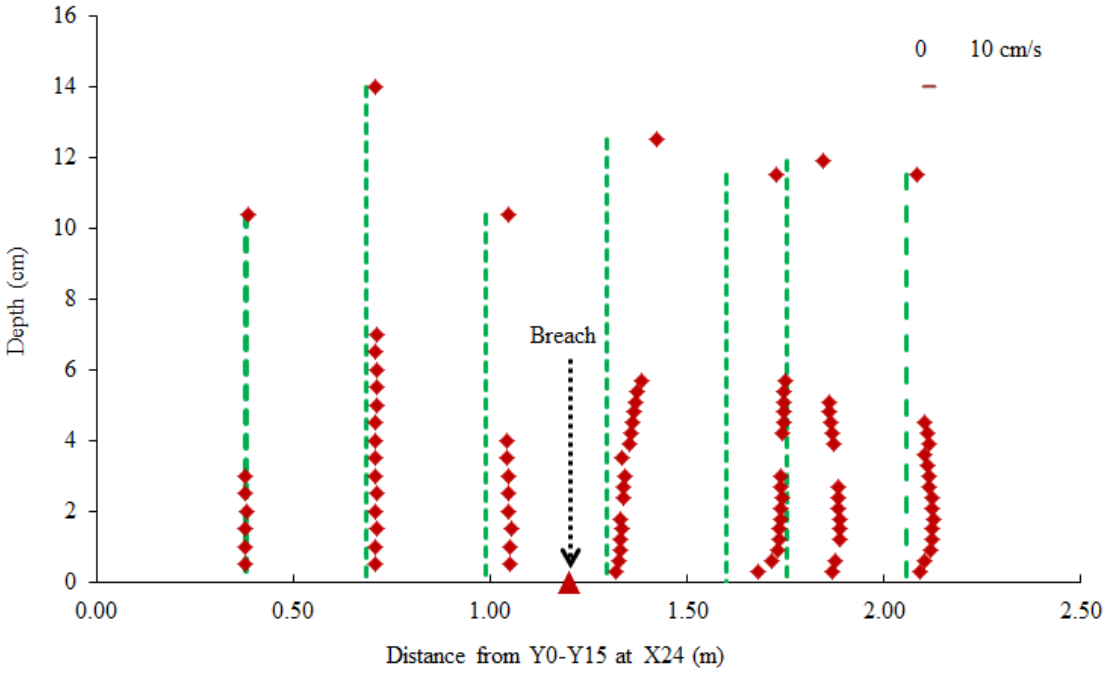

(b) Y-velocity

Fig. 5.7 Measured velocities along X24 (case 1)

The maximum Y-velocity in this zone is 22.2 cm/s and it occurs at the X26-Y7. The velocity field in the lateral direction (along X24) is shown in Fig. 5.7. The X-velocity decreases significantly beyond the breach. However, the y-velocity is significant outside the breach. The magnitude of the maximum Y-velocity is 50 cm/s and it is even higher than the maximum velocity in the main channel. The indicated water surface velocities in Figs. 5.4-5.7 are obtained from the camera. The locations of these velocities also indicate the water surface.

The flow is three dimensional in the breach region and is with high degree of turbulence. As shown in Fig. 5.8, the z-velocity is significant only in the breach region and it is negligible beyond it. Majority of the z-velocity values are positive, indicating that the

velocity is in the upward direction. This may be attributed to the undulations (ditch) on the bed. When flow impacts the lowered bed, there is an upward velocity. However, negative (downward) z-velocity also occurs when the flow enters into the ditch (Fig. 5.8 a). The maximum upward and downward vertical velocities are 3.5 cm/s and 1.60 cm/s, respectively. Note that the velocity on the water surface cannot be measured by the camera. The dashes (-) in Fig. 5.8 indicate the water surface location. Variation of the depth averaged velocities for case 1 is presented in Fig. 5.9. Different hydraulic zones described earlier may be identified from the velocity vectors. The discharge from the inlet is passing through the breach. However, a recirculating zone is created in the main channel, downstream of the breach. Net discharge across the channel in this zone is zero. A map showing the contours of Froude Numbers for case 1 indicates that the flow is subcritical in the entire domain. The observed maximum Froude Number is 0.6 and occurs near the upstream of the breached section (Fig. 5.10).

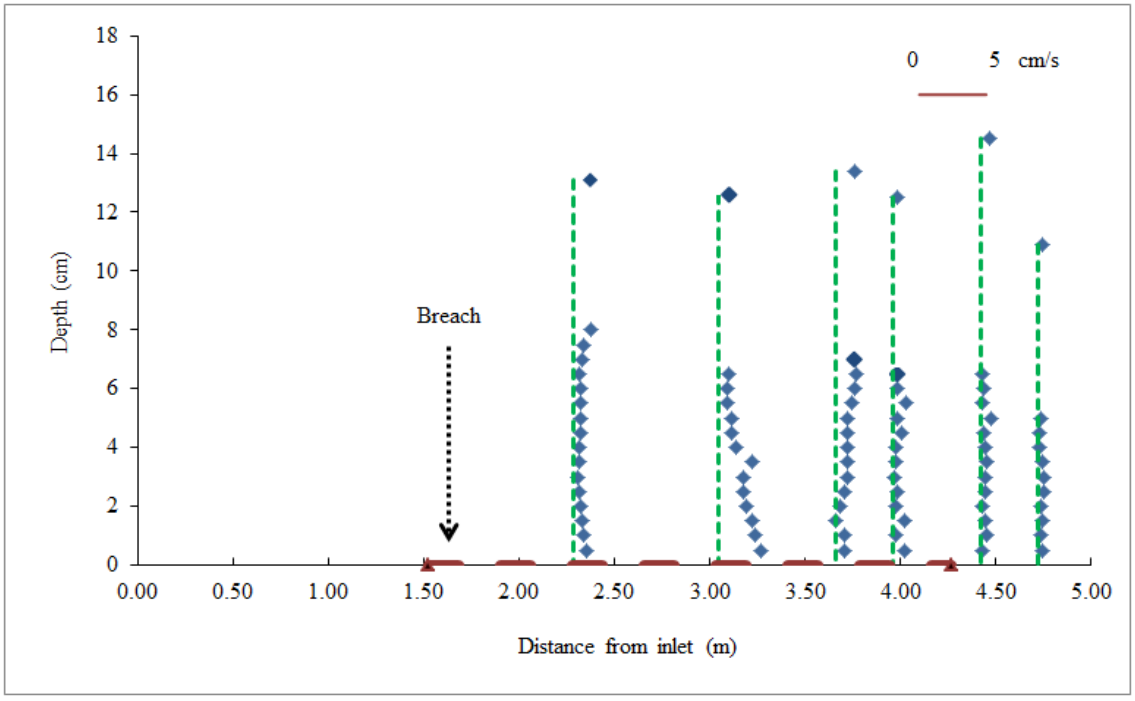

(a) Along Y6

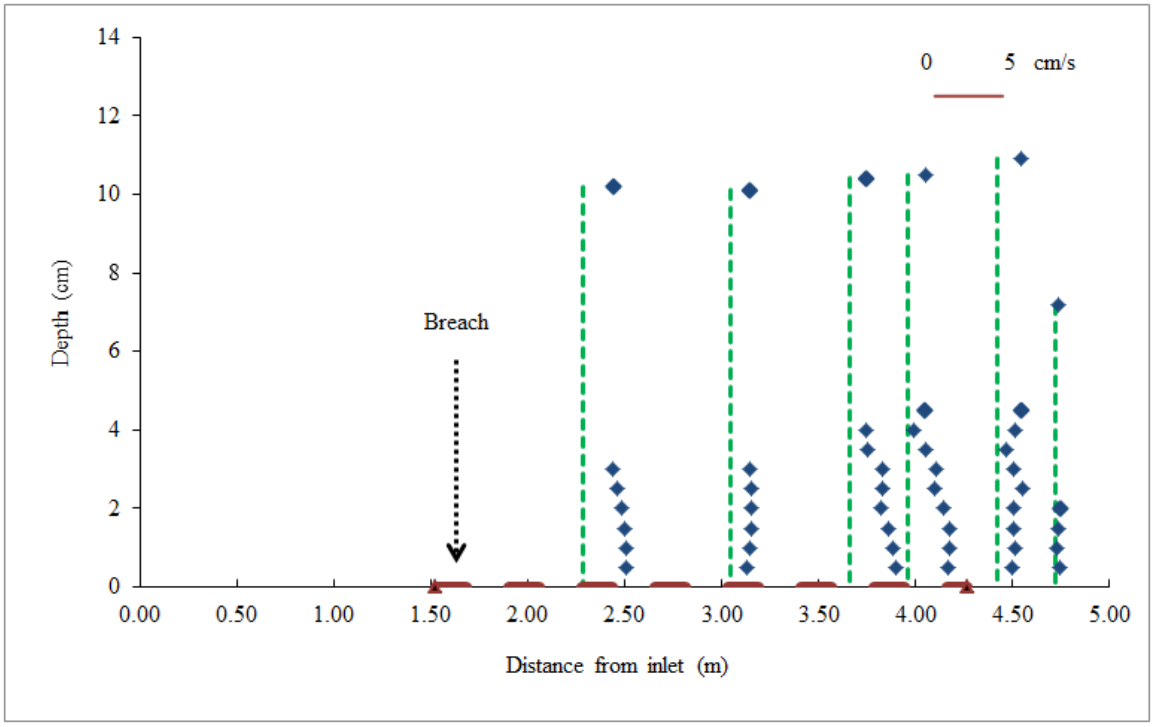

(b) Along Y7

Fig. 5.8 Measured Z-velocities (case 1)

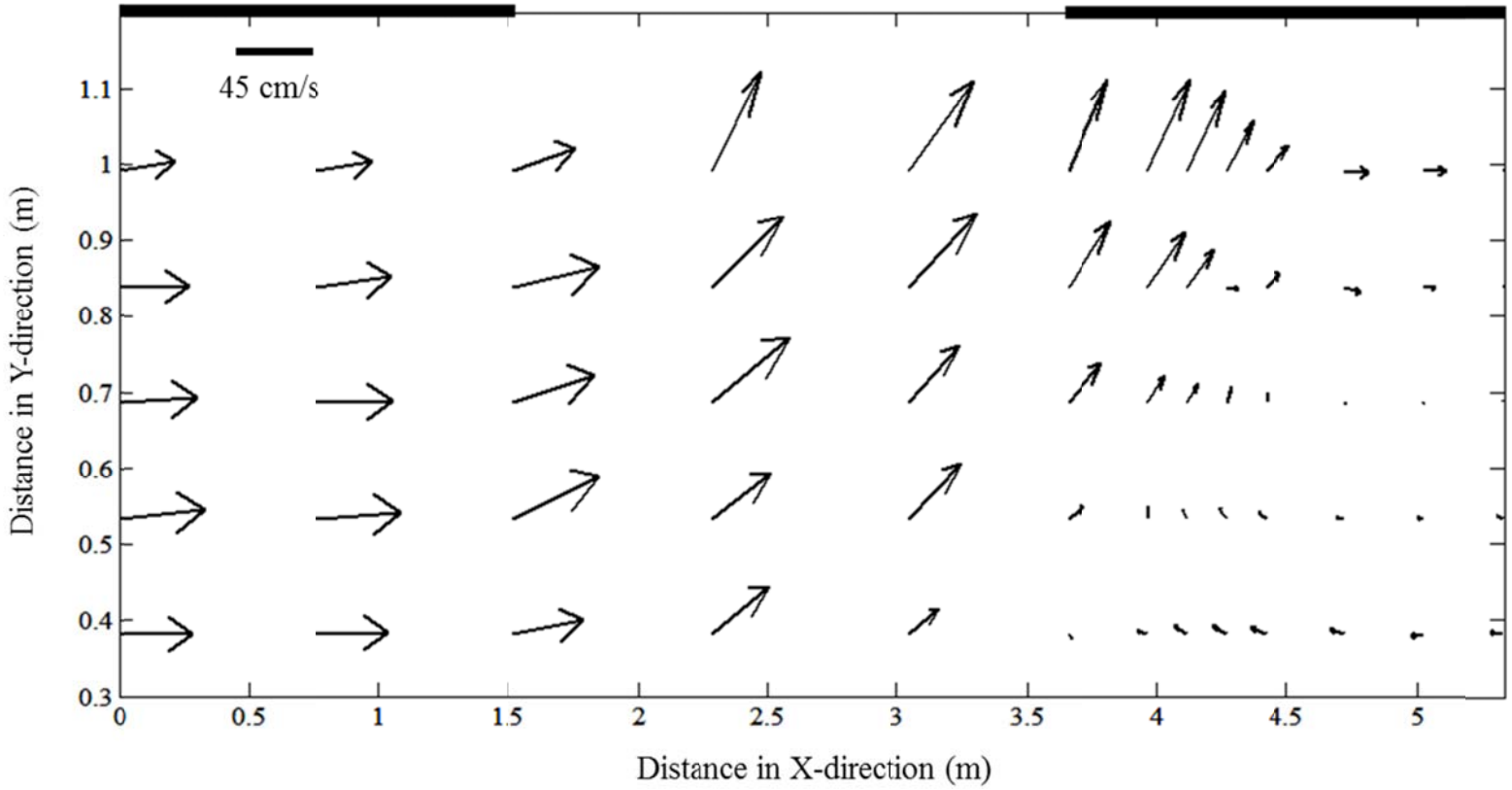

Fig. 5.9 Depth averaged velocities in the channel (case 1)

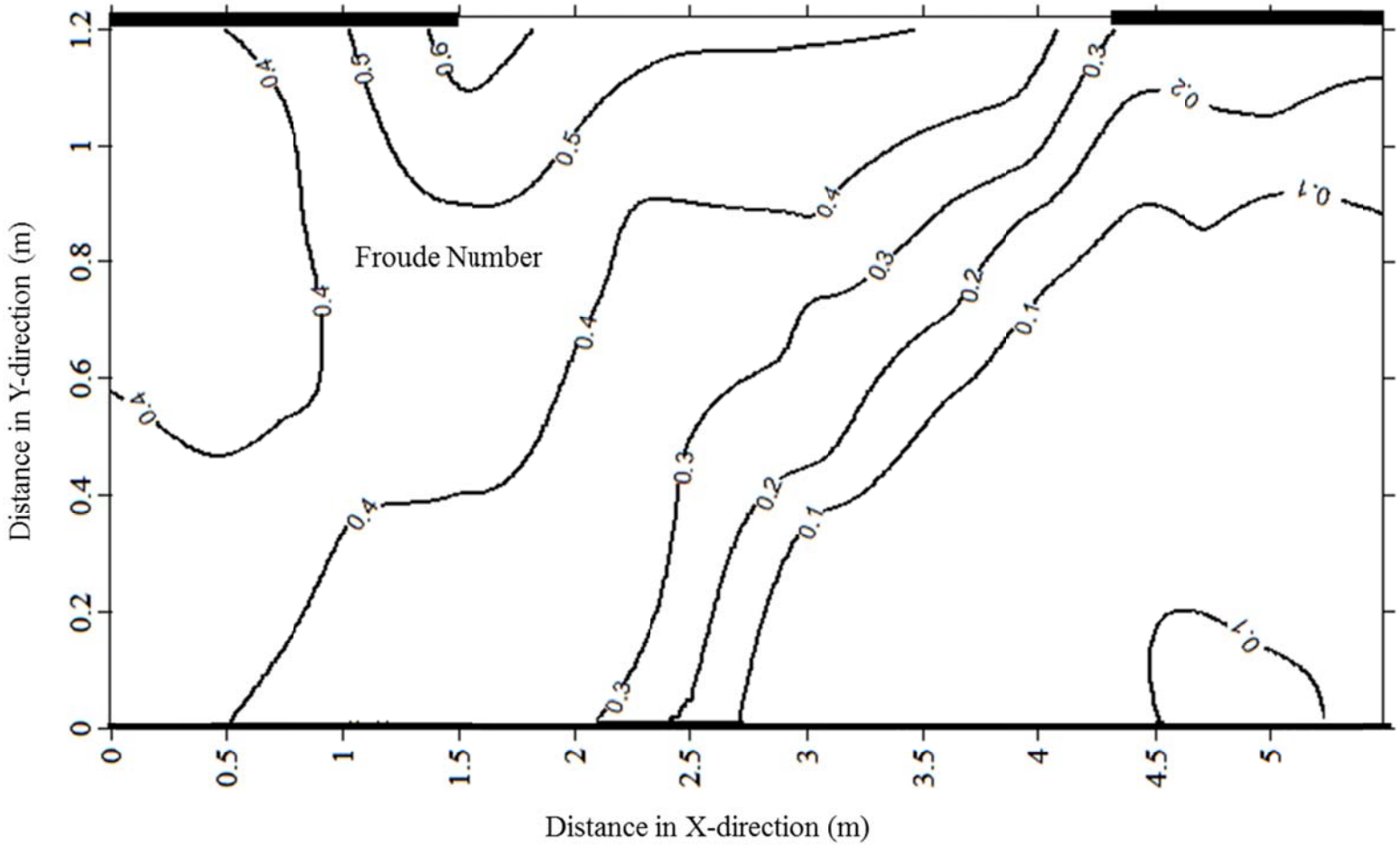

Fig. 5.10 Froude Numbers variation (case 1)

5.5 Water surface profile

The contours of the measured flow depths in the main channel and in the flooding zone for Case 1 are presented in Fig. 5.11. The maximum flow depth is 15.9 cm and it occurs at X28-Y5. Although, the flow depths vary in the longitudinal direction, the water surface is more like a horizontal line along Y3). However, as expected, close to the breach, the water surface is deformed. There is a dip of about 3 cm near the breach. The maximum water surface slopes in the longitudinal and lateral directions are 0.01 and 0.1, respectively. The presence of the ditches in the model is indicated by the higher flow depths and closely spaced contours of flow depths. The inundation in the flood-plain indicates that the structures located downstream of the breach are subjected to more impact due to flooding. Note that the present study assumes a rigid bed model, and the bed topography has been adopted from USACE (2007). The ditches formed on the bed by flow velocity due to the breaching affect.

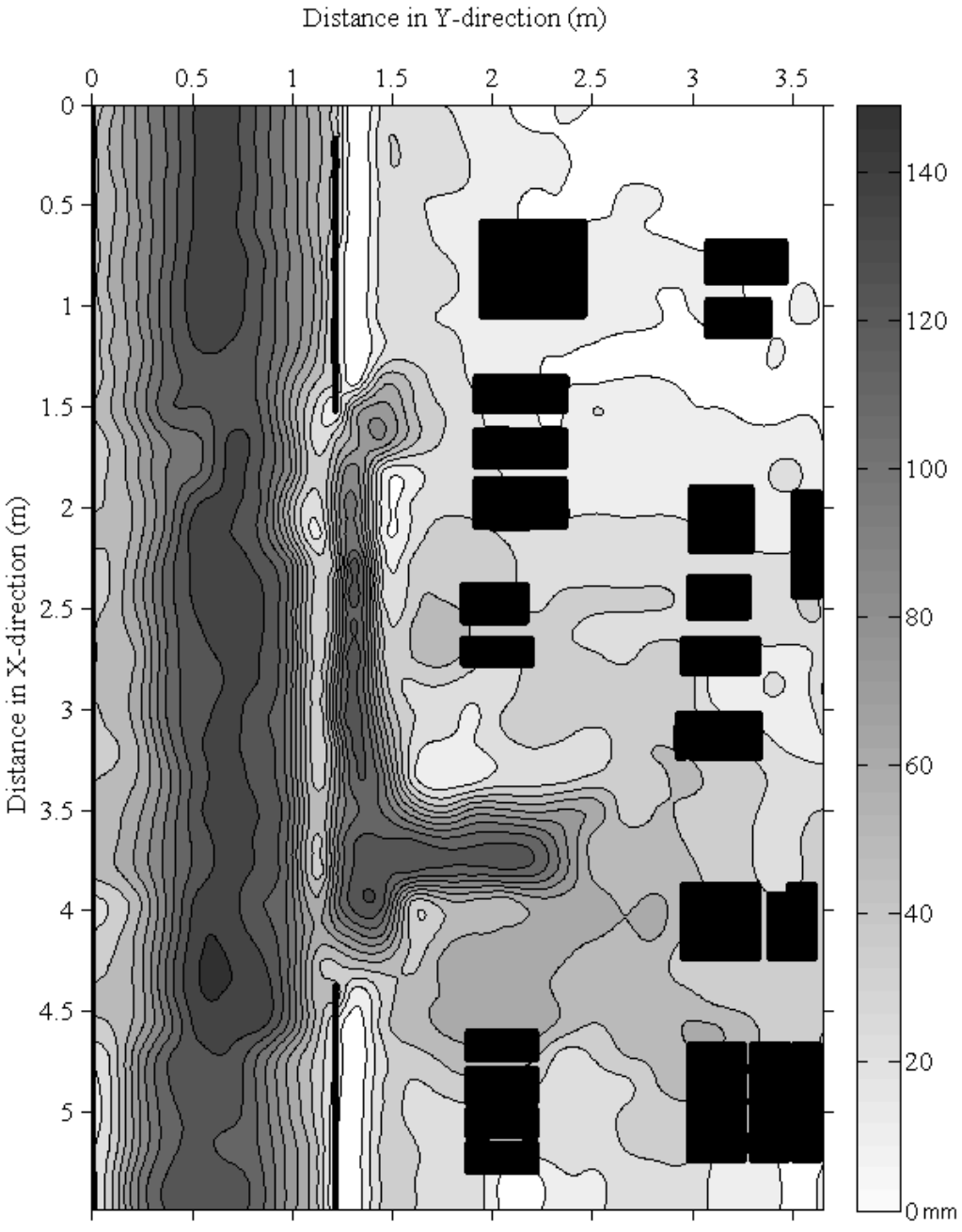

Fig. 5.11 Contours of flow depth (case 1)

5.6 Turbulent Kinetic Energy

The experimental data can be used to identify the mechanism of production of turbulent kinetic energy (TKE) in divided open channel flow past a breached levee. TKE is calculated from the acoustic Doppler velocimeter (ADV) data, since the ADV provides time series of the three components of velocity fluctuations. Consider the instantaneous x-component of velocity, U, as the sum of an average value $\overline{U}$ and a fluctuating part u' such that $U = \overline{U} + u'$. The mean of these turbulent fluctuations is zero. Thus, the mean-square value may be used as a measure of the magnitude of the turbulence. The variance of the fluctuating part is denoted as $\overline{u'^2}$. Using similar notations for the y- and z-components of the measured velocities (V and W) in the flow, turbulent kinetic energy is calculated as the sum of the mean square of velocity fluctuations and is defined as

$$K = \frac{1}{2}(\overline{u'^2} + \overline{v'^2} + \overline{w'^2}) \qquad (5.1)$$

The instantaneous velocity data contain the influence of local turbulence as well as large scale unsteadiness within the flow. Therefore, a despiking analysis is adopted and the low frequency fluctuations are filtered out to ascertain the exact level of turbulence at a given point. It results in an accurate representation of fine-grained turbulence. The spatial distribution of the turbulent kinetic energy K is presented in Fig. 5.12. It is evident that a maximum in K occurs in the turbulence production region and is located close to the breach location. Note that the TKE is significant at locations close to breach (3 m – 5.5 m from the inlet). The maximum TKE at this location is 109 cm^2/s^2. As expected, the TKE at the other locations is insignificant. The ditch at X27-Y7 may be cause of higher TKE at that location.

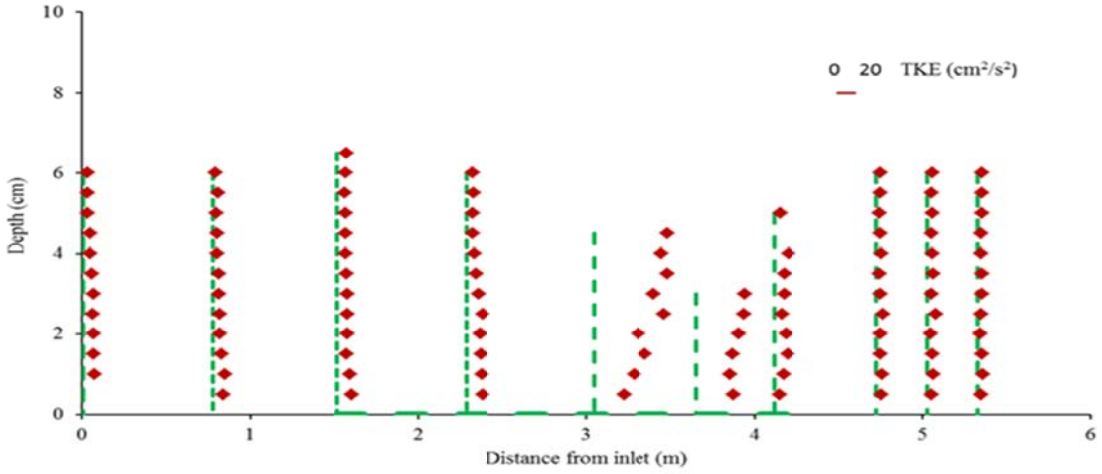

(a) Along Y3

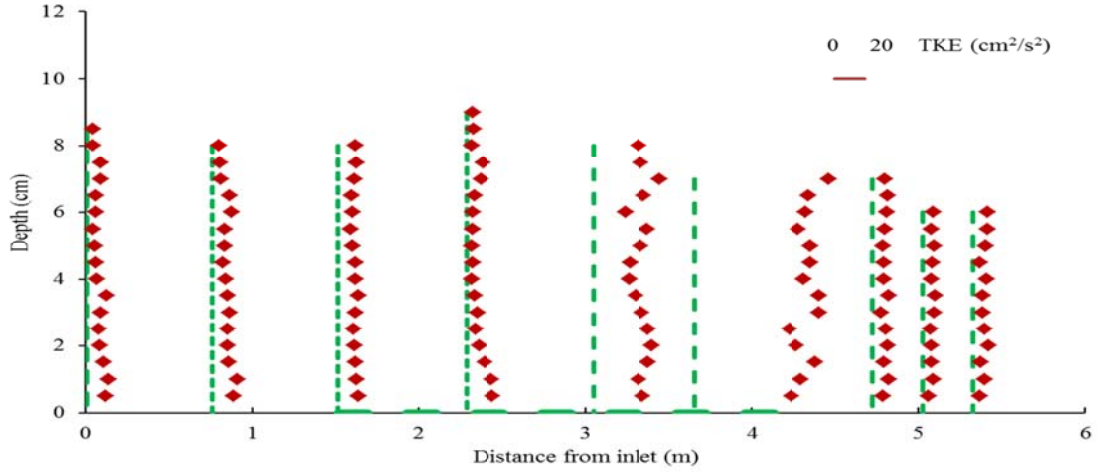

(b) Along Y5

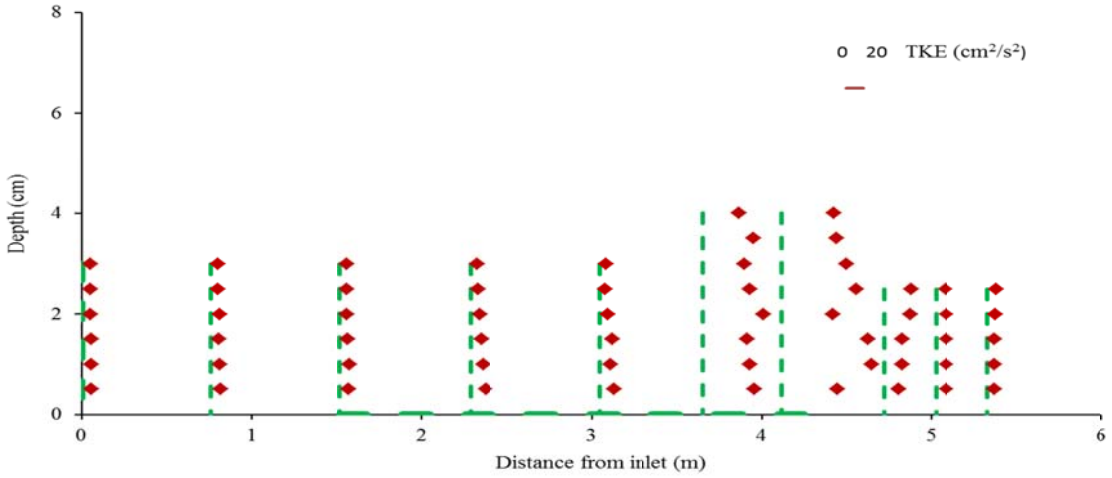

(c) Along Y7

Fig. 5.12 Variation of TKE (case 1)

5.7 Bed shear stress

Commonly employed techniques to estimate bed shear stress include: (1) Law of the Wall technique, (2) Reynolds stress measurement, (3) TKE measurement, and (4) Energy dissipation methods. The assumptions and limits of these four techniques have been reviewed by Kim et al. (2000). The authors concluded that the TKE approach is consistent and relatively easy to estimate the bed shear stress when compared to others. Simple relationships between the TKE and bed shear stress have been formulated in turbulence models (Galperin et al. 1988). Further studies have shown that the ratio of TKE to bed shear stress is constant (Stapleton and Huntley 1995). In the present work, the bed shear stress is estimated by following the method suggested by Song and Chiew (2001). The description of method follows.

The shear stress at various depths above the bed is calculated by using the equation

$$\tau_{3\text{-D}} = -\rho\sqrt{(\overline{u'w'})^2 + (\overline{u'v'})^2 + (\overline{v'w'})^2} \qquad (5.2)$$

The shear stress as a function of flow depth is plotted and a straight line is fitted by regression. The extrapolated value of shear stress at the bed (z = 0) is obtained from the regression equation.

The variation of bed shear stress for case 1 is presented in Fig. 5.13. The maximum value of 1.0 N/m^2 is observed near the downstream side of the breach. The formation of the ditch at this location may be due to the high value of bed shear stress associated with the flow.

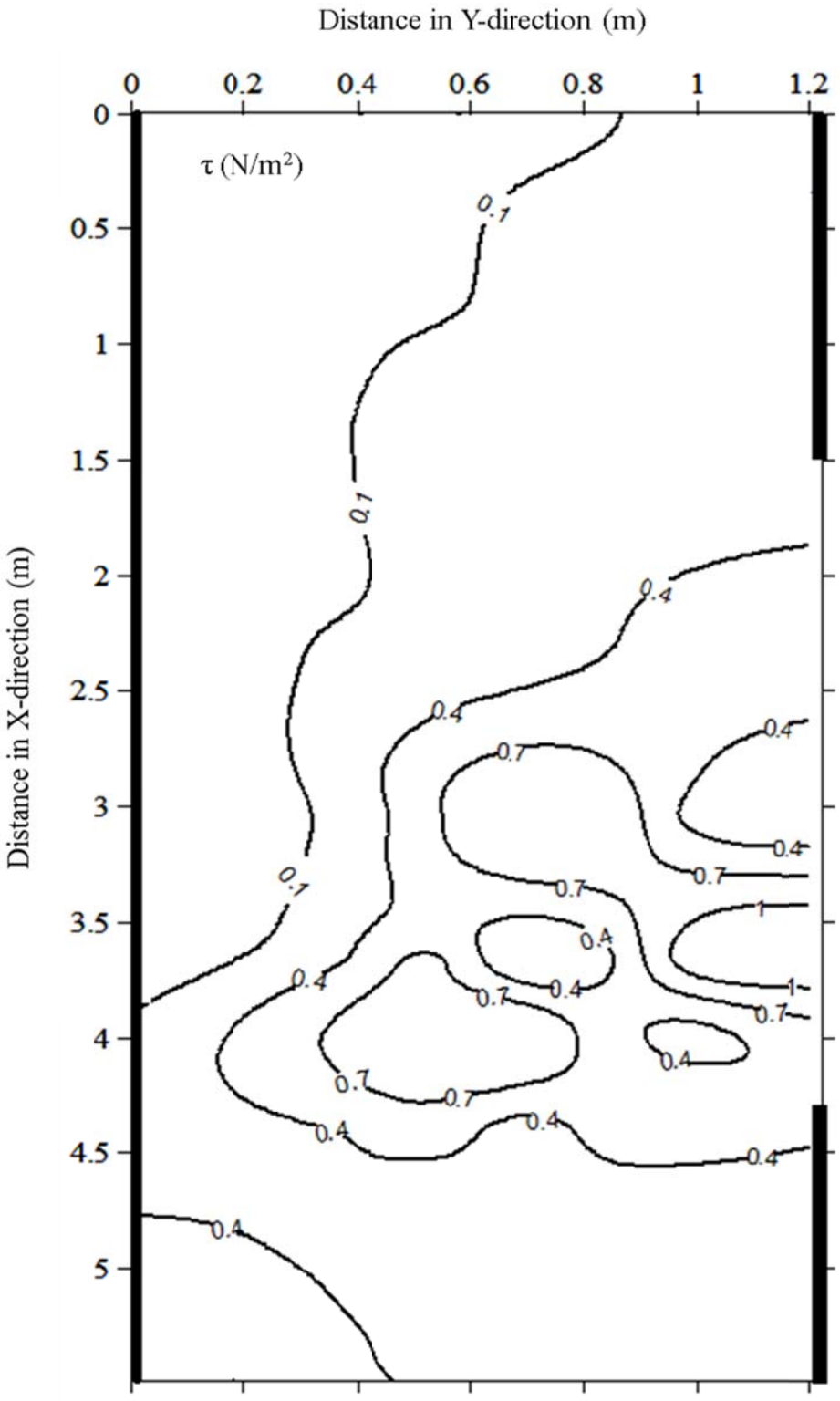

Fig. 5.13 Distribution of bed shear stress (case 1)

5.8 Effect of inlet discharge

Three different inlet discharges (0.056, 0.075, and 0.095 m^3/s) are used in the present study (Table 5.1). The trends of the velocity distribution and free surface profile are similar for all the discharges. The results for velocity (Fig. 5.10) and flow depth (Figs. 5.11 and 5.12) showing the effect of inlet discharge are presented. Velocities at two different locations (one away from the breach and the other near the breach) indicate that the velocity increases with increase in the inlet discharge. However, this increase in the velocity near the breach is a function of the depth due to the higher degree of turbulence in the breach region. The results for inlet discharge of 0.095 m^3/s shows that the increase in the velocity is towards the free surface and not near the bed. The water surface elevation in the lateral direction shows that the water surface decreases significantly near the breach (Fig. 5.11). The water flow depth increases due to increase in the inlet discharge. Similar trends are followed for all discharges. There is sharp curvature in the water surface for all discharges. The variation of water surface in the longitudinal direction shows that there is increase in water depth due to increase in the inlet discharge. Although the trend is similar for all discharges, the dip near the breach is more for an inlet discharge of 0.095 m^3/s. The role of the bed topography in the attained water surface elevation seems to be important.

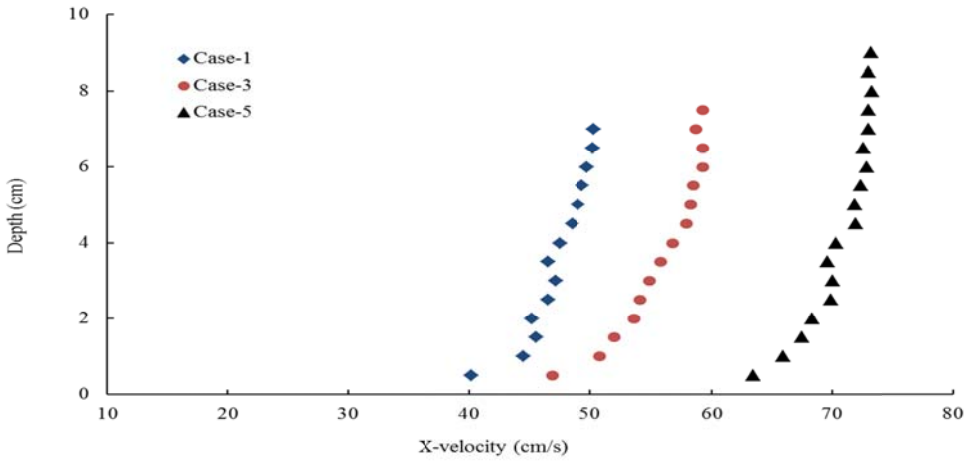

(a) X10-Y5

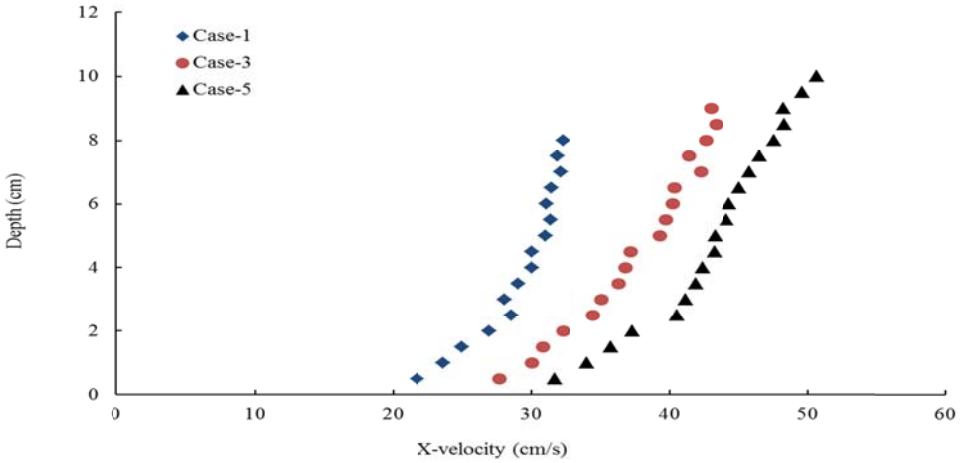

(b) X20-Y5

Fig. 5.14 Effect of inlet discharge on X-velocity

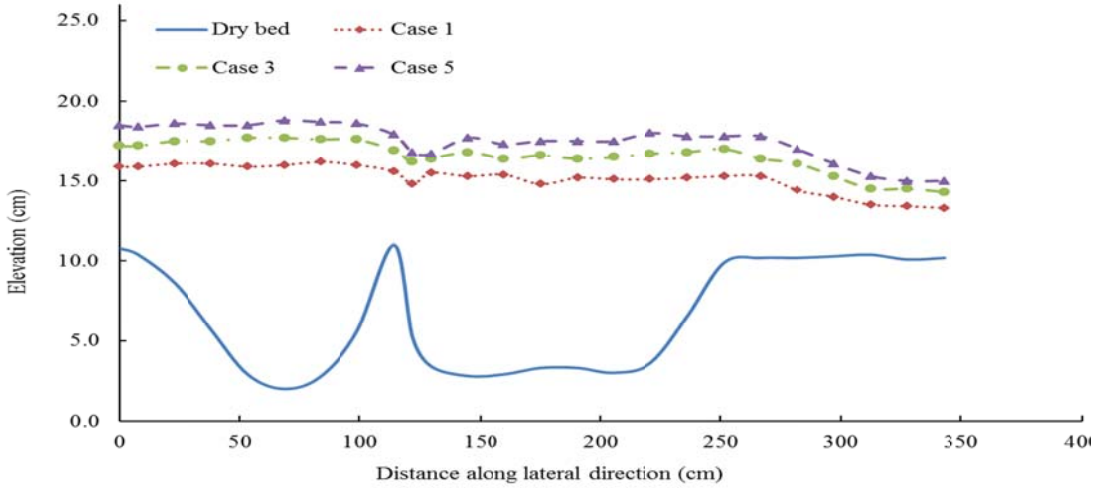

Fig. 5.15 Effect of inlet discharge on flow depth in the lateral direction

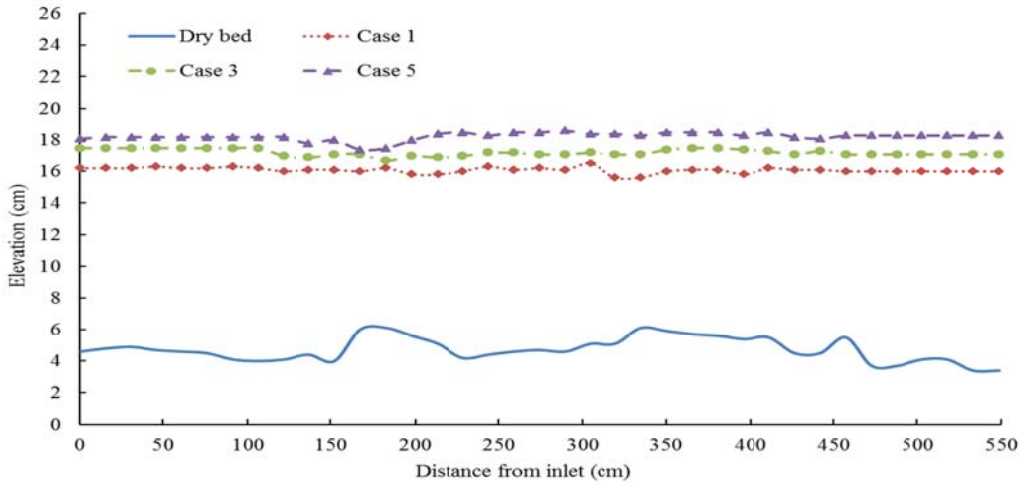

(a) Y3

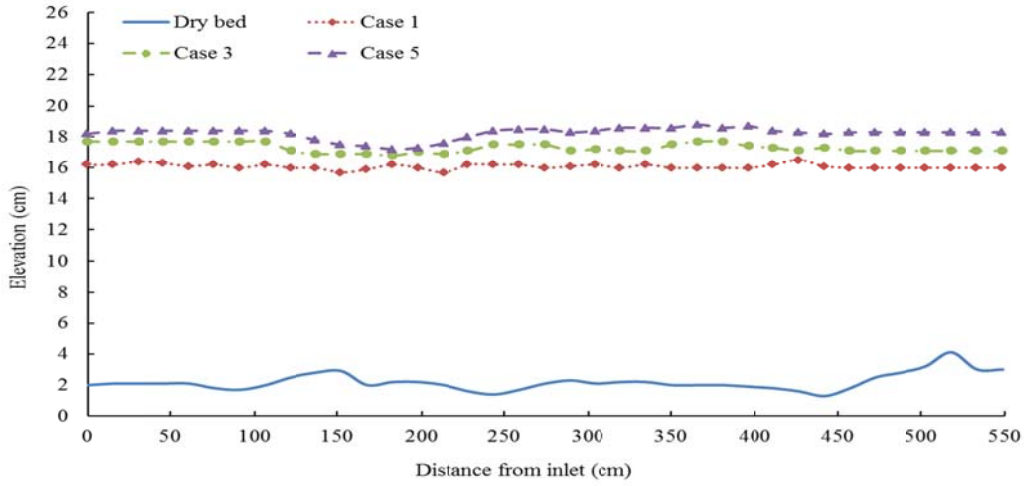

(b) Y5

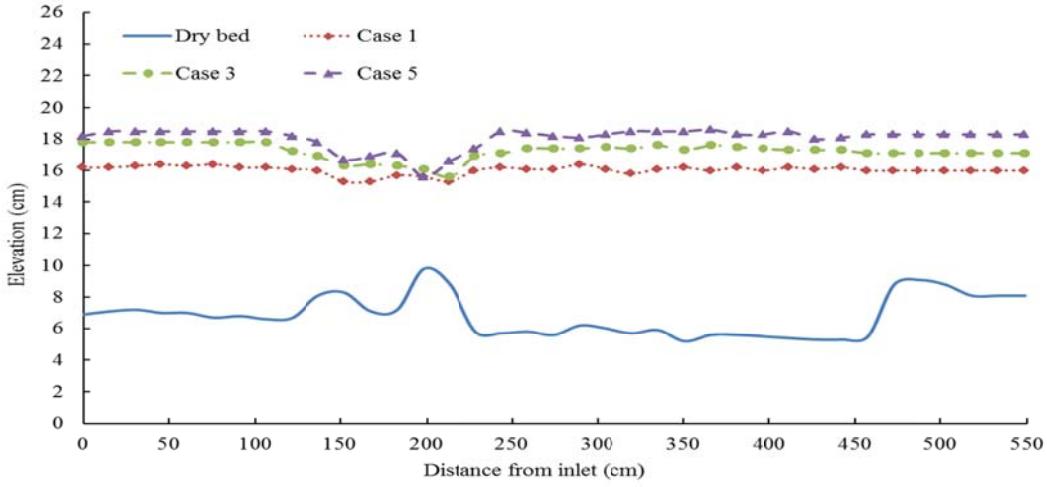

(c) Y7

Fig. 5.16 Effect of inlet discharge on flow depth along (a) Y3; (b) Y5; (c) Y7

5.9 Effect of structures from flood-plain

The outflow of the main channel through the breach impacts the structures located in these areas and the propagation of the flood wave is influenced by the local topography including these structures. Results for the flow depth with and without the structures are presented in Fig. 5.13. There is no effect of the structures on the flow field in the main channel. However, the flow in the flooded zone is influenced by the structures. The structures act like obstacles and thus, the flow area is less reduced. This results in decrease in velocity and increased flow depth near the structures. The flow depth in the flooded zone decreases significantly in the absence of the structures. Thus, the velocity could not be measured at these grid points by using ADV. The wave like water surface in case 6 has been observed in repeated experiments. This may be due to the formation of vortices at high discharge and irregular bed topography.

The next section describes the hydraulics of steady flow at the breach by using a generalized modeling approach.

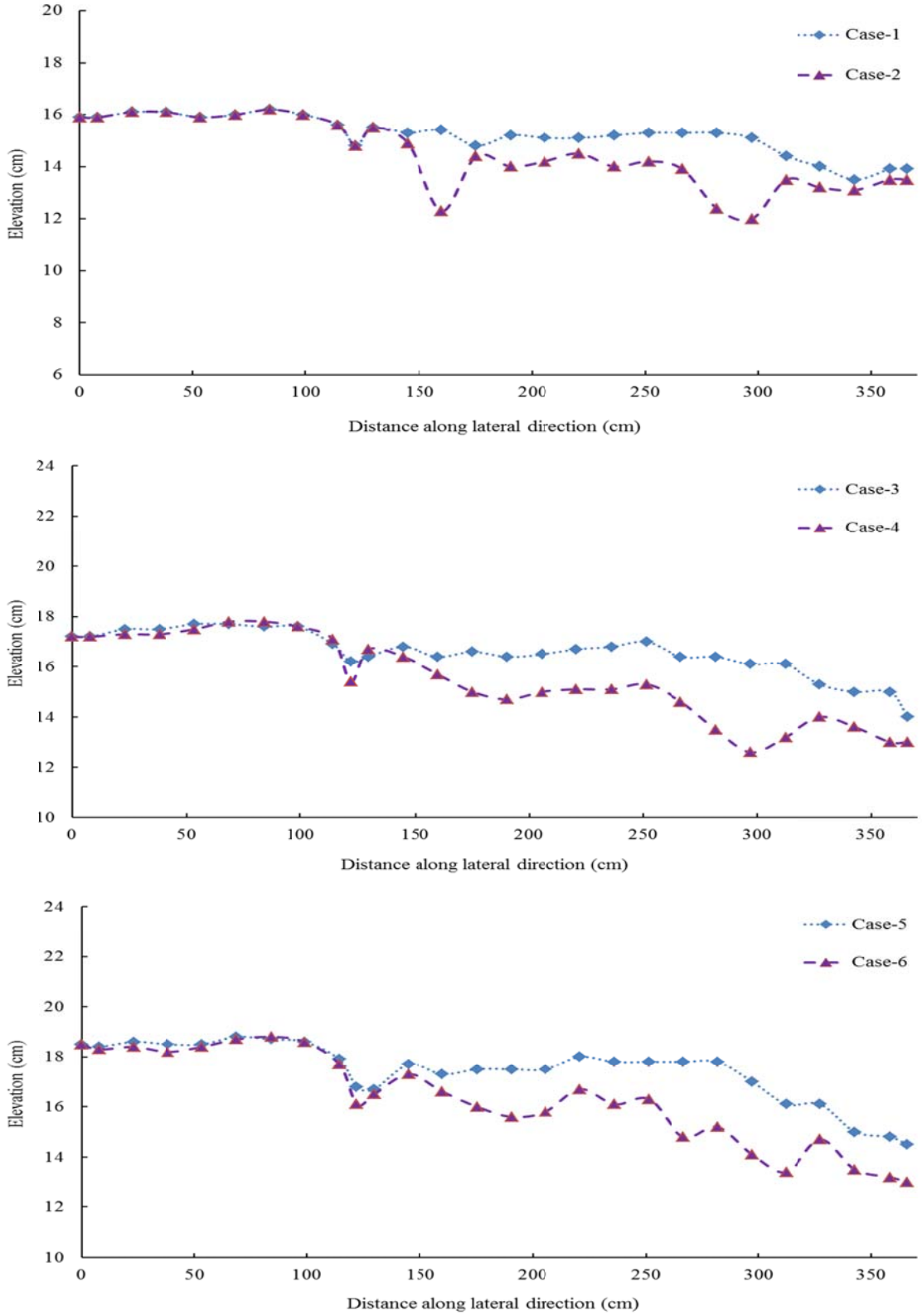

Fig. 5.17 Effect of structures on flow depth along X-24

5.10 Prediction by the generalized model

The generalized model developed in Chapter 4 is applied to predict the results for the case study, i.e. 17th Street Canal breach. The data for the generalized model as given in Table 5.2 is used for the purpose. The three cases (refer Table 5.1) with the structure in the flood plain are considered. Equations 4.11 and 4.12 are used to compute the flow depth at the breach. Note that 17th Street canal breach had a closed downstream end in the main channel, thus, $\xi = 1$. The K value is obtained by using Eq. 4.21.

Table 5.2: Prediction of the 17th Street Canal Breach by the generalized model

Model parameter	Case 1	Case 3	Case 5
Q_1 (m^3/s)	0.057	0.075	0.094
F_1	0.28	0.32	0.40
y_1 (m)	0.142	0.155	0.162
y_3 (m)	0.132	0.143	0.153
η_3 (m/m)	0.92	0.93	0.95
ω_2 (m/m)	2.34	2.34	2.34
ω_3 (m/m)	1	1	1
a (m/m)	8.45	7.74	7.40
C*	5.12	5.12	5.12
K	2.07	2.07	2.07
η_2	0.945	0.933	0.894
Predicted y_2 (m)	0.134	0.145	0.145

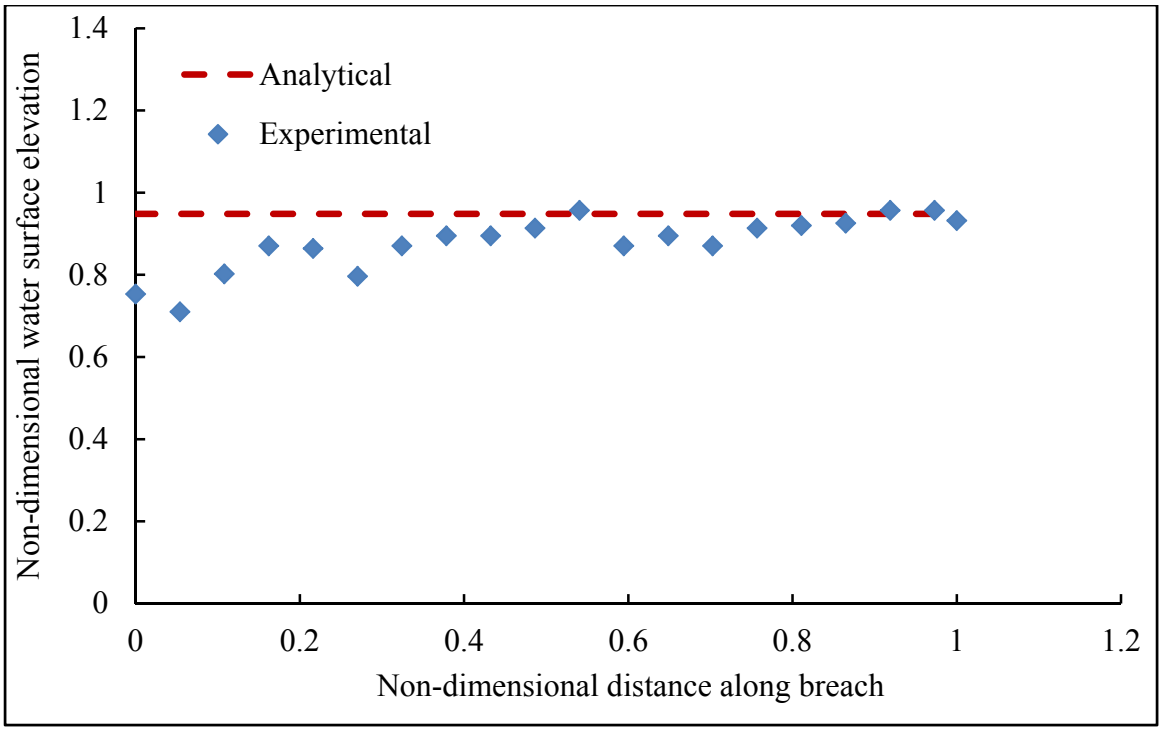

Fig. 5.18 Comparison of flow depth along the breach for Case 1

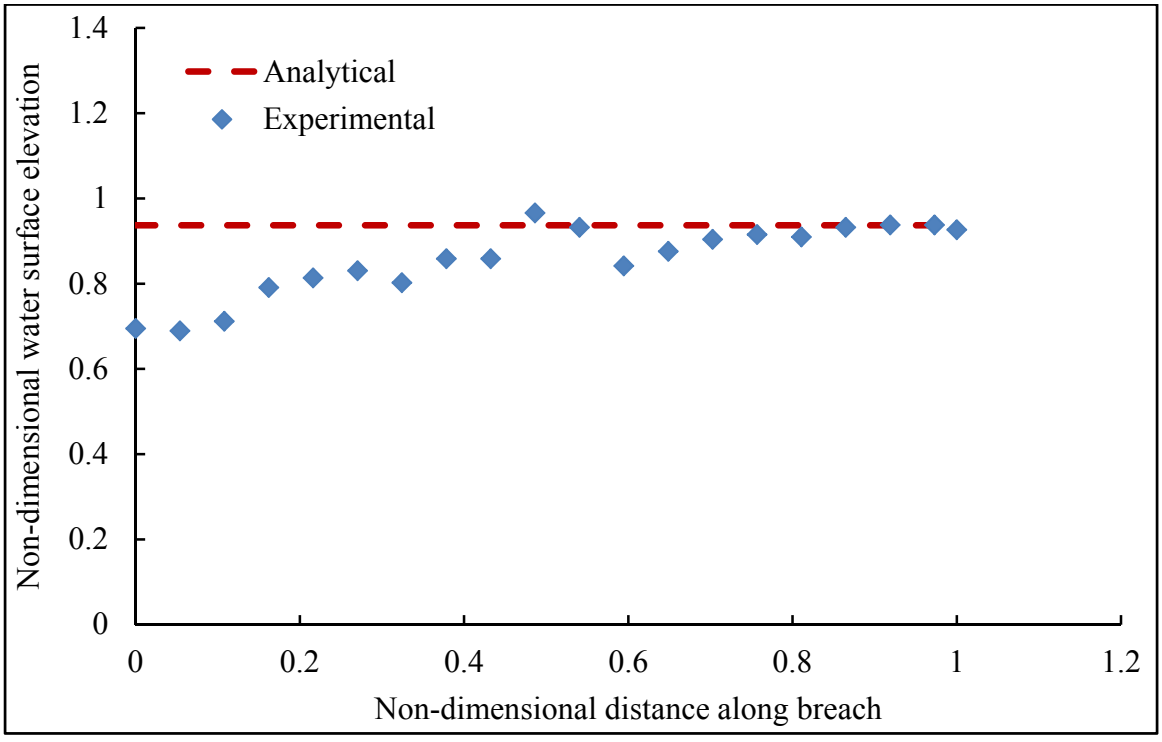

Fig. 5.19 Comparison of flow depth along the breach for Case 3

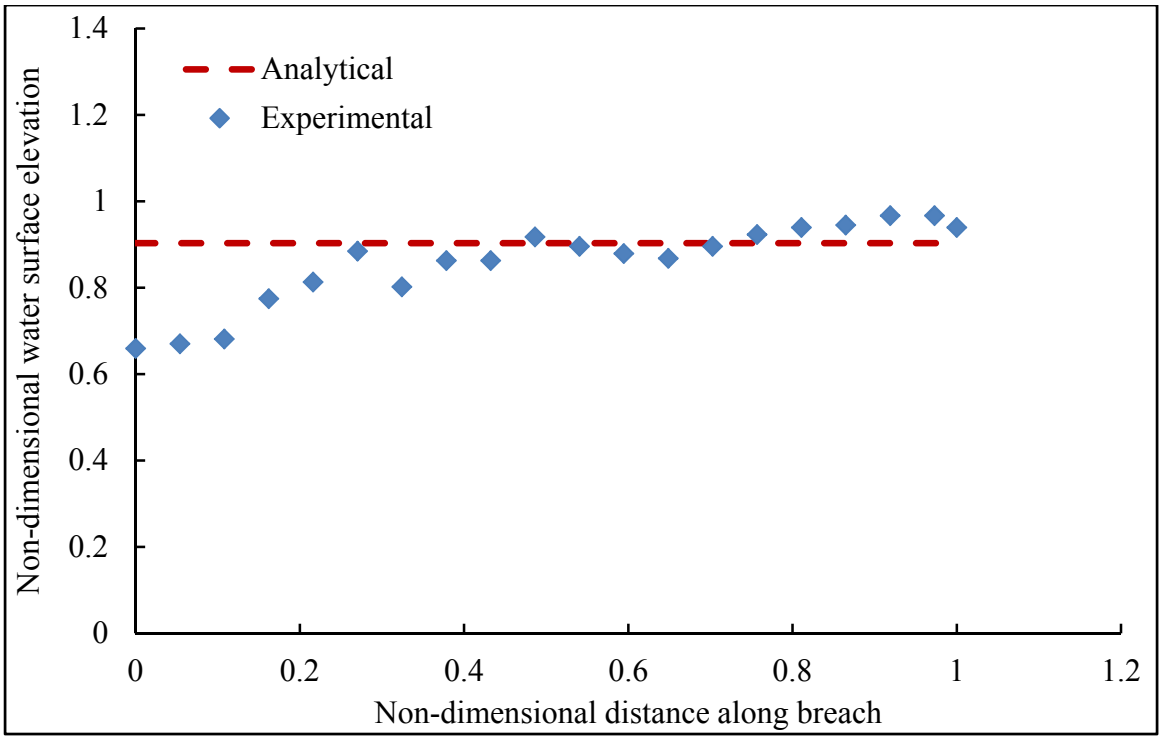

Fig. 5.20 Comparison of flow depth along the breach for Case 5

The non-dimensional flow depths at the breach computed by using the analytical model are 0.945, 0.933 and 0.894, for Cases 1, 3 and 5, respectively. A comparison of the detailed measurements and the approximate results from the analytical model indicates that the average flow depth at the breach is over-predicted by 70.0 percent, approximately. However, the water surface elevations with respect to the deepest bed level as shown in Figs. 5.18, 5.19 and 5.20, indicate that it is over-predicted by 7 percent, approximately. The difference in the results may be attributed to the undulations on the channel bed. Note that the channel cross-section is trapezoidal and there are several ditches on the bed.

5.11 Numerical simulations*

The 17th Street Canal breach is simulated by the widely used computational fluid dynamics (CFD) software FLUENT 6.3.26 (FLUENT 2006). The three-dimensional RANS equations for incompressible fluid flow for open channel flows are used. Three-dimensional, steady, pressure based solver with absolute velocity formulation and cell based gradient option are chosen as the numerical scheme. In addition, the volume of fluid (VOF) approach for tracking the free surface and the K-ε turbulence model are applied. The horizontal grid spacing is 0.02 m and the vertical grid is 0.005 m at the bottom and exponentially increases till 1.2. Details of the solution technique are given in FLUENT (2006).

Results for the water surface profile and the velocity distribution are presented in Figs. 5.21 and 5.22, respectively. The over-all match between the simulated and the experimental results is satisfactory. The water surface profiles along the longitudinal (Fig. 5.21a) and lateral direction (Fig. 5.21b) show that the numerical simulations over-predict the flow depth, marginally. The simulated velocity field indicates that the match is not that good near the bed, for few locations. Note that the 'Law of the Wall' is imposed by FLUENT while the ADV cannot be used very near the bed. In addition, high undulations on the channel bed may have contributed to this difference.

Main conclusions of the present dissertation are presented in the next chapter.

* This work is based on the following collaborative research:
Riahi-Nezhad, C. K., Reddy, H. P., Mohapatra, P. K., Chaudhry, M. H., and Imran, J. (2013). "Simulation of the 17th Street Canal Breach by a CFD approach", under preparation.

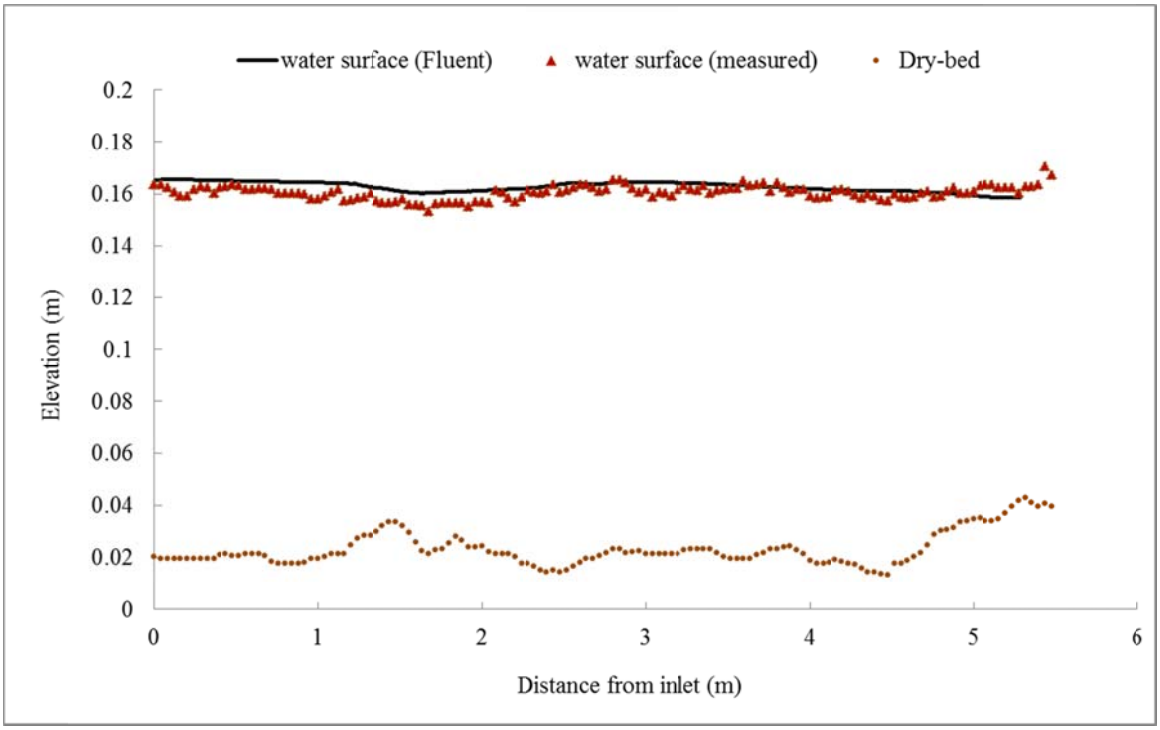

(a) Along Y5

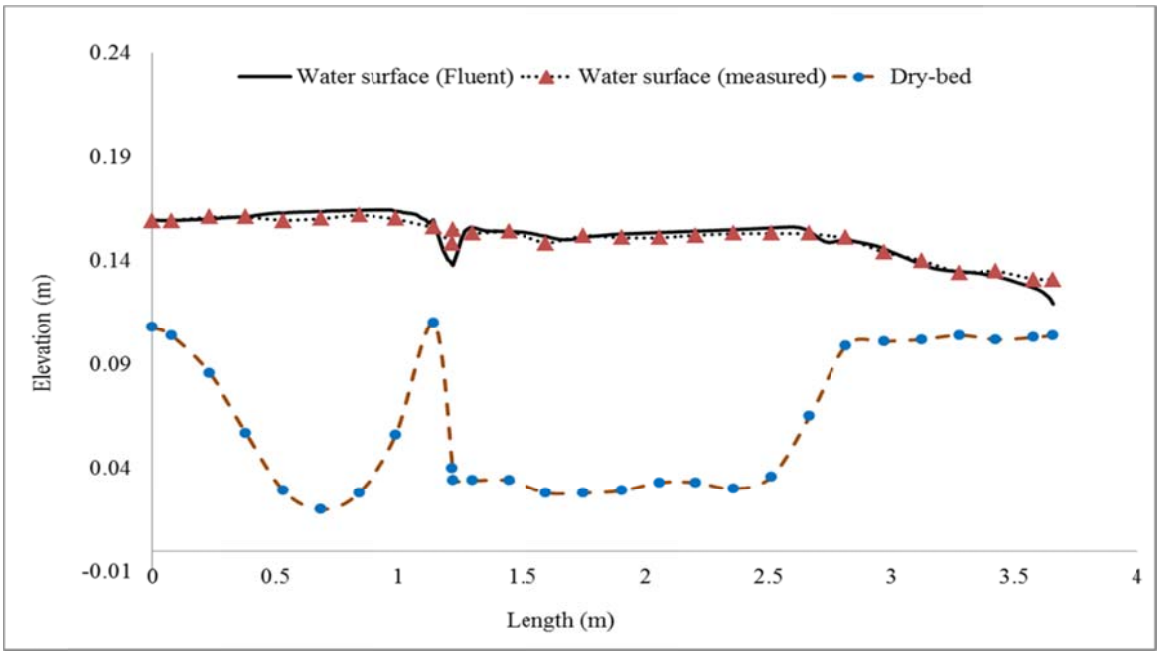

(b) Along X24

Fig. 5.21 Numerical and experimental water surface profile (Case 1)

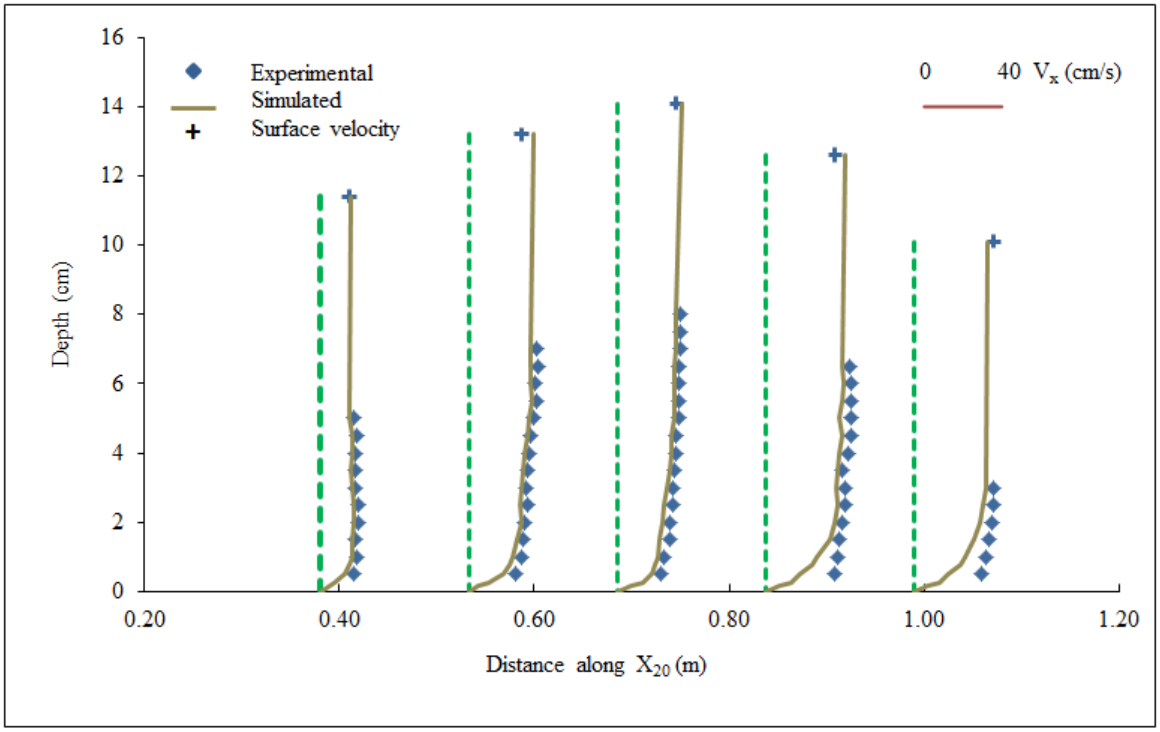

(a) X – velocity

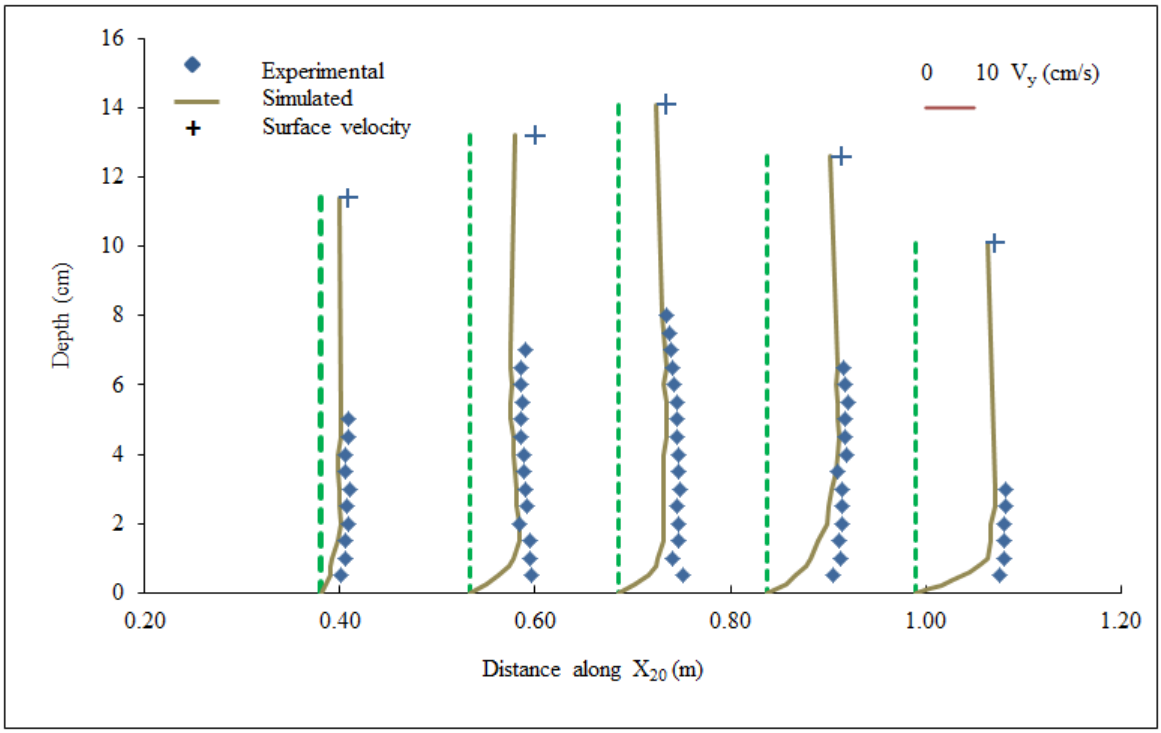

(b) Y - velocity

Fig. 5.22 Numerical and experimental velocity distribution (Case 1)

Chapter 6

SUMMARY AND CONCLUSIONS

6.1 Summary

Steady flow past a breached levee (SFBL) was studied in this dissertation through a generalized model and a case study. The generalized experimental set-up consisted of a main channel with an opening on its side wall and an adjustable sluice gate on its downstream end. Water surface elevation and the three-dimensional velocity field under the free surface were measured by a point gauge and an Acoustic Doppler Velocimeter (ADV), respectively. The ADV data were filtered before analysis. Eleven different flow conditions were considered. Time-averaged measured values of velocity field, and free surface elevation were presented. In addition, Froude Number, turbulent kinetic energy (TKE) and bed shear stress were computed from the measured parameters. A generalized analytical model was developed for SFBL by assuming that the inflow to the channel is divided into two separate zones of flow, one going out through the channel outlet and the other through the breach. The analytical model predicts the approximate flow depth and velocity at the breach from the known flow depths at inlet and outlet discharge at inlet, channel widths and breach length. The model parameters were estimated utilizing the experimental results. Simplified equations were also obtained for special cases such as (i)no flow at the channel outlet, (ii)breach length equal to channel width and (iii)equal flow depths at channel inlet and outlet. The 17th Street Canal breach was used as a

case study for SFBL. Detailed measurements of the flow field for six different flow conditions were performed on a 1:50 scale hydraulic model. The model used the actual topography of the channel bed and the area beside the breach, including the structures. Results included velocities, surface profiles, turbulent kinetic energy and bed shear stress. Effects of inlet discharge and nearby structures on the flow field were presented. The generalized analytical model was also used to predict the approximate flow depth and velocity at the breach for the 17th Street Canal breach and results obtained from the detailed measurements and from the analytical model were compared.

6.2 Conclusions

The main conclusions of the present study are presented in the following three parts.

6.2.1 Generalized experimental model

1. Flow is one dimensional at the channel inlet and outlet and it is three dimensional at the breach. Using the inlet velocity as the scale, the recorded maximum non-dimensional velocity in the breach varies from 1.25 to 2.16 for the cases considered in the present study.
2. There is a zone of depression on the water surface levels. The size of this zone is less than half of the breach length. The flow depth along the breach first decreases and attains a minimum value and then increases. The minimum breach flow depth varies from 49 percent to 79 percent of the flow depth at channel inlet.
3. The Froude Number map shows the flow tends to attain critical condition at breach.

4. The maximum bed shear stress occurs in a zone near the breach including a small part of the channel. This zone is prone to scour.
5. The maximum turbulent kinetic energy exists near the breach and it indicates a high degree of turbulence in the region.

6.2.2 Generalized analytical model

1. The estimated model parameters are C* = 5.12 and the correction factor for the stream-line curvature, K, depends on the breach length and breach discharge ratio.
2. The analytical model is easy to use and predicts only approximate values for the flow depth and discharge at the breach.
3. The predicted flow depths at the breach are more accurate than the predicted breach discharges.
4. The analytical model over-predicts the breach discharges when it is more than 70 percent of the discharge at the inlet.
5. Predicted non-dimensional breach flow depth ranges from 0.74 to 0.94 of the inflow water depth for the cases considered in this study.

6.2.3 17th Street Canal Breach

1. Flow is one dimensional at the channel inlet, becomes two dimensional as it approaches the breach and is three dimensional in the breach. There is a recirculation zone downstream of the breach due to the zero flow condition at the channel outlet.

6. Using the inlet velocity as the scale, the recorded maximum non-dimensional velocity in the breach is observed to be from 1.3 to 1.5.
7. There is a zone of depression on the water surface levels near to the breach. The maximum water surface slopes along the longitudinal and lateral directions are 0.01 and 0.1, respectively.
8. The Froude Number map shows the flow is subcritical in the entire flow domain.
9. The maximum non-dimensional bed shear stress occurs near the breach.
10. The maximum non-dimensional turbulent kinetic energy exists near the breach.
11. The structures in the flooding zone have only marginal effects on the flow field in the main channel. However, the flow depth at breach increases and velocity at breach decreases due to the structures.
12. Comparing the results obtained by detailed measurements and the analytical model, the analytical model over-predicts the flow depth by 70 percent. However, the water surface elevation with respect to the deepest bed is over-predicted by 7 percent, only. Differences in the results may be attributed to the unevenness in the bed topography.
13. The detailed measurements may be used to develop numerical models appropriate for levee breach flows.

6.3 Recommendations for future studies

The following researches may be taken up as extension of the present study.

1. All the cases considered in the present study are for rigid bed flow conditions. However, all natural channels are with mobile beds. Experiments with mobile

bed flow conditions may be performed to understand the scour pattern and sediment transport under levee breach flow.

2. The flow in the present study is steady for all cases considered. Thus, detailed flow field may be recorded for unsteady flow conditions at the channel inlet.
3. Experiments to understand evolution of the breaching process in earthen levees may be undertaken.
4. A numerical model may be developed for real-time simulation of the flood wave propagation due to a levee breach. The breach geometry as a function of time may be included.
5. Experiments to find efficient river training works for the closure of the breached levee may be conducted.

REFERENCES

1. Agelinchaab, M.; Tachie, M.F. (2008). "PIV study of separated and reattached open channel flow over surface mounted blocks". Journal of Fluids Engineering, Vol. 130, No. 6, 061206-1-9.
2. Barkdoll, B. D., Haen, B. L. and Odgaard, A. J. (1998). "Experimental Comparison of Dividing Open-Channel with Duct Flow in T-Junction", Journal of Hydraulic Engineering, ASCE, Vol. 124, No. 1, pp. 92-95.
3. Bea, R.G. (2008). "Failure of the New Orleans 17th Street canal levee & floodwall during Hurricane Katrina", GeoCongress 08, New Orleans, Louisiana, USA.
4. Chanson, H. (1999). Hydraulics of Open Channel Flow: An Introduction – Basic Principles, Sediment Motion, Hydraulic Modeling, Design of Hydraulic Structures, Second Edition.
5. Chanson, H. (2008). "Acoustic Doppler Velocimetry (ADV) in the field and in the laboratory: Practical experiences". International Meeting on Measurements and Hydraulics of Sewers. The University of Queensland, Brisbane, Australia.
6. Connell, R.J.; Painter, D.J.; Beffa, C. (2001). "Two-dimensional flood plain flow. II: Model validation", Journal of Hydrologic Engineering, Vol. 6, No. 5, pp. 406-415.

7. Dunbar, J. B.; Britsch III, Louis D. (2008). "Geology of the New Orleans area and the canal levee failures", Journal of Geotechnical and Geoenvironmental Engineering, Vol. 134, No. 5, pp. 566-582.
8. Duncan, J. M.; Brandon, T. L.; Wright, S. G.; Vroman, N. (2008) "Stability of I-walls in New Orleans during Hurricane Katrina" Journal of Geotechnical and Geoenvironmental Engineering, Vol. 134, No. 5, pp. 681-691.
9. El Kadi Abderrezzak, Kamal; Lewicki, Leszek; Paquier, Andre; Riviere, Nicolas; Travin, Gilbert. (2011). "Division of critical flow at three-branch open-channel intersection". Journal of Hydraulic Research, Vol. 49, No. 2, p 231-238.
10. Elkholy M., Chaudhry, M.H. (2009). "Tracking Sandbags Motion during Levee Breach Closure using DPTV Technique", 33rd Congress, International Association of Hydraulic Engineering and Research. Vancouver, Canada.
11. Emelen, S. V. Soares-Frazão, S. Riahi-Nezhad, C., Chaudhry, M. H., Imran, J. and Zech, Y. (2012). "Experimental and numerical simulation of the 17th Street Canal Breach", Jl of Hydraulic Research, IAHR, Vol. No. 1, pp.1-12.
12. Emiroglu, M.E.; Agaccioglu, H.; Kaya, N. (2011). "Discharging capacity of rectangular side weirs in straight open channels". Flow Measurement and Instrumentation, Vol. 22, No. 4, p 319-30.
13. Faeh, R. (2007). "Numerical modeling of breach erosion of river embankments", Journal of Hydraulic Engineering, Vol. 133, No. 9, pp. 1000-1009.
14. Fluent (2006) FLUENT user's guide, Lebanon, NH; 2006.
15. Fujita, Y.; Tamura, T. (1987). "Enlargement of breaches in flood levees on plains", Natural Disaster Science, Vol. 9, No. 1, pp. 37-60.

16. Galperin, B., Kantha, L. H., Hassid, S., and Rosati, A. (1988). „„A quasi equilibrium turbulent energy model for geophysical flows.“ “ *J. Atmosph. Sci.*, 45, 55–62.

17. Han, Kun-Yeun; Lee, Jong-Tae; Park, Jae-Hong (1998). “Flood inundation analysis resulting from Levee-break”, Journal of Hydraulic Research, Vol. 36, No. 5, pp. 747-759.

18. Hou, A.; Laws, E. A.; Gambrell, R. P.; Bae, H.; Tan, M.; Delaune, R. D.; Li, Y.; Roberts, H. (2006). “Pathogen indicator microbes and heavy metals in lake pontchartrain following Hurricane Katrina”, Environmental Science and Technology, Vol. 40, No. 19, pp. 5904-5910.

19. Hsu, Chung-Chieh; Tang, Chii-Jau; Lee, Wen-Jung; Shieh, Mon-Yi. (2002). “Subcritical 90 equal-width open-channel dividing flow”. Journal of Hydraulic Engineering, Vol. 128, n 7, p 716-720.

20. Jaffe, D.A. Sanders, B.F. (2001). “Engineered levee breaches for flood mitigation’’, Journal of Hydraulic Engineering, Vol. 127, No. 6, pp. 471-479.

21. Kesserwani, G.; Vazquez, J.; Rivire, N.; Liang, Q. ; Travin, G.; Mos, R. (2010). “New approach for predicting flow bifurcation at right-angled open-channel junction”. Journal of Hydraulic Engineering, Vol. 136, n 9, p 662-668.

22. Kim, S. C., Friedrichs, C. T., Maa, J. P. Y., and Wright, L. D. (2000). “Estimating bottom stress in tidal boundary layer from Acoustic Doppler Velocimeter data.” *J. Hydraul. Eng.*, 126(6), 399-406.

23. Kotowski, A.; Wojtowicz, P. (2007). “The new method for limiting outflow from storm overflows”. Environment Protection Engineering, Vol. 33, No. 4, p 41-53.

24. Kozak, M. (1975). "An approximate method to calculate the effect of levee breaches upon flooding of rivers having a compound section", Acta Technica Academiae Scientiarum Hungaricae, Vol. 81, No. 3-4, pp. 235-48.
25. Kraus, C. Nicholas; Lohrmann, Atle; Cabrera, Ramon. (1994). "New Acoustic Meter for measuring 3-D laboratory flow". Journal of Hydraulic Engineering, Vol. 120, No. 3, p.406-412.
26. Lakshmana Rao, N.S.; Sridharan, K.; Yahia Ali Baig, M. (1970). "Experimental study of the division of flow in an open channel". Proceedings of the 3rd Australasian conference on hydraulics and fluid mechanics, 139-42.
27. Leonardo S. N.; Manuel G.; Jose D.; Pau C.; and Juan P. "Experimental Study of Subcritical Dividing Flow in an Equal-Width, Four-Branch Junction" Journal of Hydraulic Engineering, ASCE, Vol. 137, No. 10, pp. 1298-1305.
28. Munson, B.R., Young, D.F., Okishi, T.H.(1998) Fundamentals of fluid mechanics, 3rd Ed., John Wiley & Sons.
29. Neary, V. S. and Odgaard A. J. (1993). "Three-Dimensional Flow Structure at Open-Channel Diversions", Journal of Hydraulic Engineering, Vol. 119, No. 11, pp. 1223-1230.
30. Önen, Fevzi.; Agaççioglu, Hayrullah. (2007). "Scour at a side-weir intersection located on an alluvial river". Nordic Hydrology, Vol. 38, No. 2, p 165-176.
31. Pirzadeh, B.; Shamloo, H. (2007). "Numerical investigation of velocity field in dividing open-channel flow", Applied Mathematics for Science and Engineering. Proceedings of the 12th WSEAS International Conference on Applied Mathematics, 194-8.

32. Prastowo, T.; Griffiths, R.W.; Hughes, G.O.; Hogg, A.M. (2009). "Effects of topography on the cumulative mixing efficiency in exchange flows". Journal of Geophysical Research - Part C - Oceans, Vol. 114, n C8, p C08008.
33. Ramamurthy, A. S.; Duc, M. T.; Carballada, L. B. (1990). "Journal of Hydraulic Engineering, Vol. 116, No. 3, p 449-455.
34. Ramamurthy, A. S.; Qu, J.; and Vo, D. (2007). "Numerical and Experimental Study of Dividing Open-Channel Flows", Journal of Hydraulic Engineering, ASCE, Vol. 133, No. 10, pp. 1135-1144.
35. Rickly Hydrological Company: http://www.rickly.com/sm/Lory.htm
36. Rogers, J.D.; Boutwell, G.P.; Schmitz, D.W.; Karadeniz, D.; Watkins, C.M.; Athanasopoulos-Zekkos, A.G.; Cobos-Roa, D. (2008). "Geologic conditions underlying the 2005 17th Street Canal levee failure in New Orleans", Journal of Geotechnical and Geoenvironmental Engineering, ASCE, Vol. 134, No. 5, pp. 583-601.
37. Sanders, B.F.; Katopodes, N.D. (1999). "Active flood hazard mitigation. I: Bidirectional wave control", Journal of Hydraulic Engineering, Vol. 125, No. 10, pp. 1057-1070.
38. Sanders, Brett F.; Katopodes, Nikolaos D. (1999). "Active flood hazard mitigation. II: Omnidirectional wave control", Journal of Hydraulic Engineering, Vol. 125, No. 10, pp. 1071-1083.
39. Sarma, Arup Kumar; Das, Madan Mohan. (2003). "Analytical solution of a flood wave resulting from dike failure", Proceedings of the Institution of Civil Engineers: Water and Maritime Engineering, Vol. 156, No. 1, pp. 41-45.

40. Sasanakul, I.; Vanadit-Ellis, W.; Sharp, M.; Abdoun, T.; Ubilla, J.; Steedman, S.; Stone, K.(2008). "New Orleans levee system performance during Hurricane Katrina: 17th Street Canal and Orleans Canal North", Journal of Geotechnical and Geoenvironmental Engineering, Vol. 134, No. 5, pp. 657-667.
41. Sattar, Ahmed M. Abdel; Kassem, Ahmed A.; Chaudhry, M. Hanif (2008). **"**Case study: 17th street canal breach closure procedures", Journal of Hydraulic Engineering, ASCE, Vol. 134, No. 11, p 1547-1558.
42. Savant, Gaurav; Berger, Charlie; McAlpin, Tate O.; Tate, Jennifer N. (2011). "Efficient implicit finite-element hydrodynamic model for dam and levee breach", Journal of Hydrodynamics, Vol. 21, No. 5, pp. 633-639.
43. Seabergh, W.C. (2010). "Physical model study of wave and current conditions at 17th Street Canal breach due to Hurricane Katrina", Ocean Engineering, Vol. 37, No. 1, pp. 48-58.
44. Seed, R.B.; Bea, R.G.; Athanasopoulos-Zekkos, A.; Boutwell, G.P.; Bray, J.D.; Cheung, C.; Cobos-Roa, D.; Harder Jr., L.F.; Moss, R.E.S.; Pestana, J.M.; Reimer, M.F.; Rogers, J.D.; Storesund, R.; Vera-Grunauer, X.; Wartman, J. (2008). "New Orleans and Hurricane Katrina. III: The 17th Street drainage canal", Journal of Geotechnical and Geoenvironmental Engineering, Vol. 134, No. 5, pp. 740-761.
45. Seed, R.B.; Bea, R.G.; Athanasopoulos, A.G.; Boutwell, G.P.; Bray, J.D.; Cheung, C.; Collins, B.D.; Cobos-Roa, D.; Cohen-Waeber, J.; Harder, L.F.; Kayen, R.E.; Moss, R.E.S.; Pestana, J.M.; Porter, J.; Riemer, M.F.; Rogers, J.D.; Storesund, R.; Vera-Grunauer, X.; Wartman, J. (2007). "Investigation of levee

performance in Hurricane Katrina: The New Orleans drainage canals", Geotechnical Special Publication, No. 161, pp. 1-16.

46. Shabayek, Shazy; Steffler, Peter; Hicks, Faye. (1999). "Dividing flows in open channel junctions". Proceedings, Annual Conference - Canadian Society for Civil Engineering, Vol. 2, p 11-20.
47. Shamloo, H.; Pirzadeh, B. (2008). "Numerical investigation of velocity field in dividing open-channel flow", Advanced Topics on Water Resources, Hydraulics and Hydrology. Proceedings of the 3rd IASME/ WSEAS International Conference on Water Resources, Hydraulics & Hydrology (WHH'08), 27-31.
48. Stapleton, K. R., and Huntley, D. A. (1995). „„Sea bed stress determination using the inertial dissipation method and the turbulent kinetic energy method." " *Earth Surface Processes and Landforms*, 20, 807–815.
49. Steedman, R. Scott; Sharp, Michael K.(2011). "Physical modelling analysis of the New Orleans levee breaches", Proceedings of the Institution of Civil Engineers: Geotechnical Engineering, Vol. 164, No. 6, pp 353-372.
50. Song, T. C., and Chiew, Y. M. (2001). "Turbulence measurement in nonuniform open channel flow using acoustic Doppler velocimeter (ADV)." *J. Hydraul. Eng.*, 127(3), 219–232.
51. Sontek, San Diego, CA.(2001). Acoustic Doppler Velocimeter Technical Documentation.
52. Sony:http://store.sony.com/webapp/wcs/stores/servlet/ProductDisplay?catalogId=10551&storeId=10151&langId=-1&partNumber=DCRSR47.

53. USACE (2007). Interagency Performance Evaluation Taskforce (IPET), *Final Rep.*, United States Army Corps of Engineers, March-June 2007. Available from: http://biotech.law.lsu.edu/katrina/ipet/ipet.html.

54. Van Emelen, Sylvie; Soares-Frazo, Sandra; Riahi-Nezhad, Cyrus K.; Hanif Chaudhry, M.; Imran, Jasim; Zech, Yves. (2012). "Simulations of the New Orleans 17th Street Canal breach flood", Journal of Hydraulic Research, Vol. 50, No. 1, pp. 70-81.

55. Vorogushyn, S.; Merz, B.; Lindenschmidt, K.-E.; Apel, H. (2010). "A new methodology for flood hazard assessment considering dike breaches", Water Resources Research, Vol. 46, W08541, 17 PP.

56. Voulgaris, G.; Trowbridge, J. H. (1998). "Evaluation of the acoustic doppler velocimeter (ADV) for turbulence measurements". Atmospheric and Oceanic Technology, 15:272 p.289

57. Wahl, L. T. (2000). "Analyzing ADV Data Using WinADV". Joint Conference on Water Resources Engineering and Water Resources Planning & Management. Minneapolis, Minnesota.

58. Wikipedia (2011). http://en.wikipedia.org/wiki/Levee_breach.

59. Wikipedia (2012). http://en.wikipedia.Org/wiki/effects of Hurricane Katrina in New Orleans.

60. Walsh, B (2006). "Corps chief admits to design failure", The Times- Picayune, quotation attributed to Lt. General Carl Strock, April 6.

61. Wolfautomation (2011)http://www.wolfautomation.com/assets/15/UNAM30b.pdf

62. Ye, Wen; Li, Sheng; Wu, Minquan. (1995). "Experimental investigation on dividing flow through a channel by LDA". Journal of Hydrodynamics, Vol. 7, No. 4, p 42-46.
63. YU, M.; DENG, Y.; QIN, L.; WANG, D.; CHEN, Y. (2009). "Numerical Simulation of Levee Breach Flows Under Complex Boundary Conditions", Journal of Hydrodynamics, Vol. 21, No. 5, pp. 633-639.
64. Yue, W.1; Lin, C.-L.; Patel, V.C. (2005). "Transactions of the ASME", Journal of Fluids Engineering, Vol. 127, No. 5, pp. 858-64.
65. Zhang, Xiao-Feng; Yu, Ming-Hui. (2001). "Numerical simulation of bed deformation in dike burst", Journal of Hydrodynamics, Vol. 13, No. 4, pp. 60-64.
66. Zhicheng Long.; Zheng Shen.; Dapeng Wu.; Jianhua Qin.; Bingcheng Lin. (2007). "Integrated multilayer microfluidic device with a nanoporous membrane interconnect for online coupling of solid-phase extraction to microchip electrophoresis". Lab on a Chip, Vol. 7, No. 12, p 1819-24.

Appendix – 1

HISTORICAL EVENTS OF LEVEE BREACH[1]

- 1421 - The St. Elizabeth's flood of 1421 in the Netherlands was caused when dikes were breached in a number of places during a heavy storm near the North Sea coast and the lower lying polder land was flooded. A number of villages were swallowed by the flood and were lost, causing between 2,000 and 10,000 casualties.
- 1570 - The All Saints' Flood caused dike breaches on the west coast of the Netherlands. The total number of dead, including in foreign countries, must have been above 20,000, but exact data is not available. Tens of thousands of people became homeless. Livestock was lost in huge numbers. Winter stocks of food and fodder were destroyed.
- 1651 - During the St. Peter's Flood the city of Amsterdam was flooded after several breaches of the dikes, the coasts of Netherlands and Northern Germany were heavily battered.
- 1686 - The St. Martin's flood flooded large parts of the province of Groningen in the Netherlands. 1558 people, 1387 horses and 7861 cows died. 631 houses were swept away and 616 houses damaged.

[1] Adopted from http://en.wikipedia.org/wiki/Levee_breach.

- 1703 - The Great Storm of 1703 caused havoc between Wales and Friesland, it was the most severe storm or natural disaster ever recorded in the southern part of Great Britain. Several dikes were breached in the Netherlands. Between 8,000 - 15,000 lives were lost overall.
- 1717 - The Christmas flood of 1717 was the result of a northwesterly storm, which hit the coast area of the Netherlands, Germany and Scandinavia on Christmas night of 1717. In total, approximately 14,000 people drowned. It was the last large flood in the north of the Netherlands.
- 1809 - When De Biesbosch in the Netherlands froze ice dams caused a rapid rise in waterlevels in the Meuse, Waal and Merwede, which resulted in dike breaches.
- 1820 - The Alblasserwaard in the Netherlands flooded after a dike breach
- 1825 - Parts of Groningen, Friesland and Overijssel in the Netherlands were flooded after dike breaches
- 1855 - Large parts of the central Netherlands were flooded after the Lower Rhine was dammed by ice and dikes were breached
- 1916 - A storm surge on the Zuiderzee coincided with a large volume of water flowing down the Rhine and Meuse rivers causing dozens of dike breaches
- 1927 - The Great Mississippi Flood of 1927 occurred when the Mississippi River breached levees and flooded 27,000 square miles (70,000 km2), killing 246 people in seven states and displacing 700,000 people.
- September 1928: Storm surge from the Okeechobee Hurricane breaches levees surrounding Lake Okeechobee, killing an estimated 2500 people.

- Dec 24, 1955 - Just after midnight, a levee on the west bank of the Feather River collapsed just south of Yuba City, Ca., resulting in the drowning of 38 residents.
- Jan 3, 1976 - A dike failed on the Vliet, a tributuary of the Rupel in Belgium. The village of Ruisbroek was flooded to a depth of 3m and over 2000 people had to be evacuated. This disaster prompted the drafting of Belgium's Sigma Plan as a counterpart to the Dutch Delta Plan.
- Feb 20, 1986 - A levee on the south bank of the Yuba River collapsed at the northern Sacramento Valley community of Linda, California in Yuba County, inundating 36 square miles (93 km2) and destroying 600 homes.
- Jan 31, 1995 - 250,000 people were evacuated from central parts of the Netherlands after river dikes had become dangerously unstable. The dikes were not breached after intensive works to stabilize the embankments, aided by military engineers.
- Jan 2, 1997 - A levee on the west bank of the Feather River collapsed at the northern Sacramento Valley community of Arboga, California in Yuba County, killing three people. More than 100,000 people in Yuba and Sutter counties were evacuated.
- 26 Aug 2003 - A dike near Wilnis in the Netherlands failed and flooded that town due to the dike not having enough weight to withstand the water pressure of the canal after a long drought. 1,500 inhabitants were evacuated with no loss of life.
- 3 June 2004 - Jones Tract, an inland island that is protected by a series of levees located in the Sacramento-San Joaquin Delta, failed.

- January 5, 2008 - A levee in Fernley, Nevada burst, flooding portions of the town and forcing the evacuations of 3,500 residents.
- September 14, 2008 - a levee in Munster, Indiana broke on the Little Calumet River resulting in flooding in most of Munster.
- August 8, 2009 - Levees fail in Southern Taiwan due to Typhoon Morakot causing widespread flooding in many regions.
- February 26, 2010 - Levees were submerged by wind and a huge tide in Vendée, in Western France because of the Xynthia storm.
- April 26, 2011 - A levee on the Black River in Poplar Bluff, Missouri failed, sending water rushing into rural Butler County, Missouri.
- October 30, 2012 - A levee on the Hackensack River was breached by Hurricane Sandy, flooding city of Moonachie, Little Ferry and Carlstadt with 1.2 to 1.5 m of water.

Appendix – 2

RESULTS OF GENERALIZED EXPERIMENTAL MODEL

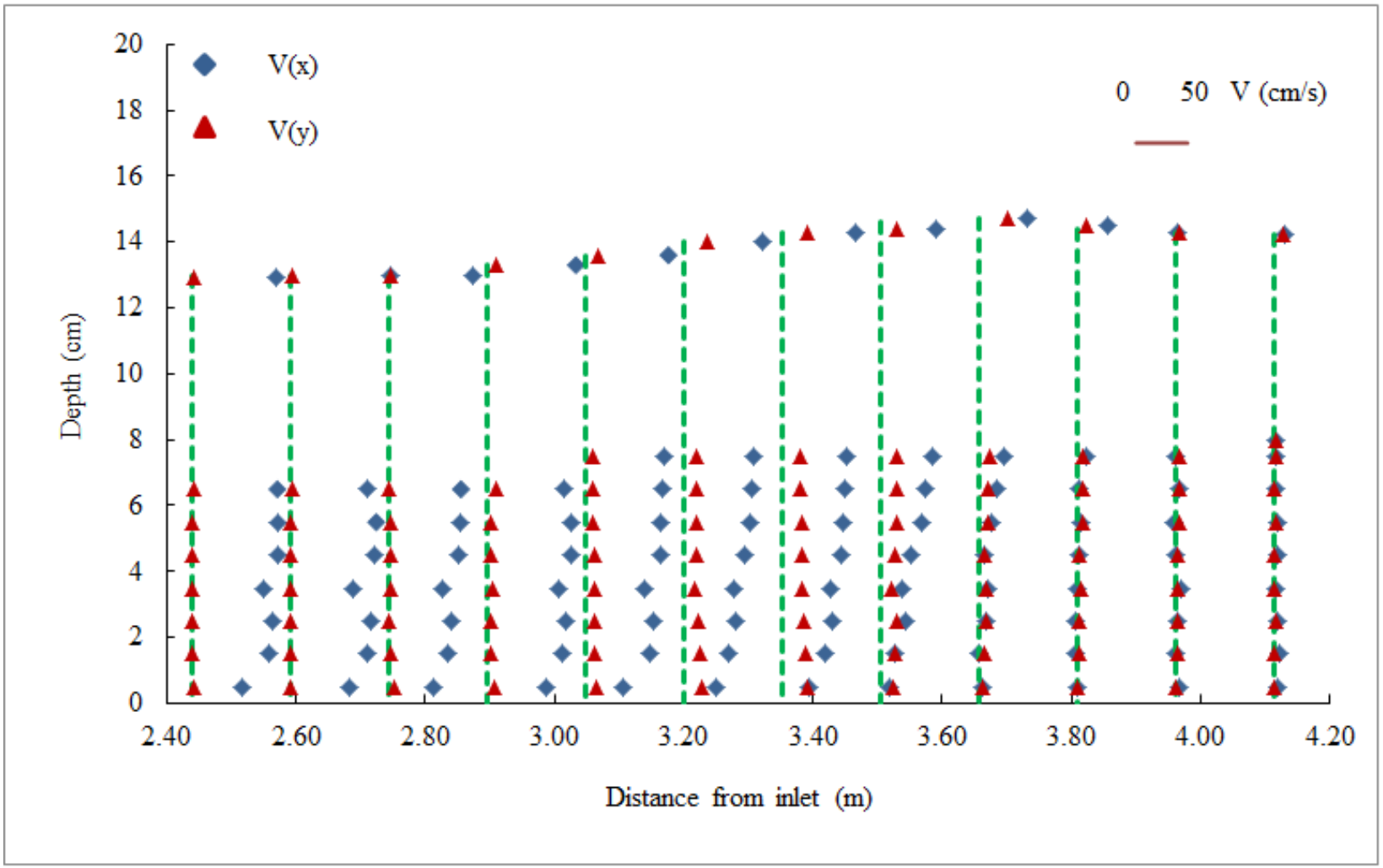

(a) Along Y1

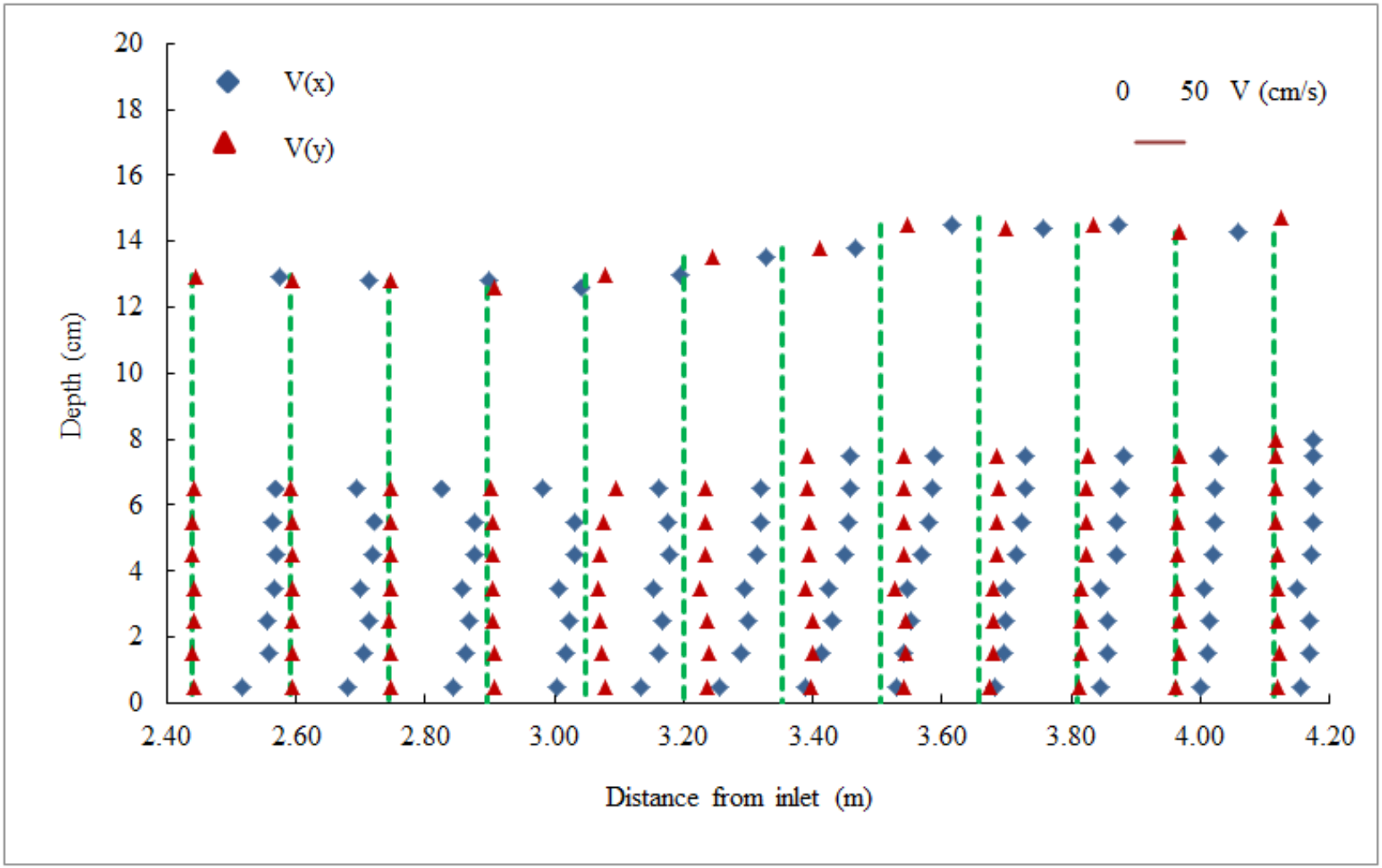

(b) Along Y2

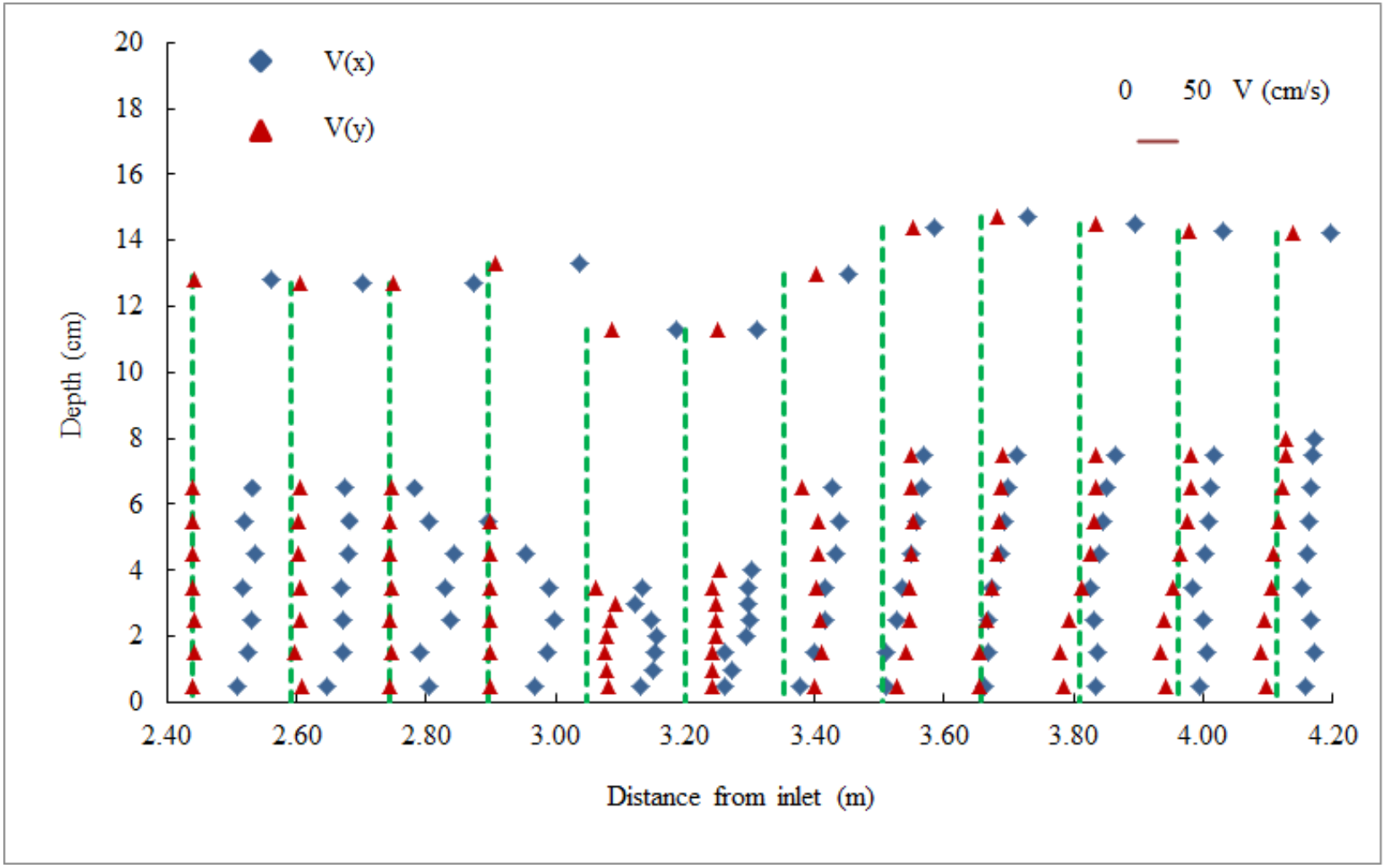

(c) Along Y3

Fig. A2.1 Measured results for velocity distribution (Case G5)

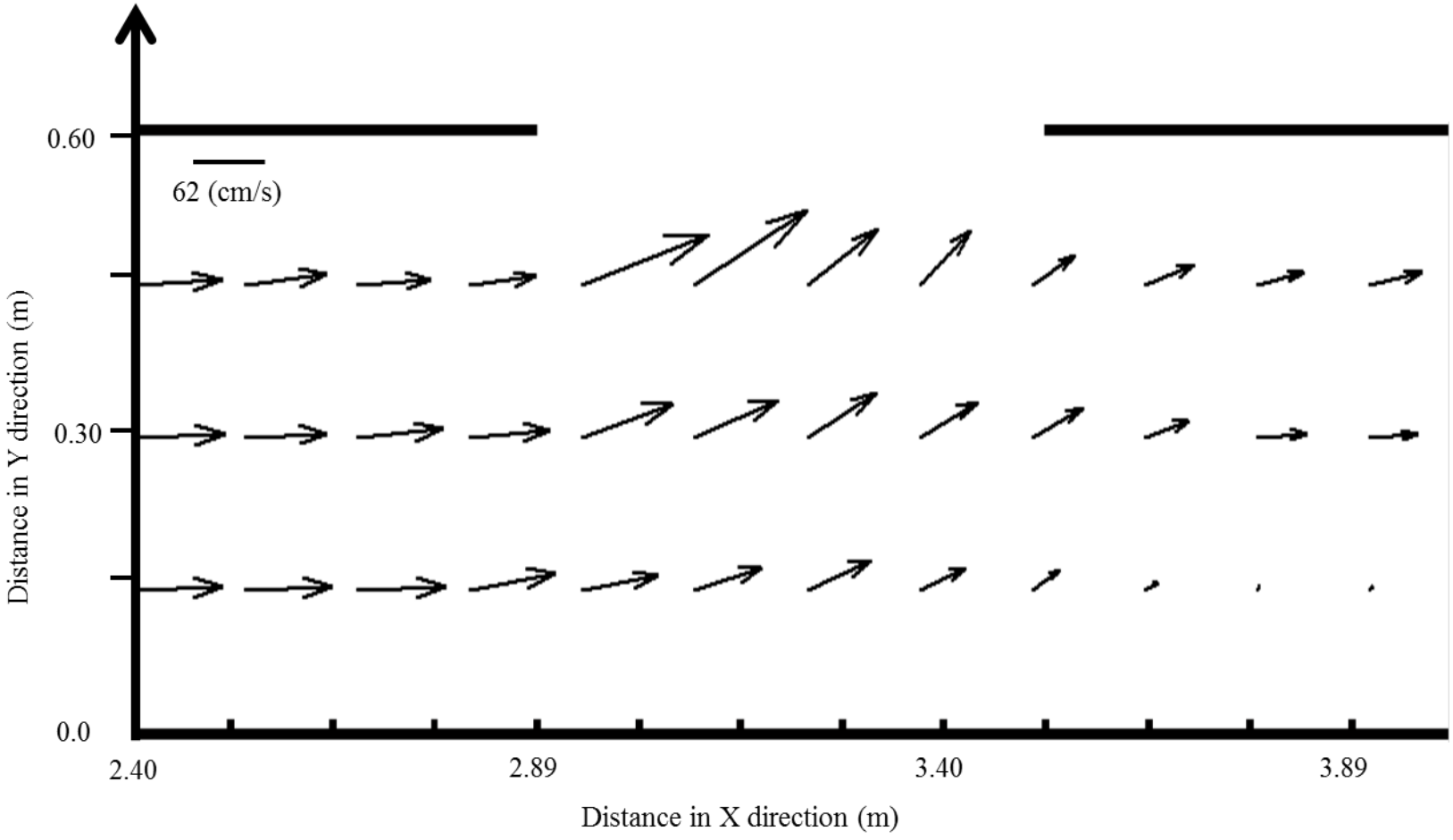

Fig. A2.2 Average velocities (Case G5)

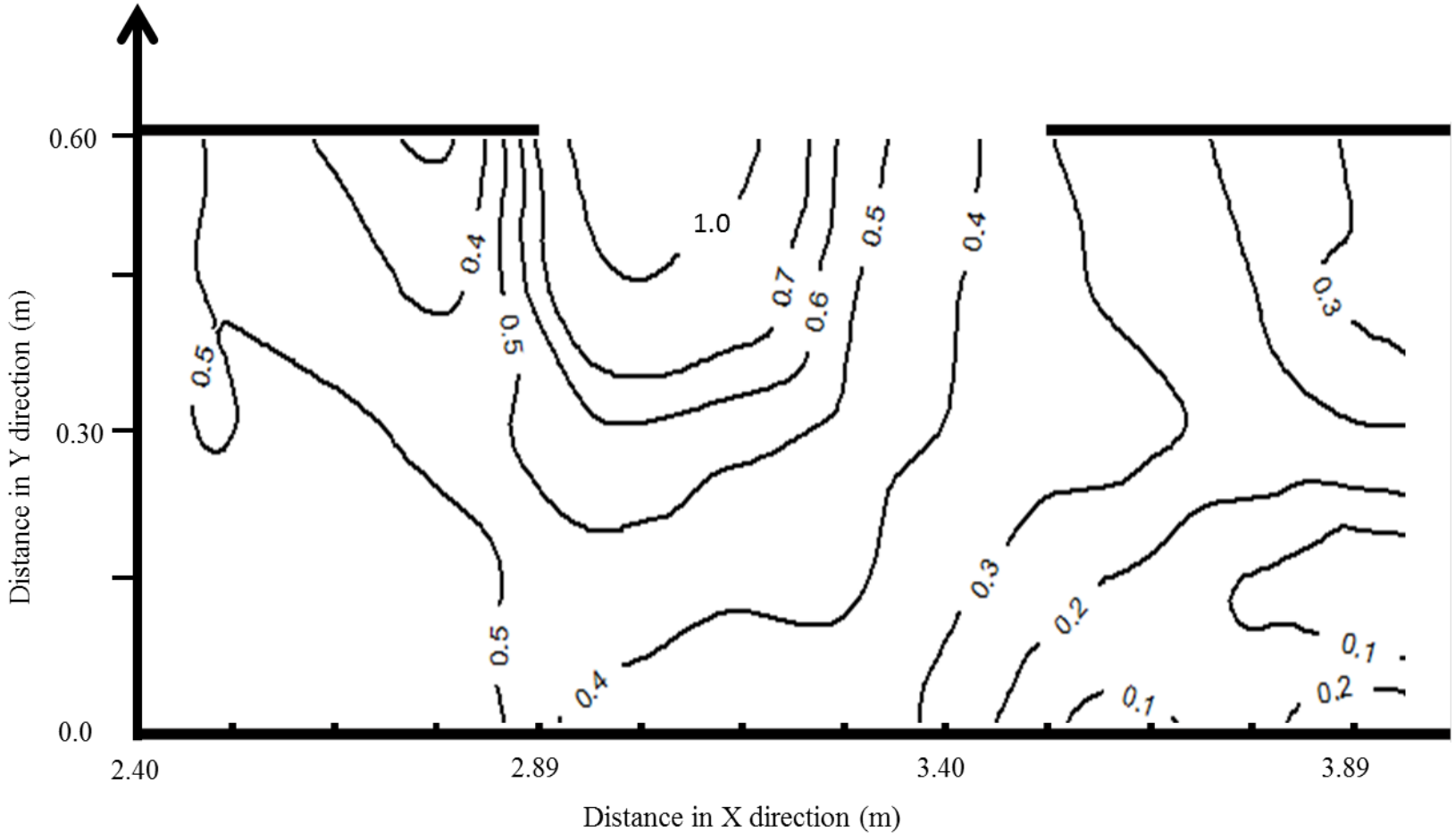

Fig. A2.3 Distribution of Froude Number (Case G5)

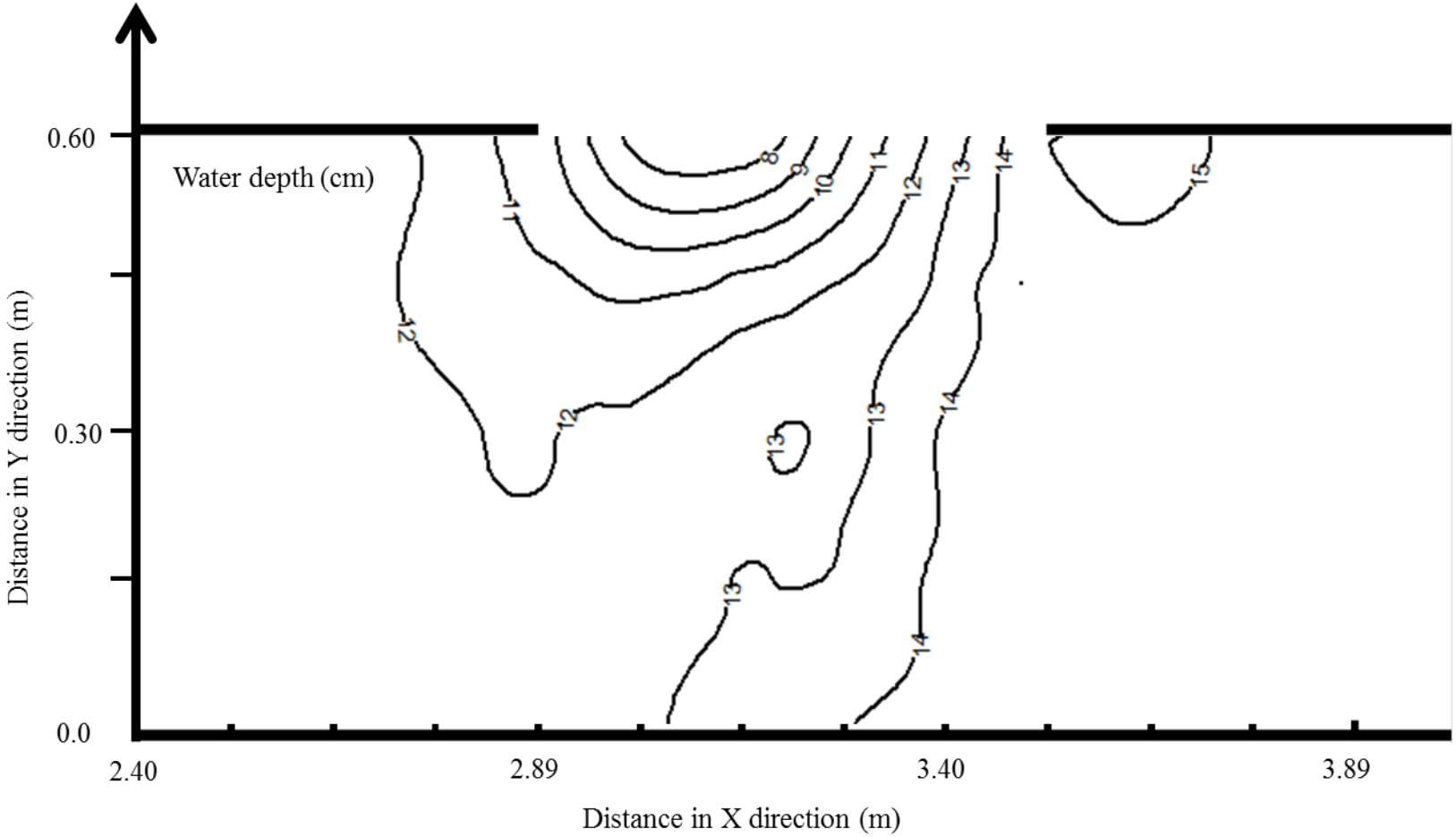

Fig. A2.4 Contours of flow depth (Case G5)

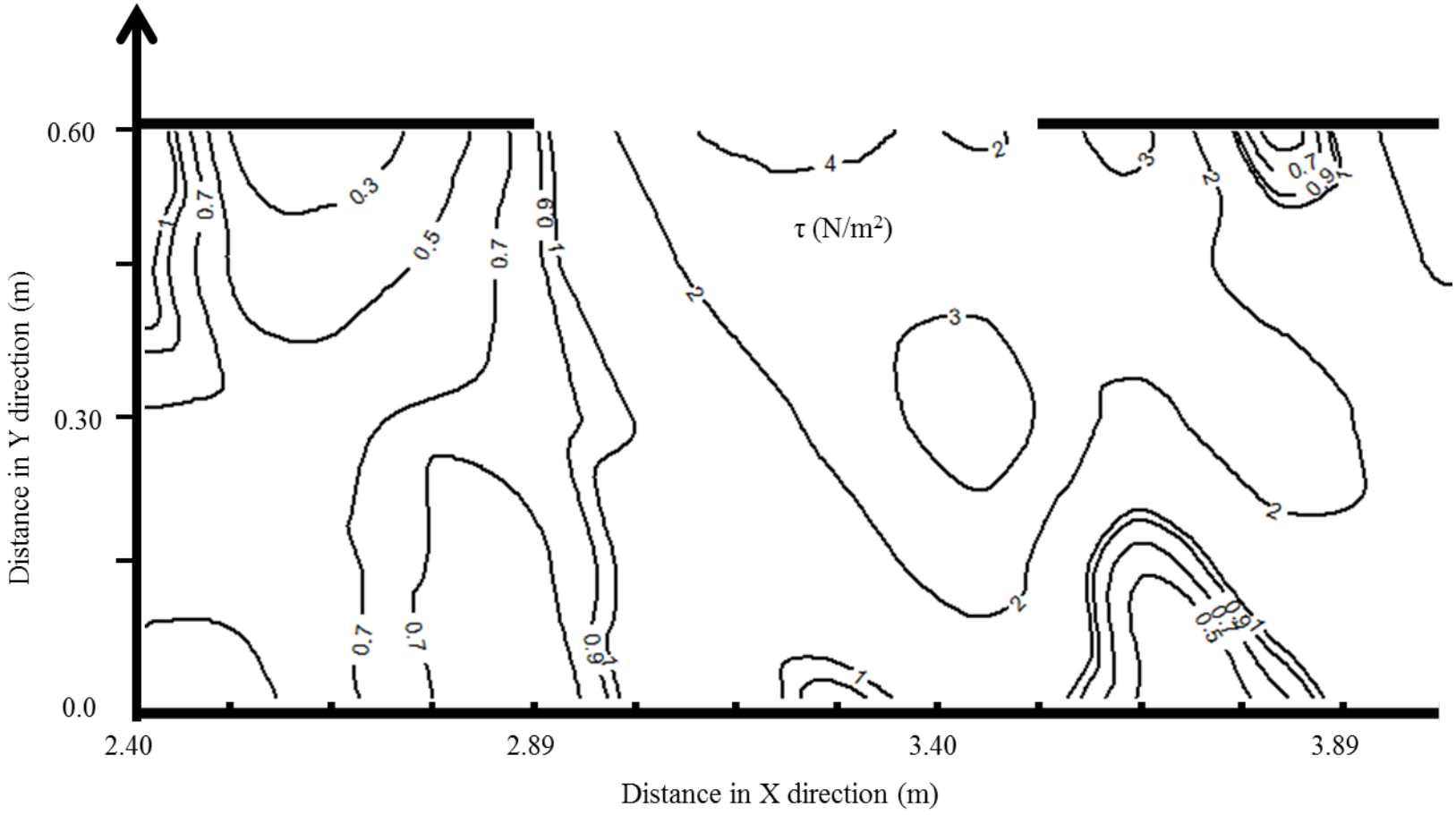

Fig. A2.5 Contours of bed shear stress (Case G5)

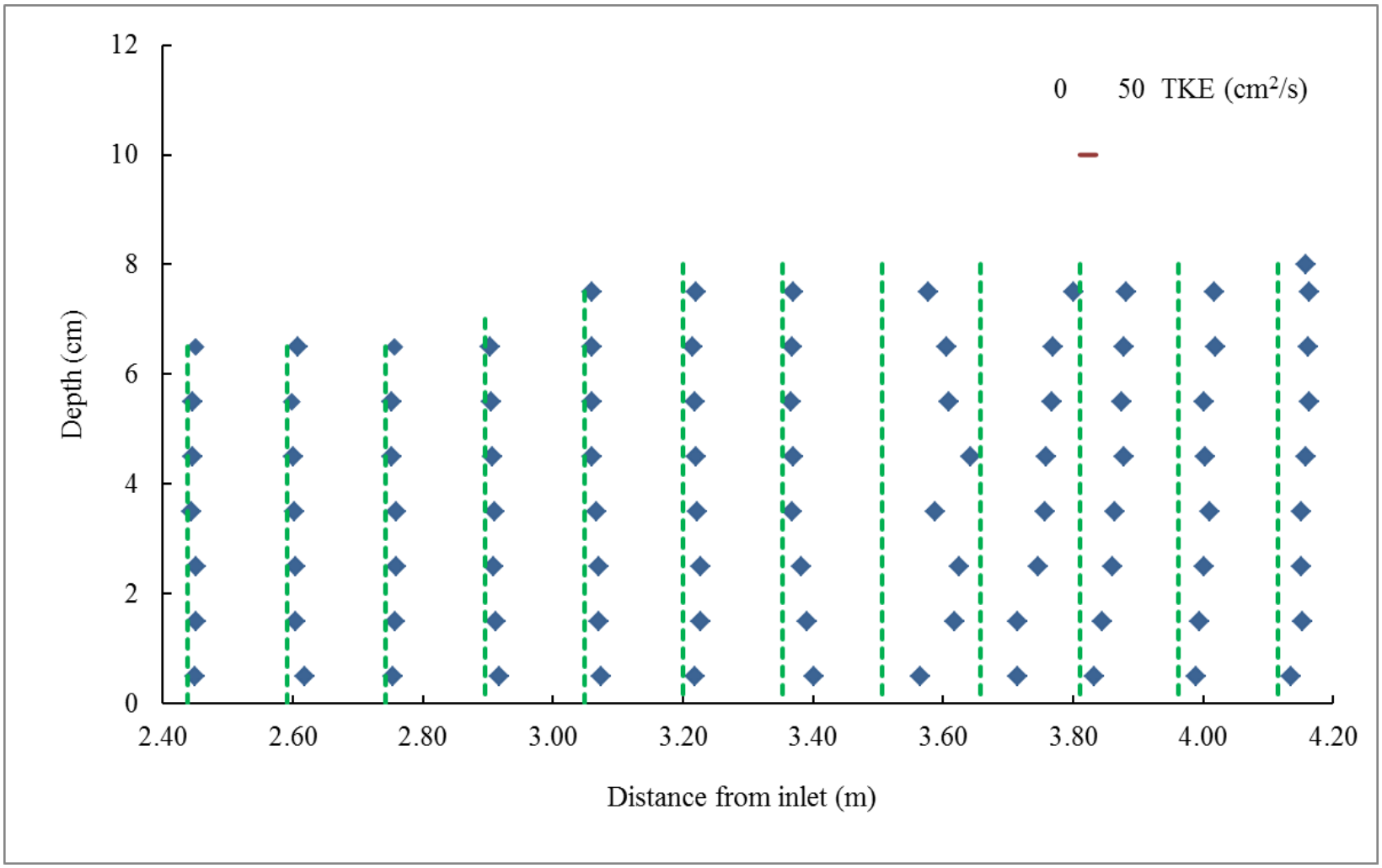

Fig. A2.6 (a) Distribution of TKE along Y1 (Case G5)

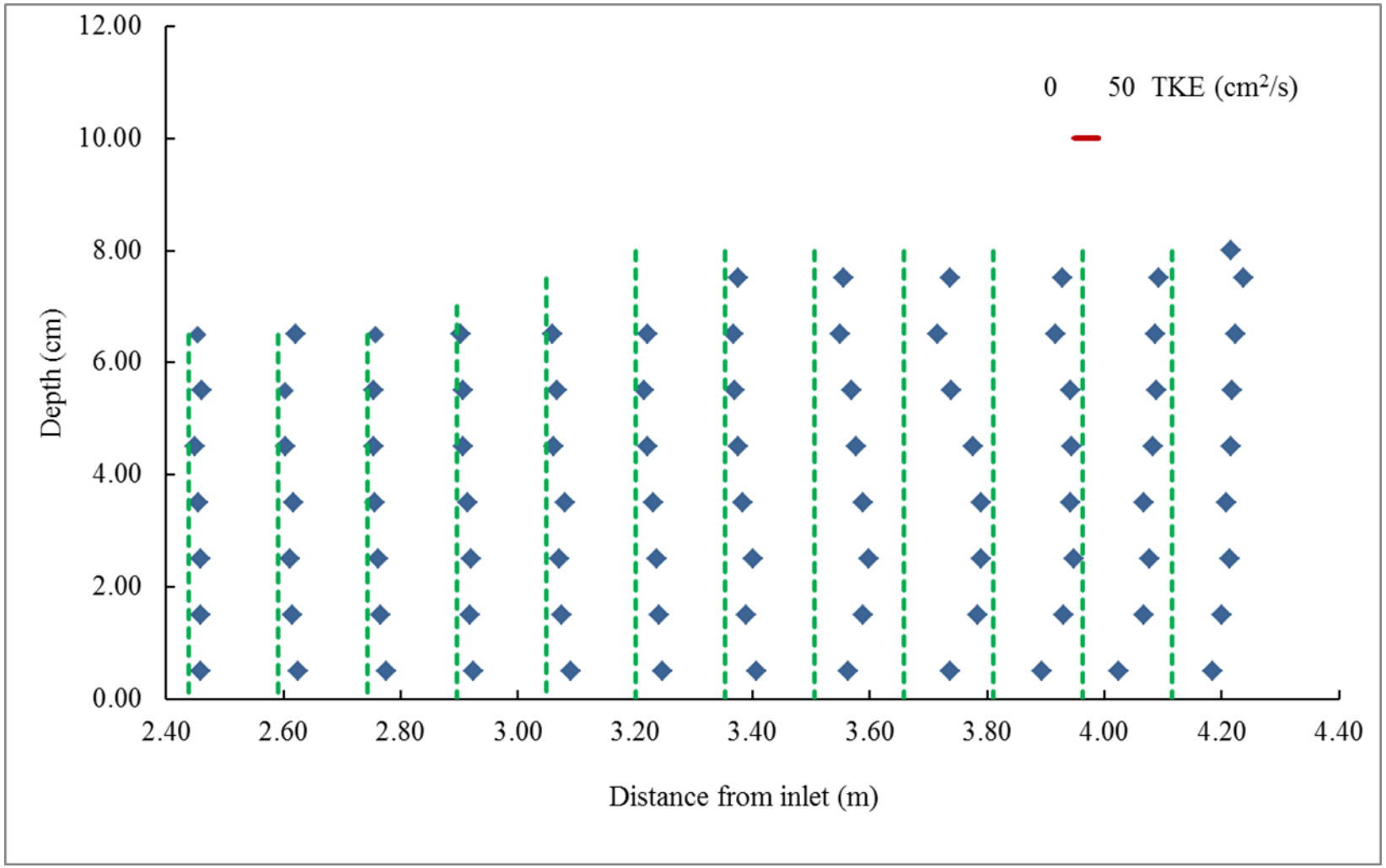

Fig. A2.7 (b) Distribution of TKE along Y2 (Case G5)

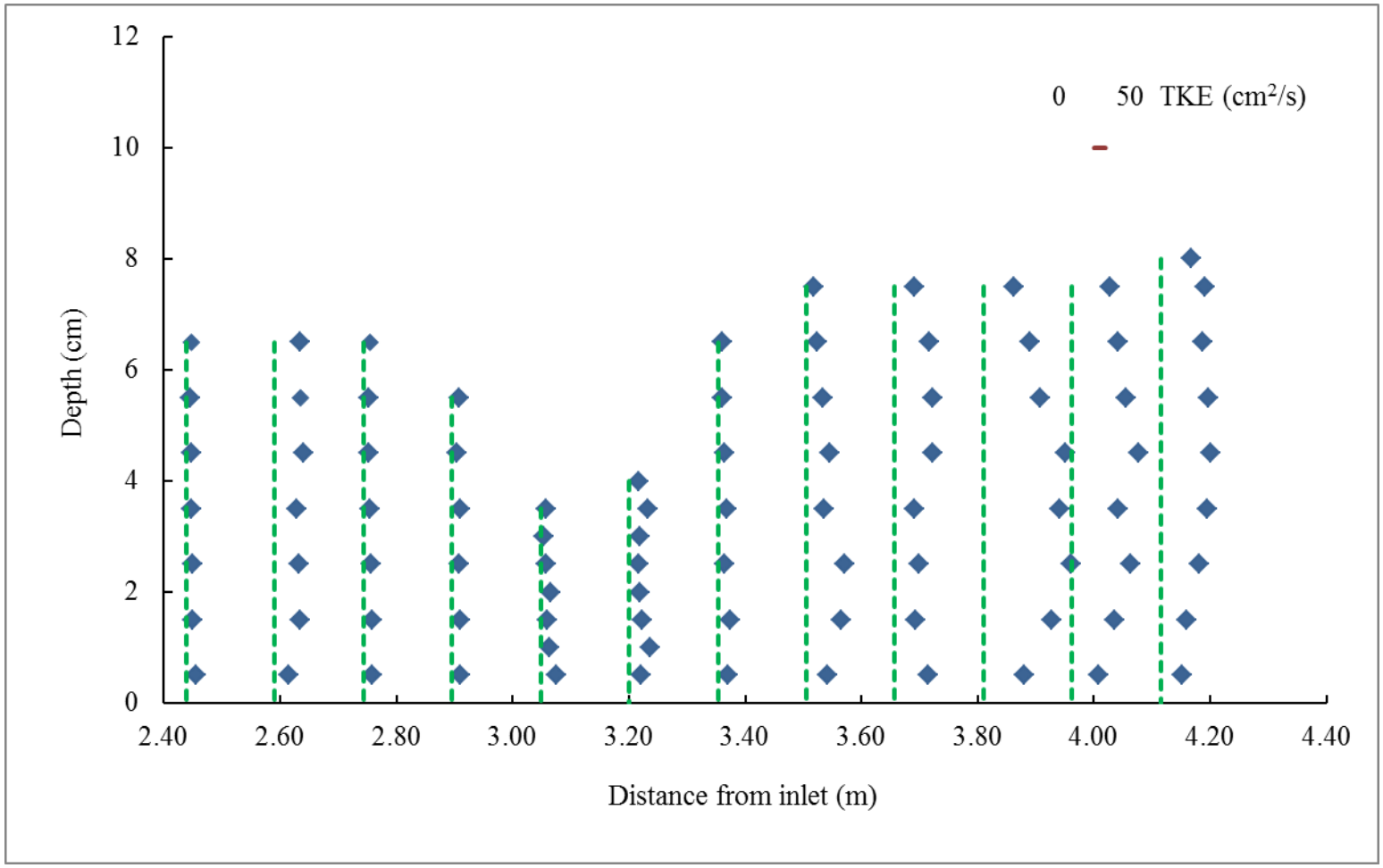

Fig. A2.8 (c) Distribution of TKE along Y3 (Case G5)

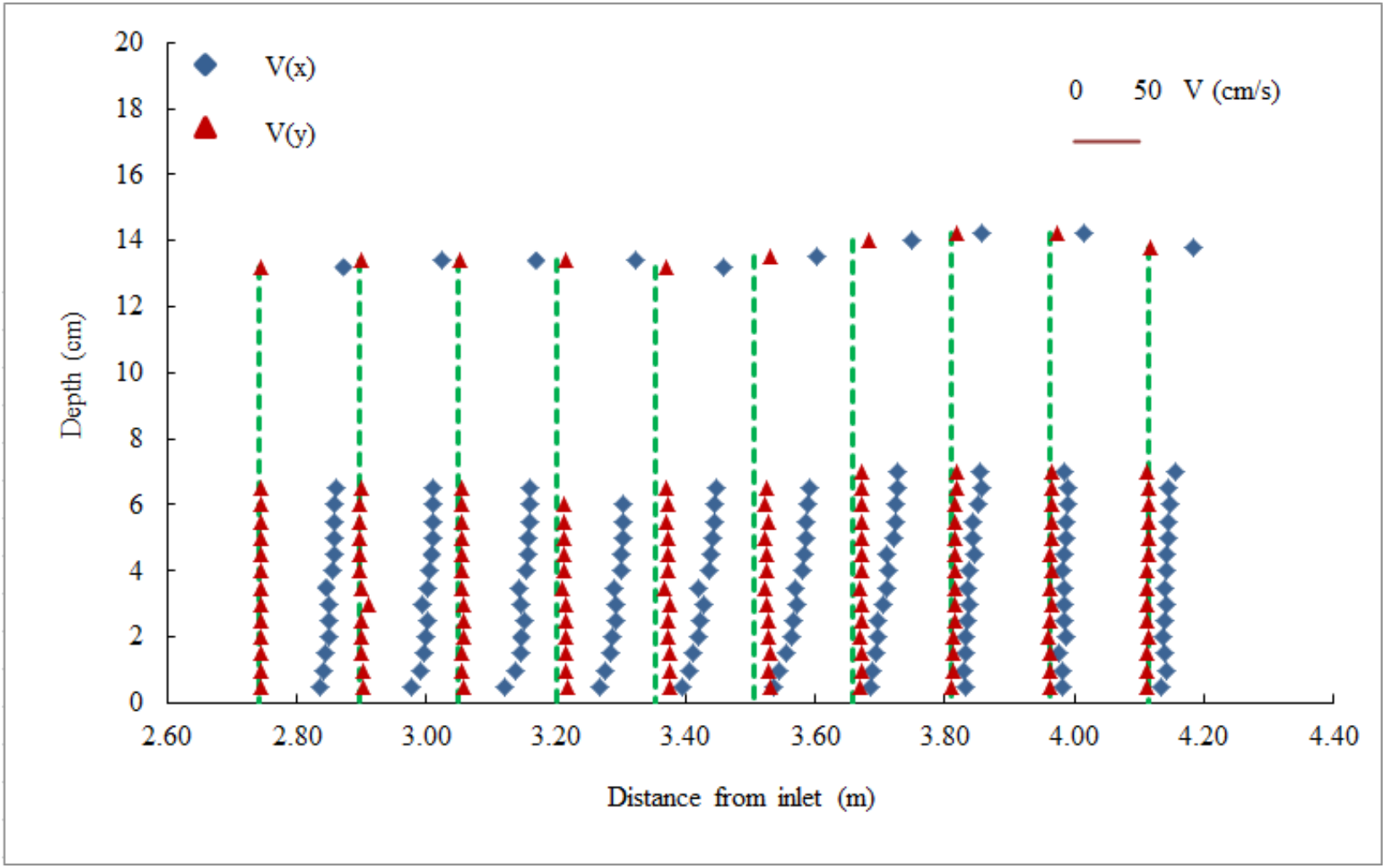

(a) Along Y1

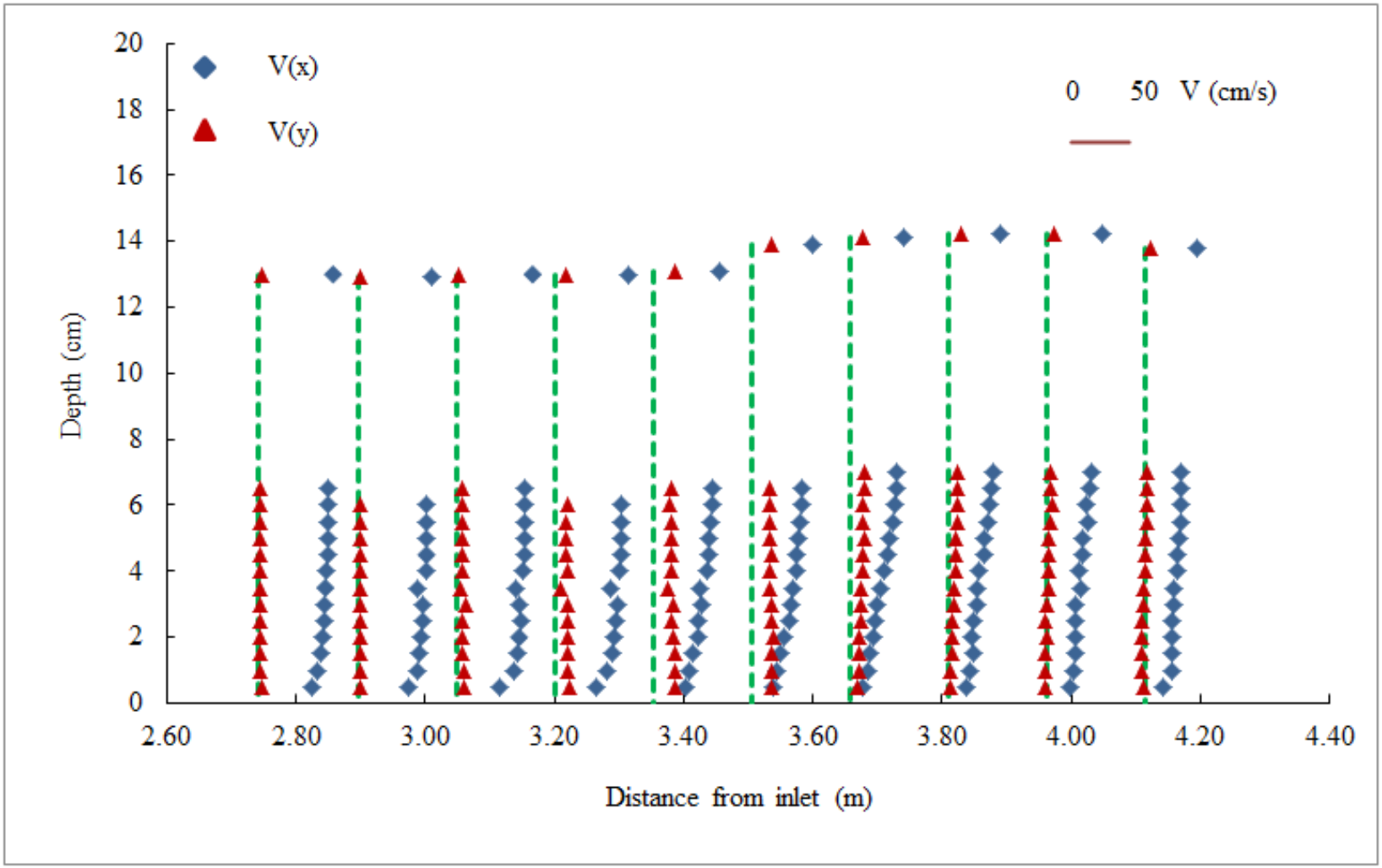

(b) Along Y2

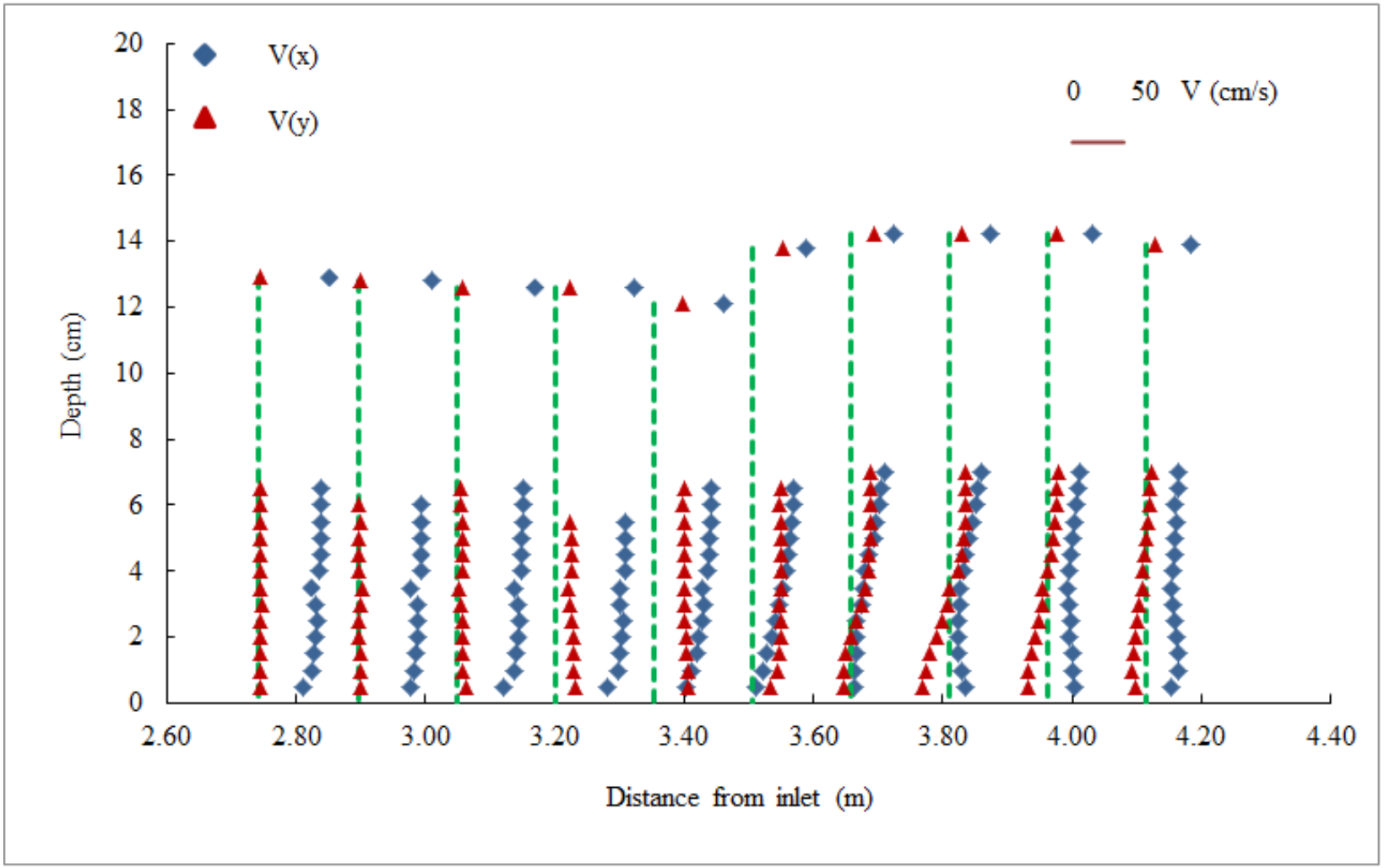

(c) Along Y3

Fig. A2.9 Measured results for velocity distribution (Case G6)

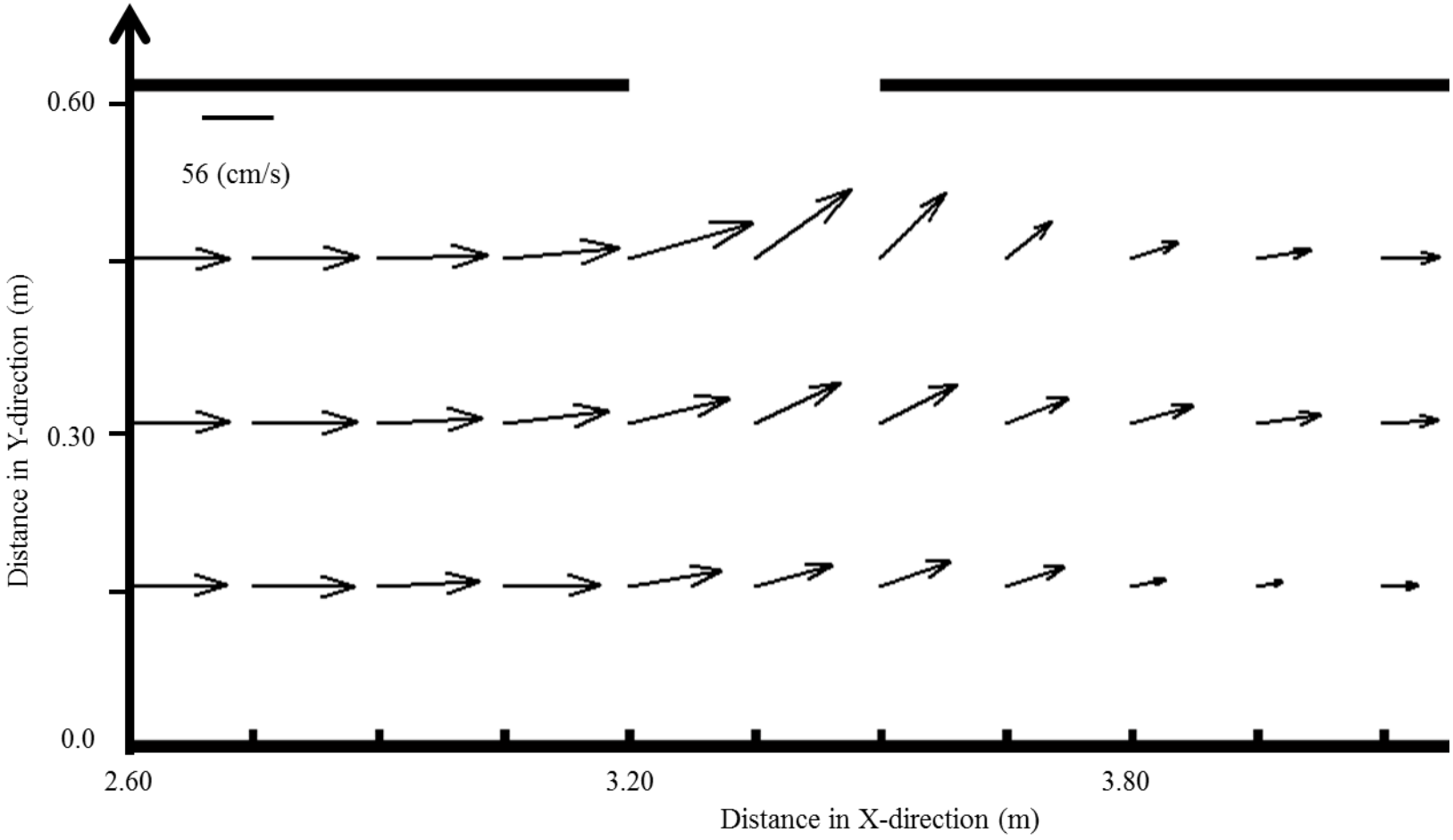

Fig. A2.10 Average velocities (Case G6)

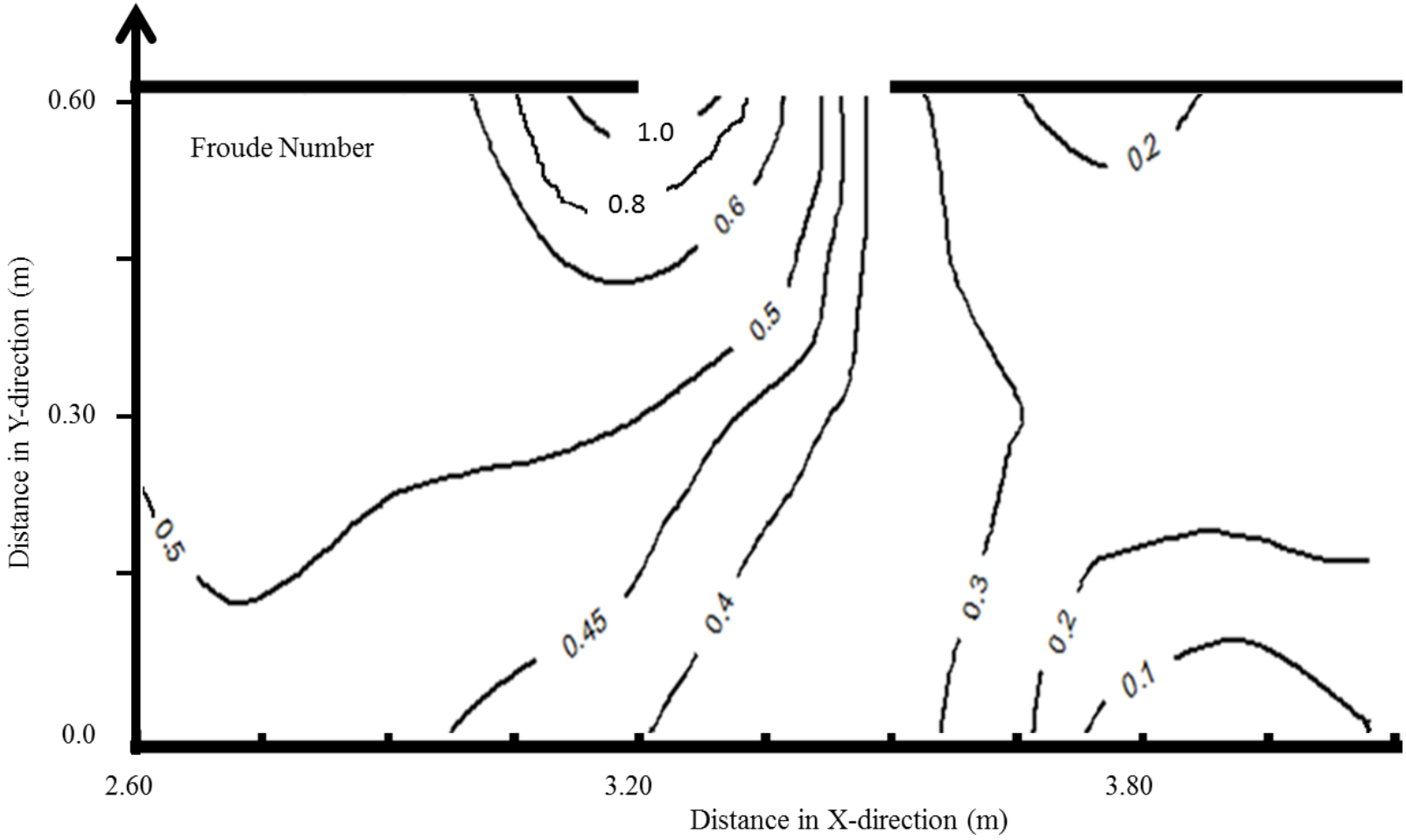

Fig. A2.11 Distribution of Froude Number (Case G6)

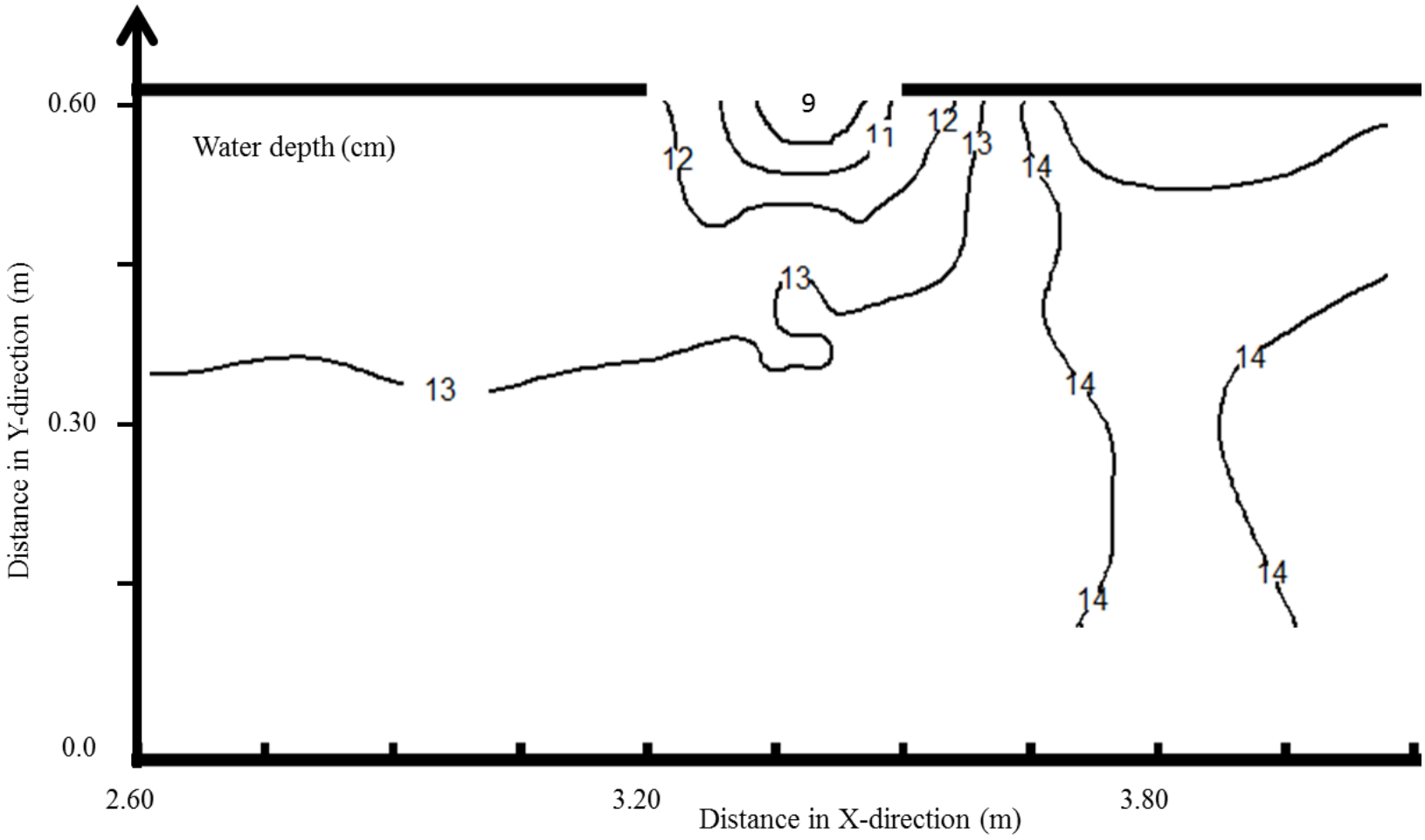

Fig. A2.12 Contours of flow depth (Case G6)

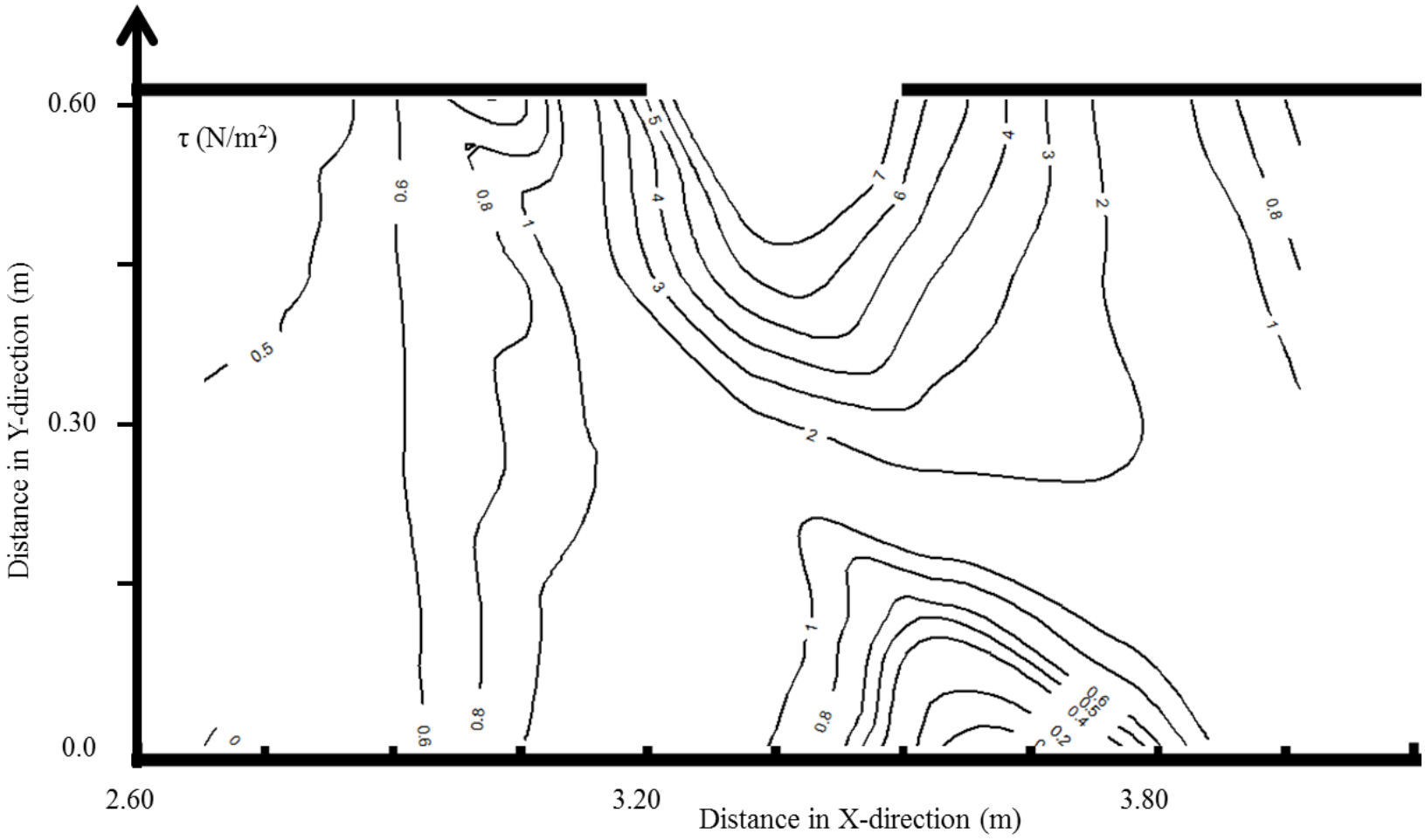

Fig. A2.13 Contours of bed shear stress (Case G6)

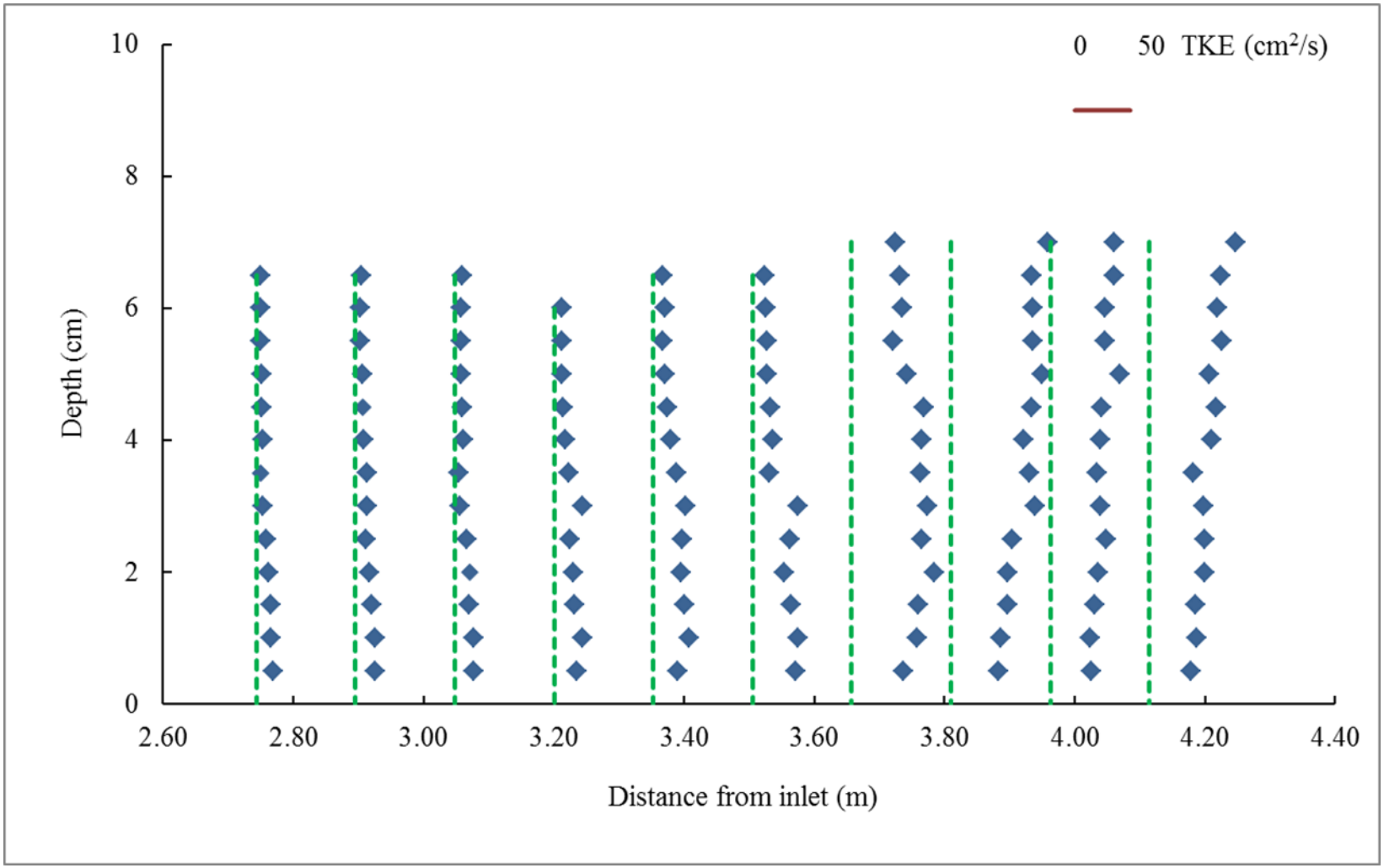

Fig. A2.14 Distribution of TKE along Y1 (Case G6)

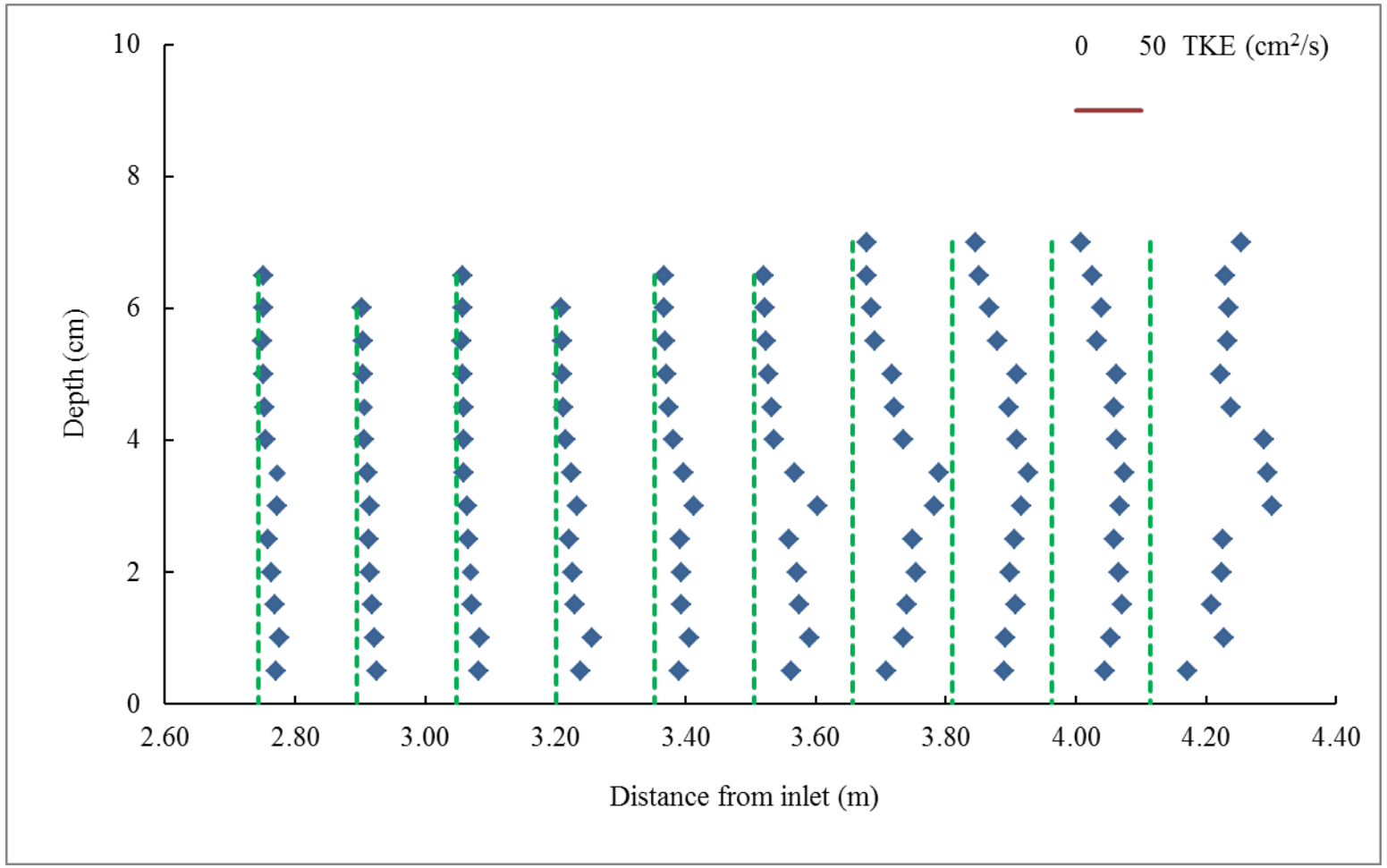

Fig. A2.15 Distribution of TKE along Y2 (Case G6)

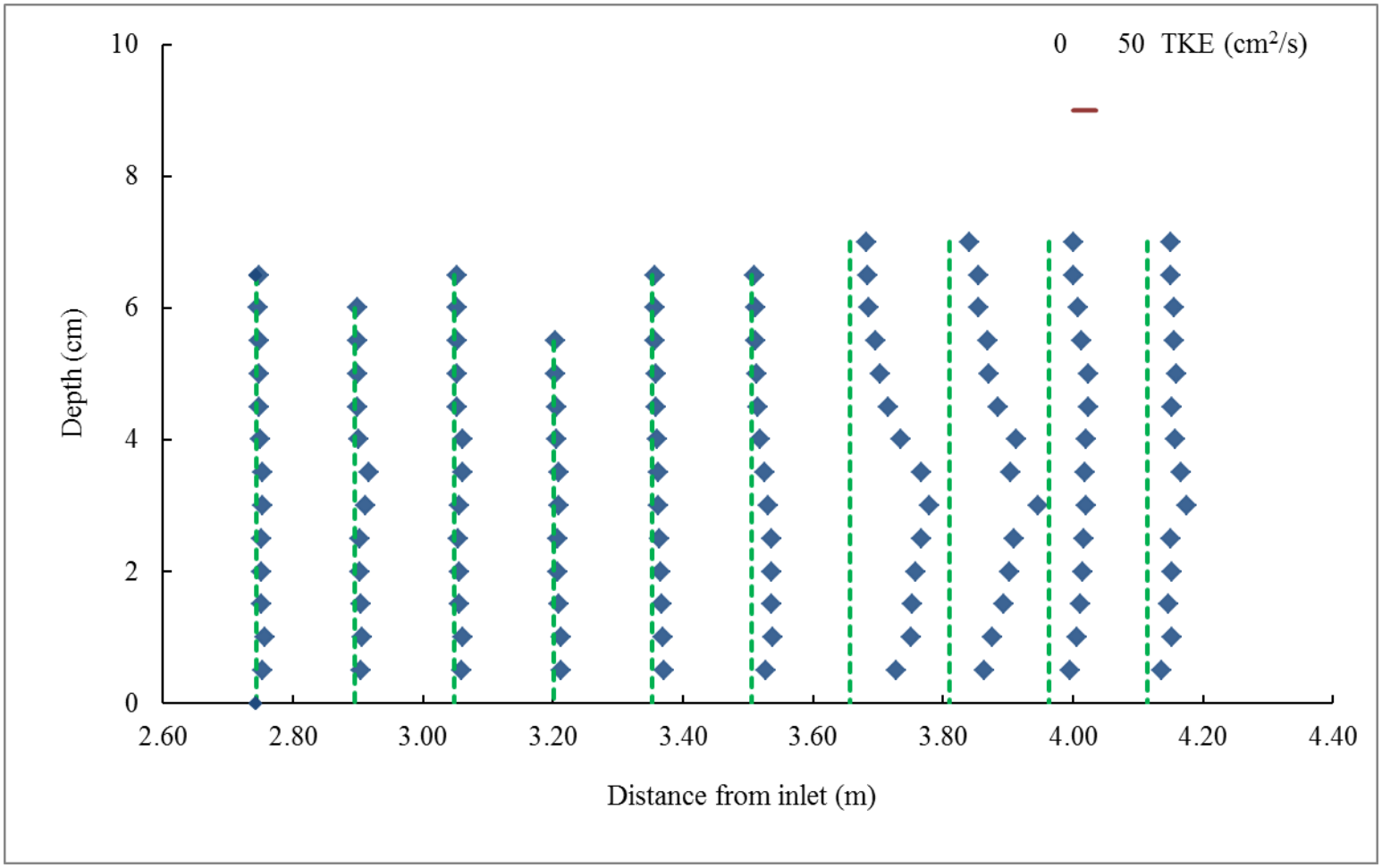

Fig. A2.16 Distribution of TKE along Y3 (Case G6)

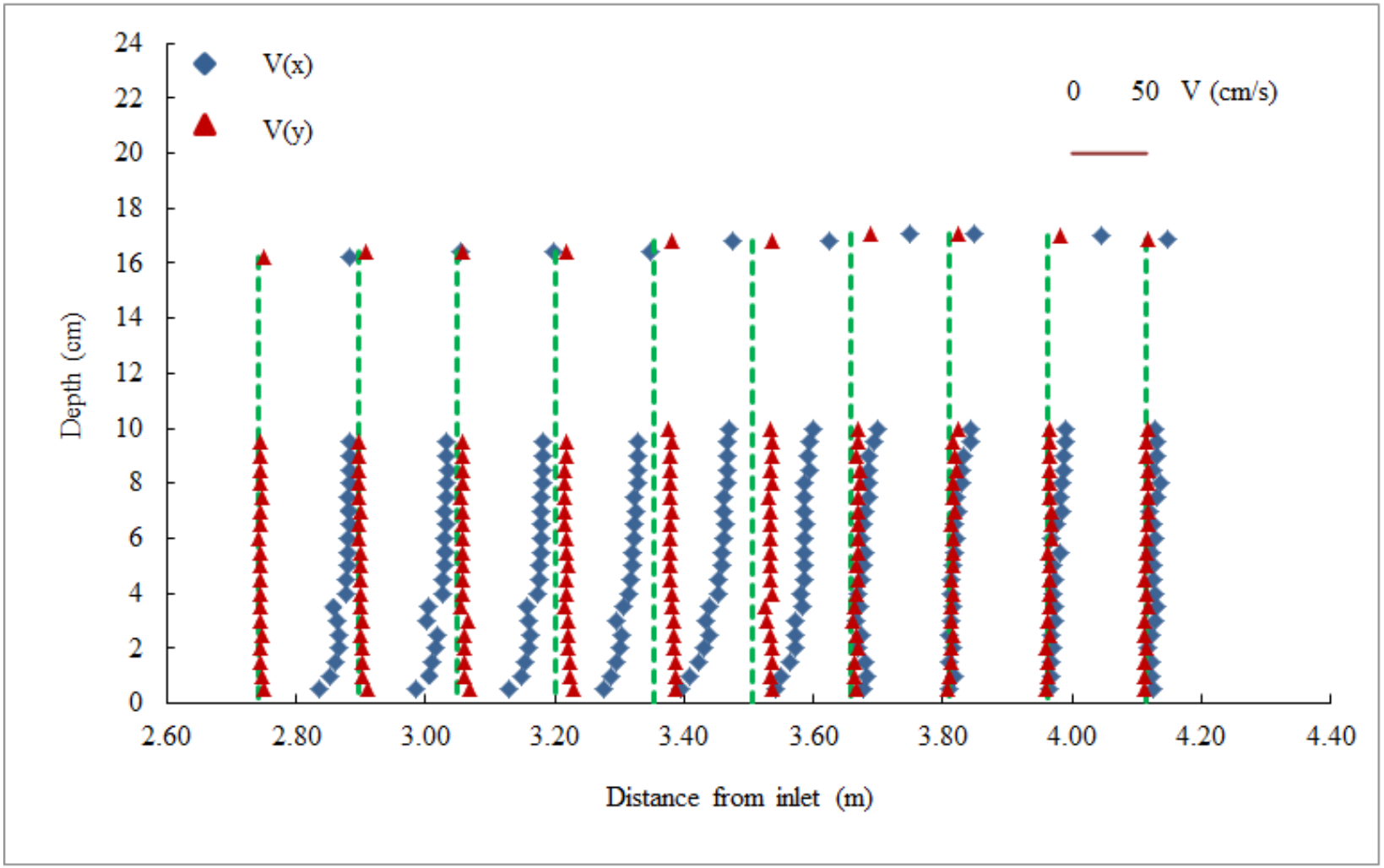

(a) Along Y1

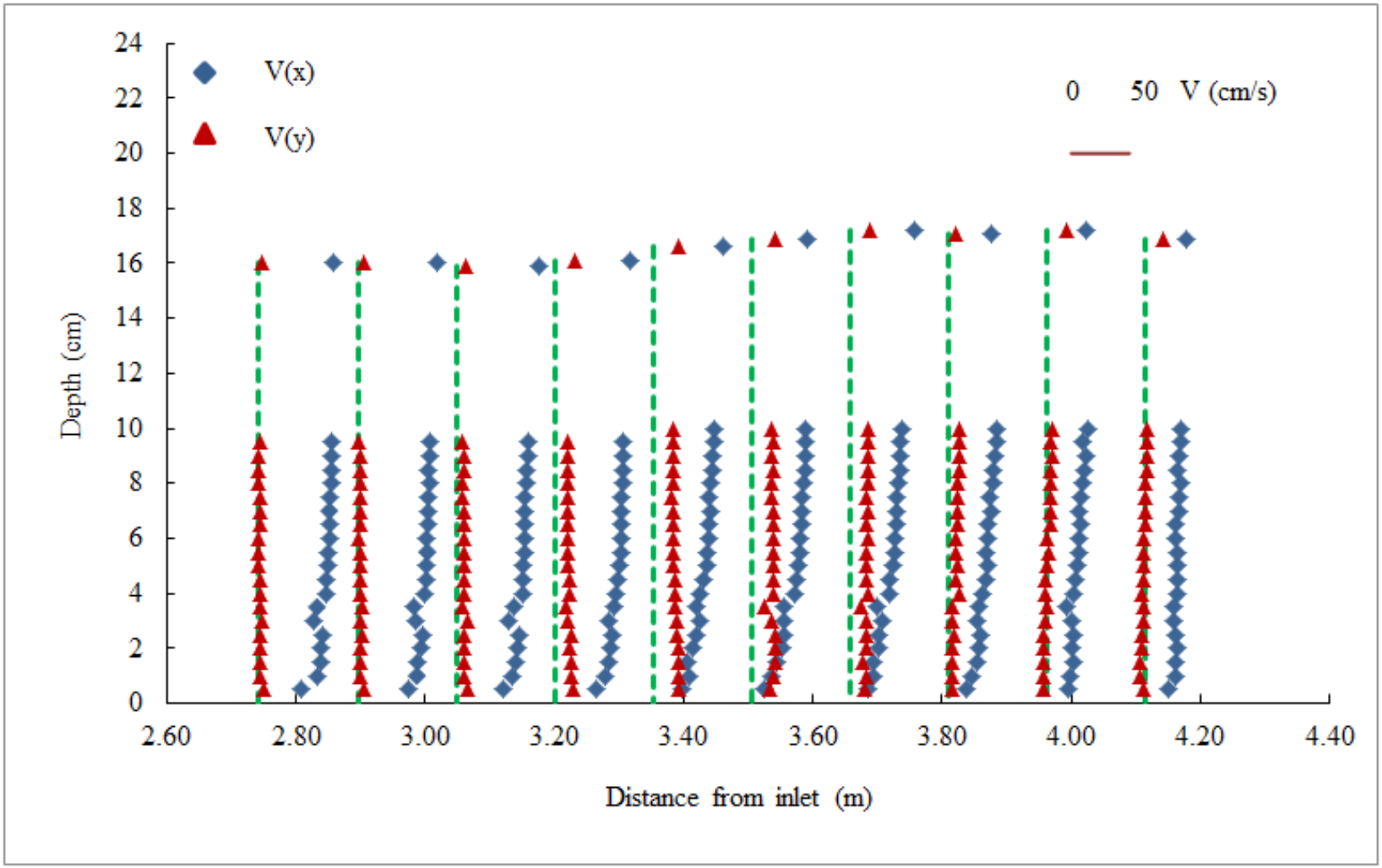

(b) Along Y2

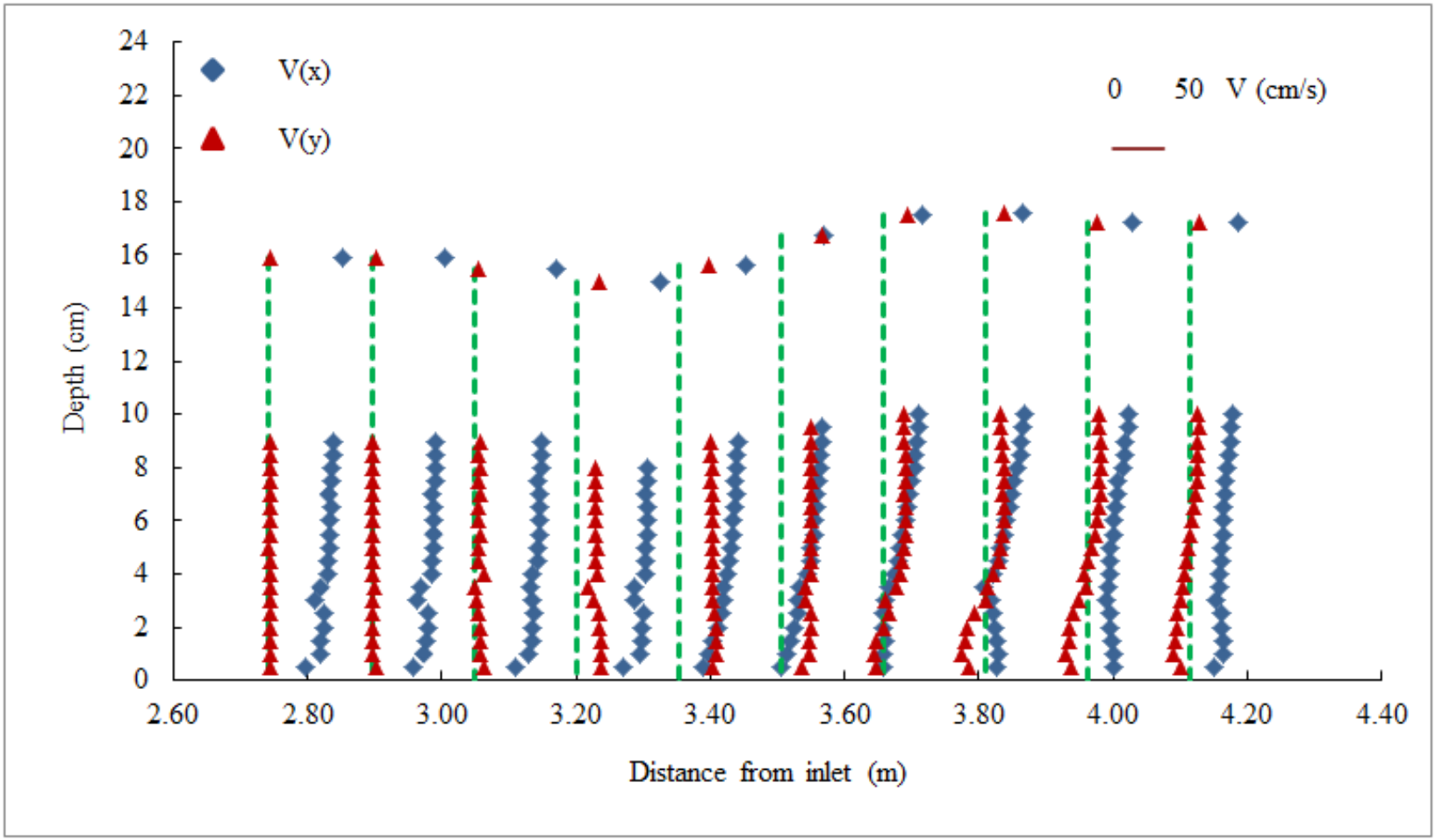

(c) Along Y3

Fig. A2.17 Measured results for velocity distribution (Case G8)

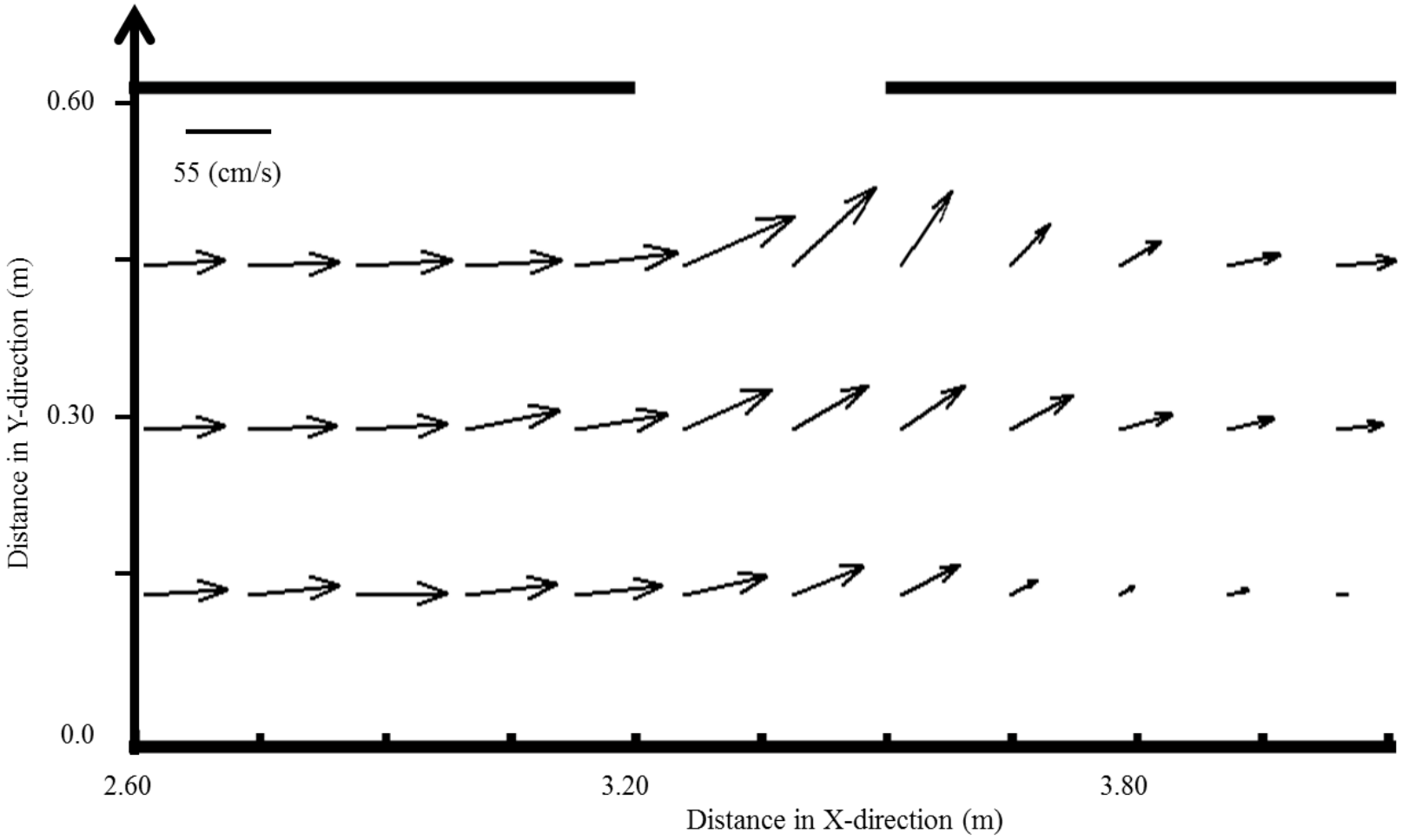

Fig. A2.18 Average velocities (Case G8)

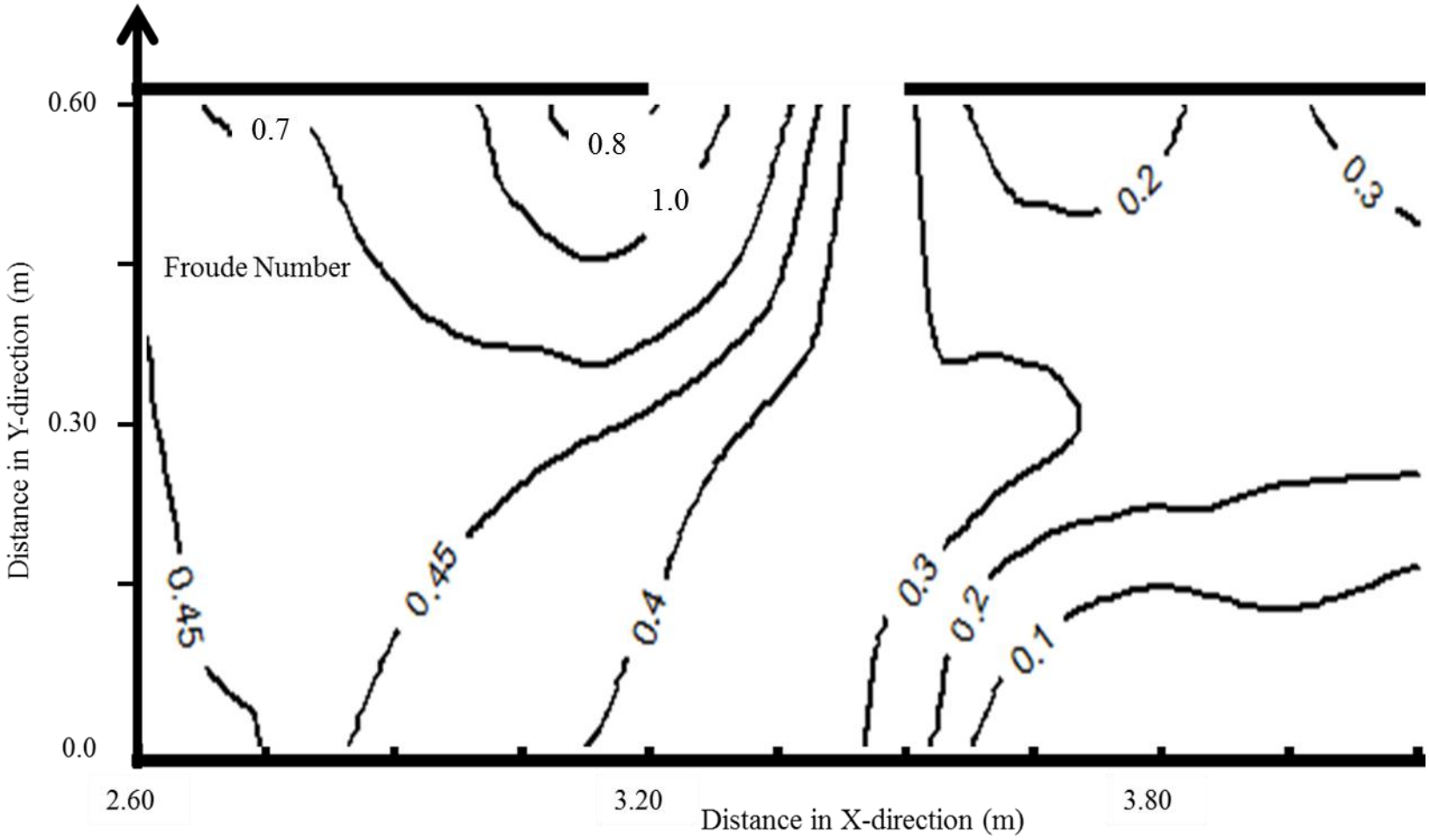

Fig. A2.19 Distribution of Froude Number (Case G8)

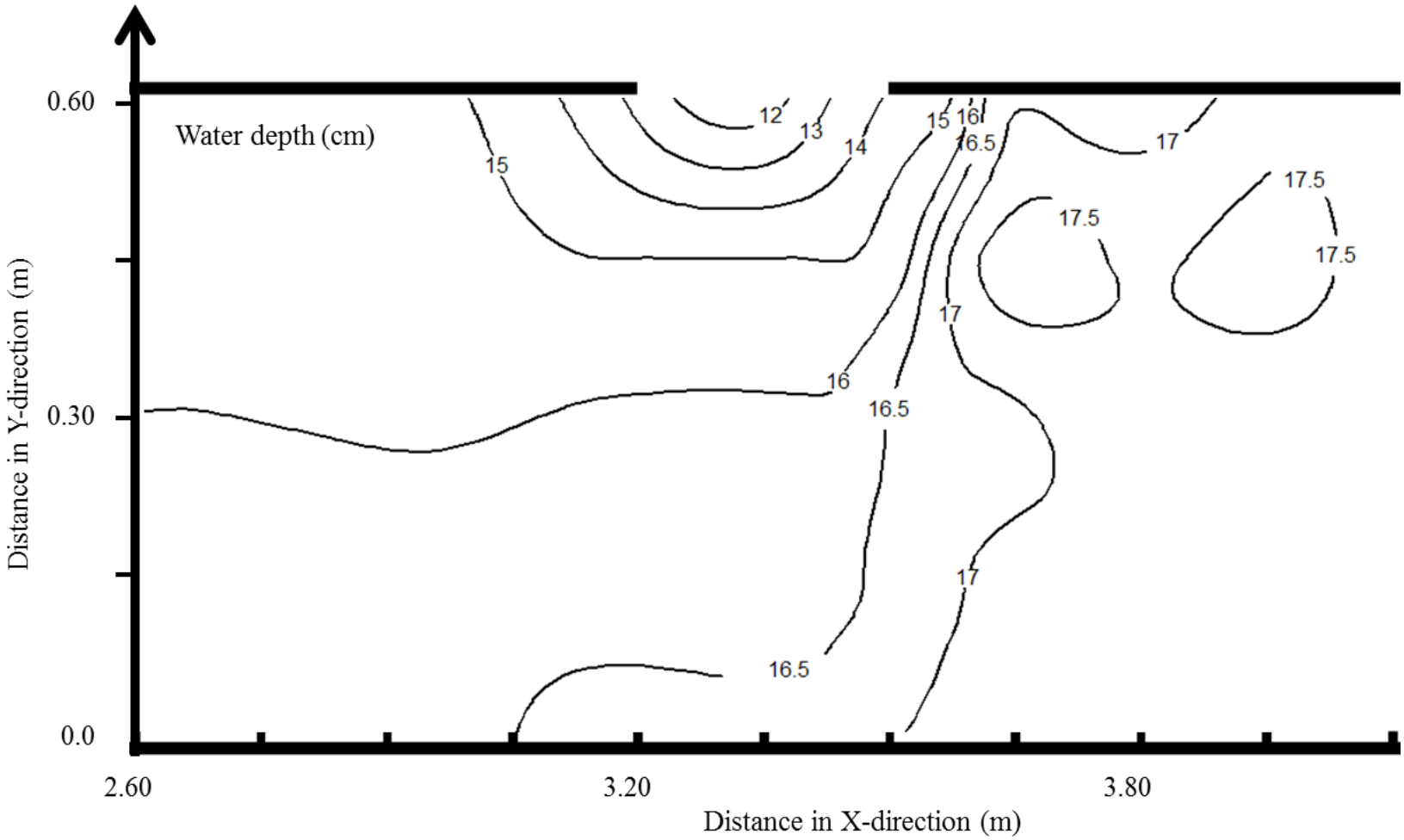

Fig. A2.20 Contours of flow depth (Case G8)

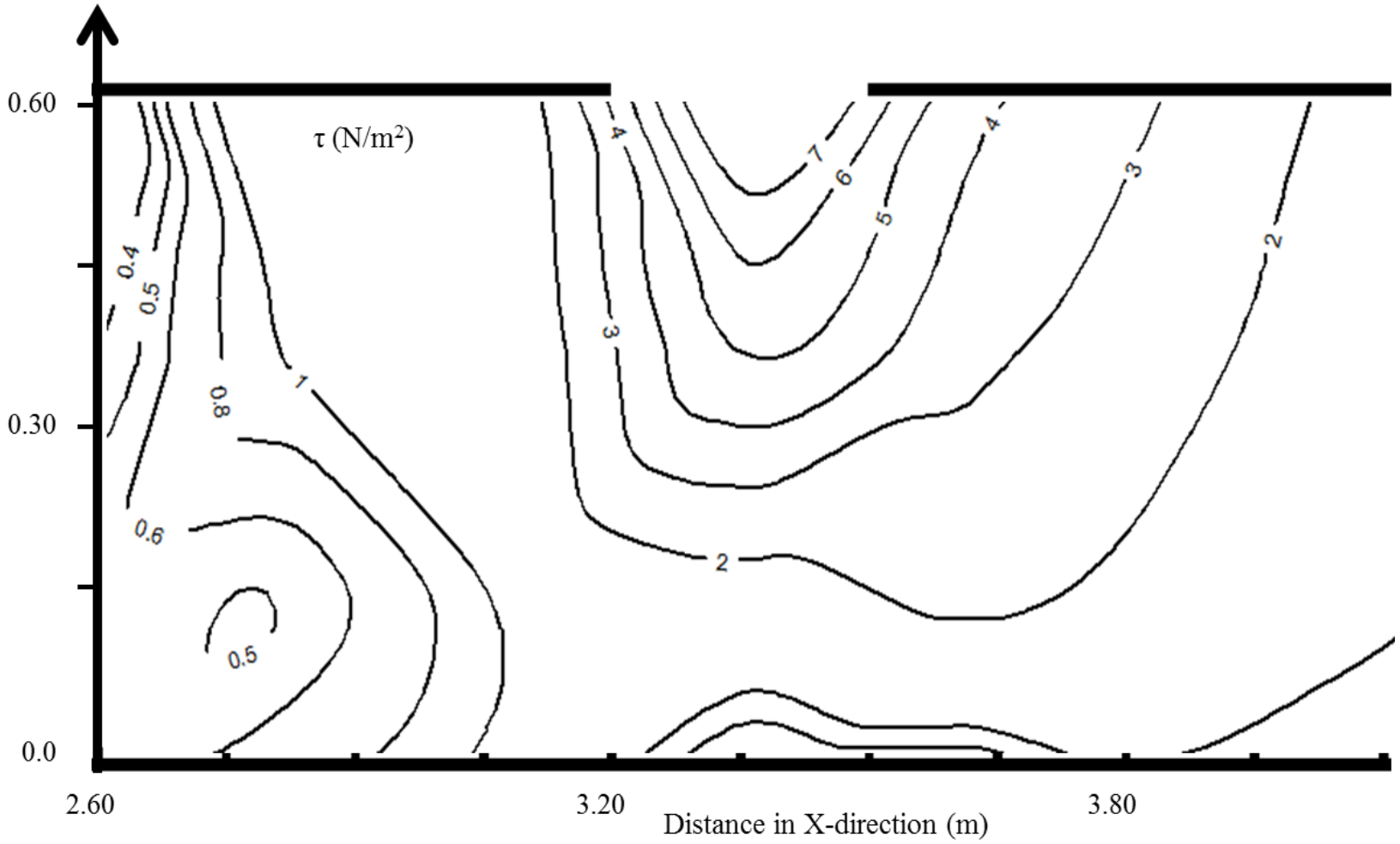

Fig. A2.21 Contours of bed shear stress (Case G8)

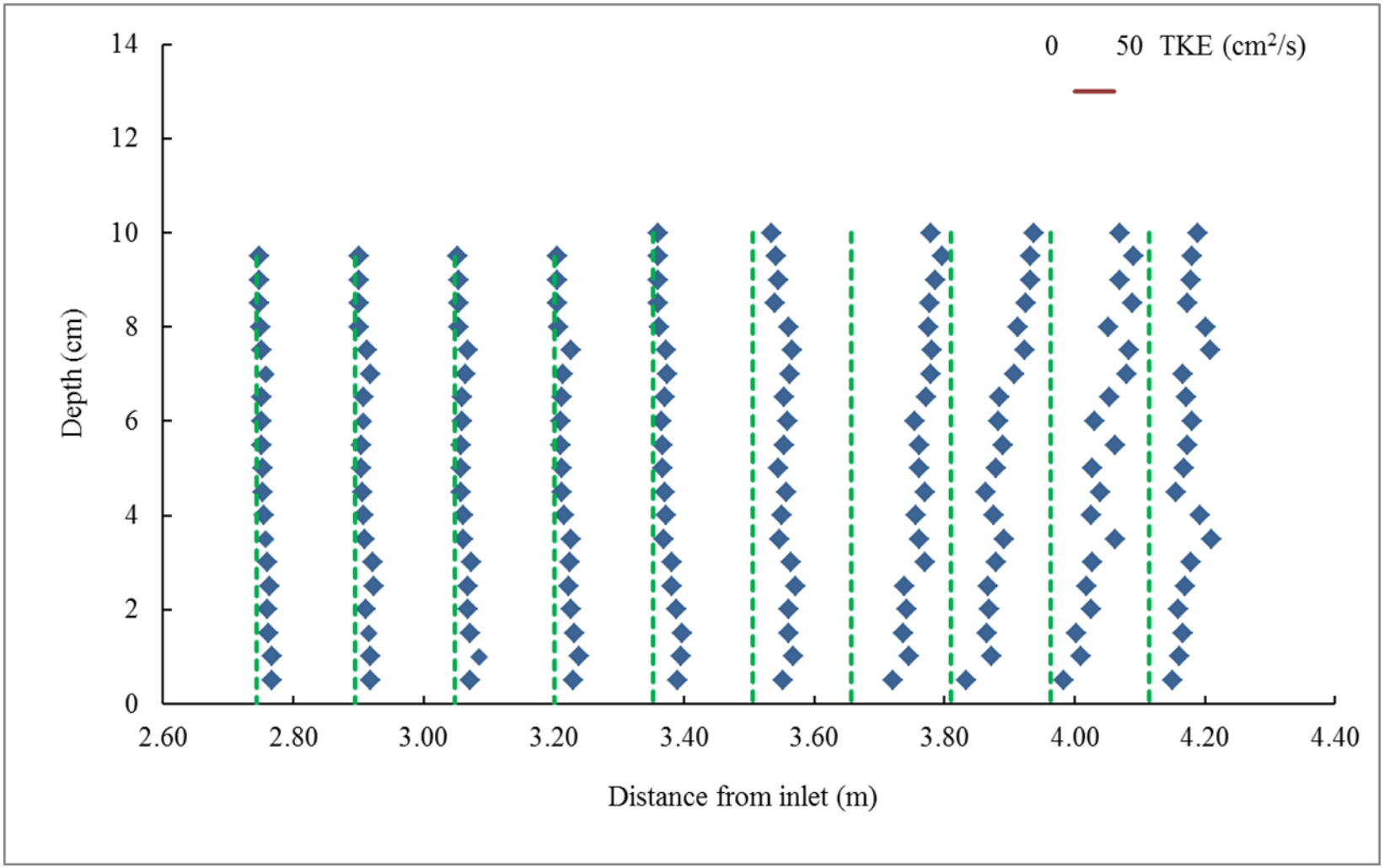

Fig. A2.22 Distribution of TKE along Y1 (Case G8)

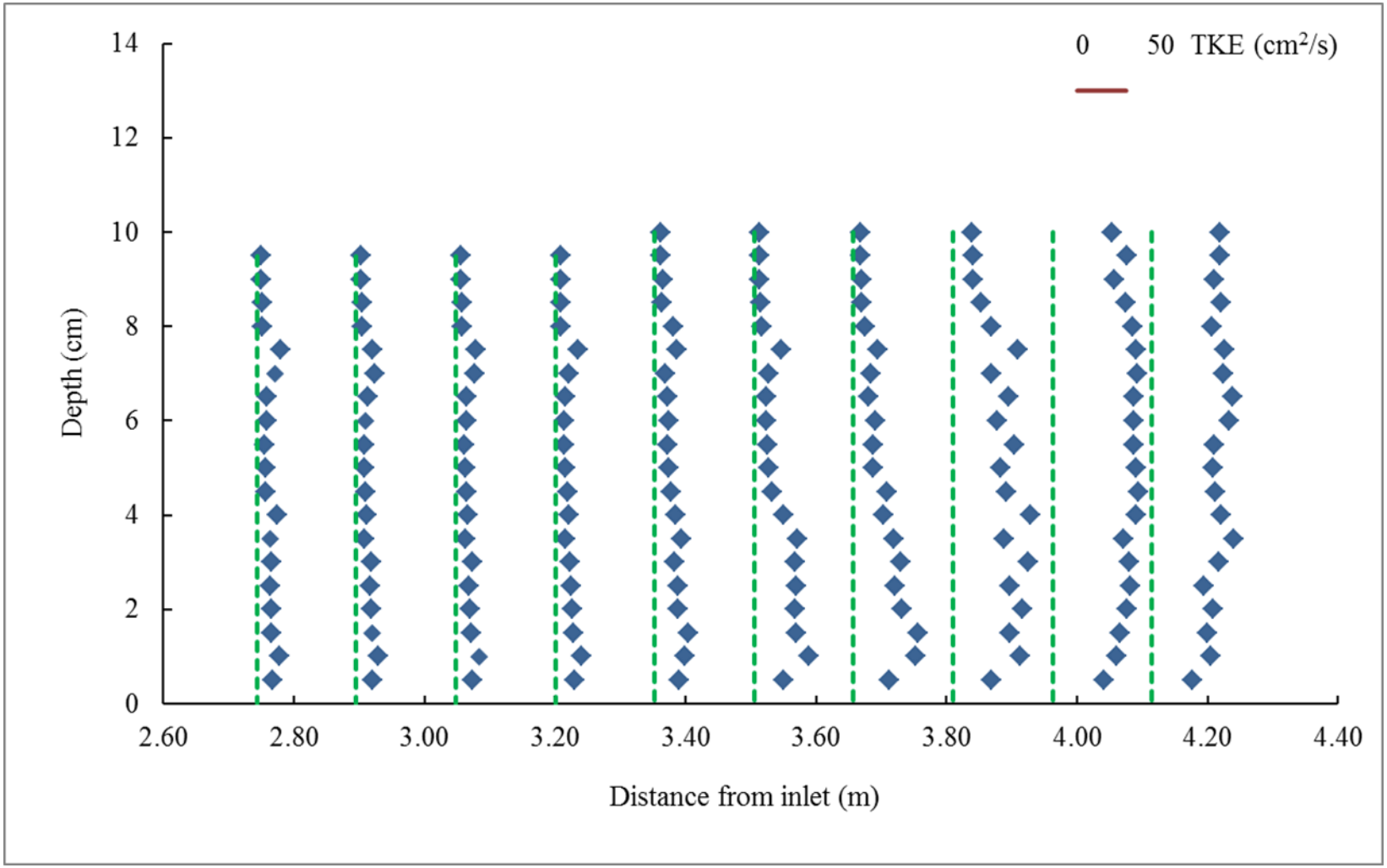

Fig. A2.23 Distribution of TKE along Y2 (Case G8)

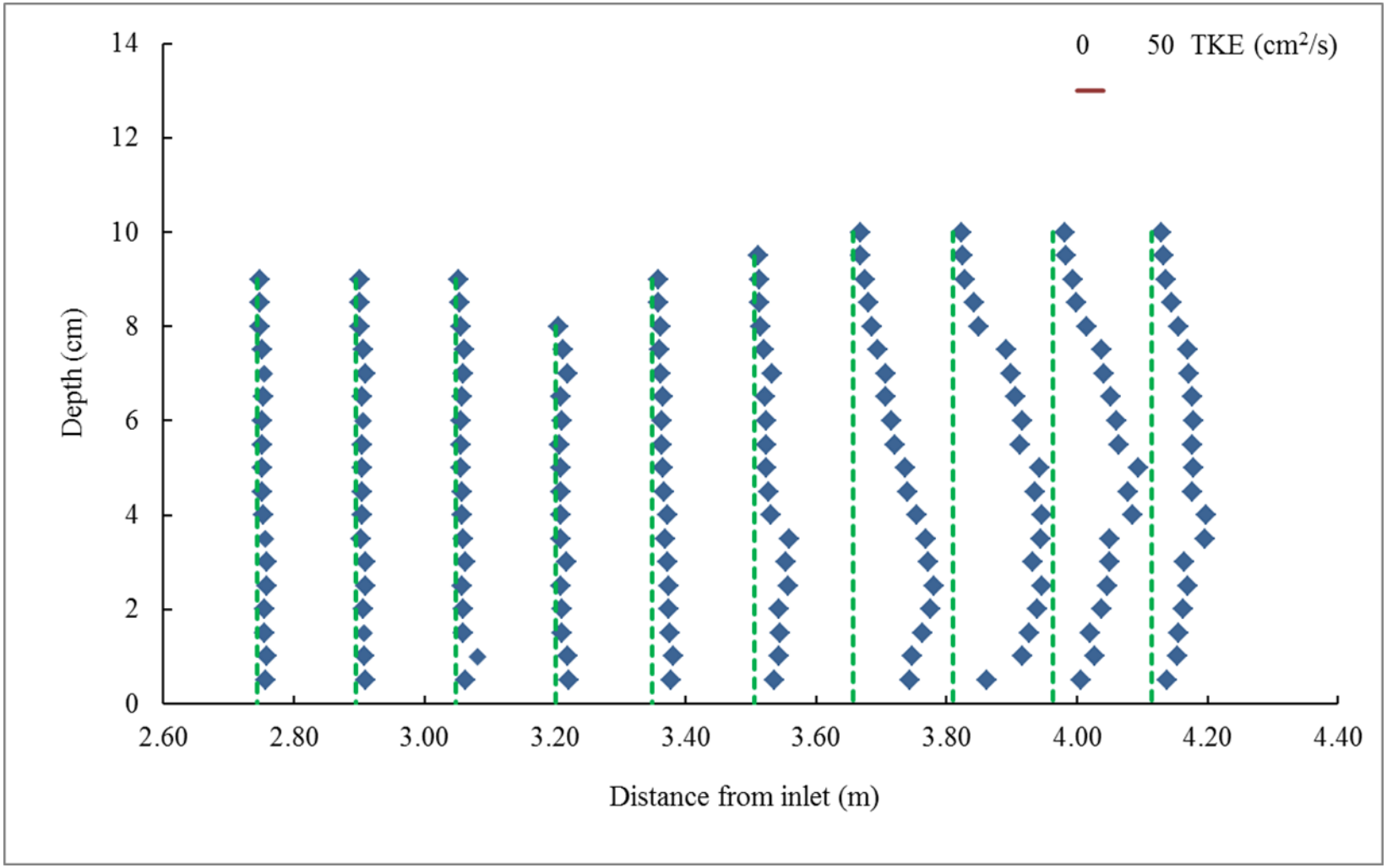

Fig. A2.24 Distribution of TKE along Y3 (Case G8)

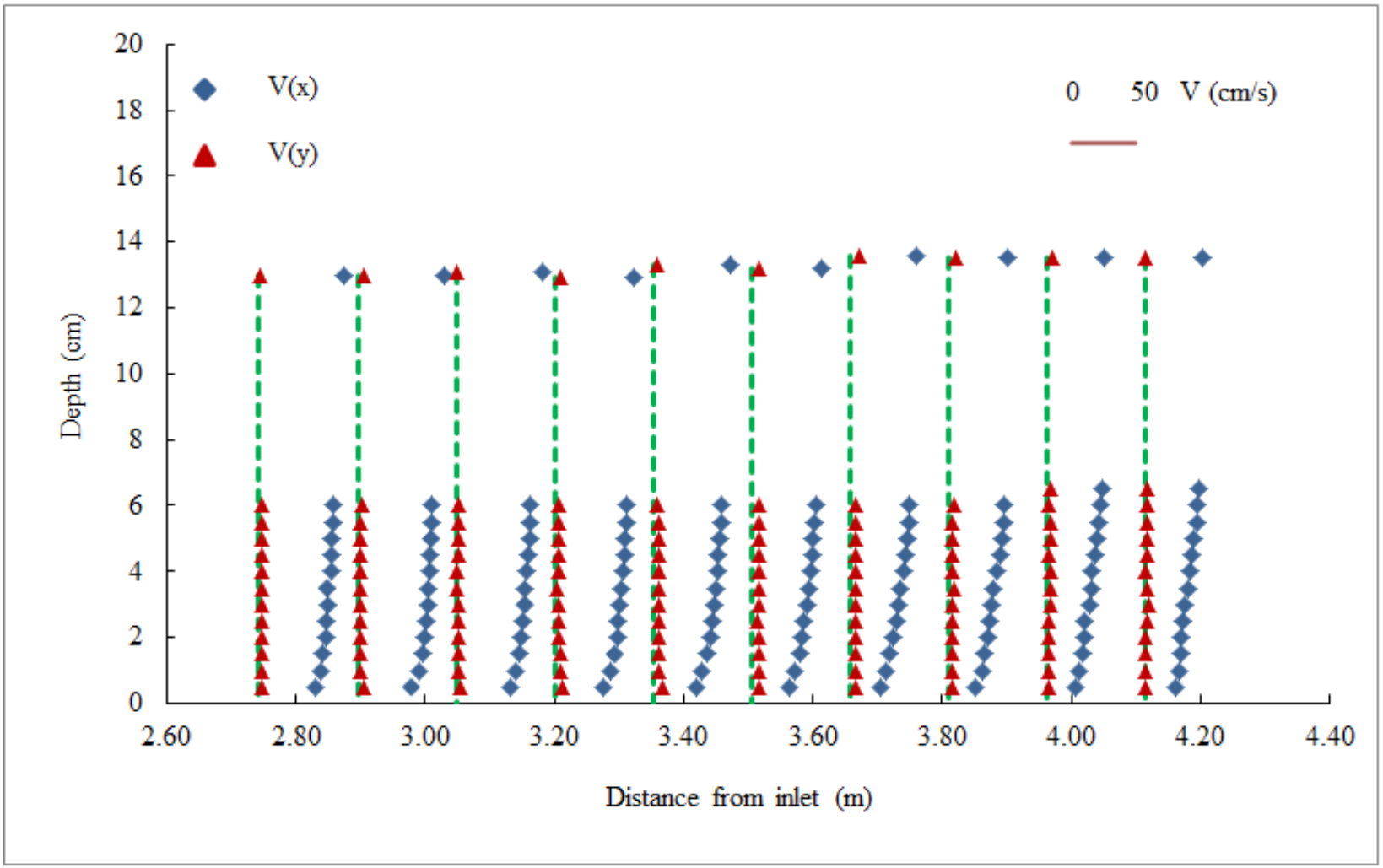

(a) Along Y1

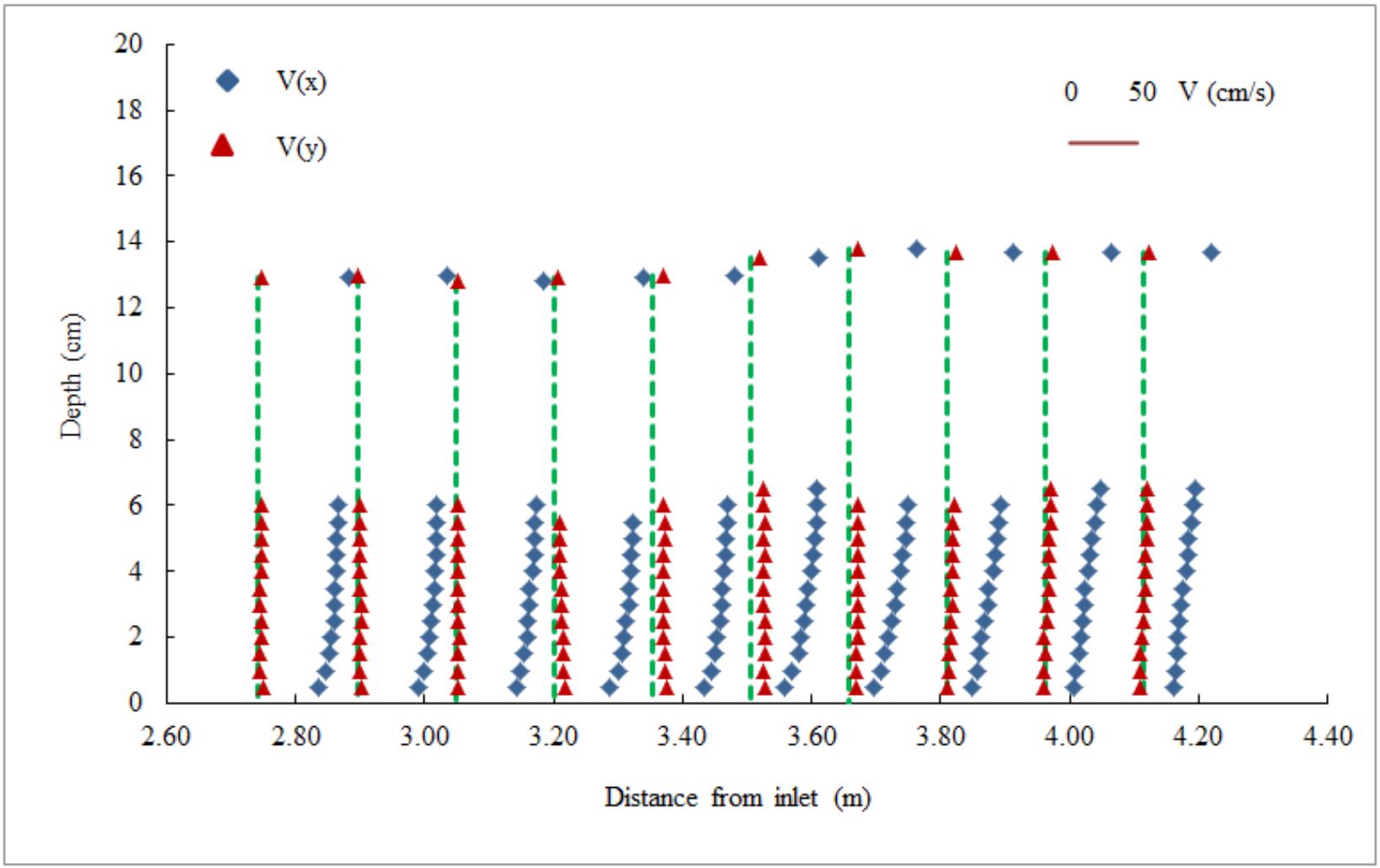

(b) Along Y2

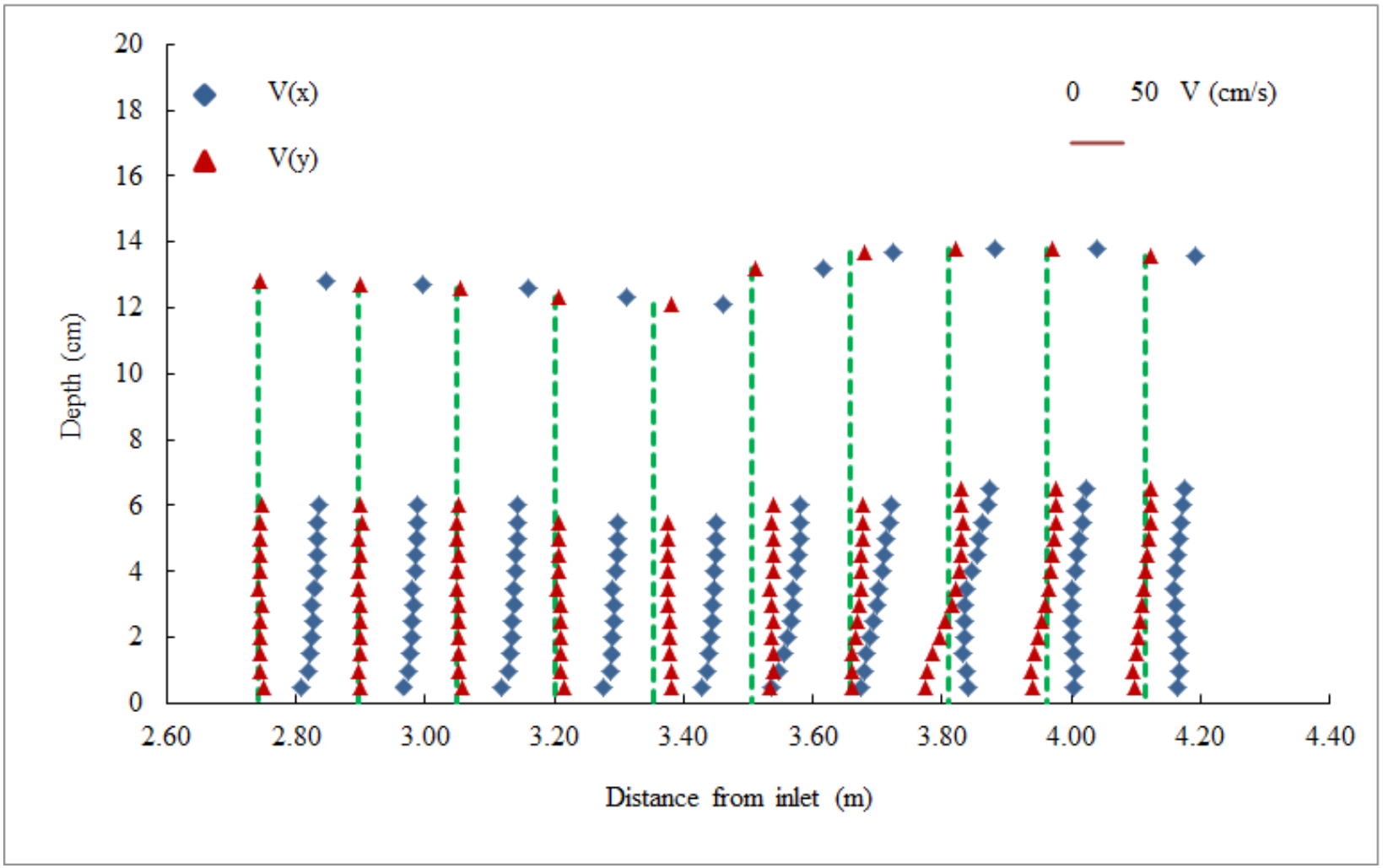

(c) Along Y3

Fig. A2.25 Measured results for velocity distribution (Case G9)

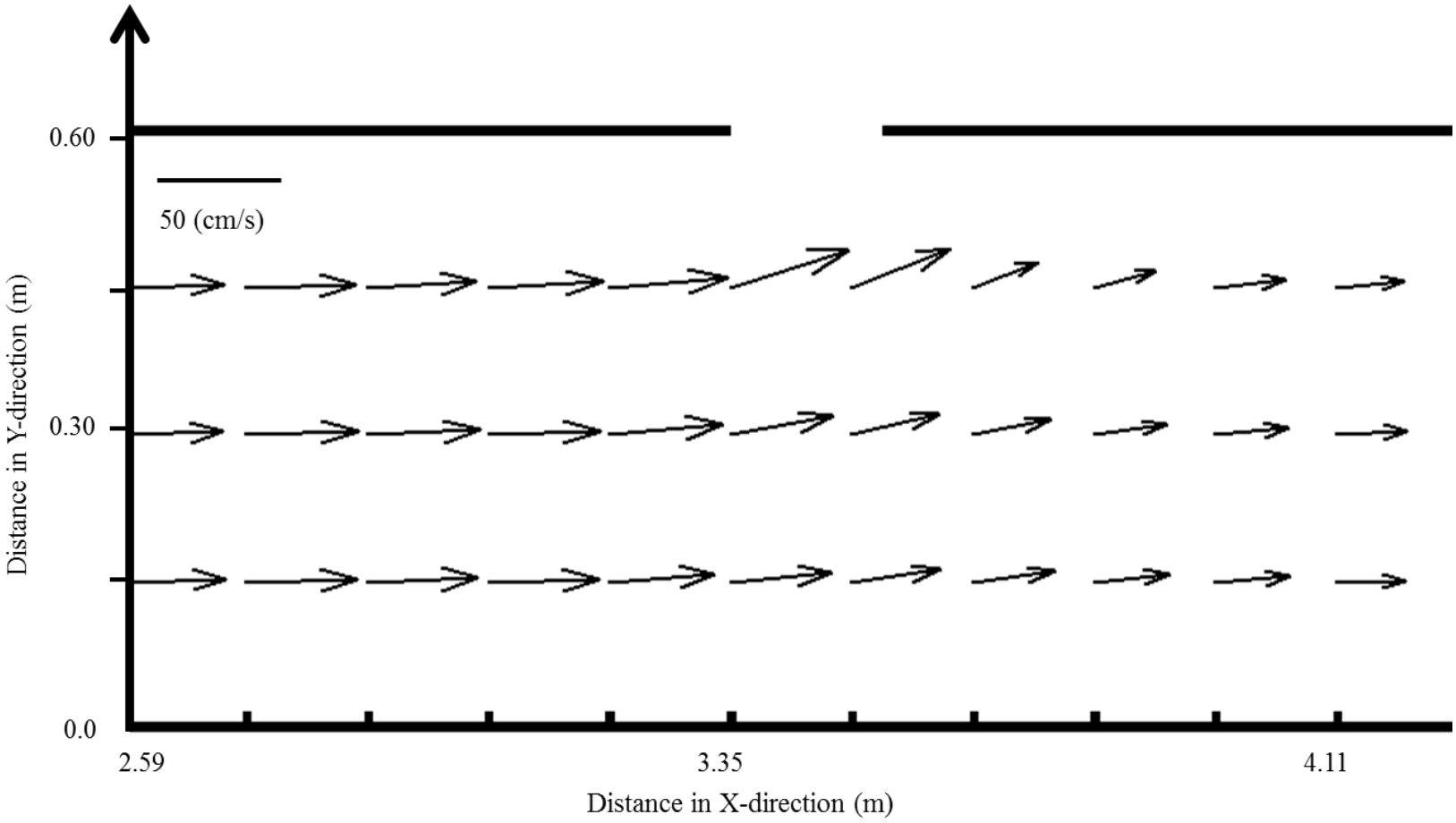

Fig. A2.26 Average velocities (Case G9)

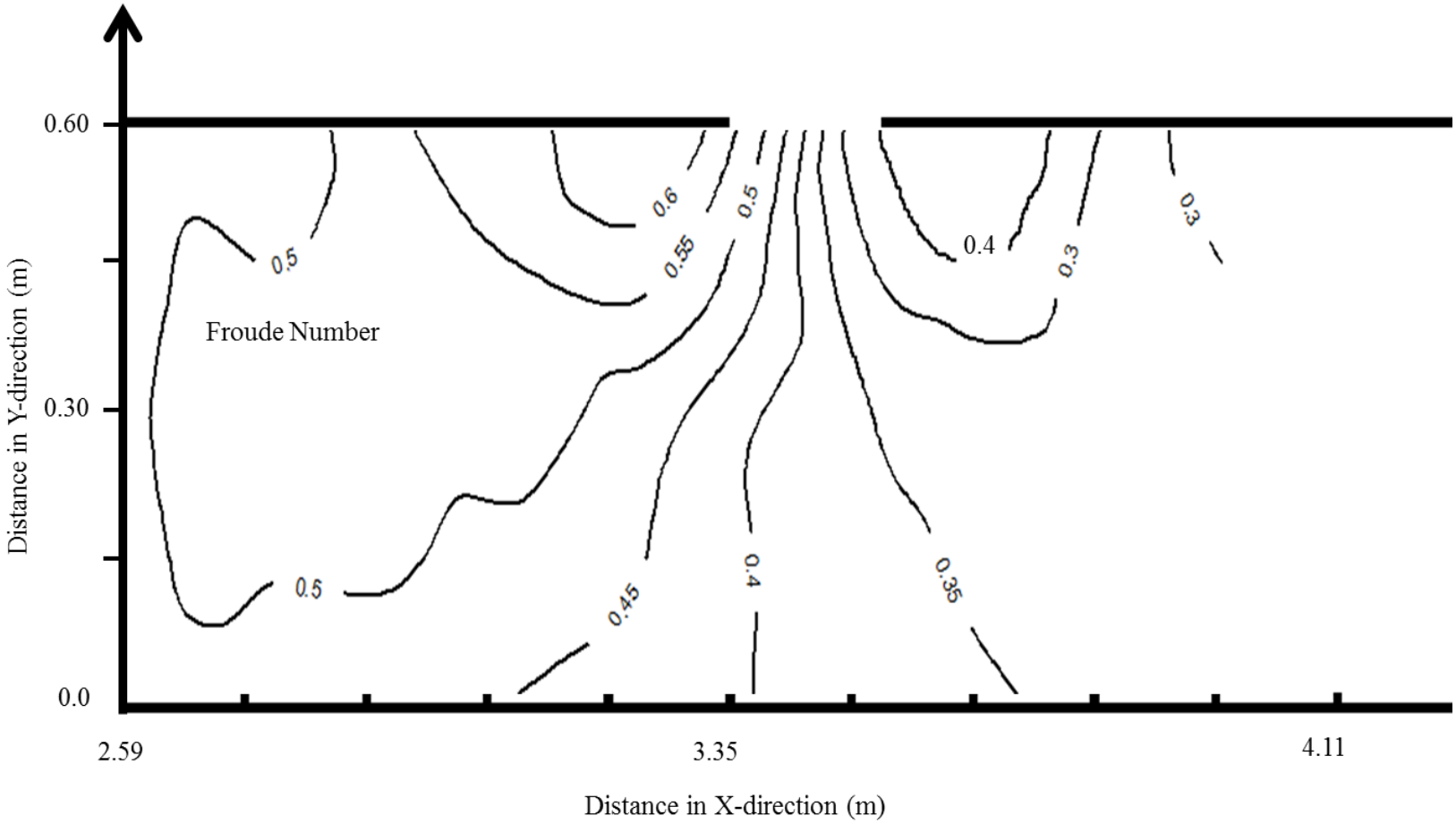

Fig. A2.27 Distribution of Froude Number (Case G9)

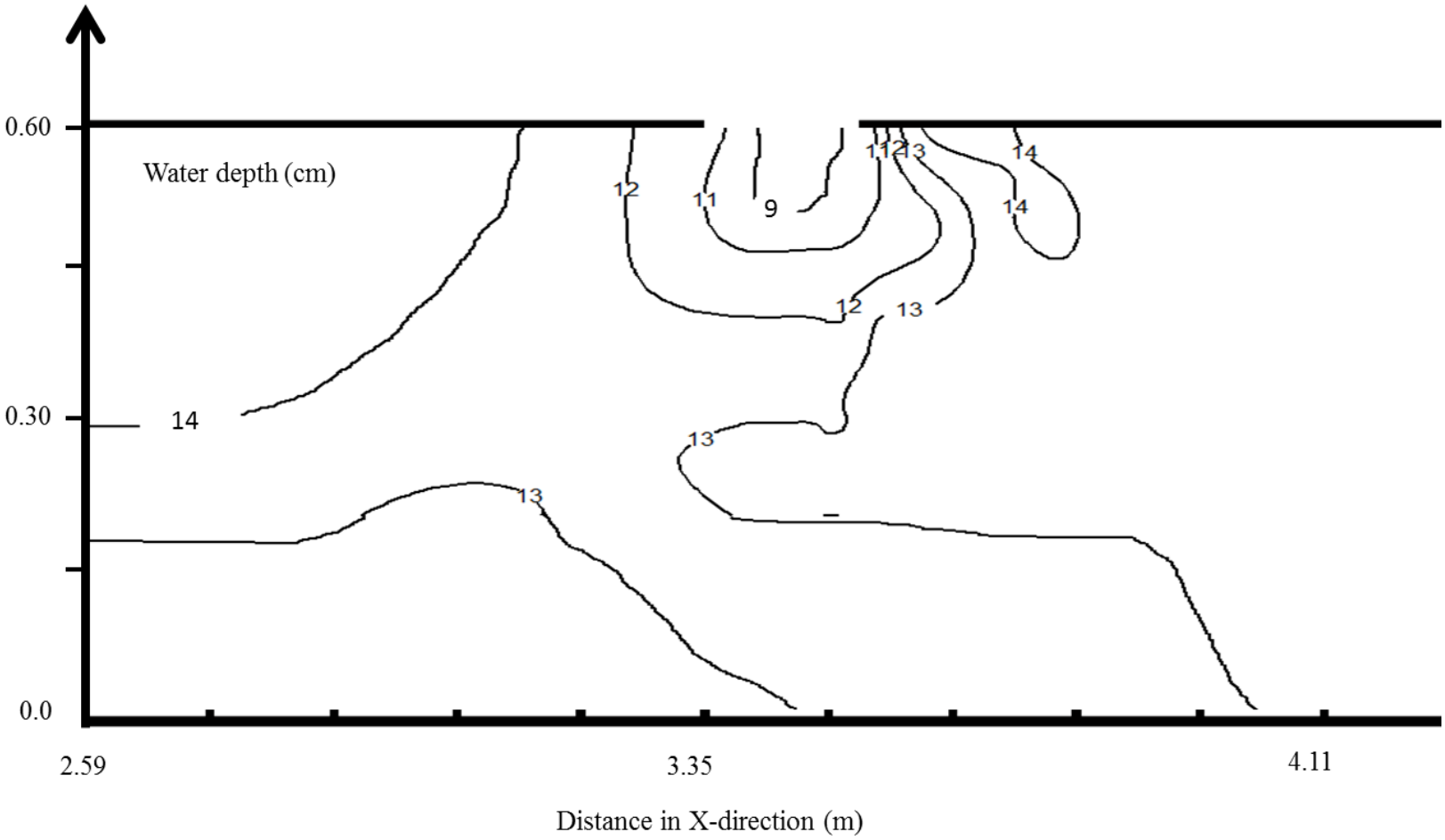

Fig. A2.28 Contours of flow depth (Case G9)

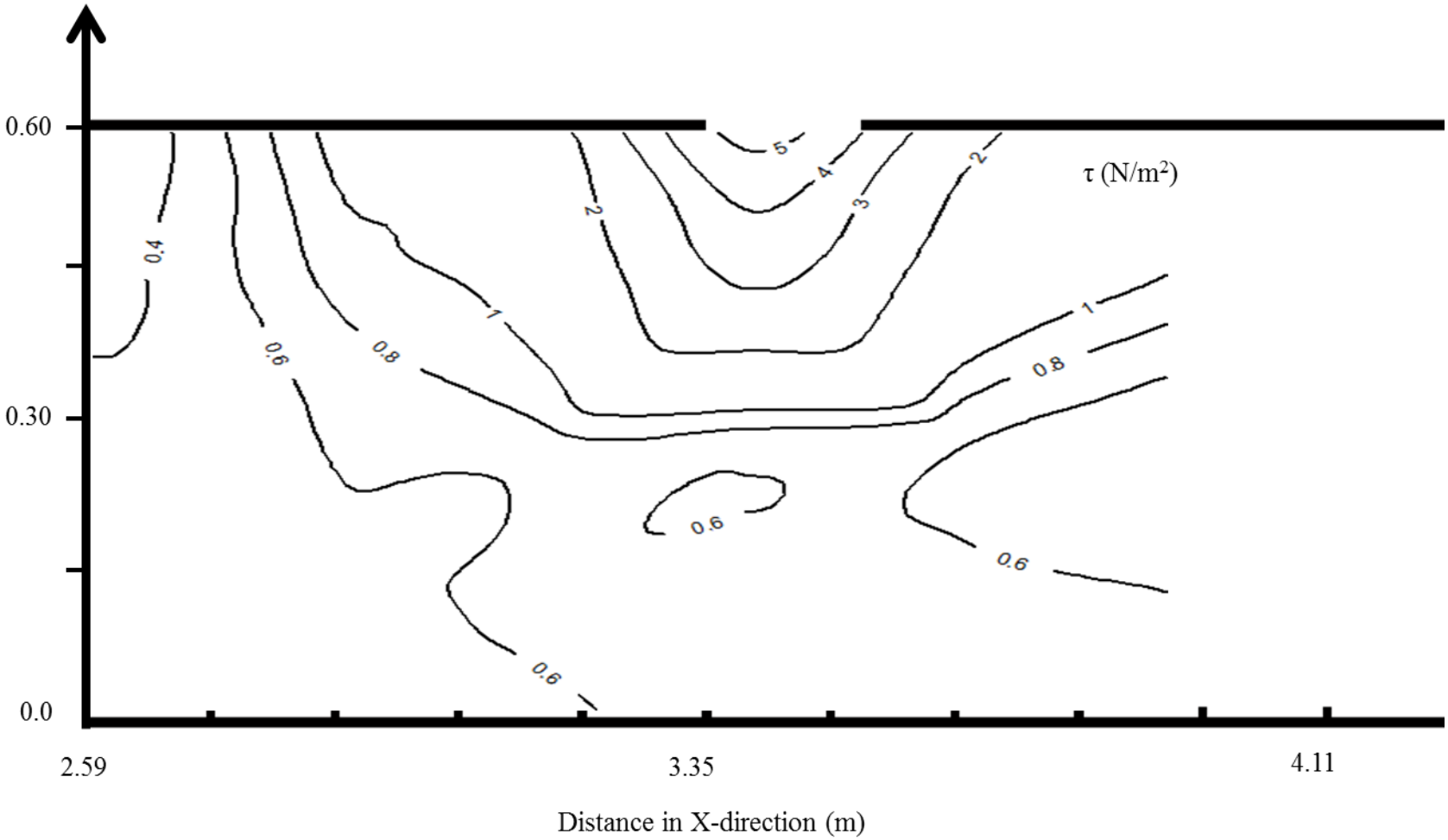

Fig. A2.29 Contours of bed shear stress (Case G9)

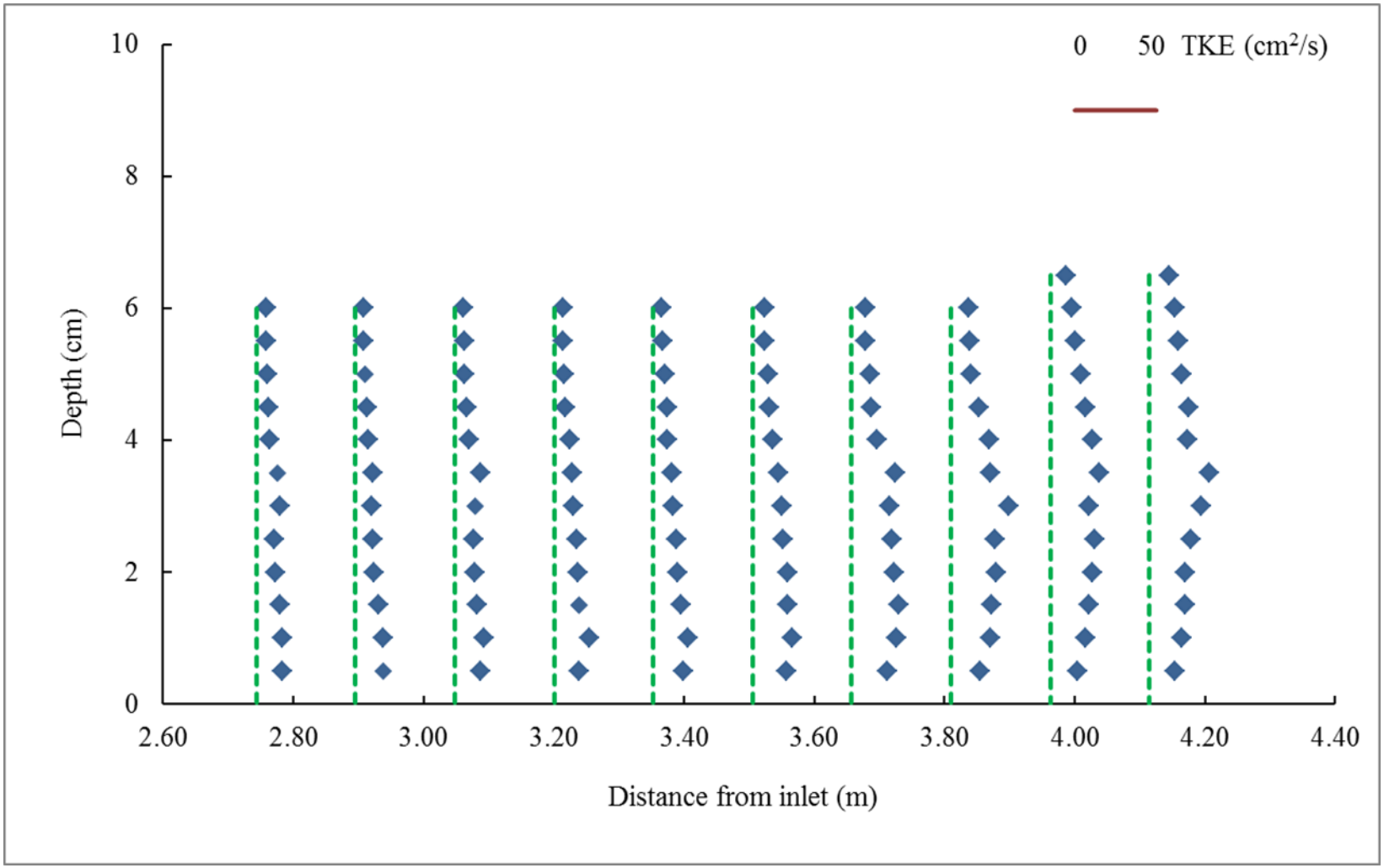

Fig. A2.30 Distribution of TKE along Y1 (Case G9)

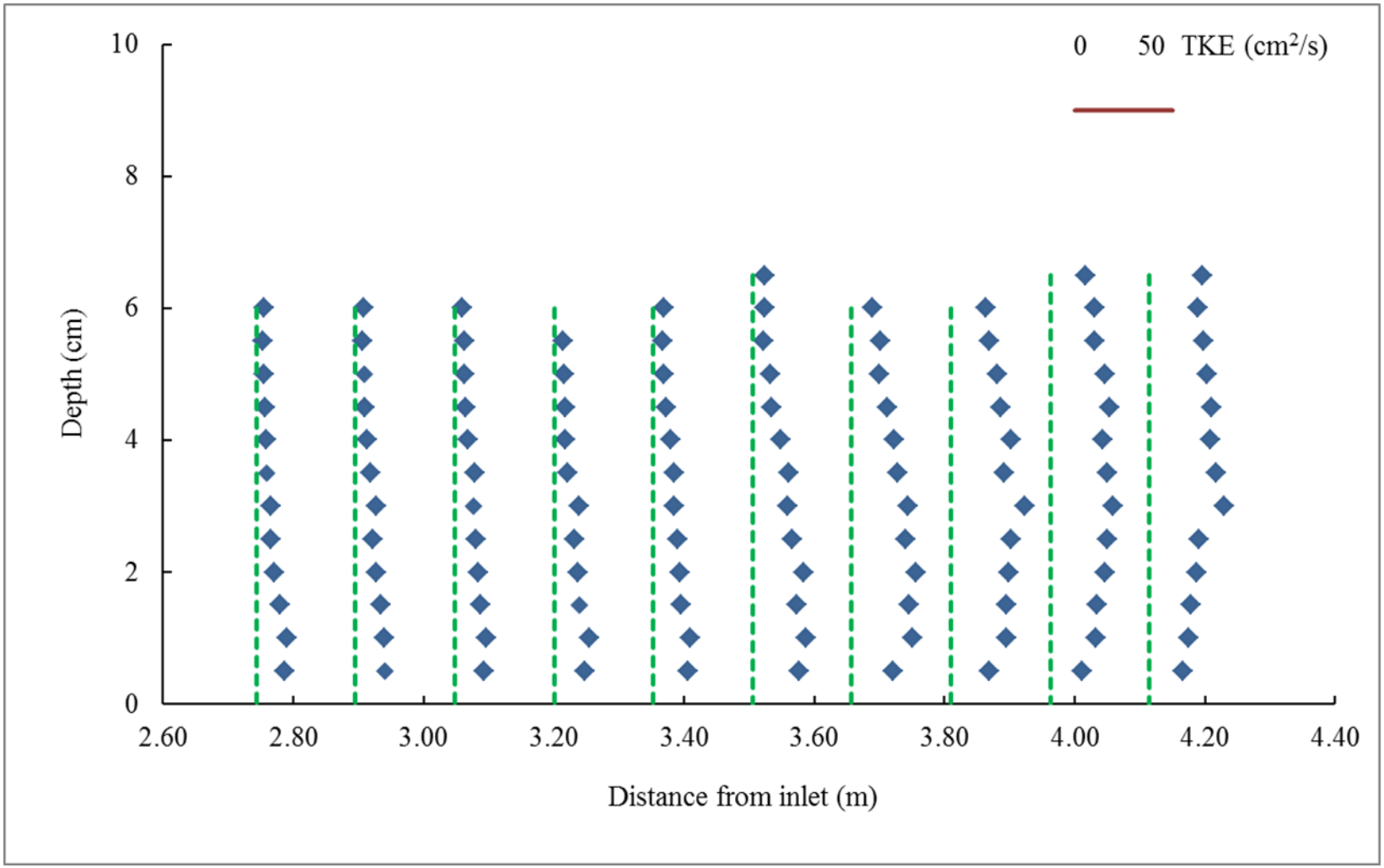

Fig. A2.31 Distribution of TKE along Y2 (Case G9)

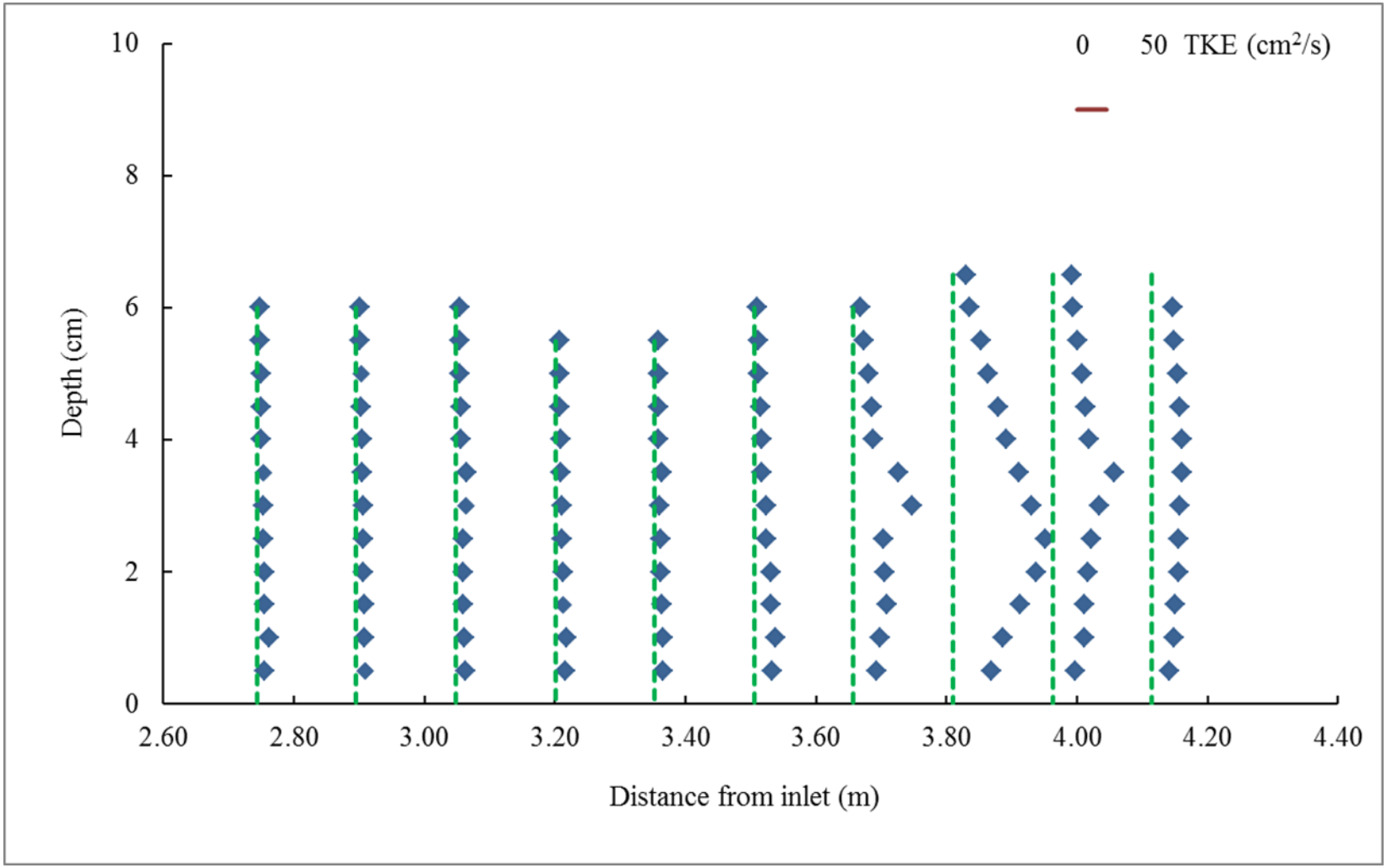

Fig. A2.32 Distribution of TKE along Y3 (Case G9)

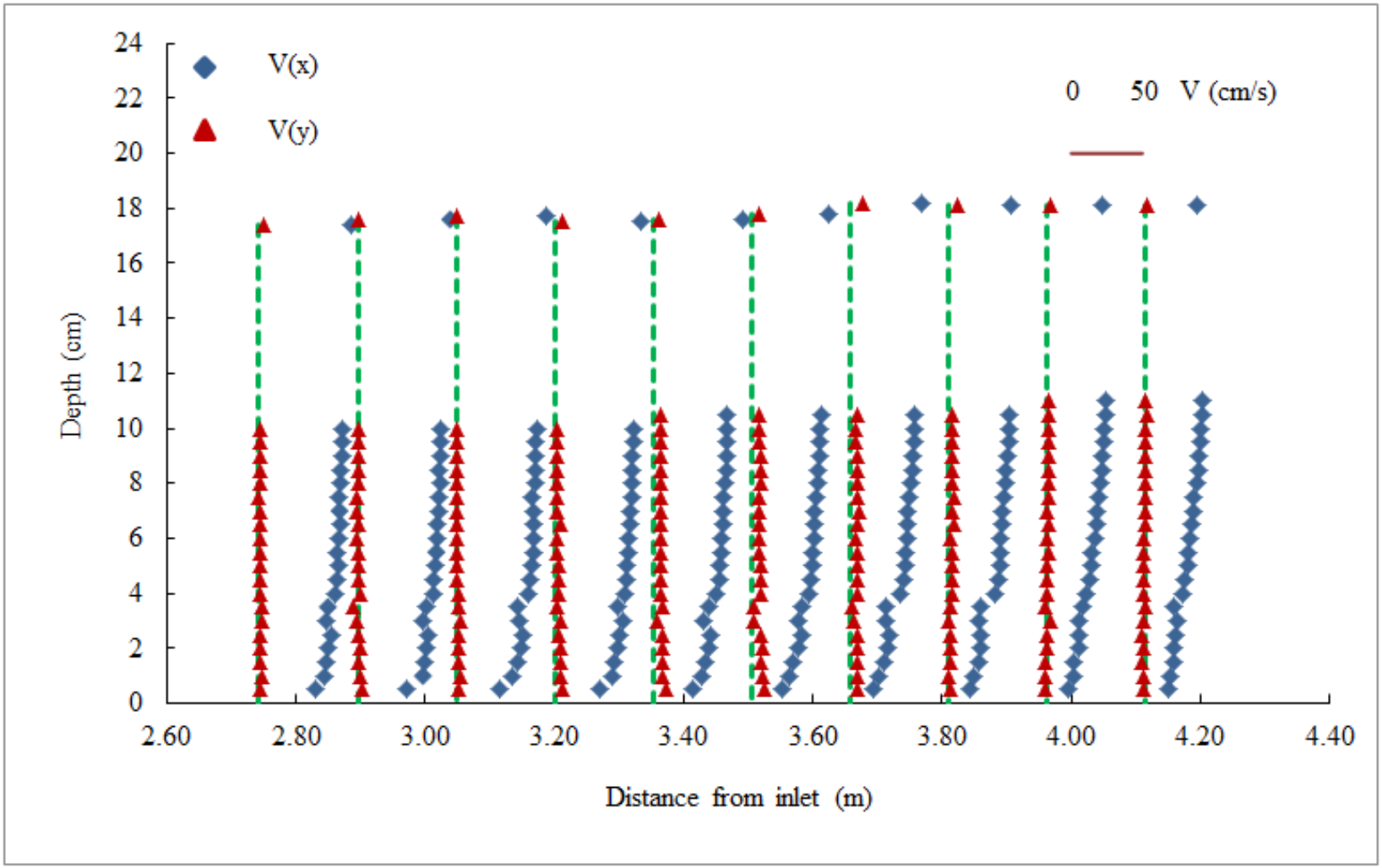

(a) Along Y1

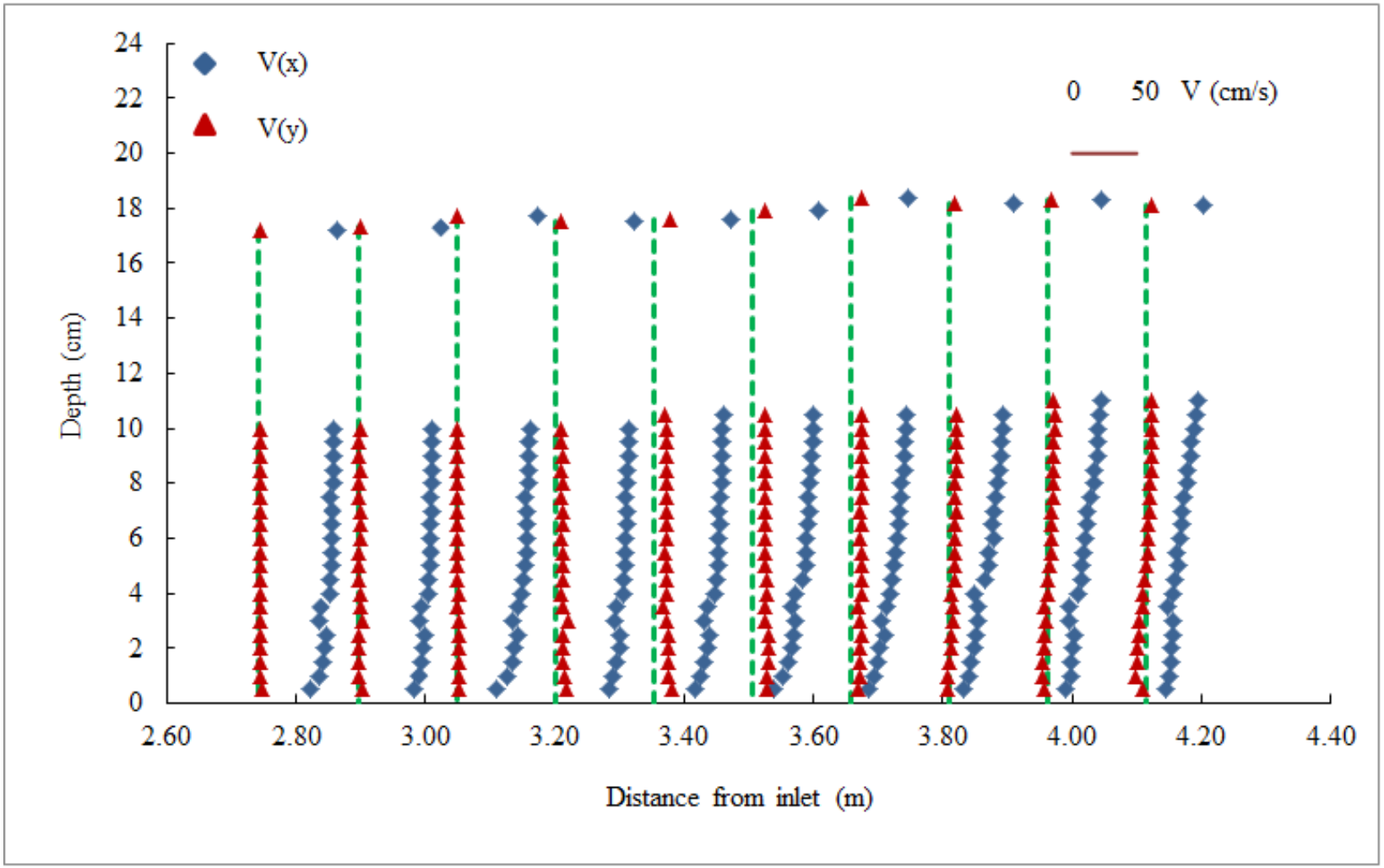

(b) Along Y2

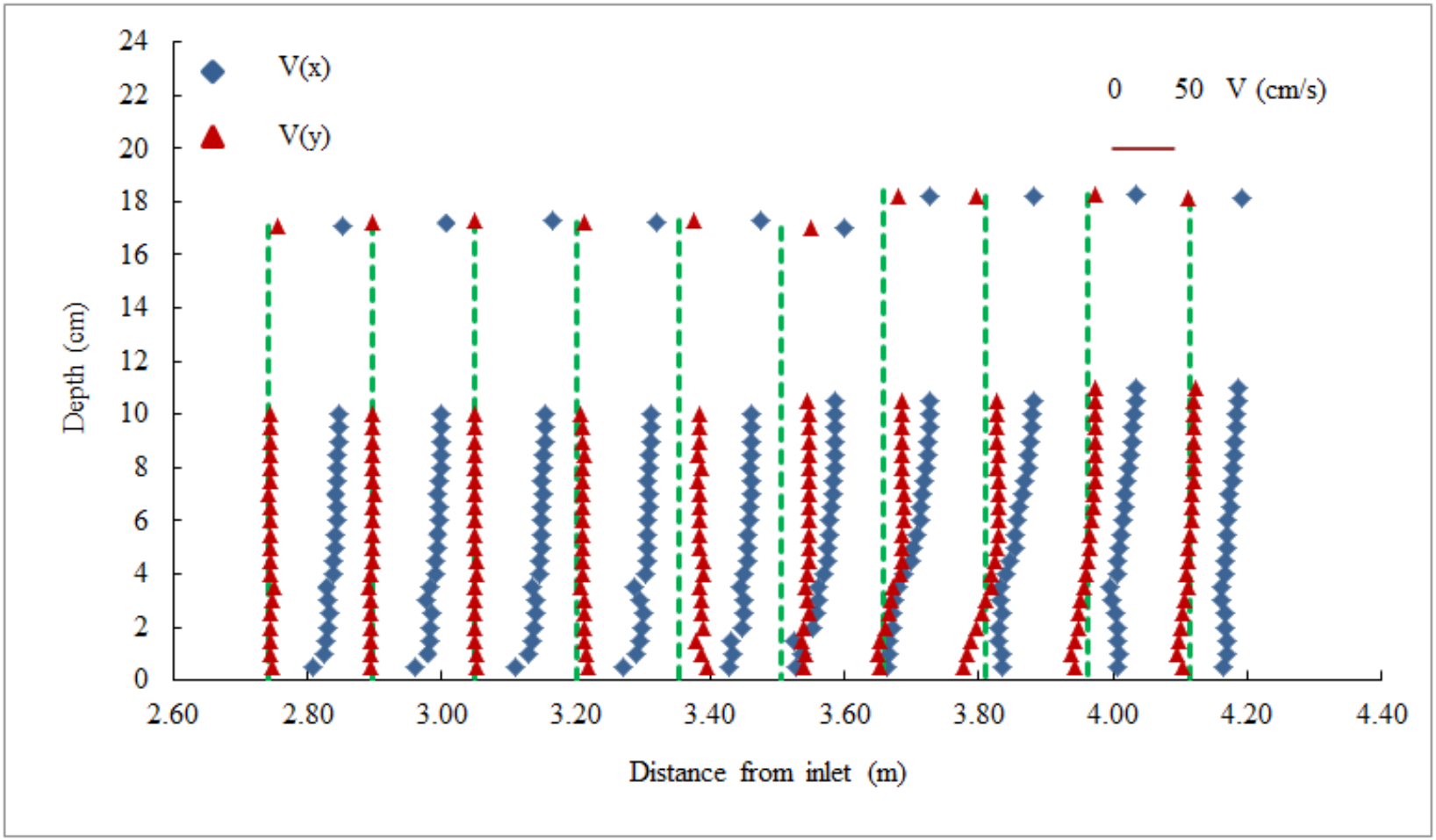

(c) Along Y3

Fig. A2.33 Measured results for velocity distribution (Case G11)

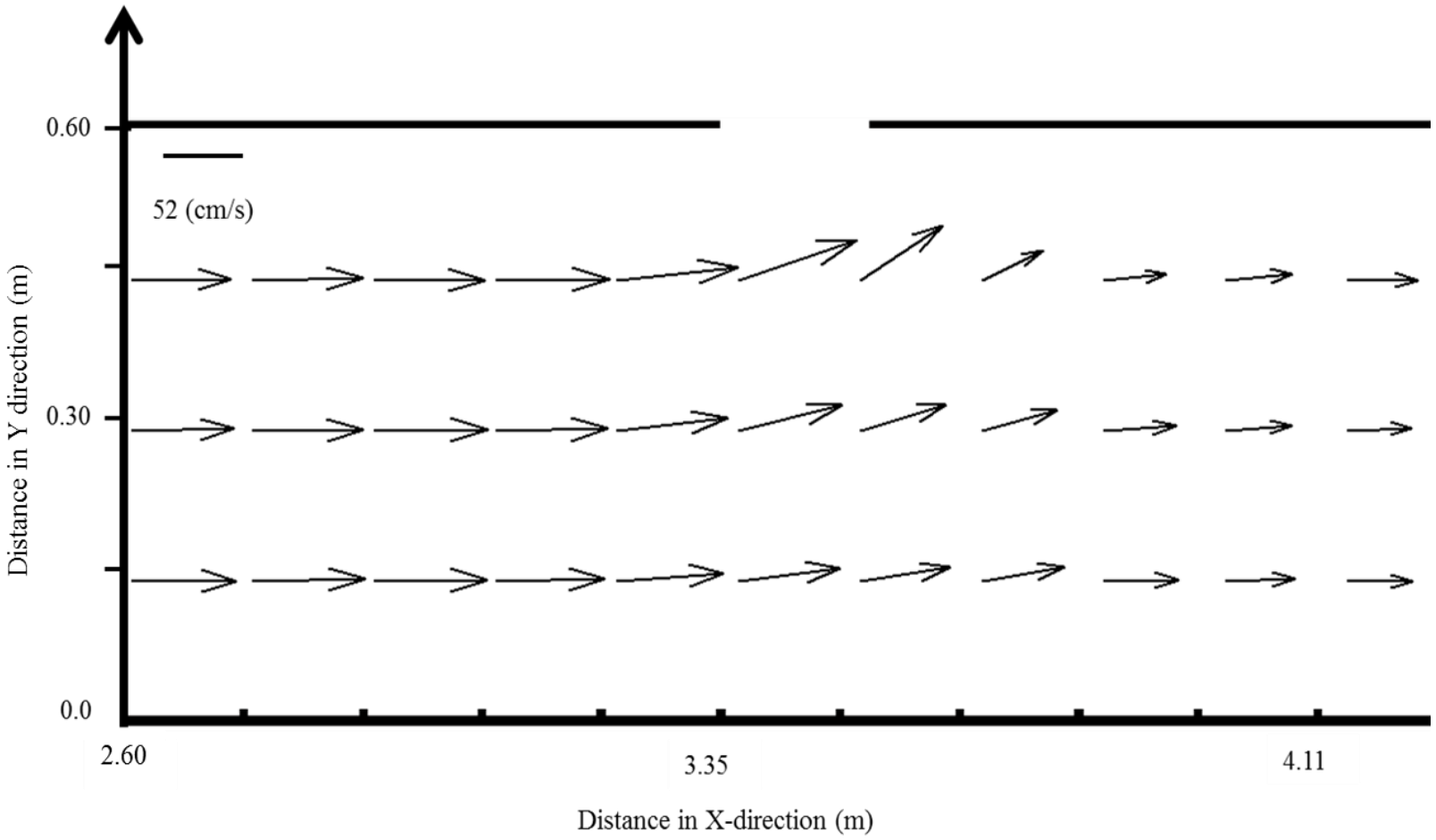

Fig. A2.34 Average velocities (Case G11)

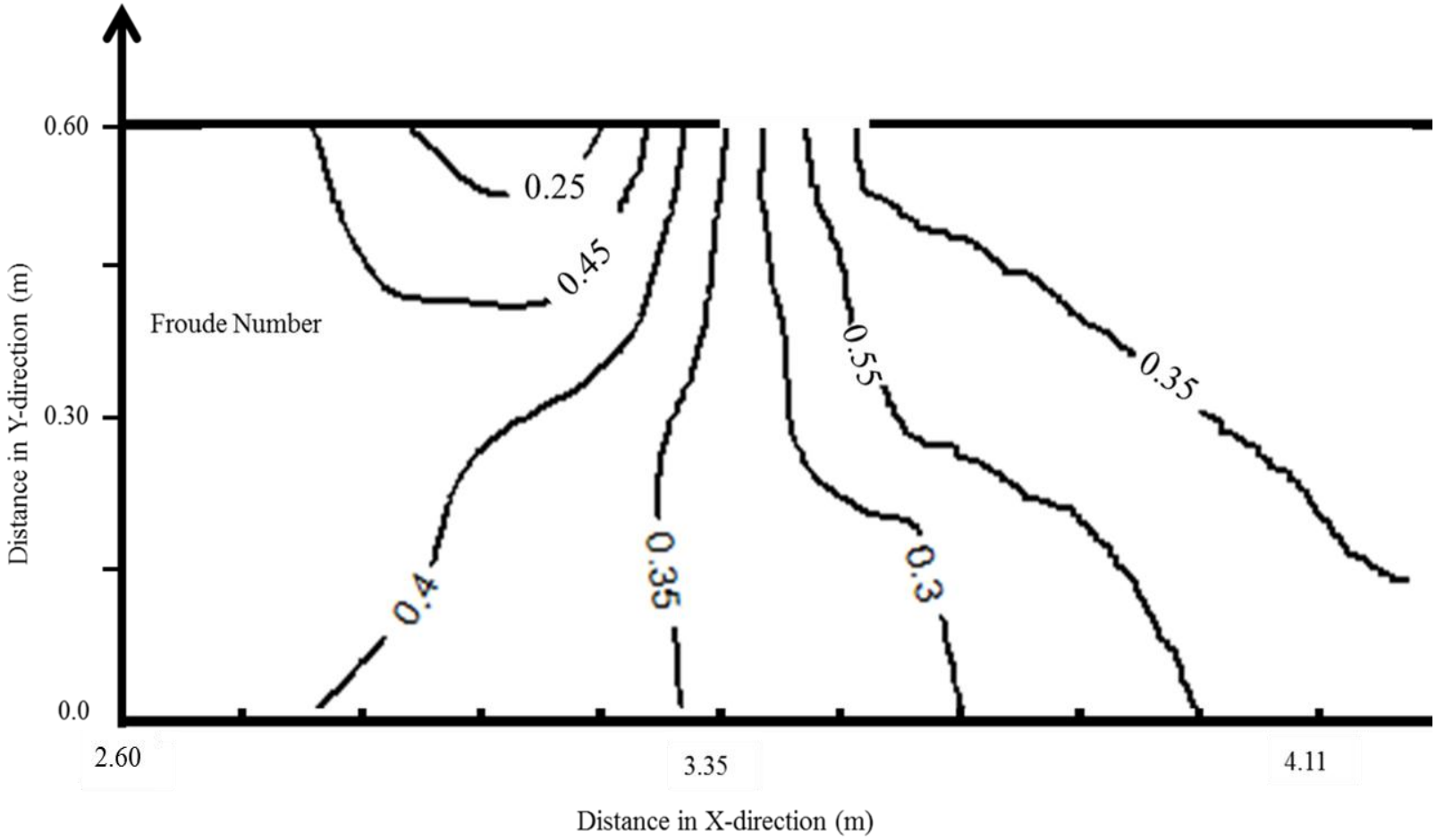

Fig. A2.35 Distribution of Froude Number (Case G11)

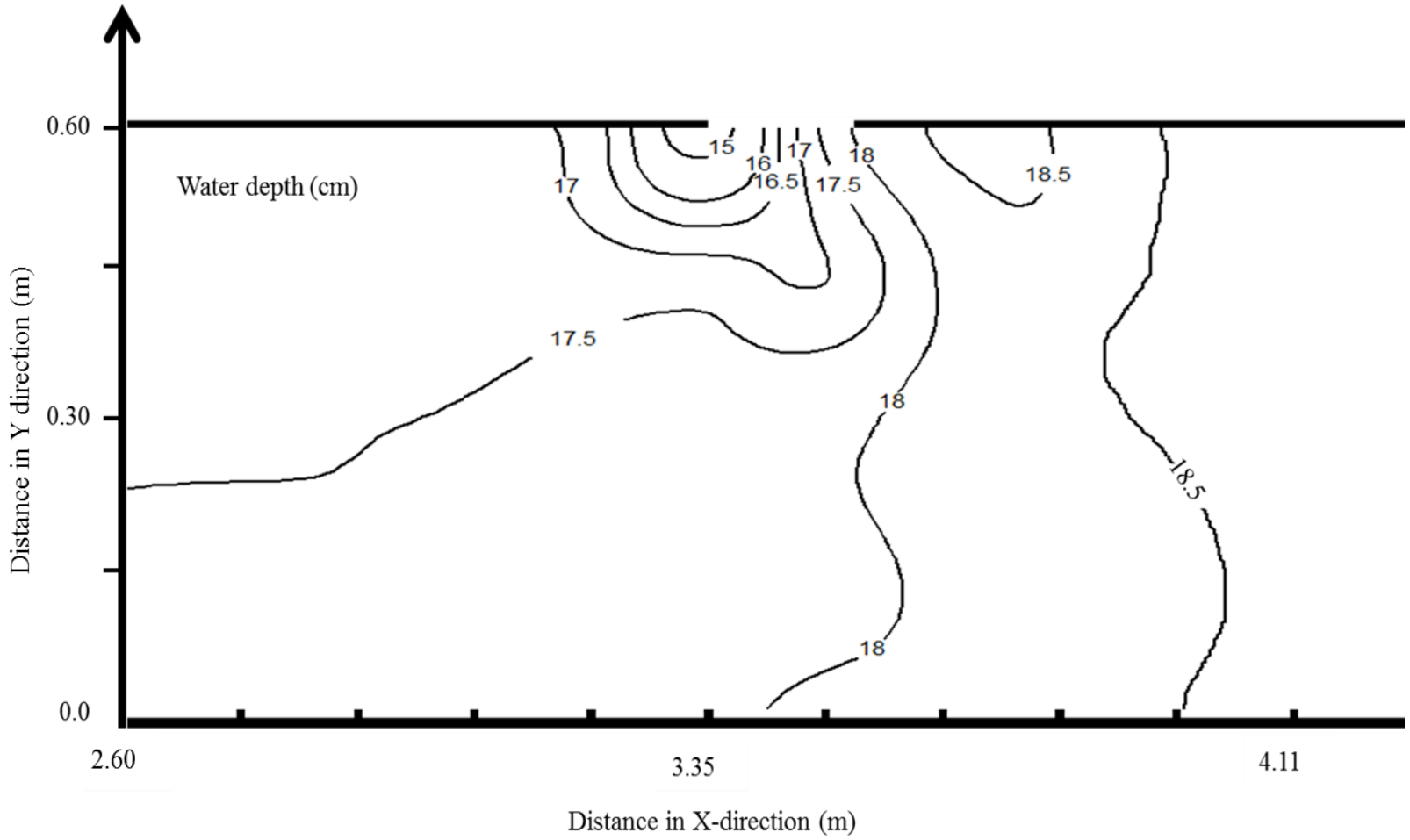

Fig. A2.36 Contours of flow depth (Case G11)

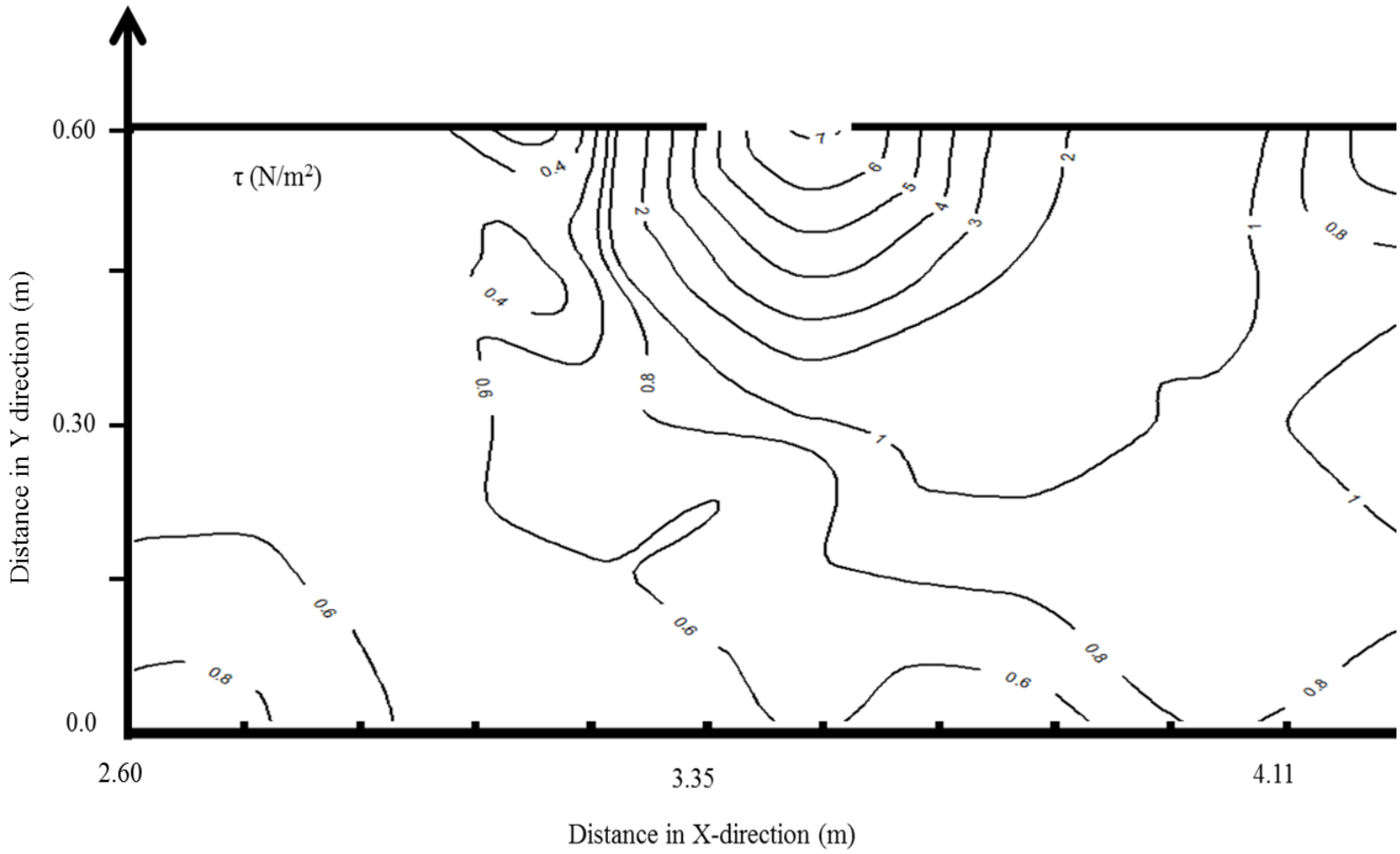

Fig. A2.37 Contours of bed shear stress (Case G11)

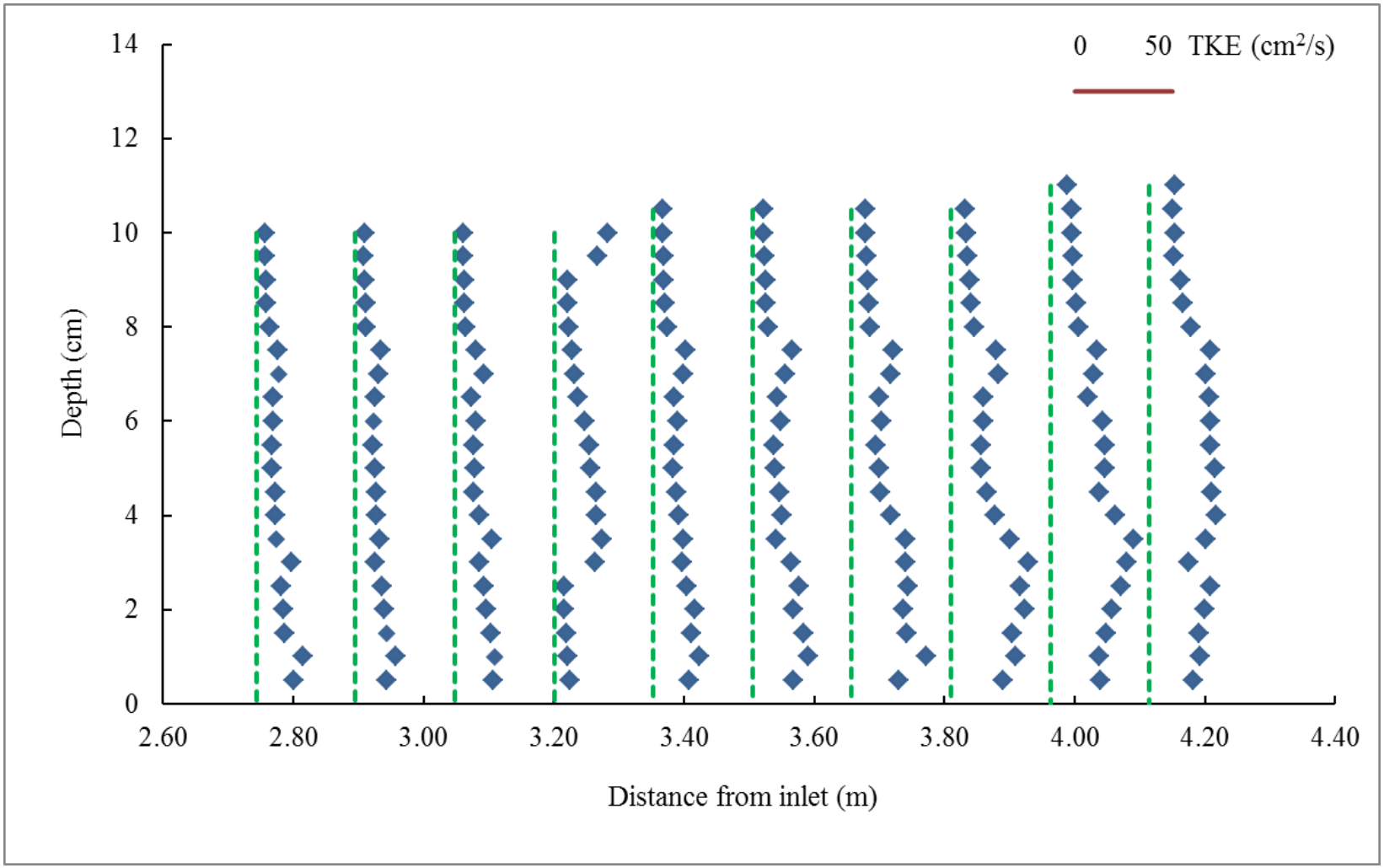

Fig. A2. 38 (a) Distribution of TKE along Y1 (Case G11)

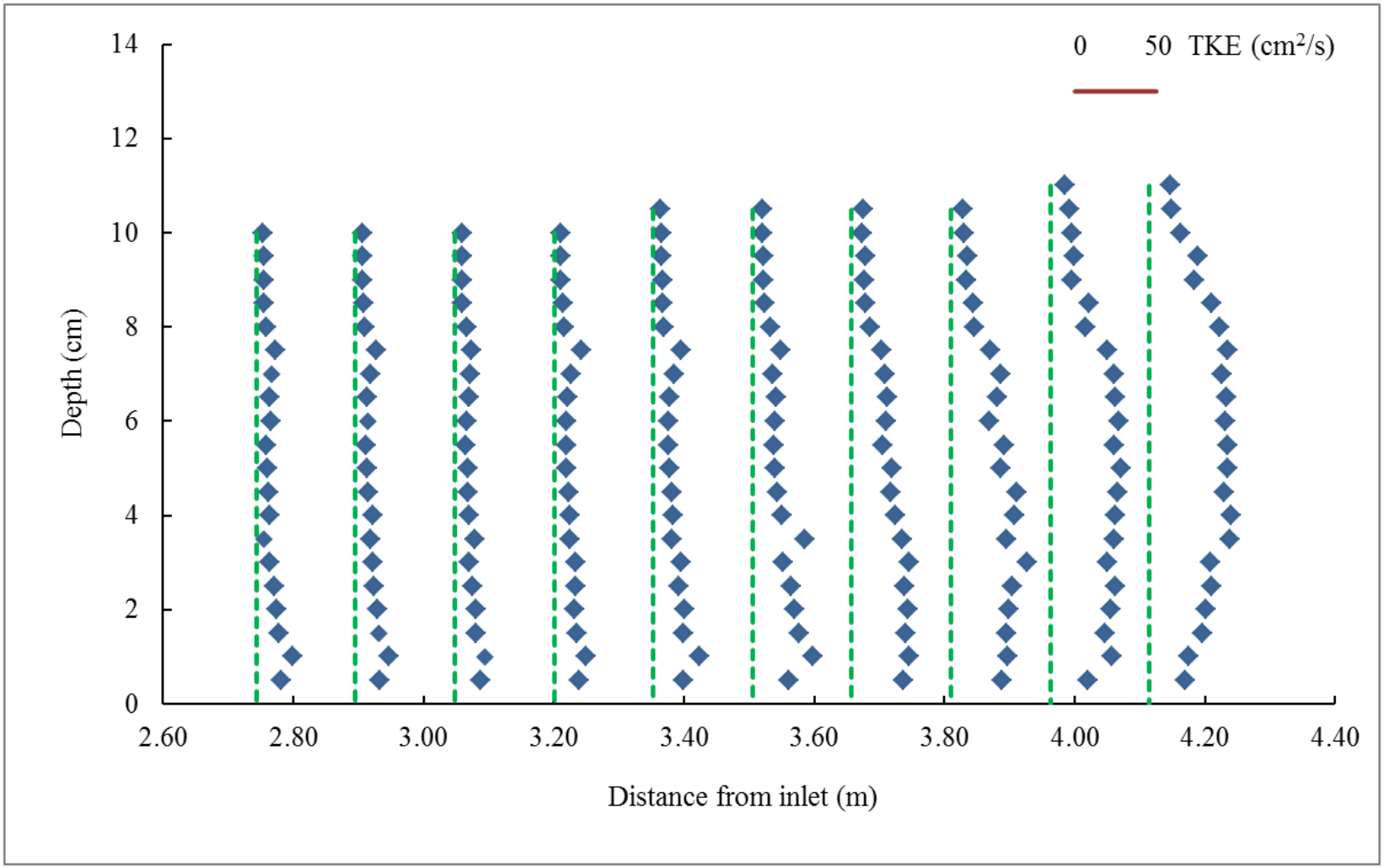

Fig. A2. 39 (b) Distribution of TKE along Y2 (Case G11)

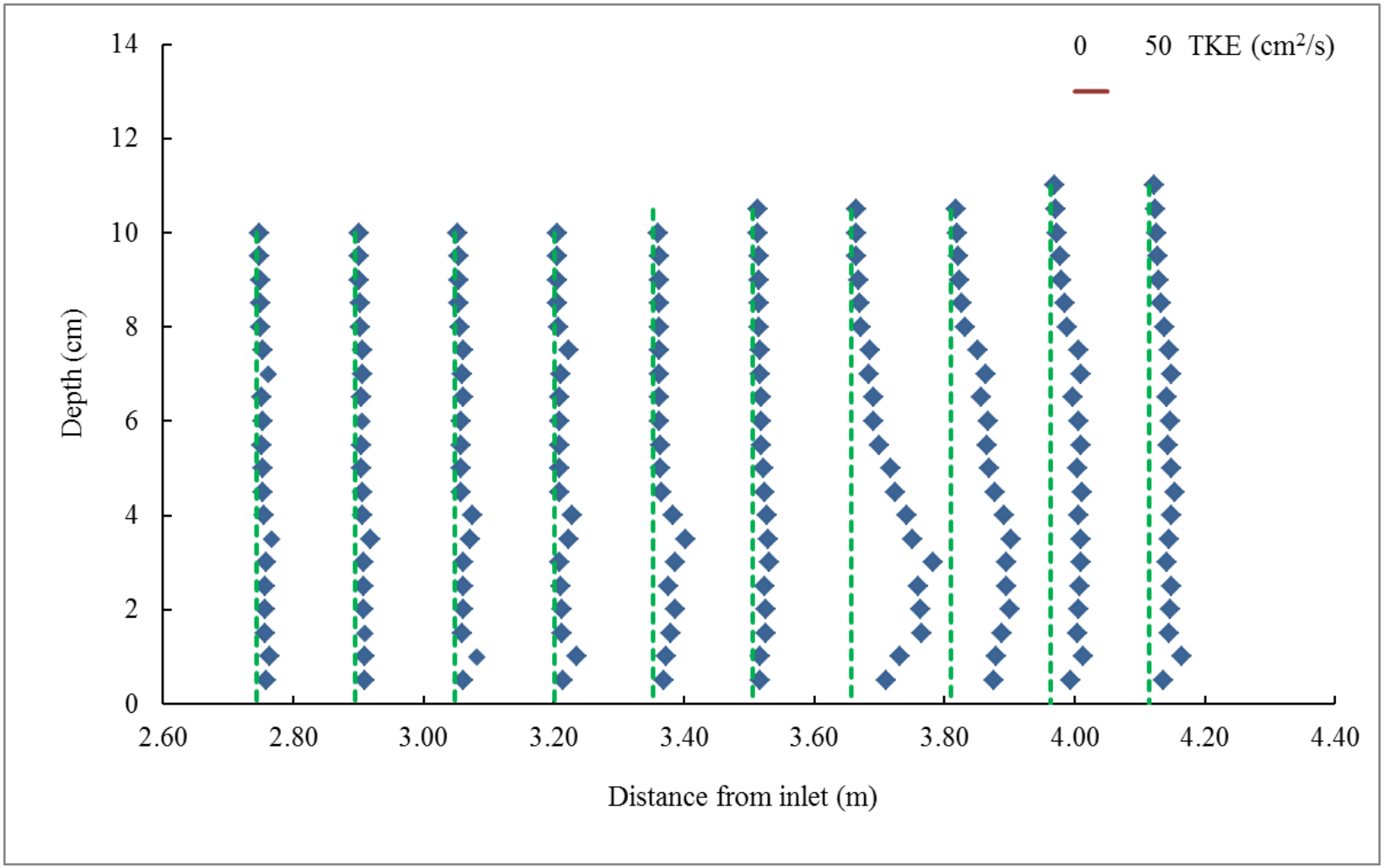

Fig. A2. 40 (c) Distribution of TKE along Y3 (Case G11)

Appendix – 3

RESULTS OF 17TH STREET CANAL BREACH

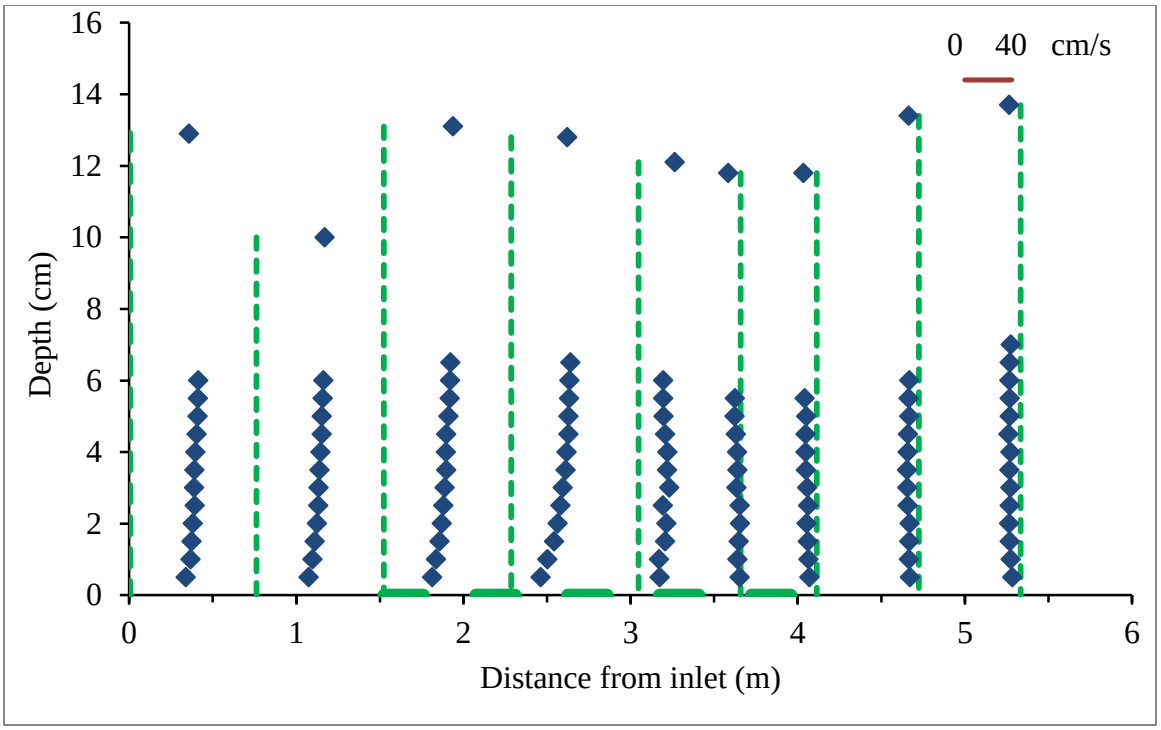

(a) X-velocity

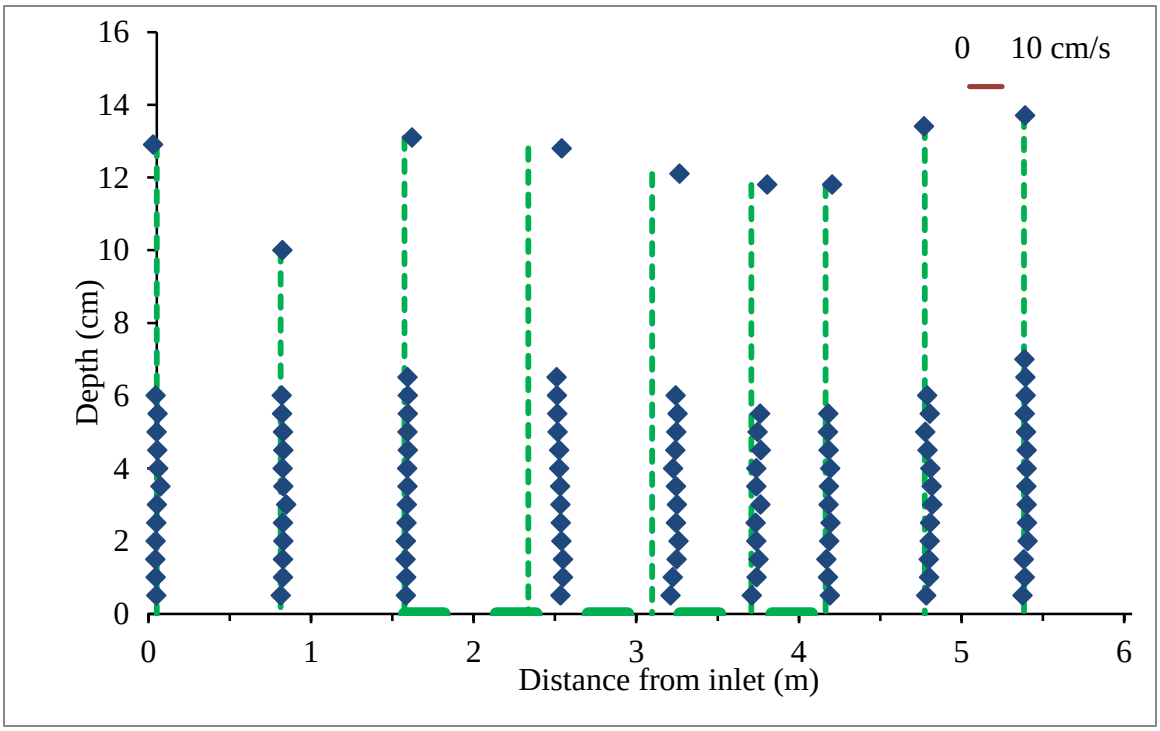

(b) Y-velocity

Fig. A3.1 Measured velocities along Y3 (case 3)

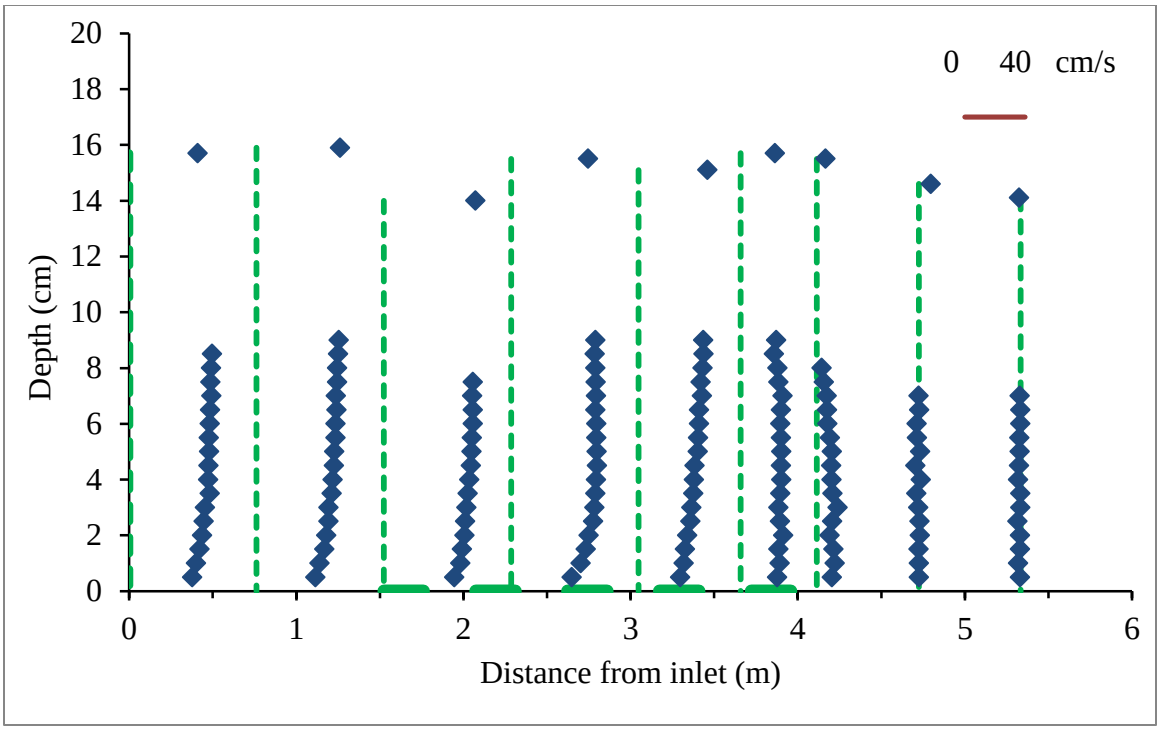

(a) X-velocity

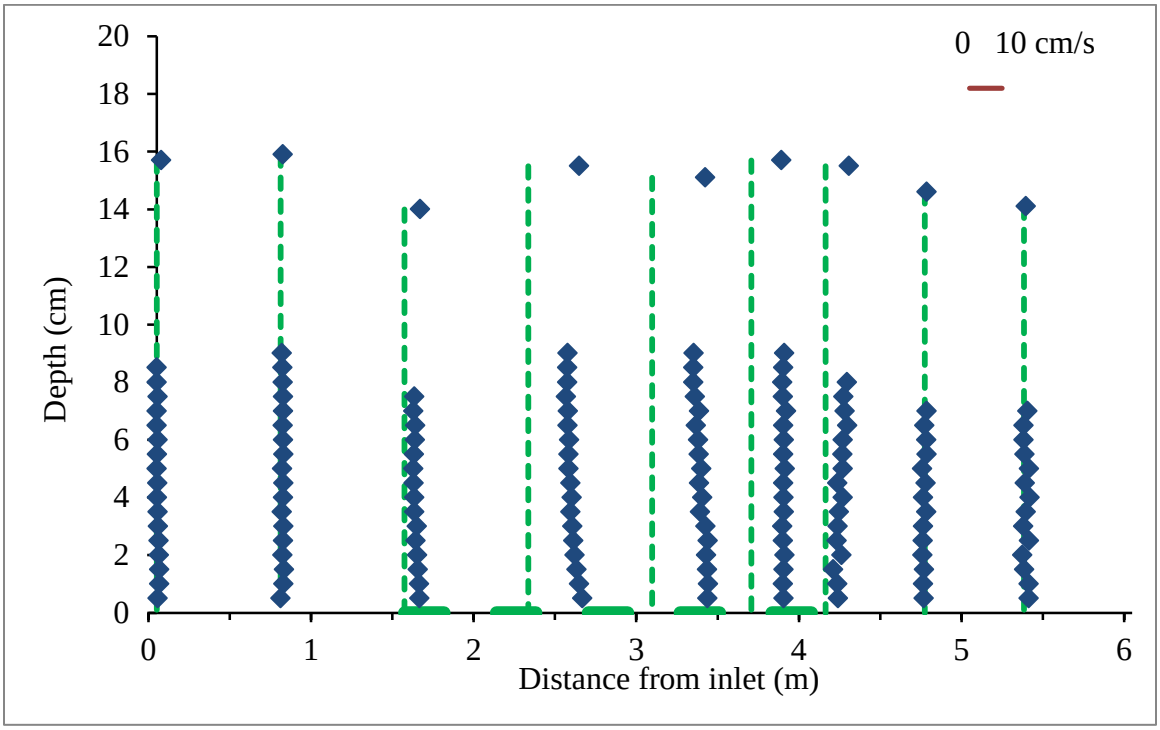

(b) Y-velocity

Fig. A3.2 Measured velocities along Y5 (case 3)

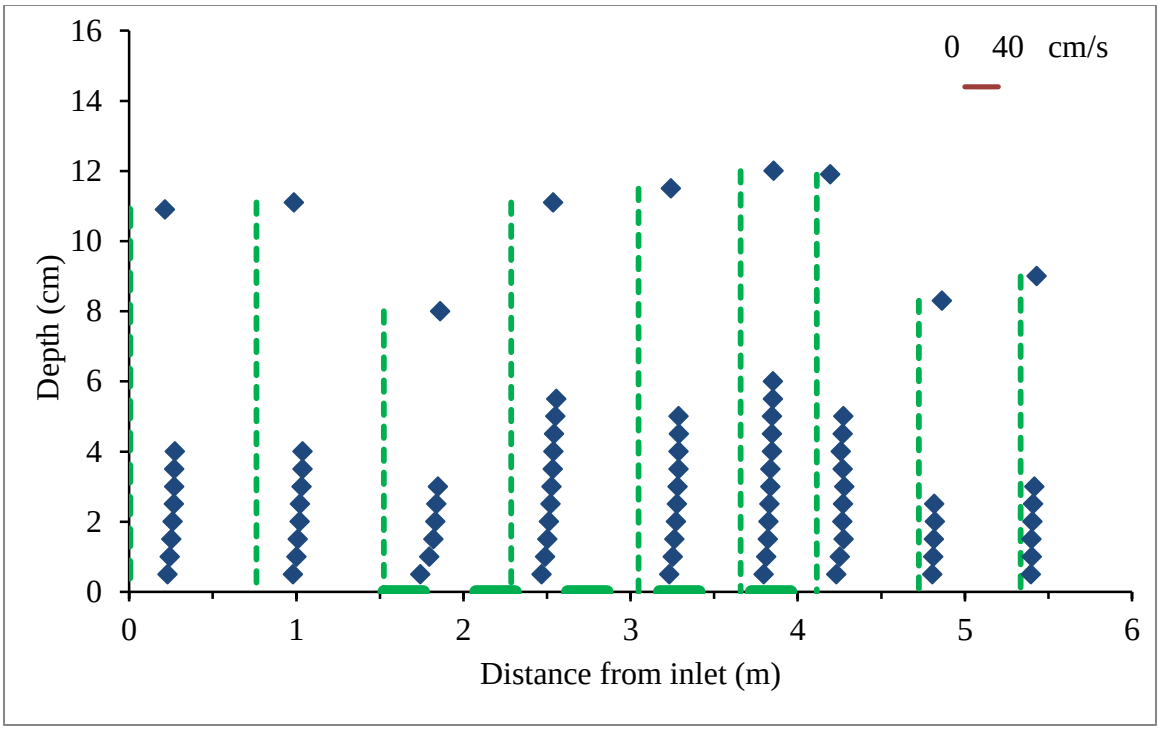

(a) X-velocity

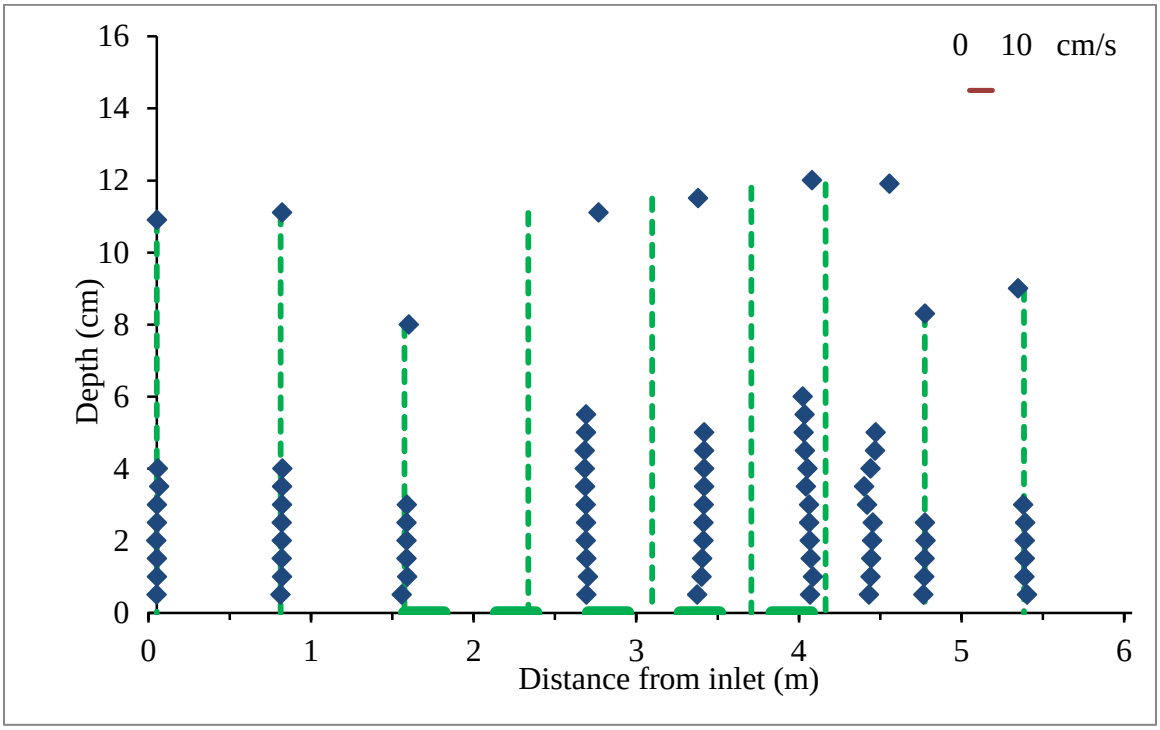

(b) Y-velocity

Fig. A3.3 Measured velocities along Y7 (case 3)

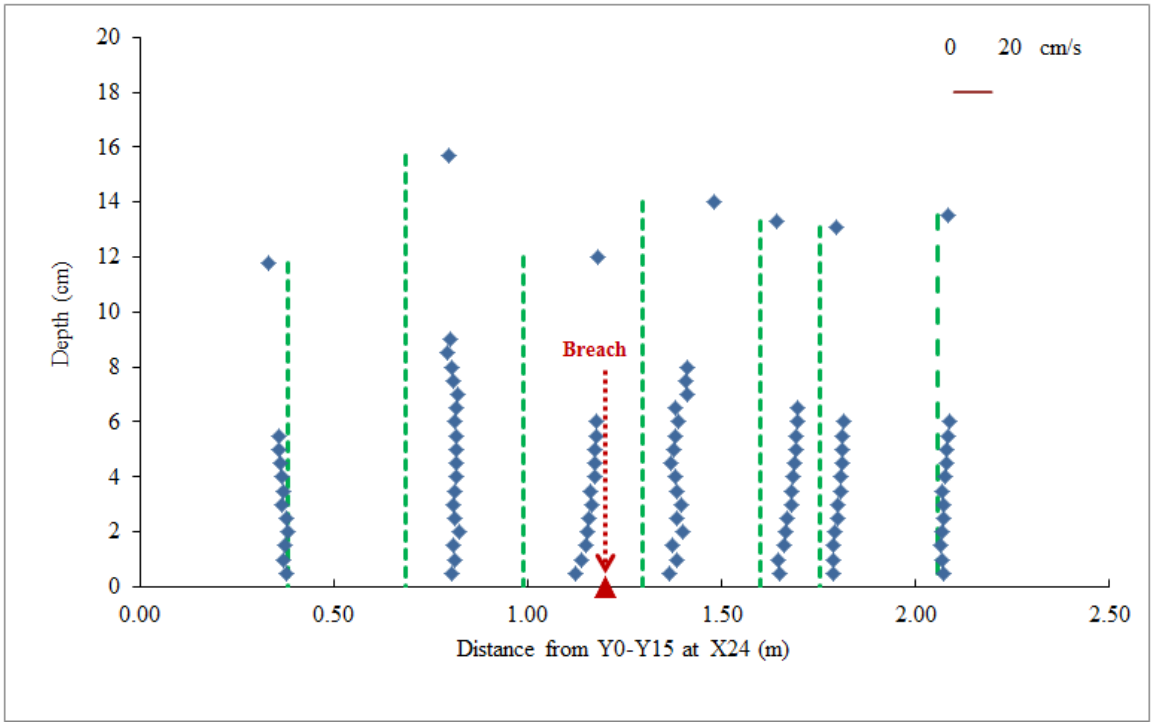

(a) X-velocity

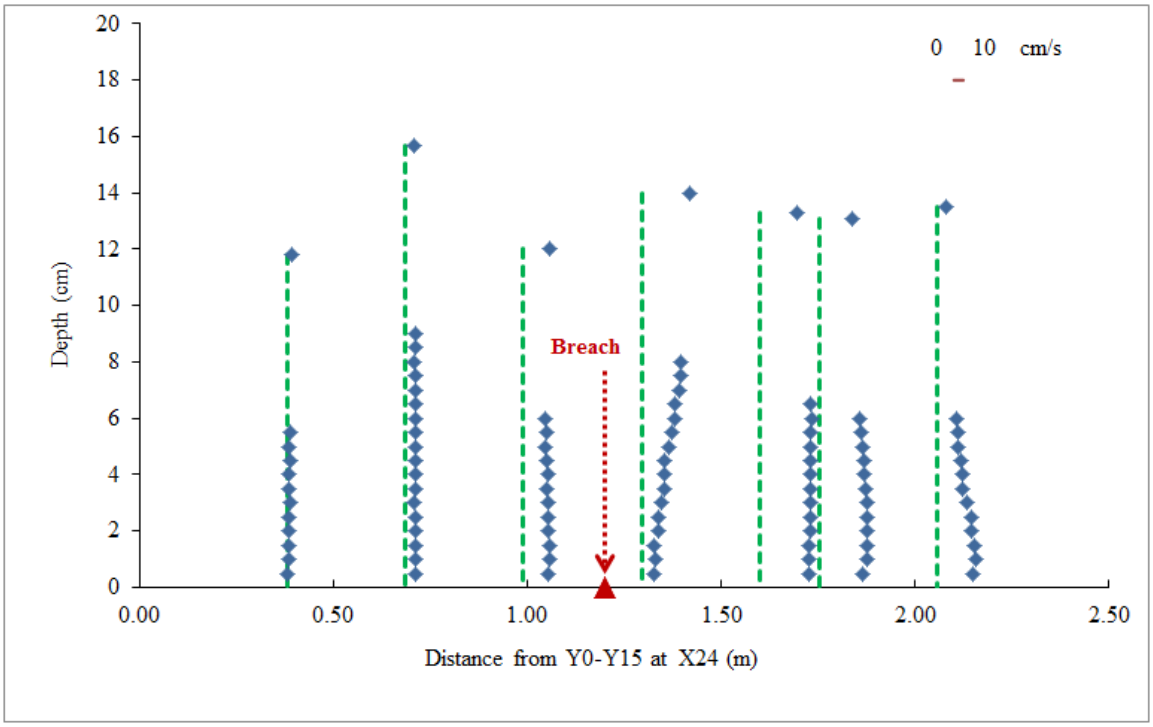

(b) Y-velocity

Fig. A3.4 Measured velocities along X24 (case 3)

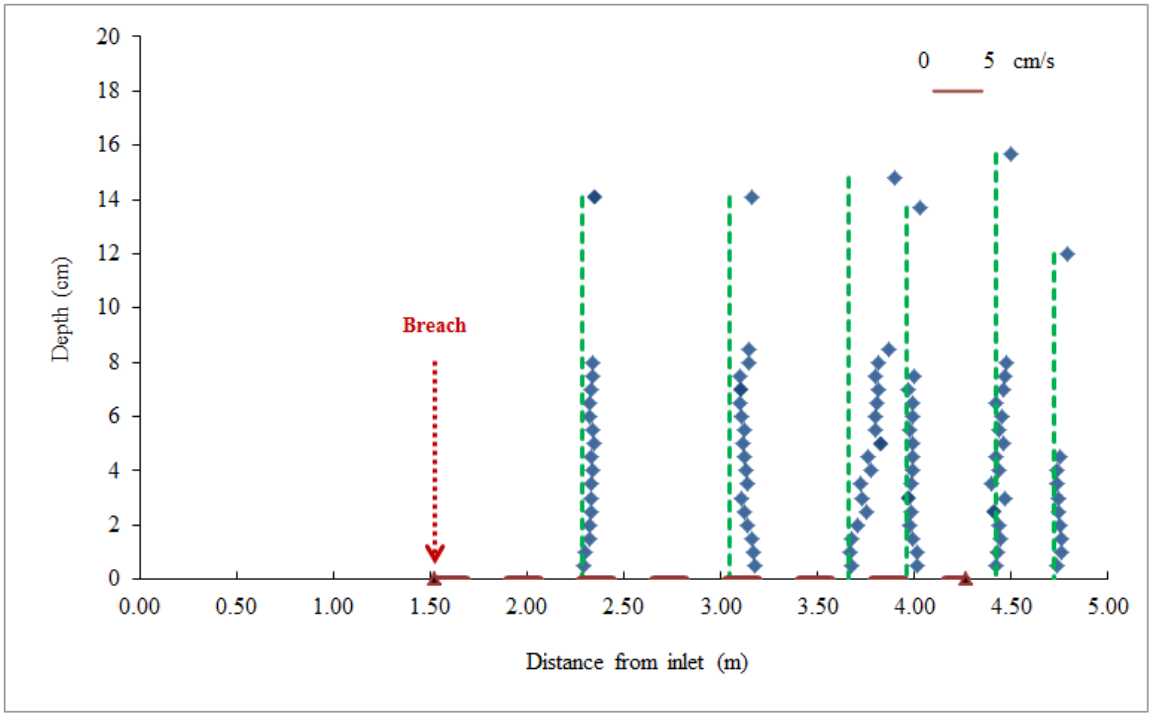

(a) Along Y6

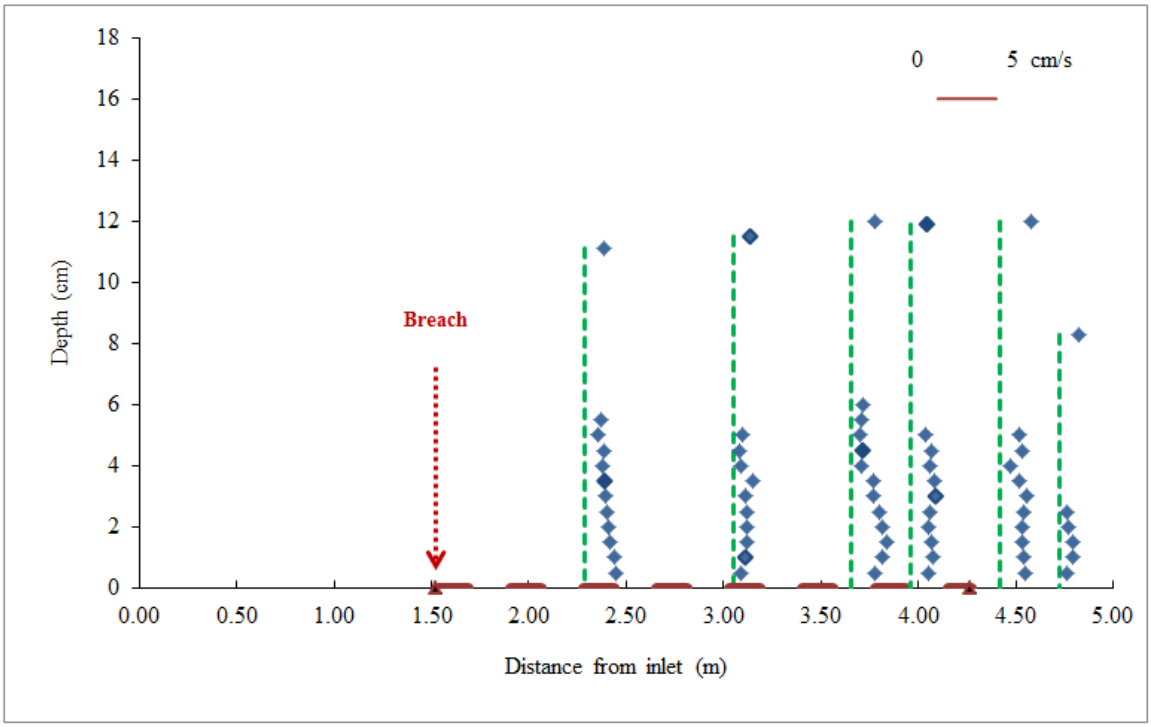

(b) Along Y7

Fig. A3.5 Measured Z-velocities (case 3)

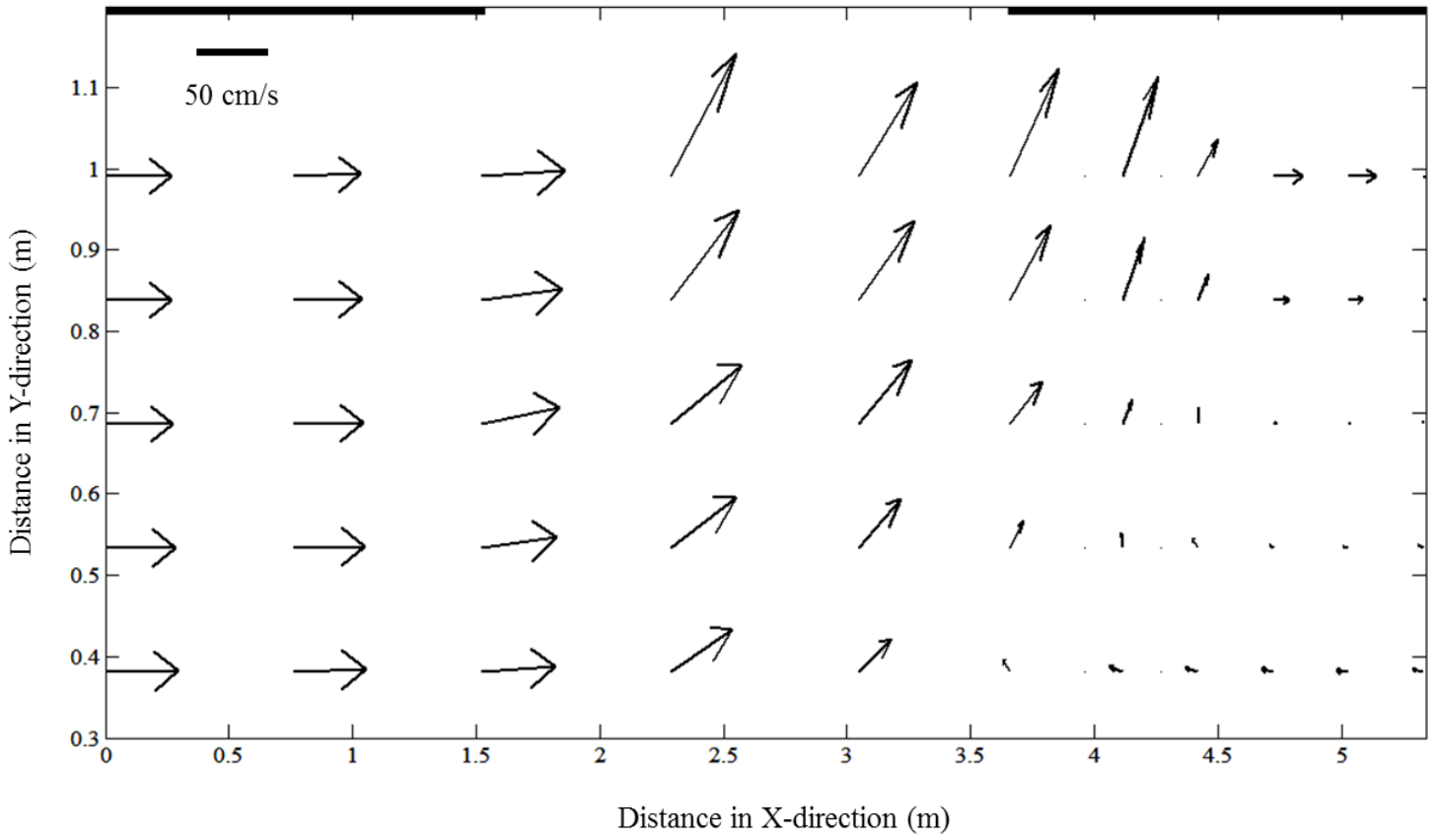

Fig. A3.6 Depth averaged velocities in the channel (case 3)

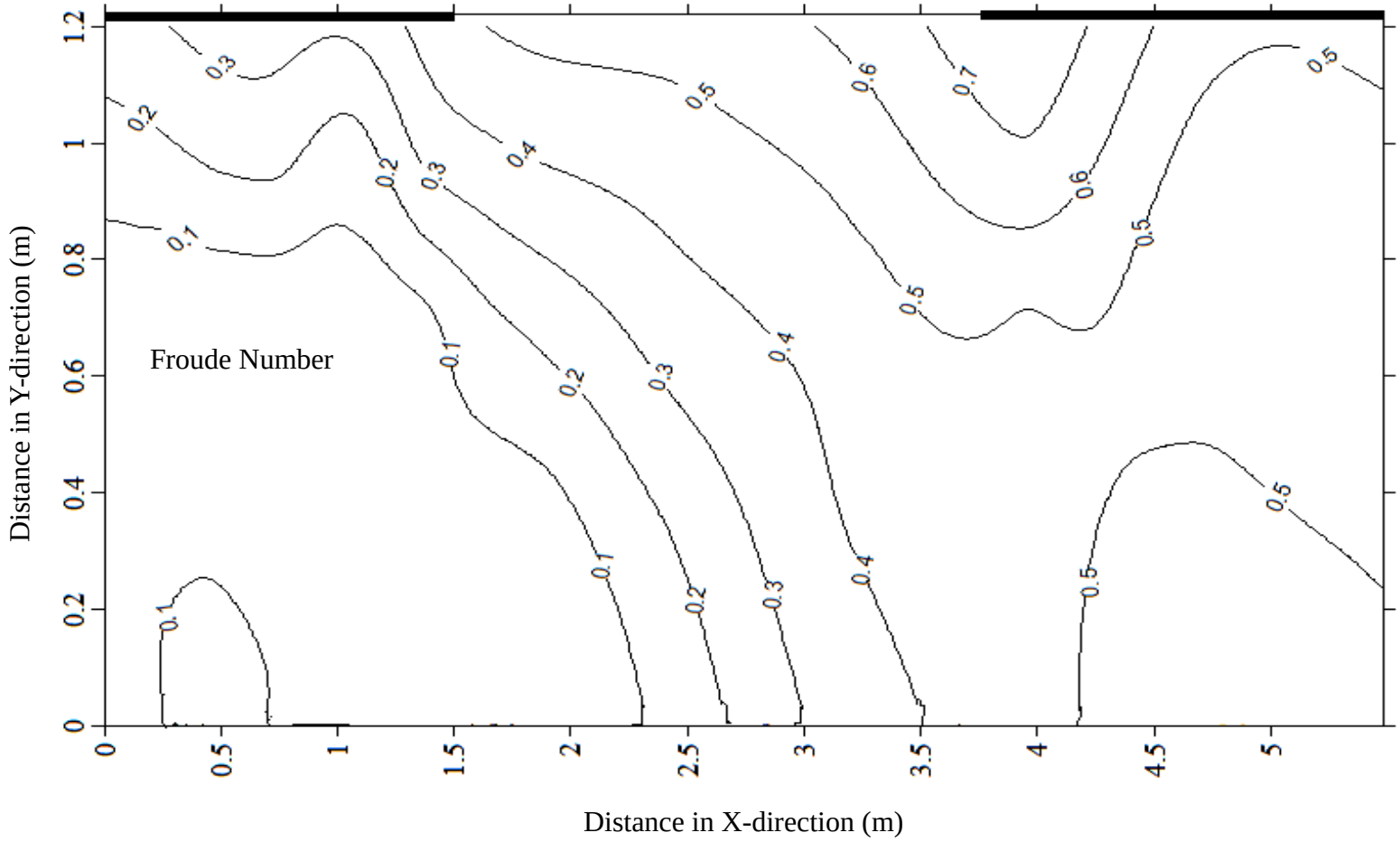

Fig. A3.7 Froude Numbers variation (case 3)

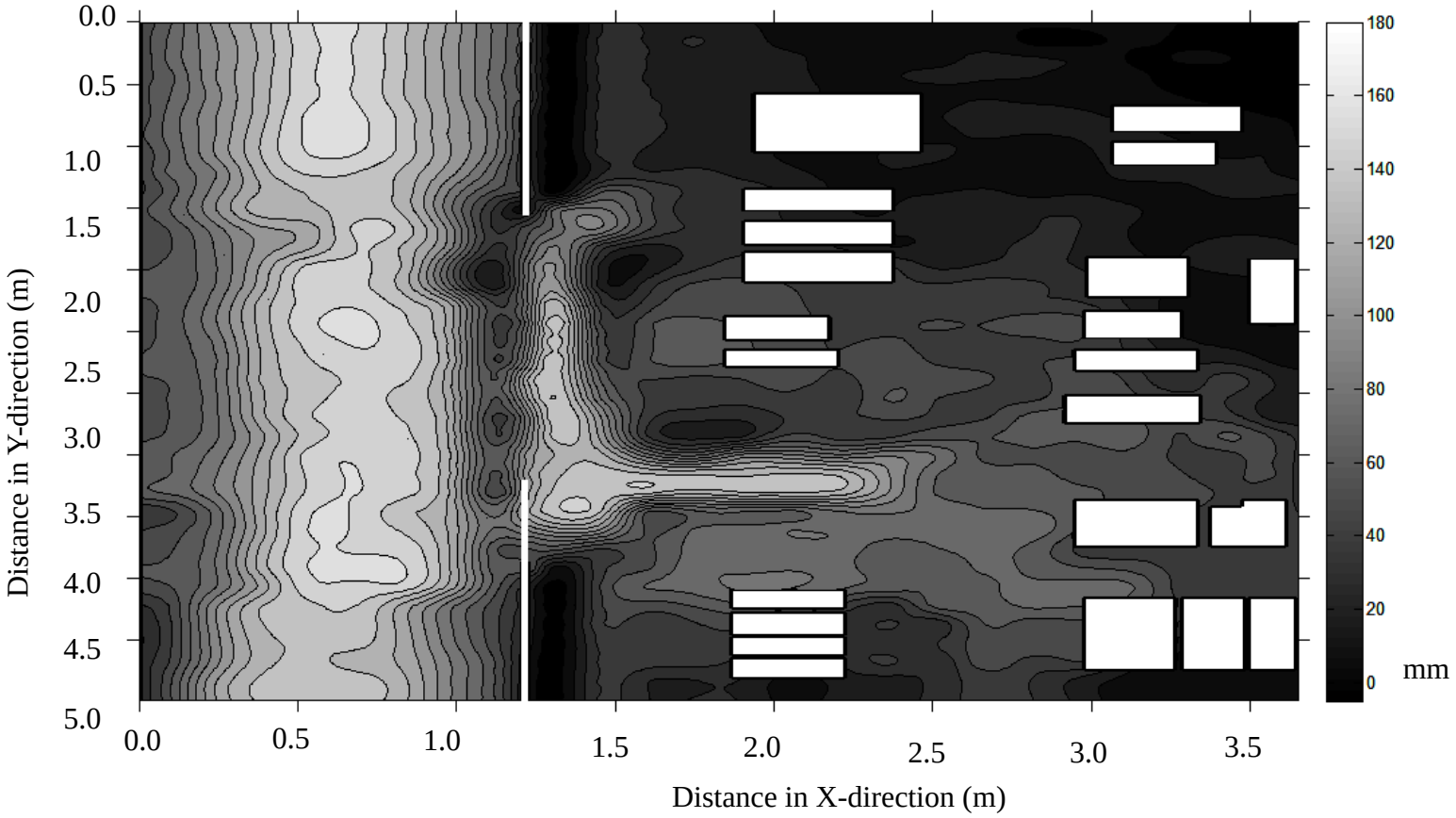

Fig. A3.8 Contours of flow depth (case 3)

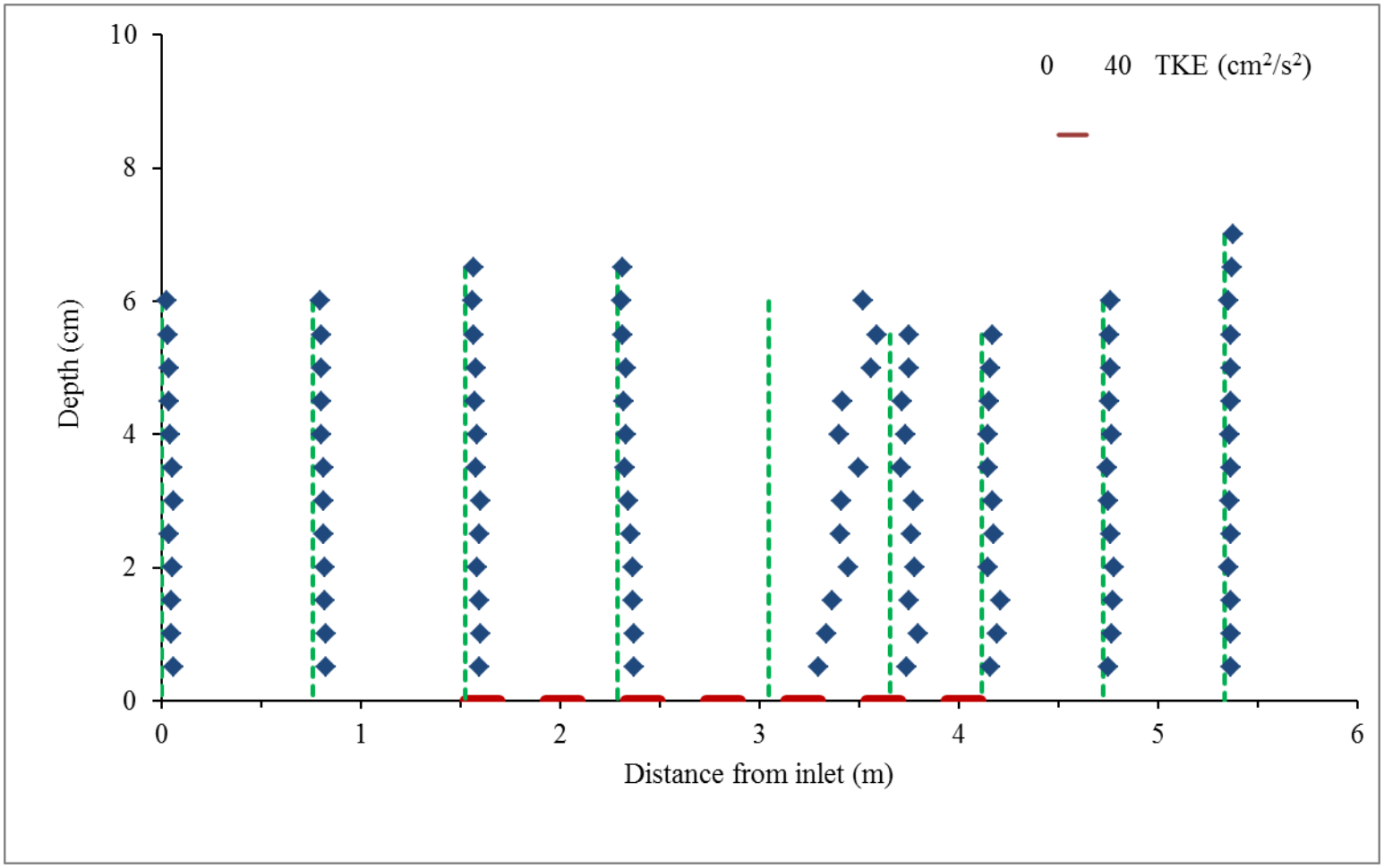

(a) Along Y3

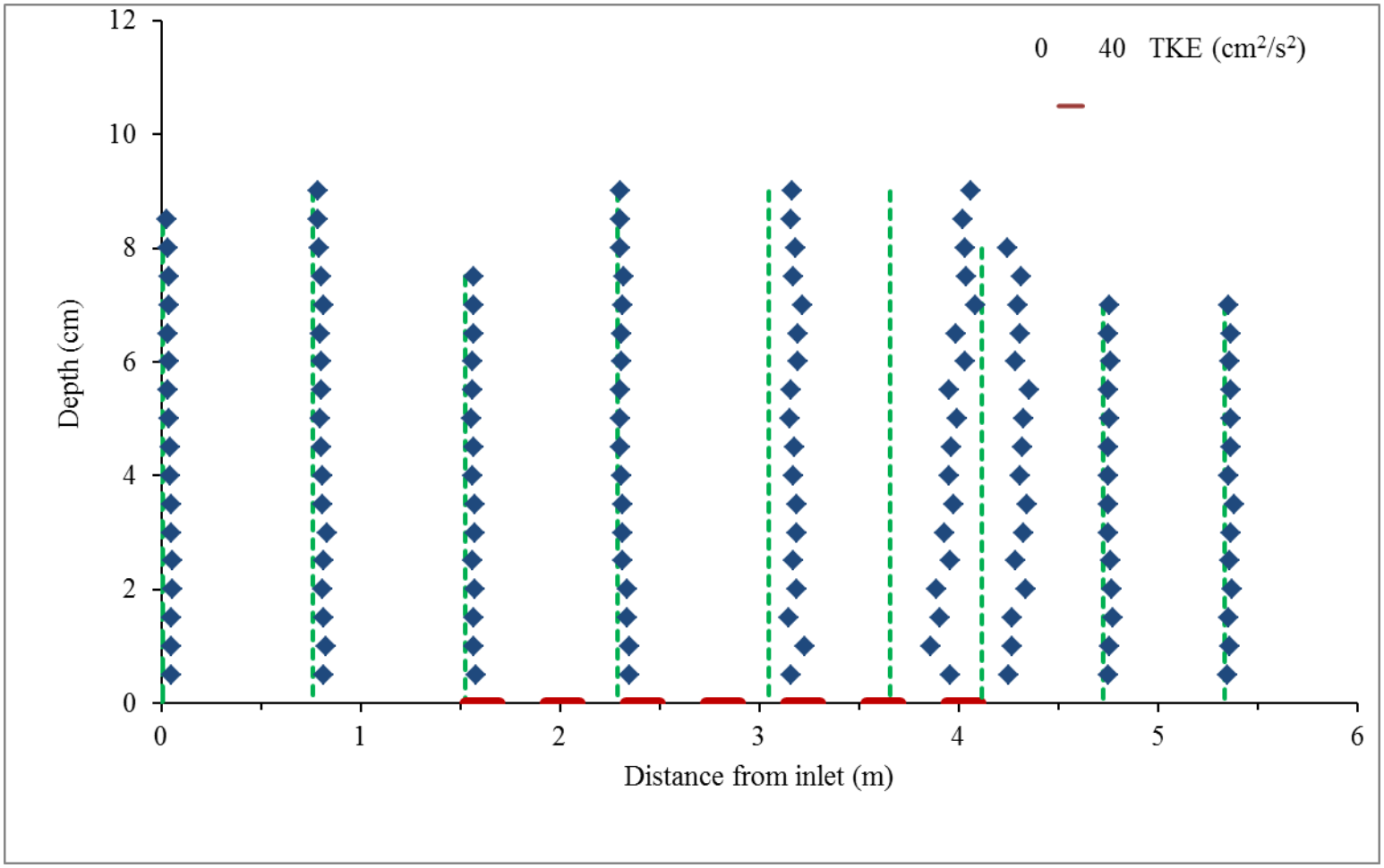

(b) Along Y5

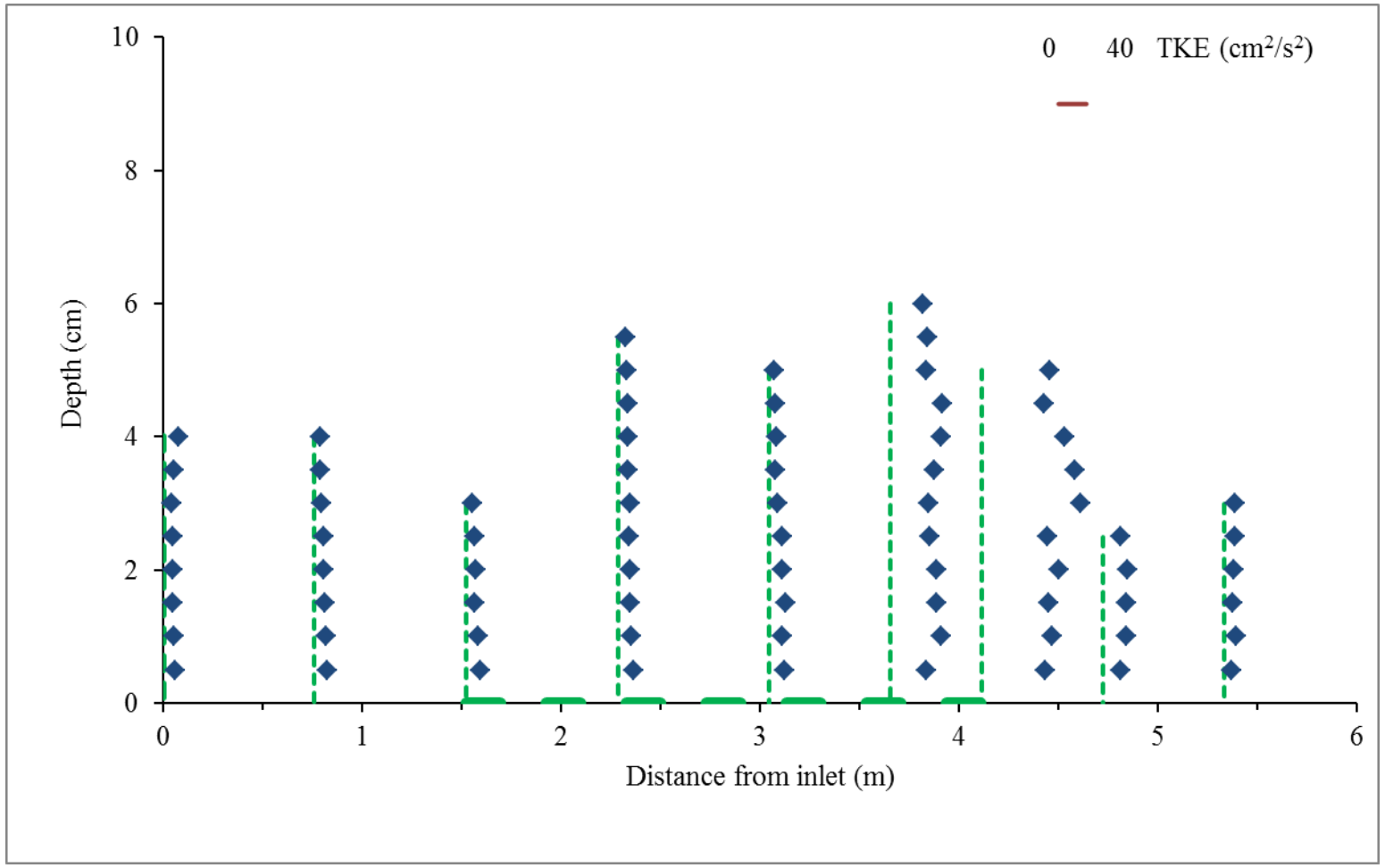

(c) Along Y7

Fig. A3.9 Variation of TKE (case 3)

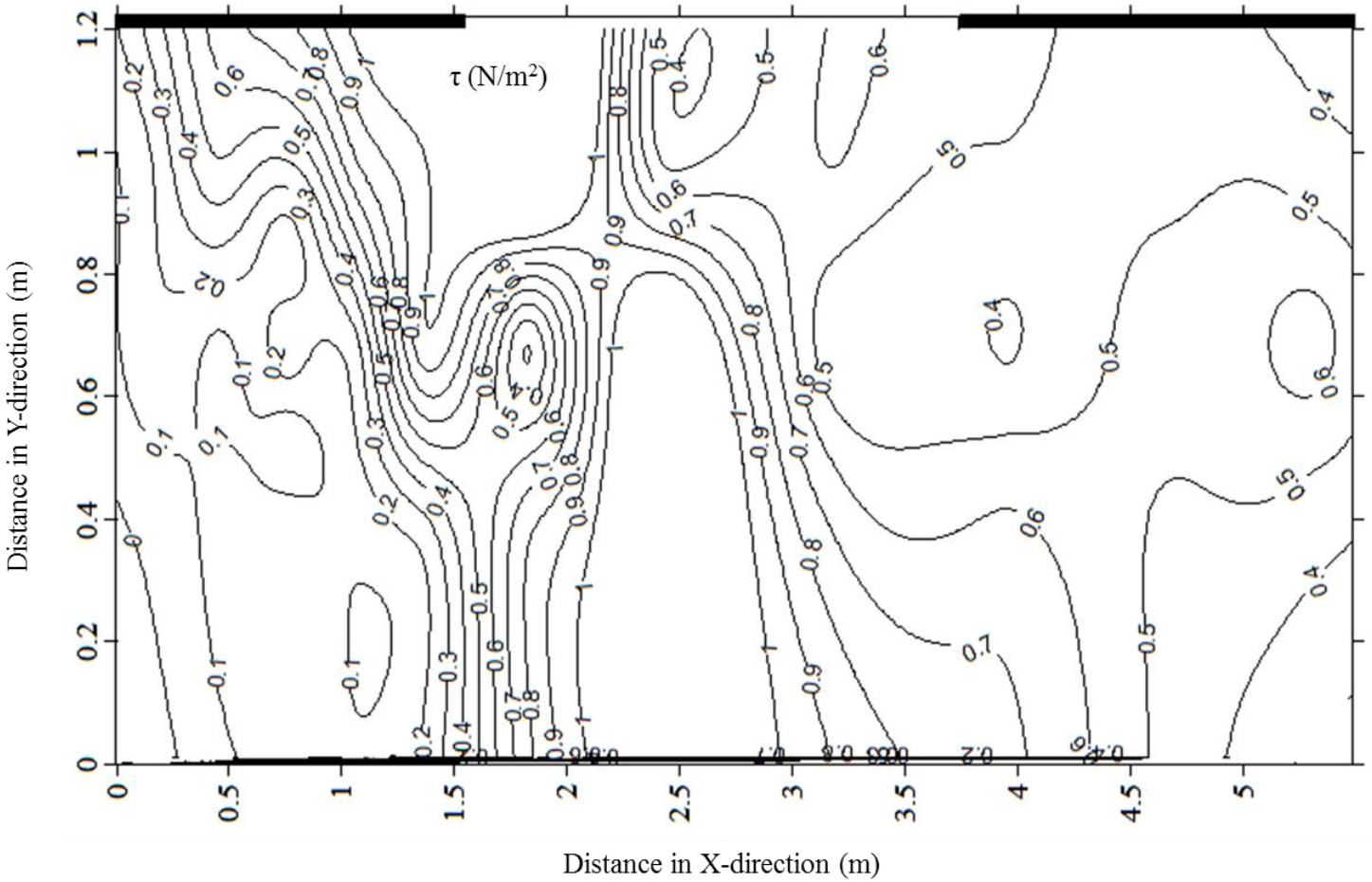

Fig. A3.10 Distribution of bed shear stress (case 3)

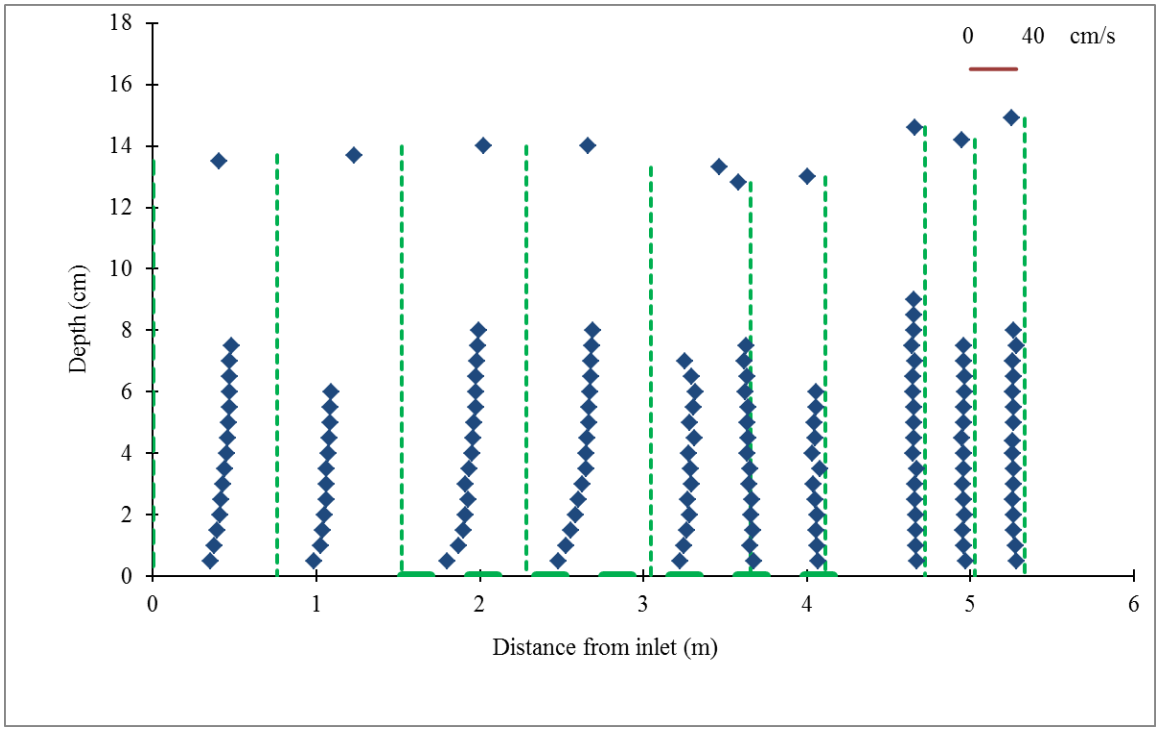

(a) X-velocity

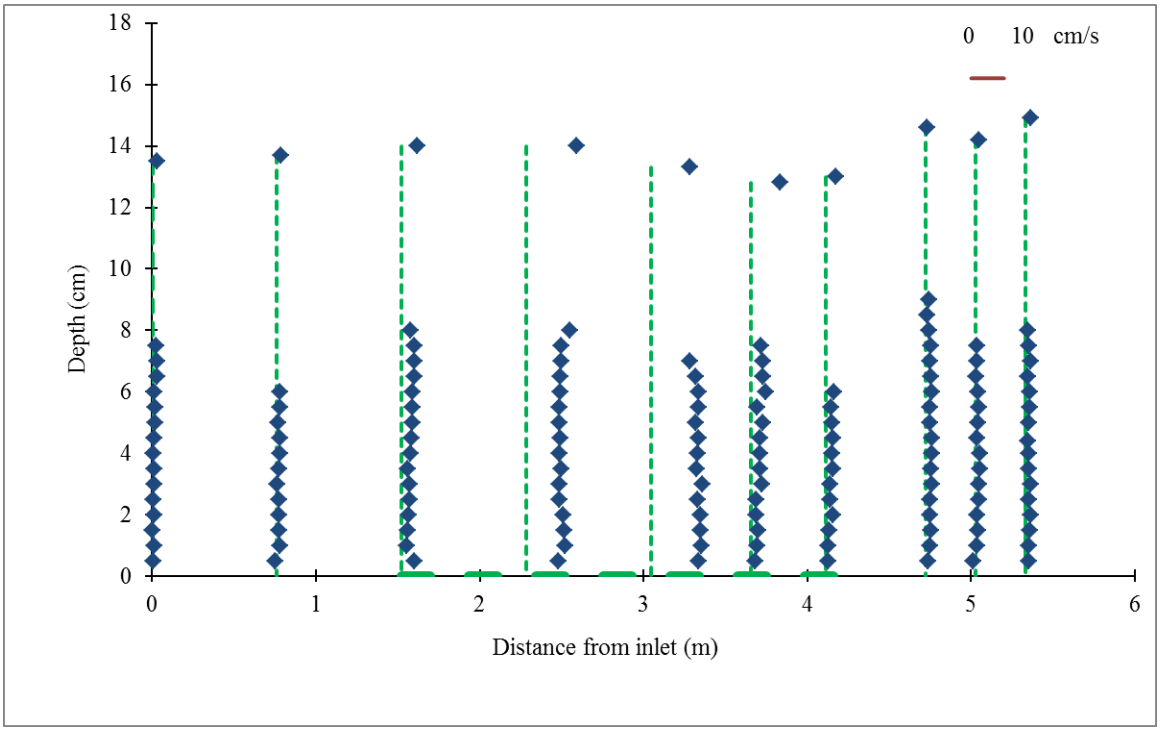

(b) Y-velocity

Fig. A3.11 Measured velocities along Y3 (case 5)

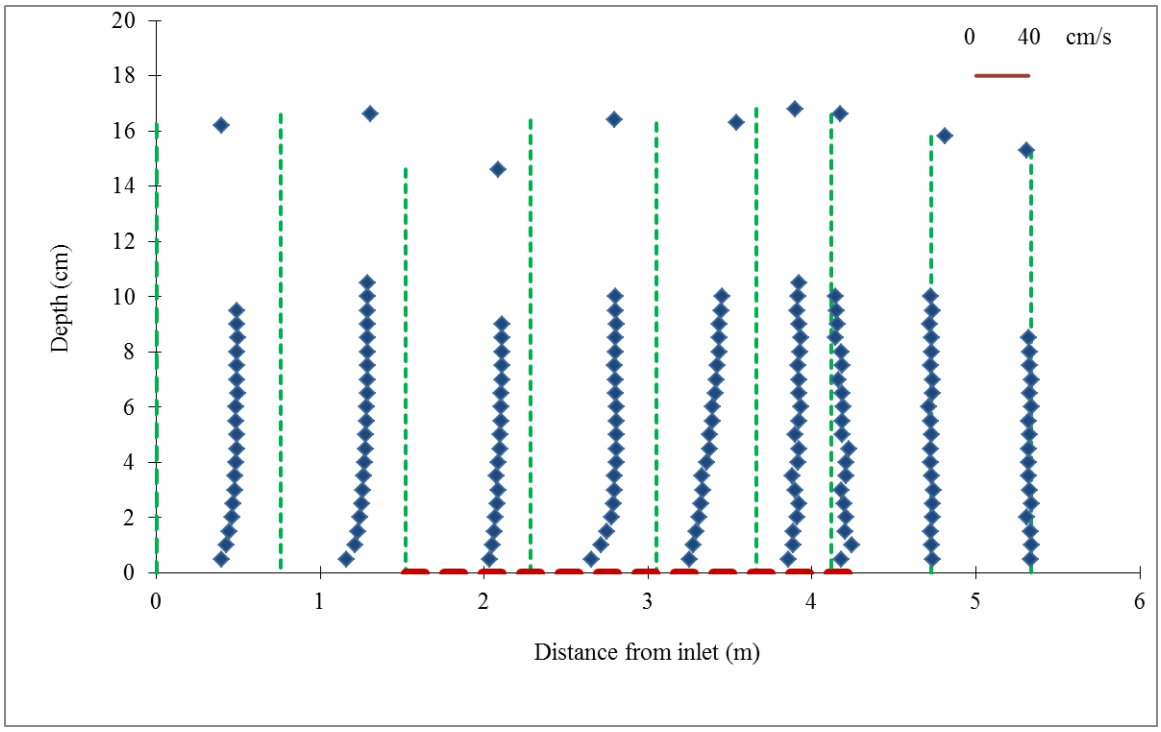

(a) X-velocity

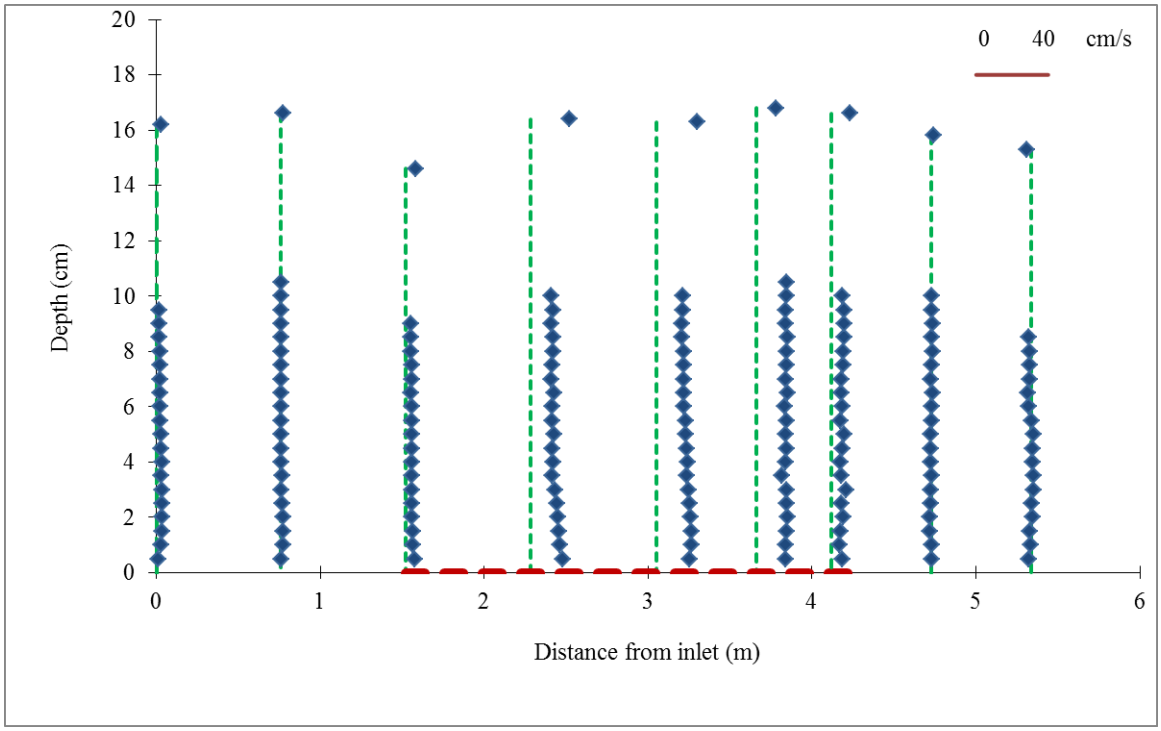

(b) X-velocity

Fig. A3.12 Measured velocities along Y5 (case 5)

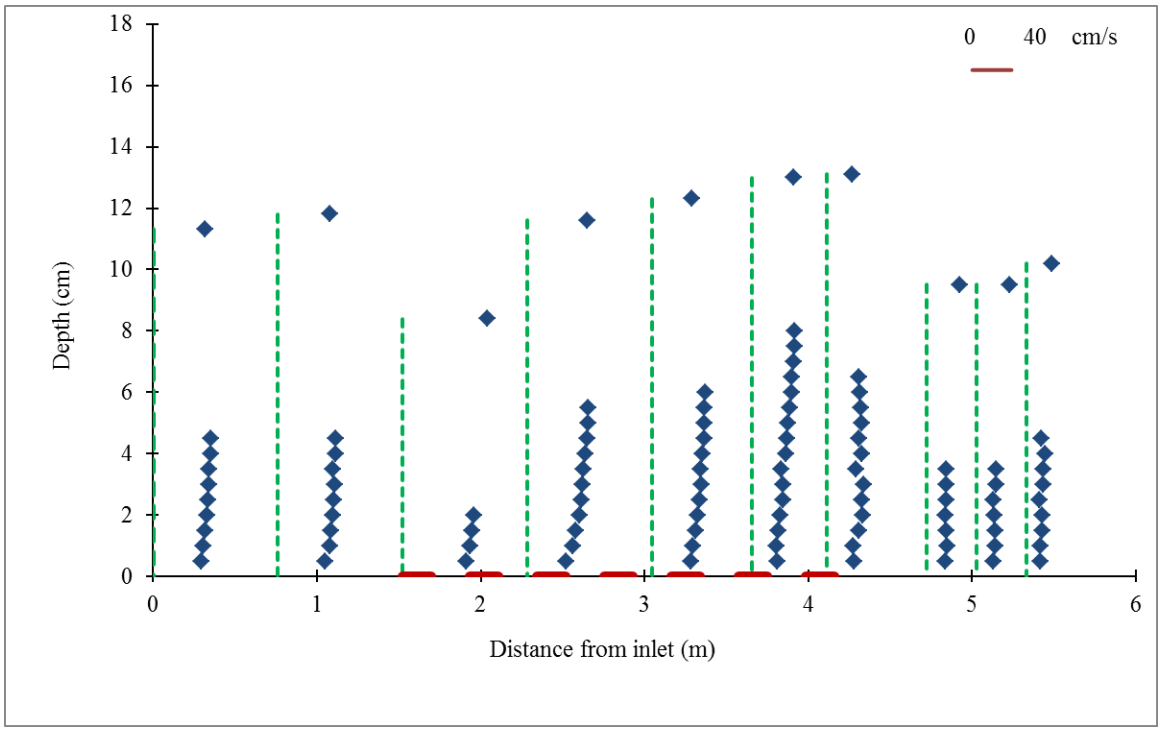

(a) X-velocity

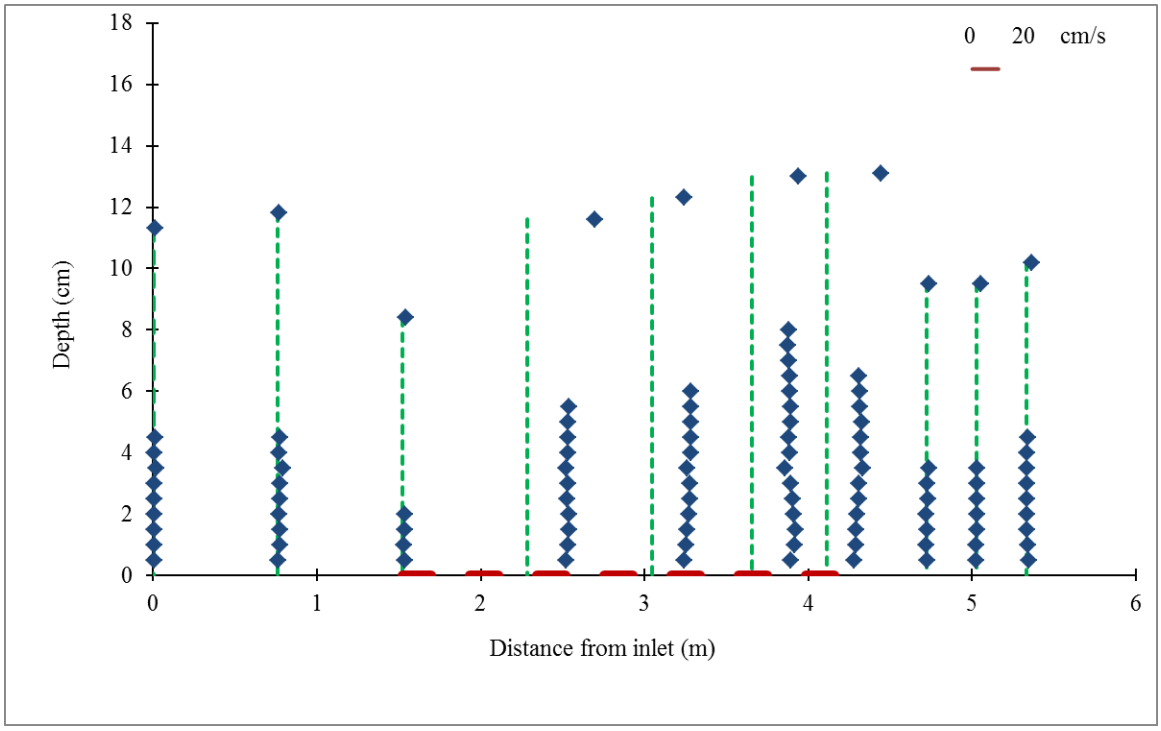

(b) Y-velocity

Fig. A3.13 Measured velocities along Y7 (case 5)

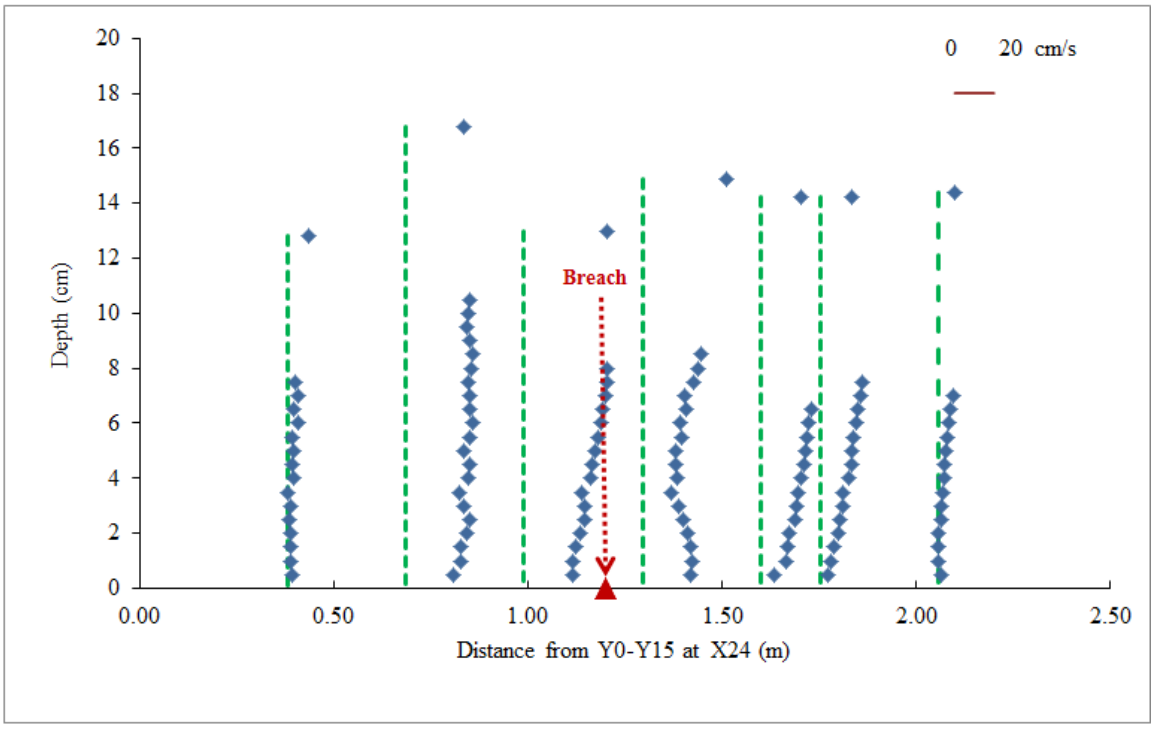

(a) X-velocity

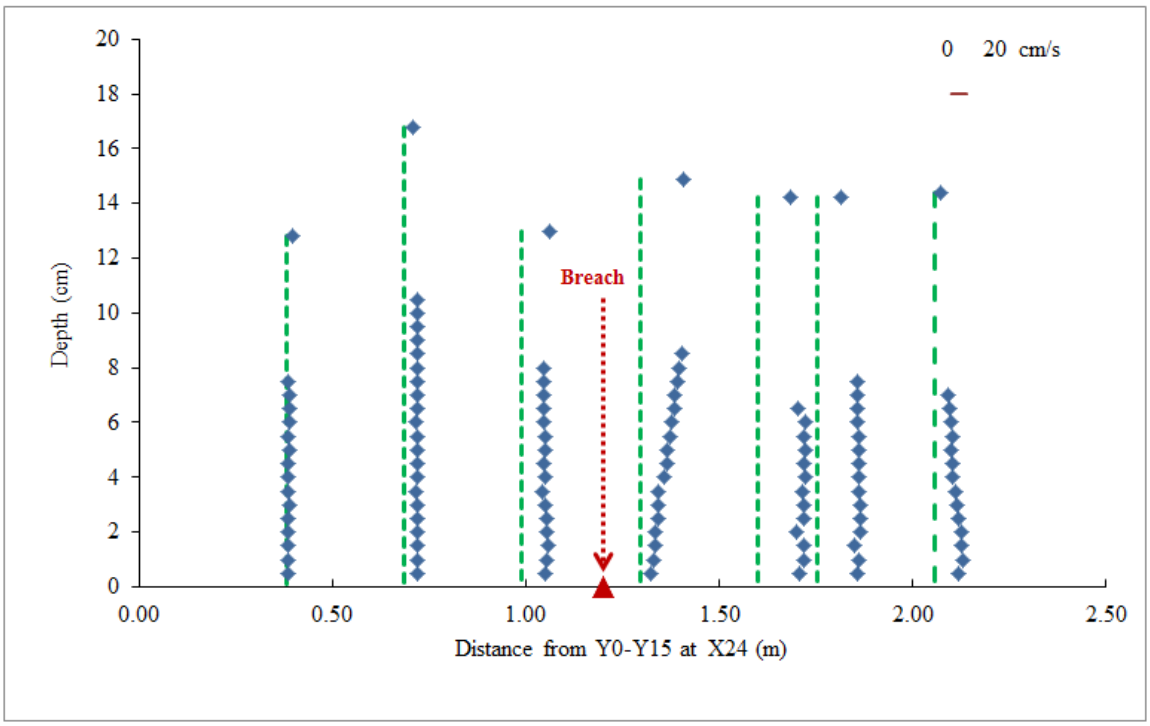

(b) Y-velocity

Fig. A3.14 Measured velocities along X24 (case 5)

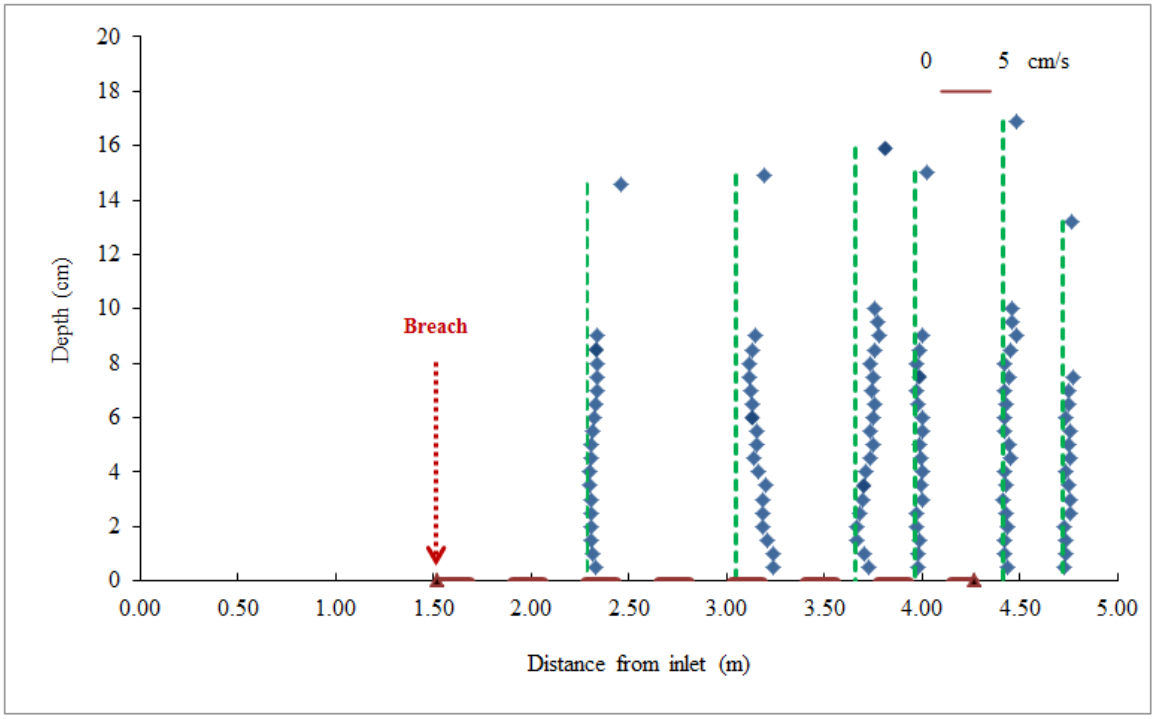

(a) Along Y6

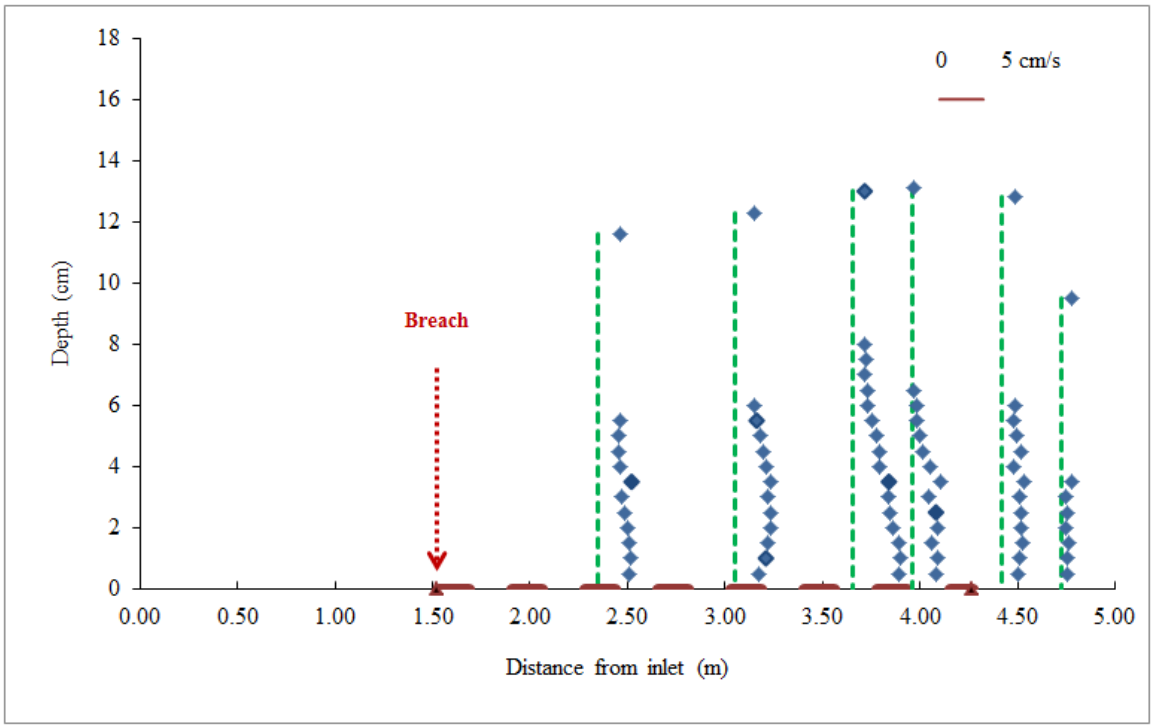

(b) Along Y7

Fig. A3.15 Measured Z-velocities (case 5)

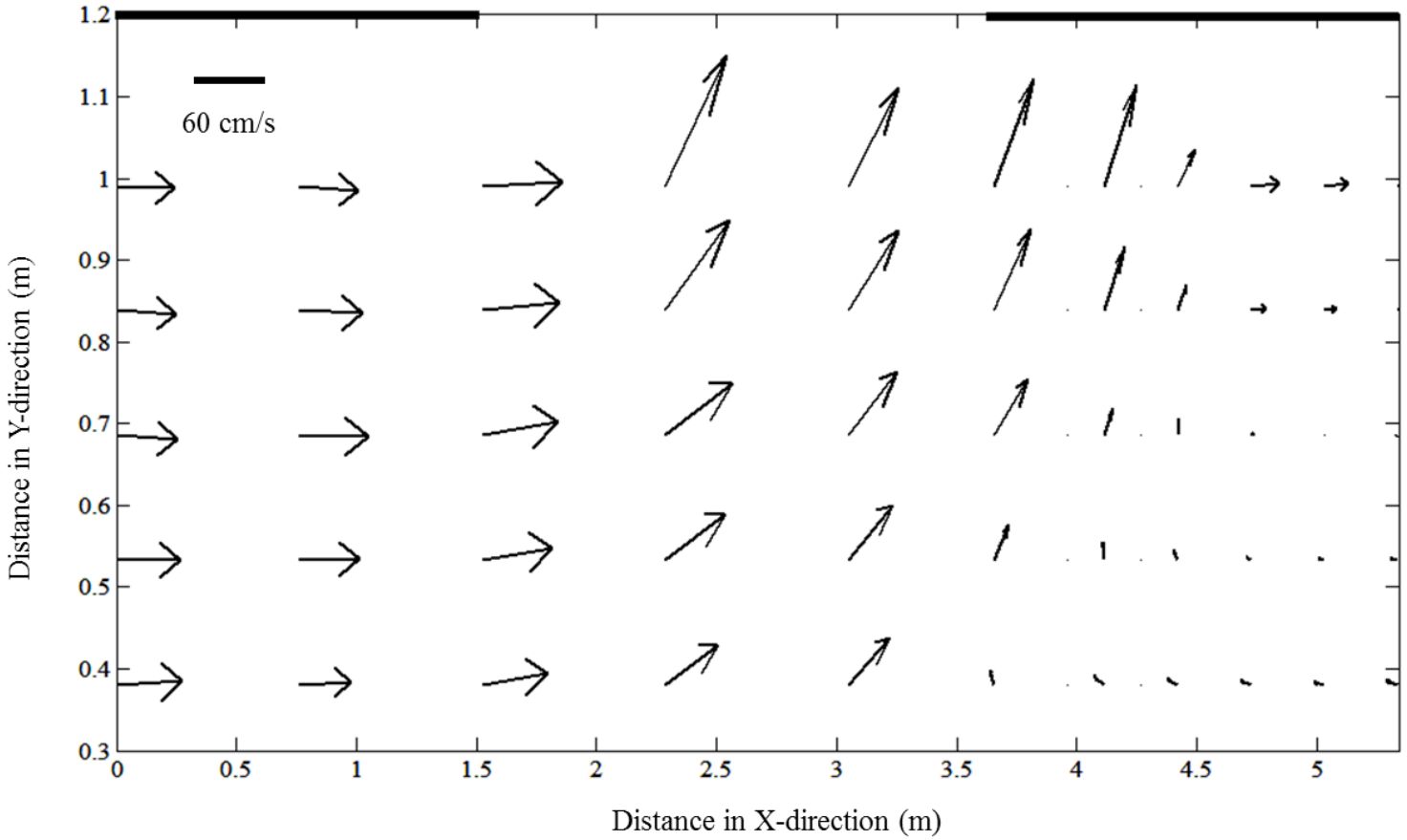

Fig. A3.16 Depth averaged velocities in the channel (case 5)

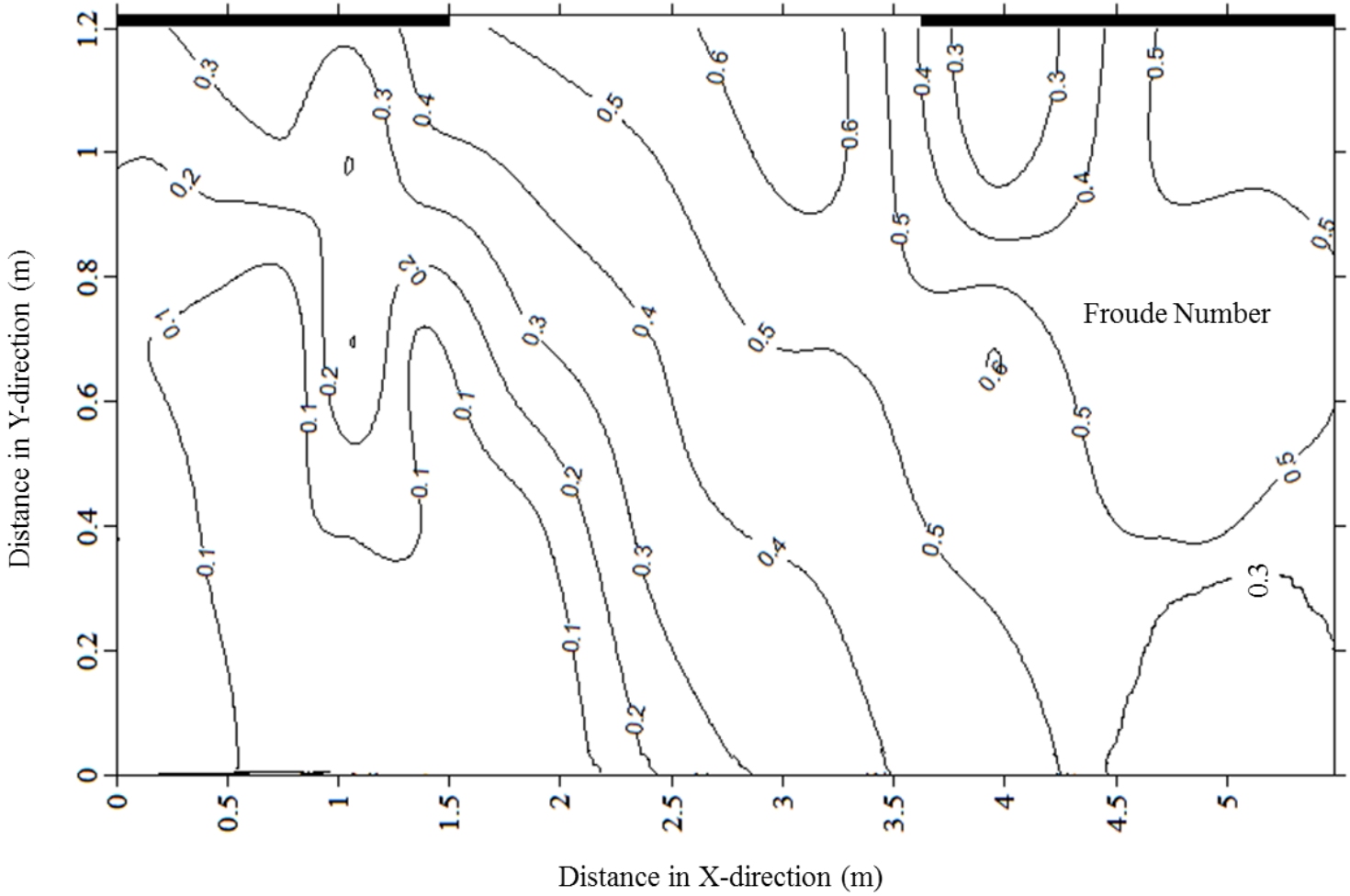

Fig. A3.17 Froude Numbers variation (case 5)

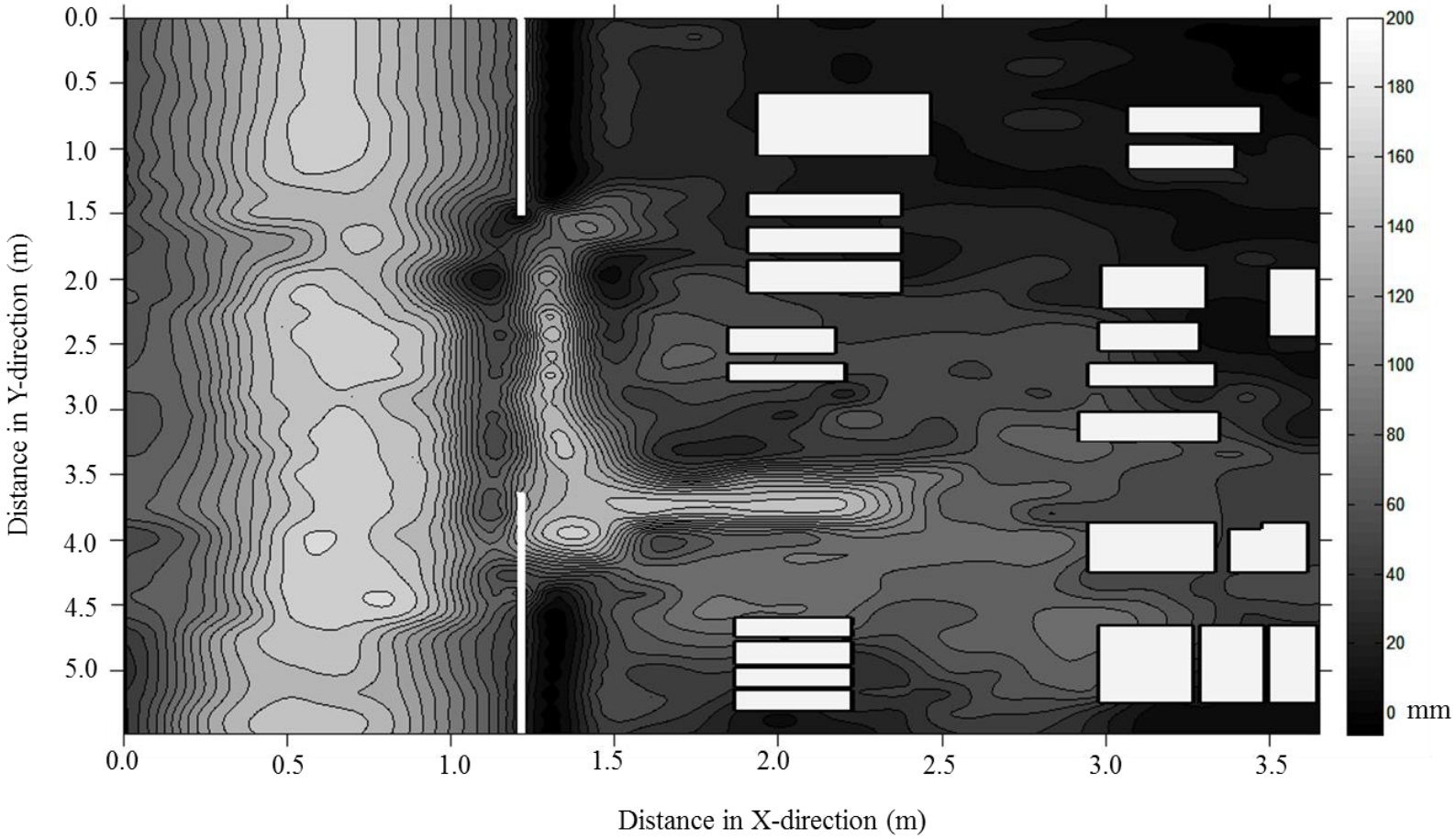

Fig. A3.18 Contours of flow depth (case 5)

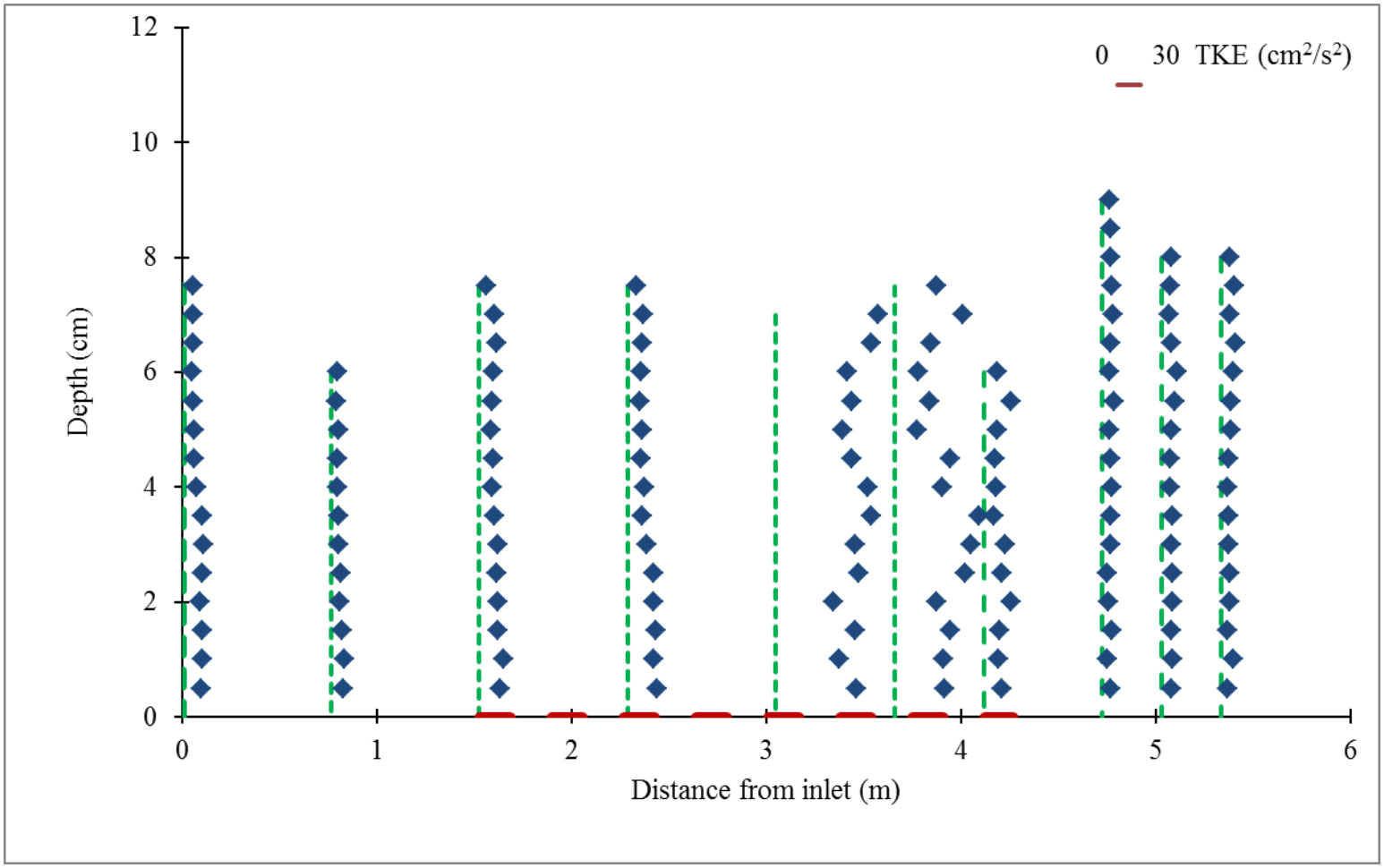

(a) Along Y3

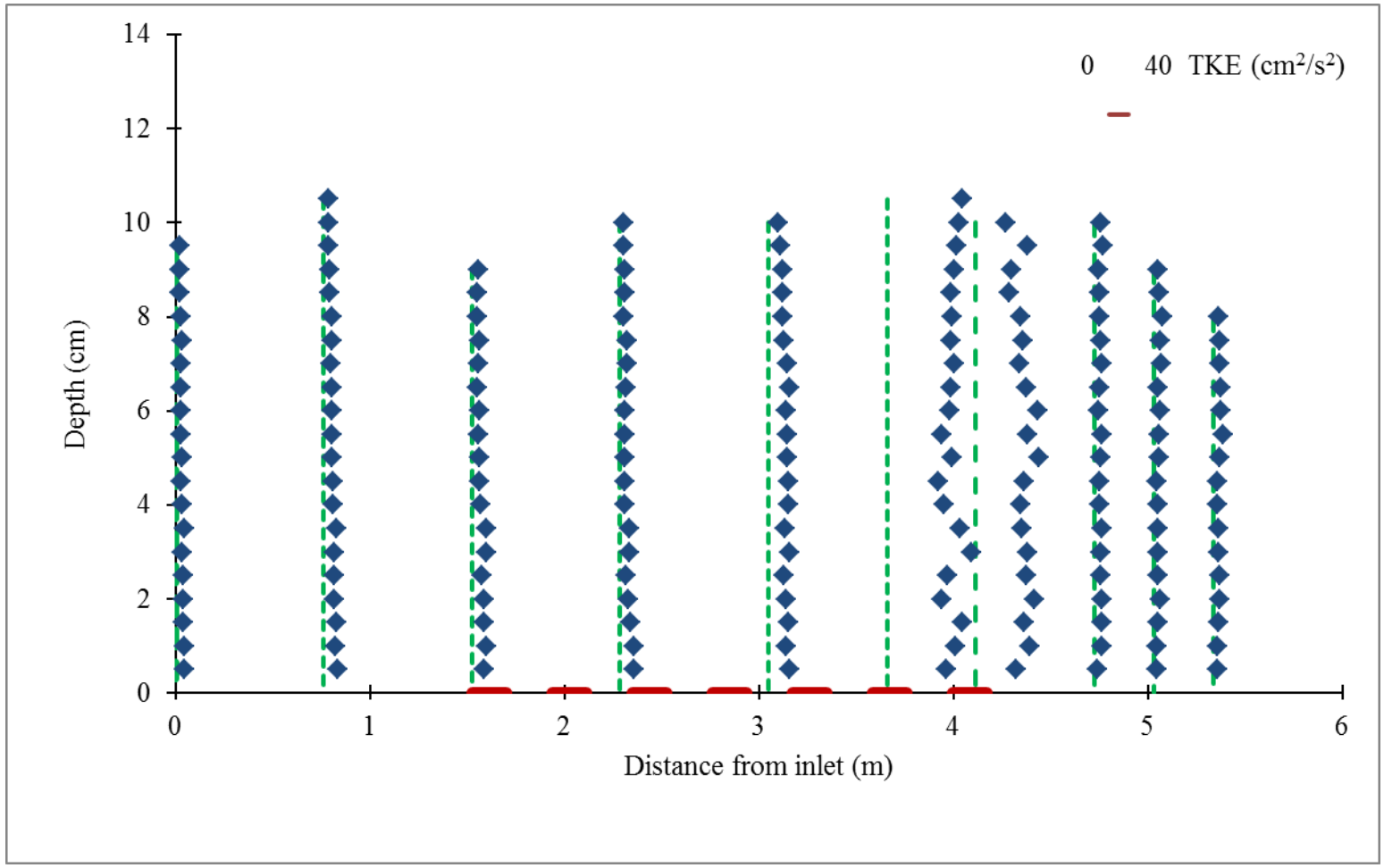

(b) Along Y5

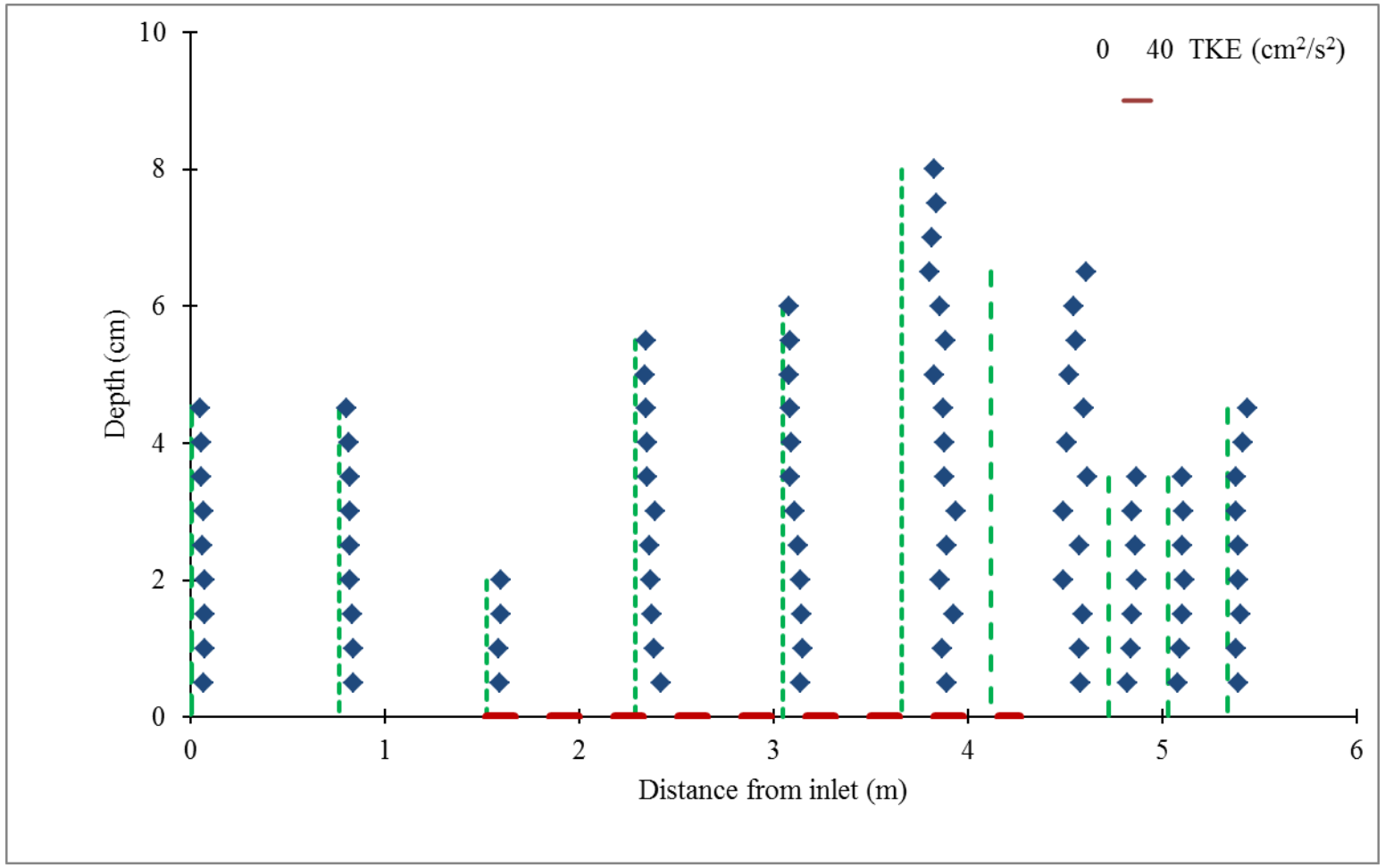

(c) Along Y7

Fig. A3.19 Variation of TKE (case 5)

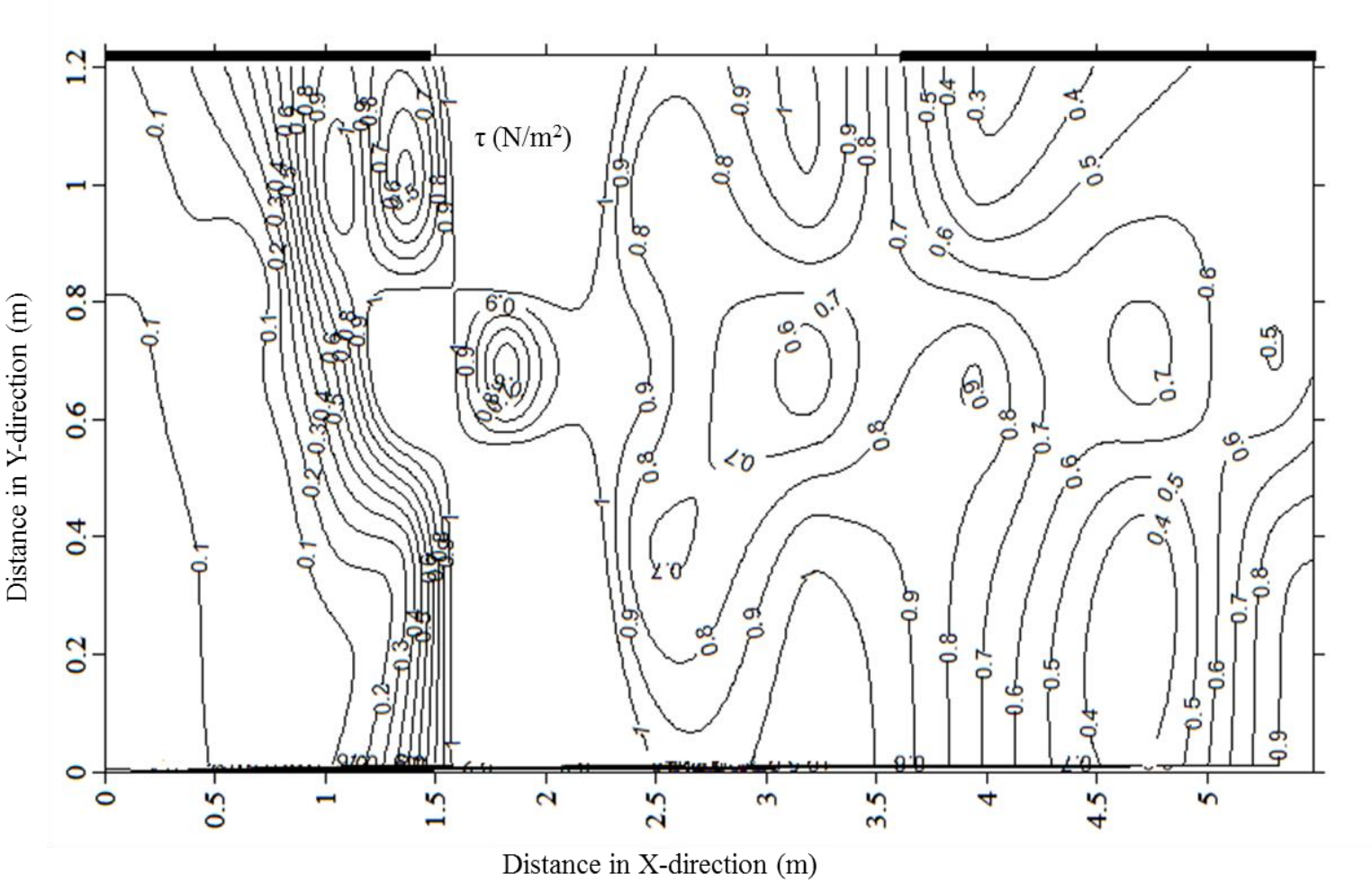

Fig. A3.20 Distribution of bed shear stress (case 5)